ATLSS

LEHIGH
University

Residual Strength and Repair of Damaged and Deteriorated Offshore Structures

CORROSION DAMAGE -- EFFECT ON STRENGTH

# TUBULAR COLUMNS WITH MULTIPLE CORROSION PATCHES

**By**
**Alexis Ostapenko and Onur Gulec**

**Research Sponsored by**

**Exxon Production Research Company**
**Minerals Management Service (U.S. Dept. of the Interior)**
**(Technical Assessment and Research Branch)**
**Mobil Technology Company**

**ATLSS Report No. 99-15**

**December 1999**
**[Distribution restricted until March 2001]**

**ATLSS is a National Center for Engineering Research on Advanced Technology for Large Structural Systems**

117 ATLSS Drive
Bethlehem, PA 18015-4729

Phone: (610)758-3535
Fax: (610)758-5553

www.Lehigh.edu/~inatl/inatl.html
Email: inatl@lehigh.edu

# DISCLAIMER

# TABLE OF CONTENTS

Page

# ABSTRACT

Offshore structures are exposed to harsh marine environment that causes corrosion damage on structural members. Actual tubular columns typically have irregular and complex corrosion patterns. When the damage is mainly local with the irregular thickness reduction concentrated over small portions of the tube (patch corrosion), the failure can develop in the weakened area and spread over the affected cross section leading to the collapse of the whole member. Except for the columns with one corrosion patch, no simple tools are presently available for analyzing the effects of such localized damage. In the current project, a simplified engineering procedure for evaluating the ultimate capacity of tubular columns with fixed and pinned ends damaged by three corrosion patches was formulated.

Tests were conducted on two specimens with multiple corrosion patches simulated by grinding. One specimen had two corrosion patches positioned at the mid-length in the same circumference, and the other had three patches, two at the mid-length as in the first specimen and the third between the two and offset longitudinally.

Finite element analysis program ABAQUS, which can consider geometrical and material nonlinearities, was used in the analytical study. Comparison of the ultimate loads and the load-deformation relationships from the tests and computations indicated that the FE analysis was sufficiently accurate, and that the analytical results can be used in parametric studies.

Finite element analysis was performed to determine the ultimate load capacity of tubular columns to generate a database for over 500 different combinations of the following parameters:

- the number of corrosion patches (two or three),
- the relative location of the patches to each other in the circumferential and longitudinal directions,
- the column length,
- the yield stress,
- the end conditions (fixed or pinned).

The effect of these parameters was investigated, and approximate "engineering type" formulas were derived for the columns with three corrosion patches and fixed or pinned end conditions.

The formula for fixed-end columns was obtained by linear regression analysis supplemented with a nonlinear approximation and has twelve (12) regression constants. The resultant accuracy of the approximation was: COV%=2.89%, the Coefficient of Determination $R^2$=0.999 and the maximum error of 6.98%.

The formula for pinned-end columns required a procedure with four-stages of nonlinear regression analysis and resulted in 18 constants (three sets with six constants in each). The accuracy of the approximation was: COV%=2.08%, the Coefficient of Determination $R^2$=1.0001 and the maximum error of 6.11%.

Since these formulas are based on the patch size used in the database, an approximate procedure was also formulated for analyzing columns with corrosion patches of other sizes.

#### *1.2.2.1 "Shifted-Circles" Model*

The "Shifted Circles" model approximated the thickness variation around the circumference as shown in Fig. 1-3.[9] In this model, the damaged cross section is defined by the circle of the inside surface and the outside circle which touches the outside point at the location of minimum thickness and the outside point of the maximum thickness. The maximum thickness point, if necessary for computational purposes, is moved to be diametrically opposite the point of minimum thickness. However, the results of this idealization were not very promising since the stresses in the idealized cross section often significantly differed from the stresses computed using the actual thickness variations.

#### *1.2.2.2 "Cosine Patch" Model*

In another idealization, the thickness reduction was defined by a cosine curve over a portion of the circumference and similarly in the longitudinal direction. This model named "Cosine Patch" Model is shown in Fig. 1-4.[5,12,13] The two main drawbacks of this model are that the reduction of the thickness outside the patch is not considered, and that, similarly to "Shifted Circles", the variation of thickness in the area of minimum thickness is totally controlled only by the overall dimensions of the patch.

#### *1.2.2.3 "Constant-Thickness Patch" Model*

The "Constant-Thickness Patch" model is an idealization of the thickness variation in the corrosion patch as shown in Figs. 1-5 and 1-6. It was developed as a generalization of the "Cosine Patch". A greater flexibility in modeling the circumferential thickness variation was achieved by introducing a constant-thickness portion "a" with minimum thickness $t_p$ in the patch and a reduced thickness $t_d$ outside the main patch. Note that, the "Constant-Thickness Patch" model reduces to the "Cosine Patch" if $a = 0.0$, $c = w$, $t_p = t_{min}$ and $t_d = t$. Although more sophisticated, this model still has the disadvantage of creating a symmetrical section as an approximation of generally unsymmetrical actual patterns.

Figure 1-7 illustrates an application of the "Constant-Thickness Patch" to an idealization of a typical corroded cross section having a very irregular thickness variation. [10]

In general, the model gave reasonably good results in comparison with the cross sectional properties computed from the actual thickness measurements. One of the convenient advantages of this model is that once the geometrical parameters ($a$, $c$, $t_p$, $t_d$) are defined, the cross sectional properties can be readily computed. Although good correlation between the estimated and actual properties and stresses can be achieved, the model is still highly dependent on intuitive consideration of equal areas, moments of inertia and centroidal shift, which is very subjective and may be inconsistent.

#### *1.2.2.4 "Linear Segments" Model*

The "Constant-Thickness Patch" model has then led to another model, called the "Linear Segments" model, in which the irregular thickness variation is approximated with a series of segments with a linear variation of the thickness in each segment.[10] Figure 1-8 illustrates the idealization of a corroded section by five thickness values at five angle locations around the circumference. The thickness variation is also shown on the unfolded circumference (to a different scale), where the corroded surface becomes a series of straight lines.

The most important advantage of this model over the others is that the subjective approximation is limited to matching the areas in each segment, which is easily done by inspection and requires very little intuition. Normally, five to twelve segments are sufficient to approximate a typical irregular cross section.

## 1.3 Summary of Current Project

In summary, this report describes the tests conducted on two tubular columns with multiple corrosion patches simulated by grinding. The results served to validate the accuracy of the finite element analysis that was used to generate database for developing engineering design formulas. Basically, the report consists of the following four parts:

**(1) Chapter 2:** *Description of the specimens and test procedures.*

**(2) Chapter 3:** *Finite element analysis.*

The chapter describes the finite element modeling and analysis of the columns damaged with multiple corrosion patches. Given are the details of modeling techniques for tubular columns with different lengths having one, two or three corrosion patches at various locations. Discussed are also the comparison and selection of different types of elements in the finite

# 2. TESTS ON SHORT TUBULAR COLUMNS WITH MULTIPLE CORROSION PATCHES

Tests were conducted on two short specimens with multiple corrosion patches: one with two patches and the other with three. The main purpose of these tests was to help in the development of the discretization models for the finite element analysis used in the preparation of the database. The corrosion damage was simulated by manual grinding of the originally intact tubular members. These tests were needed since all the previous experimental work had been performed on columns either with only one patch or with very irregular corrosion damage.[e.g., Ref 9,10] A detailed description is given of the preparation of the test specimens and of the testing procedure in the hope that this information would be helpful in any similar research.

## 2.1 Description of Test Specimens

The two specimens were cut from the undamaged portions of a previously tested Specimen P8, which, in its turn, was made from a longer specimen that had been tested with a dent at mid-length.[9,10] Figure 2-1 shows the layout of all these specimens. The first specimen, MP1, had two corrosion patches positioned at mid-length. The second, MP2, had three corrosion patches; two were in the same position as in Specimen MP1, and the third directly above the two.

The patches are shown in the unfolded views of the two specimens in Fig. 2-2. The longitudinal reference lines designated by compass points N(North), NE, etc., were used together with the distance from the bottom end (End A) as a coordinate grid for locating the corrosion patches, strain gages, measuring points for initial imperfections and out-of-straightness, etc. The N(North) line was along the weld, and the S(South) line served as a centerline for positioning the corrosion patches with respect to the half-length distance between the ends. (The compass point labeling corresponded to the actual orientation of the specimen in the testing machine.)

The geometry of the individual corrosion patches was selected to be of the typical type used in the predecessor project in which the effect of a single patch was studied.[10] This way, the results from the two projects could be compared to each other. As shown in Fig. 2-3, the patch was of essentially rectangular shape with dimension ‘a’ circumferentially and ‘h’ longitudinally. The middle portion of the constant reduced thickness $t_p$ measured 'c' circumferentially and 'b' longitudinally. The cosine-type transitions between the original thickness t and the reduced thickness tp were 'v/2' circumferentially ad 'w/2' longitudinally along the respective sides. Thus, each patch consisted of two regions: a region of constant reduced thickness, and a transition region from the constant thickness to the full thickness.

The actual positioning and dimensions of the patches are shown in Fig. 2-4. Specimen MP1 had two patches with a circumferential spread g=3.20 inches. Specimen MP2 had the same two patches as specimen MP1 and a third patch offset longitudinally at a spacing of s=1.40 inches. The dimensions of the reduced constant-thickness portion were a=1.70 in. circumferentially, b=0.50 in. longitudinally, and the thickness $t_p$=0.03 in. In combination with Specimen P21 of Ref.10, Specimens MP1 and MP2 provide a transition of the effect of damage by one patch (P21), two (MP1) and three (MP2).

## 2.2 Preparation of Specimens -- Tools and Procedures

Some special tools and procedures were employed in the preparation of the specimens for testing. In particular, tools were needed for measuring wall thickness during the grinding of the simulated corrosion patches.

### 2.2.1 Angle Tool

The angle tool was used for measuring the depth of the depression made in the wall during grinding a patch. The angle tool is shown in Fig. 2-5. It was made from a piece of aluminum angle about six inches long and a dial gage with 0.001-inch accuracy. At the midpoint of the angle, a hole was drilled at a 45° angle to the legs of the angle. The shaft of the dial gage was inserted through the hole. A C-clamp fixed the gage to the angle and also provided support against the outside surface of the tube so that the shaft of the gage was always perpendicular to the specimen.

During the operation, the tool measured the depth of the grinding rather than the thickness of the wall in the patch. The remaining patch wall thickness $t_p$ was obtained by subtracting the reading from the original thickness t.

### 2.2.2 Fork Tool

The fork tool was also used for measuring the wall thickness, but it was much more accurate than the angle tool, and it measured the thickness directly although more awkwardly. It was made from three pieces of aluminum angle. Two pieces were about 15 inches and the third about 6 inches long, respectively. As shown in Fig. 2-6, the longer pieces formed the inside and outside arms (forks), and the shorter piece held these arms together by means of two small C-clamps thereby creating the 'Fork' Tool. At the end of the outside arm angle, a hole was drilled that accepted the shaft of a 0.0001inch dial gage. A small bracket was used to attach the dial gage to the angle with a small C-clamp. At the corresponding end of the inside arm angle, a short tip was attached to oppose the gage tip. The tips were custom fabricated to have sharp points which made the thickness measurements more accurate than using rounded tips since the sharp tips were not affected by the curvature of the specimen as much. Care was taken to make the tips lined up exactly against each other.

A block of wood taped to the fork arm with the dial gage served as a pivot bar. This bar was necessary to make sure that the fixed tip was in contact with the inside of the tube wall and to serve as a spacer to keep the dial gage tip some distance from the angle.

To use the tool, the fork with the fixed pointer (inside arm) was inserted longitudinally into the tube. With both pointers opposite each other, the patch wall thickness could be read directly from the dial gage. Due to the sensitivity of the tool, it was necessary to take measurements with the fork in a vertical position. If the fork had been horizontal, the self-weight of the tool could have caused elastic deformations, which could have produced an error of several ten-thousandths of an inch.

### 2.2.3 Lathe Method – Specimen Topography

The lathe method was used to define the topography of the tube surface and specifically to measure the diameter at any location along the length and around the circumference. An arrangement in a lathe was found to be most convenient for this purpose. One end of the tube was supported by the lathe chuck that was tightened just enough to hold the specimen in position and not introduce detrimental distortions of the tube. The opposite end of the specimen was hanging free and positioned with respect to the axis of the specimen so that it would not significantly move as the specimen was rotated about its axis. The arrangement is similar to that shown in Fig. 2-8 except that the right end was not supported in order to exclude any distortions that might be introduced at that end.

The cutter tool carriage, which can ride on the lathe bay (rail) parallel to the axis of rotation of the tube, was used to support a 0.0001-inch dial gage for measuring the radial position of the specimen surface. The attachment of the gage was provided through an adjustable rod assembly that was bolted to a magnetic base that was stuck to the cutter mount. In this arrangement, a radial dial gage reading could be taken at any point of the specimen by rotating it in the lathe and moving the cutter mount parallel to the specimen axis. Readings were taken at the eight longitudinal reference lines at one-inch intervals. Three readings were averaged at each point.

The geometry of the specimen surface was related to an imaginary reference cylinder whose axis was the axis of rotation of the lathe chuck. The diameter of this reference cylinder is given by Eq. 2-1.

$$D_r = D_m - (g_1 + g_2) \tag{2-1}$$

Where

$D_r$ is the diameter of the reference cylinder,

$D_m$ is the diameter of the specimen measured with a 6-inch micrometer between two diametrically opposite points,

$g_1$ and $g_2$ are the dial gage readings at these two points.

To account for the slight inaccuracy of the measuring system, one should obtain this reference cylinder diameter from the micrometer and dial gage readings at several locations along the specimen and around the circumference and average these diameters into the $D_r$ value to be used in further operations. (In application, the variation was within 0.001 inch.)

With the value of $D_r$ established, the specimen diameter $D_i$ can be computed from Eq. 2-2 without the cumbersome micrometer measurements, by using the dial gage readings at opposite points at any i$^{th}$ location on the specimen.

$$D_i = D_r + (g_1+g_2) \tag{2-2}$$

Readings were taken on the eight longitudinal reference lines at one-inch intervals. For better accuracy, three readings were averaged in each case. It was noted that no matter how loosely the chuck was tightened, there would still be some deformations of the tube near the clamped end. Therefore, the ends of the tube were reversed in the lathe, and dial gage readings taken at the three one-inch intervals at the end that was formerly at the chuck. The new diameters were recomputed and used as the actual diameters.

Inspection of the values obtained showed that the diameter variation in the region of corrosion patches was quite insignificant and that the nominal diameter of D=5.5 inches was acceptable for use in FE analysis.

The diameter of the reference cylinder $D_r$ can be used for defining the topography (contour map) of the specimen surface with respect to a base cylinder with the diameter $D_b$ equal to the average of the measured diameters. The axis of this base cylinder is coincident with the axis of the reference cylinder. The elevation $r_i$ from the base cylinder to the specimen surface at the $i^{th}$ point is then given by Eq. 2-3.

$$r_i = g_i - (D_b - D_r) \tag{2-3}$$

where

$r_i$ is the elevation at the $i^{th}$ point, positive outward and negative inward.

$g_i$ is the dial gage reading.

$D_b$ is the diameter of the base cylinder equal to the average of the measured specimen diameters.

$D_r$ is the diameter of the reference cylinder as defined by Eq. 2-1.

### 2.2.4 Grinding of Corrosion Patches

Corrosion damage on the specimens was simulated by grinding the patches with a hand-held rotary grinder. A patch consisted of two regions: a region of reduced constant thickness and a transition region from the constant thickness to the full thickness. The dimension variables are defined in Fig. 2-3, and the actual dimensions are given in Fig. 2-4.

As the first step in the grinding operation, a template of the corrosion patches drawn on paper was taped to the tube wall and the corners of the constant-depth and transition areas of each patch were marked with a center punch. For reference, a few points around the perimeters of both areas were also punched.

The transition profile from the constant-thickness portion to the full thickness was selected to be a cosine curve. The depth halfway between the constant depth and full thickness was ground at one half the depth of the patch. The other points in the transition area were not measured due to the inaccuracy of the measuring devices in the curved regions.

#### *2.2.4.1 Coarse Grinding*

The operation began by rough grinding the constant thickness portion of the patch. The centerline of the grinding stone was placed in line with the perimeter of the constant thickness portion and allowed to grind an oval-shaped pattern. The oval shape went outside of the constant thickness portion, but this helped to maintain a constant thickness to the edge of the region and to form the transition region. This process was repeated around the entire perimeter. Figure 2-7 shows the layout of the initial grinding zones. The ridges between the ovals were then smoothed over so that the entire area was at a constant depth. In this process, the thickness of the patch was measured with the angle tool. Once the patch was within ten to fifteen thousandths of an inch of the desired thickness, the grinding was made much more refined, and measurements were taken much more frequently until the patch thickness was within a few thousandths of an inch of the target thickness.

#### *2.2.4.2 Fine Grinding*

After this, a quarter inch grid was drawn over the patch, and thickness measurements were taken with the fork tool. Additional grinding was done as necessary. The fork tool was used at this stage since the angle tool was not as accurate. The final polishing ended when the thickness was within one to two thousandths of an inch of the desired thickness.

#### *2.2.4.3 Measuring and Recording Patch Thickness*

Then, an eighth-inch grid was drawn over the patches with a ballpoint pen, and careful measurements were taken with the fork tool at each grid point three times. If the wall was still too thick at some point, the area was ground some more to the proper thickness and the thickness measurements repeated. Each time, three measurements were taken to eliminate any error that could be caused by inadvertent rocking of the fork tool. The average of the thicknesses at all points in the patch was taken as the patch thickness $\mathbf{t_p}$.

### 2.2.5. Milling of Specimen Ends

Although the specimen ends did not need to be exactly perpendicular to the longitudinal axis since the end bearing fixtures compensated for any deviations, the end surfaces had to be perfectly plane. Otherwise, the stresses at the end would be non-uniform and, due to the short length of the specimens (12.5 inches), this may affect the behavior of the corrosion patches. Milling in a lathe was found to be the most reliable method of achieving this.

Figure 2-8 shows the lathe and specimen setup for milling the ends. The lathe head (chuck) held one end of the specimen by expanding the jaws so that they would press against the inside wall of the tube. The free end, however, needed to have something solid at the center so the center lathe support could have something on which to press. A cylindrical wooden block with the diameter slightly smaller than the inside diameter of the specimen was placed inside the tube. The block was held in place by wooden wedges inserted at both ends of the block. Each successive wedge was pushed in slowly and evenly in order to minimize any distortions of the tube. To provide a more stable point for the center support to push against, an aluminum plate was nailed to the wooden block. To find the center of rotation of the block, the aluminum plate was center-punched and placed at the middle point of the center support. The center support was slowly moved closer to the specimen until it came in contact with the block. At this point the plate was nailed into place and milling could begin.

The tool bit (cutter) surface of the lathe was placed as close to parallel to the cross section of the specimen as possible. It was important to avoid milling a conical shape at the ends. Otherwise, the applied load would not be evenly distributed through the specimen wall. The cutter was slowly moved longitudinally toward the specimen end until it just began to remove some steel. If the cutter were advanced too fast, the force on the edge of the specimen might be too high, and the lathe center support could move from its central point. The cutter was gradually advanced until it cut the whole way around the circumference. To ensure that the end did not have a conical shape, the tool bit was moved perpendicularly to the line of rotation without changing the longitudinal position. With one end perfectly flat, the specimen was turned end for end and the procedure repeated.

## 2.3 Instrumentation and Test Setup

Several steps needed to be taken in order to fully prepare the specimens for testing. The strain gages were cemented to the tube surface at specified locations. The bearing fixtures were set up. Then, the dial gages were attached and, finally, the specimen was whitewashed. After these steps were completed, the specimen was ready for testing.

### 2.3.1 Strain Gages and Instrumentation

Strain gages were applied to each specimen to determine the stresses in the specimen and to detect initiation of buckling as the loads were applied. One-eighth-inch gages were placed at the center of each corrosion patch. These gages helped to determine when local buckles started to form. Quarter-inch gages were placed at other locations on specimen to determine the stress distribution over the specimen. The smaller gages were used at the center point of each corrosion patch in order to get a more accurate strain reading. Advantage was taken of the gages still remaining from the source specimen (Fig. 2-1, Specimen P8 [10]), and the additional gages were located in coordination with them.

**Specimen MP1**

Specimen MP1 had a total of ten strain gages: two eighth-inch gages and eight quarter-inch gages. Figure 2-9 shows the location of the gages. The eighth-inch gages were placed in the centers of the corrosion patches. The quarter-inch gages were placed at other locations. Four were two inches from the end (end B) at or near the north, south, east and west reference lines. The last four were placed just below the corrosion patches in line with the four near the end.

### Specimen MP2

Specimen MP2 had three eighth-inch gages and eleven quarter-inch gages. Figure 2-10 shows the layout of the gages on this specimen. Again, the eighth-inch gages were put at the centers of the corrosion patches. Similarly to Specimen MP1, four quarter-inch gages were placed two inches from one end and four just below the corrosion patches. Also, one gage was placed directly above the third corrosion patch. Its distance above the patch was the same as the distance the four gages were placed directly below the other two patches. The last two gages were salvaged gages. They were located about three-quarters of an inch from end B and were slightly offset from the north and south reference lines.

## 2.3.2 Bearing Fixtures

Both tests were conducted with cylindrical bearing fixtures to provide free rotation at the ends. Due to the shortness of the specimens it was necessary to have these end conditions. The cylindrical bearings were selected in favor of spherical bearings because in a previous project the spherical bearings were found not to provide fully free rotation under higher loads, and this resulted in somewhat ambiguous results.[10]

Figure 2-11 shows the setup for cylindrical bearing fixtures. Square steel plates were used to transmit the load evenly to the cylindrical bearing bars. The bearing bars were attached to 2-inch thick circular plates that evenly distributed the loads to the specimen ends.

To assure the square bearing plates had sufficiently high yield strength in order not to get indented by the cylindrical bars, they were tested with a portable hardness tester. The Rockwell B and C scales were used to determine the hardness. Two scales were used for comparison of the results to one another. Table 6-1 shows the results of the hardness tests. Table 6-2 shows an abbreviated listing of steel tensile strengths versus the hardness numbers for typical steels.[14] The averages of the measured hardness numbers in Table 2-1 for both scales (B = 102.4 and C = 26.9) fell somewhat above the values listed in Table 2-2. However, approximately straight-line extrapolations resulted in essentially the same value of $F_u$=127.5 ksi for both scales. Conservatively assuming the yield stress to be 67% of the ultimate strength, the yield stress was estimated to be $F_y$= 85 ksi which was judged to be adequate for the expected column loads (less than 65 kips).

The cylindrical bearing bars were attached with Epoxy to the thick circular plates. These plates needed to be at least two inches thick so that they would not deform and also so that dial gage fixtures would not interfere with the machine base. (In previous tests, thinner plates deformed under the load, and this caused an uneven stress distribution in the specimen ends.[10]) On the other side of the plates, small wooden blocks were Epoxied to the surface as indicated in Fig. 2-12. These blocks and wooden wedges were used to center and hold the specimen in position on the plate.

### 2.3.3 Setup Procedure

Figures 2-11, 2-12 and 2-13 illustrate the setup procedure described here as a series of steps.

**Bottom Square Plate**

The procedure was started by spreading a plastic sheet over the base of the testing machine in the area directly below the machine head. A small pile of Hydrostone* was placed in the middle and covered by a 9×9 square steel plate with a plastic sheet draped over its bottom. The plate was subjected to pressure and some wiggling as Hydrostone was squeezed from under the plate till only a layer of 1/16 to 1/8 on an inch remained.(See Fig. 2-11.) Hydrostone was needed to compensate for any nicks and uneven spots in the contact surfaces. The plastic sheets protected the metal from marring by Hydrostone.

**Bottom Round Plate with Cylindrical Bearing Bar**

The excess Hydrostone was cleaned up, and the bottom 6-inch diameter plate with the attached cylindrical bar positioned over the center of the square plate. The round plate was oriented with the cylindrical bar in the East-West direction and propped from rocking with small pieces of wood. A bubble level was used to make the top surface perfectly horizontal in the North-South direction, that is, perpendicularly to the cylindrical bar.

**Test Specimen on Bottom Round Plate**

After covering the top of the round plate with an aluminum foil, the test specimen was carefully placed on it and centered and secured with wedges against the wooden centering blocks at the

---

* Hydrostone Gypsum Cement, United States Gypsum, Chicago, IL

edges.(Figs. 2-11 and 2-12) The aluminum foil was needed to compensate for any nicks or burrs in the interface between the plate and the end of the specimen.

### Top Round Plate with Cylindrical Bearing Bar

After verifying that the specimen was vertical in the North-South direction and, if necessary, adjusting the props under the round plate, an aluminum foil was placed over the top of the specimen. The second round plate was then put on the top end of the specimen and properly centered. It was oriented to have the cylindrical bearing be in the East-West direction.

### Top Square Plate and Clearance to Machine Head

The top square plate was then put on the cylindrical bar and propped from rocking with pieces of wood against the top of the round plate and adjusted to be horizontal. Then, the machine crosshead was lowered till it almost touched the plate. This was needed in order to determine the point where the plate and the machine head were the closest to each other. This was the point where the distance between the two would be measured in later steps. Then, the head was lifted up to provide room for further work.

### Lowering of Machine Head on Specimen

A sheet of plastic was placed over the square plate, and another one taped to the bottom surface of the machine head. A strip of masking tape was attached around the edge of the square plate to project above it in order to contain Hydrostone that was poured next. Then, the machine head was lowered on top of it. The distance at the closest point between the plate and the machine head was measured with a wooden wedge inserted between them. The head was slowly lowered and then stopped when the gap at that point was about one eighth of an inch. Usually, a small load (about 1 kip) had to be applied to force Hydrostone from under the head. Then, the head was stopped to let Hydrostone set and cure. The purpose of this layer of Hydrostone was not only to fill-in any uneven spots but, mainly, to compensate for practically unavoidable non-parallelism between the surfaces of the square plate and the machine head, for example, due to the fact that, during the milling process, the end sections of the specimen were not enforced to be parallel to each other. In this process, to prevent the squeezed out Hydrostone from splashing over the specimen and the machine base, these were covered with newspaper or plastic that were later removed. Hydrostone had to cure for at least two hours to attain adequate strength. Meanwhile, the last steps of the setup process were completed.

### Connection of Strain Gages

Connection of the strain gages to the data acquisition units was completed, and the system tested out. If necessary, faulty gages were replaced and connections resoldered.

### Whitewashing of Specimen

The specimen was whitewashed except for the strain gages. When yielding occurred, the whitewash popped off and made the areas of yielding much easier to see. After the whitewash dried, a grid pattern was drawn over the corrosion patches with pencil to accentuate buckling deformations.

### Dial Gages

The last step was the installation of four dial gages. The arrangement is shown in Figs 2-12 and 2-13. Two were called the specimen gages (SN and SS) and the other two the machine gages (ME and MW). The second letter in the designations stands for the position (North, South, East and West) with respect to the reference lines. Figure 2-12 shows these locations in plan view. The specimen dial gages were used to determine the shortening of the specimen and the relative rotation of the ends. They were attached to plastic studs that were epoxied to the specimen on the north and south reference lines about an eighth of an inch from the bottom. A thin soft wire was stretched longitudinally to bridge the distance from the gage to the stud at the top end of the specimen. To assure the wire to be straight and have no kinks, it was stretched a little beyond the point of yielding before its final attachment. The wire was kept under tension from the dial gage spring with an additional force from a rubber band that was looped around the shaft and the face of the dial gage.

The machine dial gages were used to determine the motion of the machine head with respect to the base and to check for any relative rotation of the crosshead that could be caused mainly by unequal squeezing of grease in the machine screws. These gages were attached via magnetic fixtures and bridged with thin wire similarly to the specimen gages. Figure 2-13 shows the final test setup for the two specimens, MP1 and MP2.

Once the test setup was completed, the testing began with incremental loading. After the ultimate load was reached, the test continued till the axial deformation was equal to three to four times the deformation at the ultimate load. The failure usually initiated with a local buckle occurring in the corrosion patch. Additional wall deformations developed in the post-ultimate range.

## 2.4 Testing Procedure and Results

### 2.4.1 Testing Procedure

Once the test setup was completed, the testing began by taking the first set of all strain and dial gage readings under the initial load. Then, the readings were taken at 2,000-pound load increments until the readings increased proportionally with each load step. In this range, the test system had to stabilize at each load increment. Then, in the linear range, the readings were taken every 4,000 pounds until the ultimate load was reached.

Load application continued after the ultimate load until the axial deformation was three to four times the deformation at the ultimate load. Then, the machine head was gradually raised and thereby the load slowly reduced in 5,000-pound steps until a load of 1,000 pounds was on the specimen. This load was kept on till instrumentation was disconnected and dismantled.

### 2.4.2 Behavior of Specimens

#### *2.4.2.1 Specimen MP1*

Specimen MP1 was tested first. According to the strain gages in the corrosion patches, local buckling developed in both patches between 26.9 and 30.0 kips. The dial gage readings indicated that the overall specimen buckling started between 52.2 and 54.4 kips. Specimen buckling was determined from the points where the linear loading portion of the curve became non-linear. The ultimate load of the specimen was about 57 kips. Figure 2-14 shows the individual plots of the axial shortening versus load for the four dial gages. Also, the average of the specimen gages for Specimen MP1 is given in Fig. 2-16 together with the curve for Specimen MP2.

It is appropriate to clarify some characteristics of the plots since these curves, similarly to most other experimental load-deformation curves, exhibit certain typical segments.

- At the start, the plot is nonlinear with a gradually increasing slope and decreasing positive curvature. This behavior is caused by such things as the crushing of aluminum foil, the flattening of the bearing plates, the squeezing out of the grease on the screws of the testing machine, motion of the gage attachments caused by the local specimen adjustments to some imperfections at the ends, initial friction in the gages, etc.

- The next portion has an essentially straight-line pattern of linearly elastic deformations and 'small' deflections.
- This is followed by a segment with negative curvature climbing till the curve becomes horizontal at the ultimate load. The deviation from the previous straight segment is indicative of an initiation of local yielding, local buckling and the development of overall column instability.
- The post ultimate segment, with the load gradually decreasing, is terminated by a dramatic drop-off caused by local buckling or overall failure, or by the investigator.
- The unloading segment is usually relatively linear in bigger load steps.
- Since under ideal conditions and in theory, there should be no initial nonlinear segment, it is logical to modify this portion so that the straight-line portion would pass through the origin.
- A linear regression analysis of the data points in the linear segment would give the "zero offset" needed to shift the whole curve to the left.

After such a "zero adjustment" of the curves for the four dial gages of Specimen MP1, the curves fell virtually on top of each other. To separate them for clarity in the same figure, the individual curves were plotted with a constant offset from each other as shown in Fig. 2-14.

#### *2.4.2.2 Specimen MP2*

For Specimen MP2, local buckling in the two lower patches was observed between 19.0 and 23.0 kips. In the third, the higher, patch, local buckling was between 39.0 and 43.0 kips. The overall specimen buckling took place between 47.0 and 51.0 kips. The method for determining buckling was the same as for Specimen MP1. The ultimate load for this specimen was 51.1 kips.

Figure 2-15 shows the load versus axial shortening response of the four dial gages of Specimen MP2.

#### *2.4.2.3 Comparison of Specimens MP1 and MP2*

Figure 2-16 shows the average of the specimen gages for Specimen MP1 and for Specimen MP2. The responses are quite similar except that, as would be expected, Specimen MP2 with three corrosion patches has a lower ultimate load of 51.1 kips than 57.0 of Specimen MP2 with two patches. Also, Specimen MP2 is softer in the linear segment than Specimen MP1.

Thus, the third corrosion patch noticeably reduced the strength of the specimen. The local buckling strength was reduced by 29%, and the overall specimen buckling and ultimate strengths were reduced by 10%.

# 3. FINITE ELEMENT ANALYSIS

## 3.1 Introduction

Finite element analysis is a convenient and accurate method for generating a database needed for conducting parametric studies of the effect of various parameters on the ultimate strength of patch-corrosion damaged tubular columns. The method is very time and cost effective in comparison with testing physical specimens.

The principal objective of finite element analysis was to determine the ultimate axial load and the axial load-deformation relationships of patch-corrosion-damaged tubular columns in the pre- and post-ultimate ranges while including the effects of large deformations and plastification of the material. The finite element analysis program ABAQUS was used.[1] The tests on specimens with corrosion damage simulated by grinding, described in Chapter 2, validated the FE modeling and analysis.

## 3.2 General Description of Finite Element Analysis Procedure

### 3.2.1 Solution Methodology

ABAQUS, the finite element program, generally uses the Newton-Raphson method as the numerical technique for solving the nonlinear equilibrium equations. For a regular nonlinear analysis a load step is split into a number of increments that can be defined by the user. For regular large-deformation analysis, the program finds the static equilibrium at the end of each new increment by iteration. The program fully controls the load incrementation and convergence. It can reduce the increments to very small values when extremely large geometrical changes are taking place. However, the analysis stops if a reverse curvature is sensed because the procedure can handle only positive increments.

In order to overcome this limitation, it is necessary to employ the modified RIKS method (the "arc-length method" provided in ABAQUS) for handling reversal of displacements. In this method, the increment size limitation is made by moving a given distance along the tangent line to the current solution point and then searching for the equilibrium in the plane which passes through this point and is orthogonal to the tangent line. For bifurcation problems and larger suggested increment sizes, this method is very useful since it can change the sign of the displacements to negative. Specifically, the method was found to be very convenient in analyzing long columns.

### 3.2.2 Loading

The load was applied to the finite element model by introducing a displacement of the node at the center of the top of the column as shown in Fig. 3-1. The loading point was subjected to incremental displacements to obtain the load-deflection curve.

The loading point, the central node at the top of the column, was analytically connected to the end nodes of the shell elements to provide the required pinned or fixed end conditions. For pinned end conditions, displacements of the nodes at the end of the column were all in the same plane, which was controlled by the vertical displacement and rotation of the central node about the x- and y-axes. For fixed-end models, all the nodes around the end were constrained to displace the same amount as the central node without any rotations.

### 3.2.3 Material Properties

The material for most of the cases was assumed to be the same as in the test specimens:

| | |
|---|---|
| Modulus of Elasticity, | $E = 29{,}500$ ksi |
| Poisson's Ratio, | $\nu = 0.3$ |
| Yield Stress, | $F_y = 42.11$ ksi |

However, the yield stress of the material was varied for some of the specimens to study its effect on ultimate capacity as described in Section 6.4. The strain-stress relationship was assumed to be bi-linear elastic-plastic without strain hardening.

## 3.3 Finite Element Models

Several discretization models were used depending on the column length, the number and position of the corrosion patches and on the type of end conditions. The mid-length portion, which had the corrosion patches, had the same overall dimensions as the test specimens described in

Chapter 2 (D=5.5 in., $\ell$=12.5 in., t=0.122 in.) and was modeled using shell elements. The portions to both sides of the middle portion were modeled using beam elements. In addition, the fixed-end columns had short shell-modeled segments to accommodate potential local buckling. In all cases, the "Constant-Thickness Patch" model, described in Sections 1.2.2.3 and 2.2, was used.

### 3.3.1 Modeling of Stub-Columns

As stated above, the mid-length damaged portions of tubular columns were discretized with shell elements. Some of the specimens had the same length as these portions, and they were designated as "Stub-Columns". The shell elements allowed plastification to spread and vary through the thickness and over the area of the element. 9-node thin shell elements with 5 degrees of freedom per node (S9R5) were used. As shown in Fig. 3-2, the nodes were defined at the mid-thickness only, and four integration points were generated by the program to perform the stress-strain calculations.

The mesh was refined in the corrosion patch areas, and a transition mesh was introduced between the patches and the tube. The undamaged portion of the tube was modeled with coarser elements to save computational effort. A typical element size was chosen to be square-like with an aspect ratio of approximately 1.0. The nodal points of the mesh were generatated in cylindrical coordinates (r, θ, z), and then mapped to the global (X, Y, Z) coordinate system.

The following modeling scheme, illustrated here for a one-patch half-tube model, was used for all the stub-columns. As shown in Fig. 3-3a, the surface was modeled with a coarse mesh, leaving a window at the location of the corrosion patch. Then, the patches were introduced in the model at the desired locations by modifying the node coordinates, as shown in Fig. 3-3b. The transition mesh, which has the elements of the same thickness as the elements of the original undamaged tube, was filled in as shown in Fig. 3-3c. For multi-patch models, the transition mesh was generated in such a way that it could reshape itself automatically when the patches were moved apart from each other. Considerable effort was needed to establish such an auto-adjustable transition mesh system. One of the main concerns was to keep the relative size ratios (aspect ratios) of the elements smaller than 2.0 since, especially for large deformation analysis, the aspect ratio plays an important role in obtaining accurate results.

As shown in Fig. 3-2, two small elements were connected to a bigger one. A standard method for mesh refinement of second-order elements was achieved by making use of the quadratic type Multi-Point Constraint (MPC), which constrains each degree of freedom at node p (where p is either p1 or p2) to be interpolated quadrically from the corresponding degrees of freedom at nodes a,b and c.

### 3.3.2 Modeling of Corrosion Patch

The discretization of a typical corrosion patch is shown in Fig. 3-4. Four rows of shell elements were used in both the longitudinal and circumferential sinusoidal transitions so that a constant-thickness could be used for each row of elements. By modeling this way, the corner nodes of each row of elements were located directly on the sinusoidally curved line, as shown in Fig. 3-5. The nodes between the two nodes at the corners fell on a curved line connecting the two. Thereby, the transition elements formed same-thickness approximations to the gradual thickness variation. The thickness of each row of elements was specified to be the average of the actual thickness at the node locations along the sides of the row. Four rows of elements were used in the constant-thickness portion, and they all had the same thickness $\mathbf{t_p}$ as shown in Figure 3-4.

During modeling, the nodes and elements on one half of the patch were defined and then copied to the other half to create the full patches. This was done by using the special *NCOPY and *ELCOPY commands of ABAQUS.

### 3.3.3 Naming of Specimens

Names (labels) of FE specimens/models were constructed to provide information about the following five principal parameters (within six spaces) for each specimen:

1) Number of corrosion patches (one space): 1, 2 or 3.
2) Length of the specimen designated by a letter (one space):

| | |
|---|---|
| T (for **ST**ub-column), | $\ell$ =12.5 in. |
| S (for **S**hort), | $\ell$ =90 in. |
| M (for **M**edian), | $\ell$ =136 in. |
| I (for **I**ntermediate), | $\ell$ =168 in. |
| L (for **L**ong), | $\ell$ =200 in. |

3) Circumferential spread **g** between patches in inches, designated by the first digit of the value (or by the first digit after rounding), (one space).

4) Longitudinal spacing **s** in inches was designated by the first two digits of the value (two spaces). To indicate a large spacing such that there would be no interaction between patches, '99' was used for s=9.9 in. (essentially, Infinity).

5) End support conditions designated by one letter (one space): **F**ixed or **P**inned.

When the name was used for a group of specimens with one parameter varying in value, an asterisk (*) would be used in its place. For example, 3M5**F stands for a specimen with 3 patches, $\ell$=136 in.(**M**edian), **g=5**.36 in., <u>a range</u> of **s** values (**), and fixed ends (**F**).

Other information about a specimen was either the same for all (or most) of the specimens or provided in the 7th and/or 8th space in the name, as described next.

The tube diameter (D=5.5 in.) and the original wall thickness (t=0.122 in.) were the same for all FE specimens/models and were not included in the name.

The patch thickness $\mathbf{t_p}$ was the same in essentially all specimens. The seventh space in the name was reserved for indicating the value when it was different from the common $\mathbf{t_p}$=0.03 in. The first significant digit of $\mathbf{t_p}$ in inches was used for this purpose, that is, '2' for $\mathbf{t_p}$=0.02 in., '3' for $\mathbf{t_p}$=0.03 in. and '4' for $\mathbf{t_p}$=0.04 in.

The yield stress $F_y$ was the same in essentially all specimens. The eighth space in the name was used for indicating the value when $F_y$ was different from the common $F_y$=42.12 ksi. The first digit of the value was used for this purpose, that is, '3' for $F_y$=36 ksi, '5' for $F_y$=50 ksi and '7' for $F_y$=75 ksi.

Some specimens had a non-zero load eccentricity e. This was designated with a combination '**e**N' in the 7th and 8th spaces where 'N' was for the first significant digit of **e** in inches, that is, for example, '**e4**' in specimen **2M588e4** means that **e**=0.40 in.

According to the above rules, a specimen with 3 patches, $\ell$=90 in., **g**=3.055 in., s=4.4 in., pinned ends, $\mathbf{t_p}$=0.04, and $F_y$=50 ksi would be named/labeled as **3S344P45**.

A summary of this system of naming specimens and the specific values of respective parameters used in this research are given in Table 3-1.

### 3.3.4 Stub-Columns with One Corrosion Patch

In previous studies, the tubular columns with a single corrosion patch were modeled as a quarter-tube by taking advantage of the double-symmetry in the longitudinal and circumferential directions as shown in Fig. 3-6. [10] To check the accuracy of the previous assumptions made for the quarter-tube models and also in anticipation of expanding the model in this study to two patches, the columns with one patch were analyzed by full-tube modeling as shown in Fig. 3-7. Table 3-2 shows that the difference between these two models is quite small (~2%). Also, the deformation patterns of the specimens and the models were essentially the same as shown in Fig. 3-8. Therefore, it can be concluded that the two models agreed with each other and both can be considered to be equally accurate.

### 3.3.5 Stub-Columns with Two Corrosion Patches

The stub-column specimens ($\ell$=12.5 in.) with two corrosion patches were modeled as full-tube and had the two patches straddle the mid-length point of the column as shown in Fig. 3-9 over the unfolded surface of the specimen. Thus, these specimens had skewed-symmetry with respect to the mid-length of the tube and therefore had to be modeled over the full tube surface.

Figure 3-10 shows the models for two values of circumferential spread, $\mathbf{g}_2$=2.68 and $\mathbf{g}_5$=5.36 inches, and zero longitudinal spacing (s=0.0 in.). Additional examples for different values of longitudinal spacing s are shown in Fig. 3-11. When the patches were moved apart from each other so that there was no interaction between them, the specimen was assumed to have only one patch at the mid-length as shown in Fig. 3-7.

In order to examine the effect of the thickness of the constant-thickness portion, models with $\mathbf{t}_{p2}$=0.02 and $\mathbf{t}_{p4}$=0.04 inches were also modeled for some selected combinations of **g** and **s** as shown in Fig. 3-15.

### 3.3.6 Stub-Columns with Three Corrosion Patch

Due to the single symmetry of the geometry and loading of the specimens with three corrosion patches as shown in Fig. 3-12, only one half of the tubular column had to be modeled. The central point and the displacement and rotations of the ends of the column were handled as described Section 3.2.2. Proper boundary conditions (YSYMM) were imposed along the longitudinal edges of the half tube to simulate the behavior of the whole specimen.

The following four values of **g** distance were studied: $g_1$=1.60, $g_2$=2.68, $g_3$=3.055 and $g_4$=3.384 inches. Figure 3-13 shows the discretization for three of these **g** values and the longitudinal spacing between the middle corrosion patch and the lower two patches of **s**=1.65 in. For **s**=0.00 in., the three patches were aligned in one cross section. In the case of $g_1$=1.60 in. and **s**=0.00 in., the patches overlapped each other to form one long single patch. Figure 3-14 shows the patterns for **s**=1.60 in. and three different values of **g**.

When the longitudinal spacing **s** becomes sufficiently large, the interaction between the patch sets disappears, and the member fails as if it had only two patches (with **s**=0) rather than three (or, for larger **g** values, only one). Such three-patch specimens were designated by "99", that is, as if they had **s**=9.9 in. (essentially, Infinity). The half-tube models of the specimens with three patches, when the middle patch was moved far away and the full-tube models of the specimens with two patches for **s**=0.00 in. are compared in Table 3-3. The small differences between the two modeling techniques verified the accuracy of the two approaches. In analysis, the longitudinal spacing of **s**=4.40 inches was accepted as the maximum value for the specimens with three patches since the middle patch approached the end of the column, and the ultimate capacity showed very slight difference from the specimens with two patches. (This is further discussed in Subsection 6.2.3.)

Determination of the effect of the thickness of the constant-thickness portion of the patch on the ultimate capacity was one of the objectives. Therefore, specimens were also modeled with three different values of $\mathbf{t_p}$, 0.02, 0.03, and 0.04 inches, as shown in Fig. 3-15.

The effect of yield stress on the ultimate capacity was also an objective of the research, and models were modified by changing the yield stress value of the material from the original 42.11 ksi value to 36, 50, or 75 ksi.

### 3.3.7 Long Columns

Since long tubular columns with larger $\ell/r$ ratios than of the stub-columns are the more usual in offshore structures, it was necessary to study the effect of length. The tests have shown that the strength was controlled by the wall distortions only in and in the immediate vicinity of the damaged area and well within the length of the middle portion (stub-column length), with the outside portions behaving essentially as elastic beams with a constant cross section.

Correspondingly, these outside portions were represented by beam elements, which were added at both ends of the damaged tubular portion as shown in Fig. 3-16a. The element type was chosen to be the 2-node hollow pipe section (PIPE31) with the thickness and diameter of the undamaged column. This technique is a common approach in finite element analysis, and it benefits the computational effort. For all column lengths, the beam-column portions were each subdivided into seven elements between the middle shell portion and the ends.

For the pinned-end long specimens, the vertical (axial) displacement was applied to the top end node of the beam-stem portion. For the specimens with two patches, the node was permitted to displace in the vertical direction and rotate about the x- and y-axes, and the bottom node could rotate similarly to the top end, but not displace. Figures 3-16b and 3-16c show the deformed shape of the damaged middle portion of a long specimen with pinned ends.

For the fixed-end specimens, segments with shell elements were introduced at the ends since it was expected that the restraining end moments could cause local buckling of the tube wall as shown in Fig. 3-17a, and the beam elements could not accommodate it. These end portions were approximately equal to 70% of the diameter of the tube and were discretized into five segments of shell elements as shown in Fig. 3-17b. This length was found to be sufficient to accommodate potential local buckling and short enough to minimize computation time. Since local buckling could develop on the side opposite to the location of the corrosion damage, the mesh was further

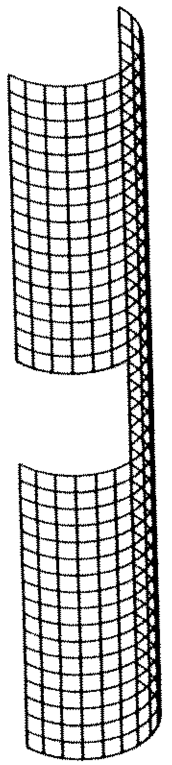

Figure 3-3a: Undamaged Portion

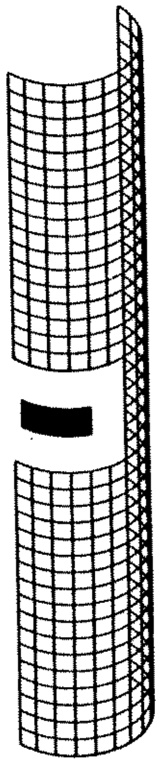

Figure 3-3b: Addition of Corrosion Patch

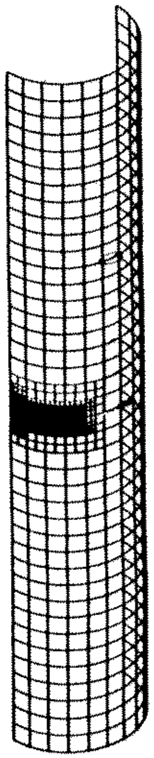

Figure 3-3c: Completed Model

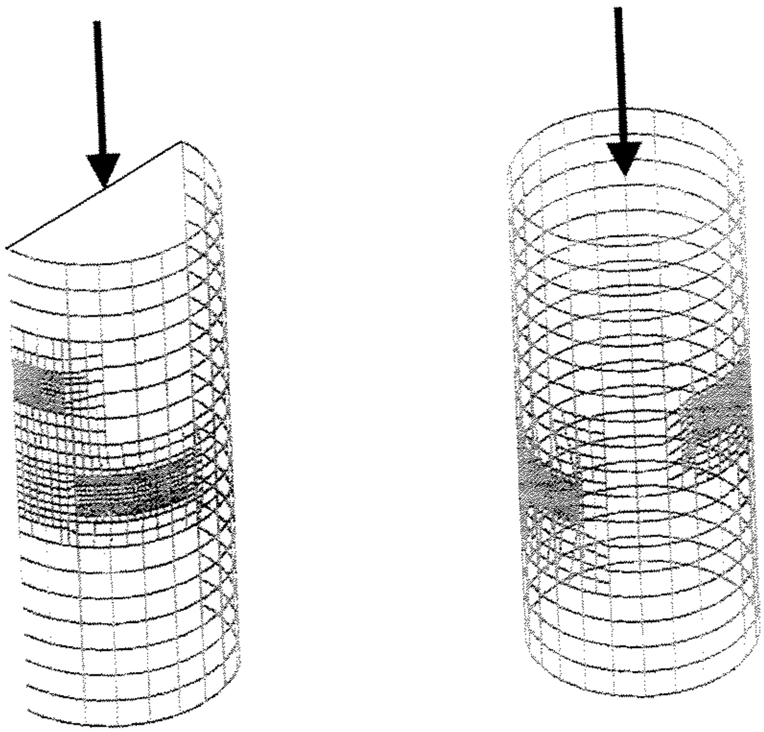

Figure 3-1: Loading of a Typical FE Model for Half-Tube and Full-Tube Models

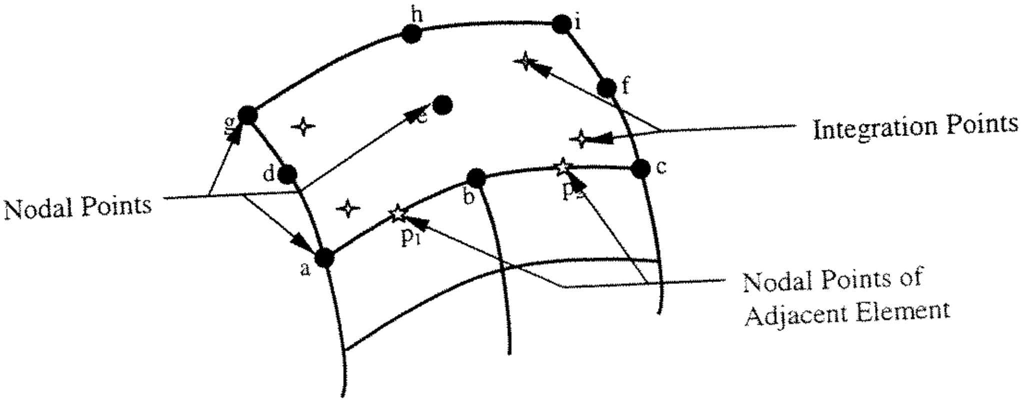

Figure 3-2: A typical 9-node Shell Element and Transition Mesh

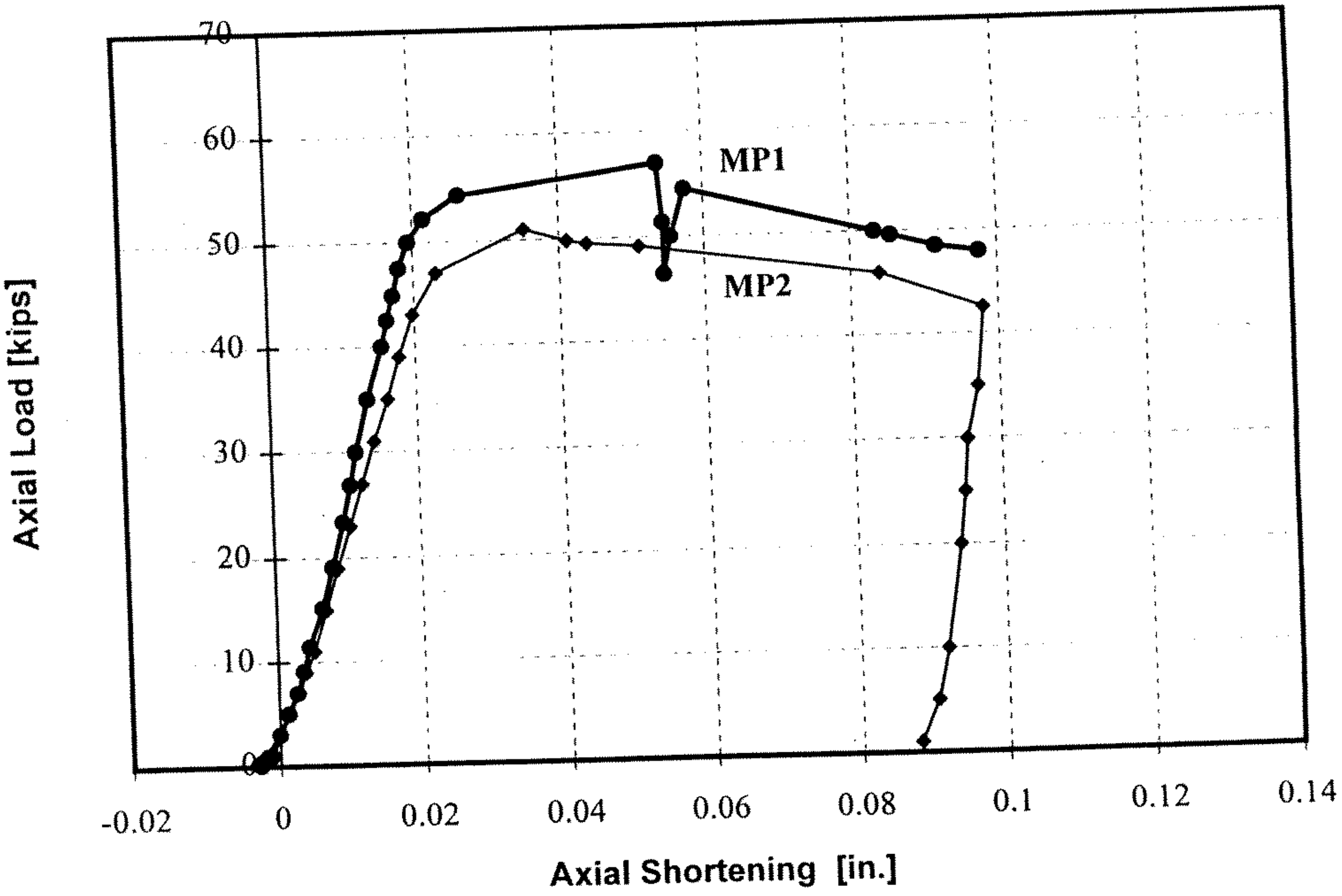

Figure 2-16: Axial Load vs. Axial Shortening Comparison for Test Specimens MP1 and MP2

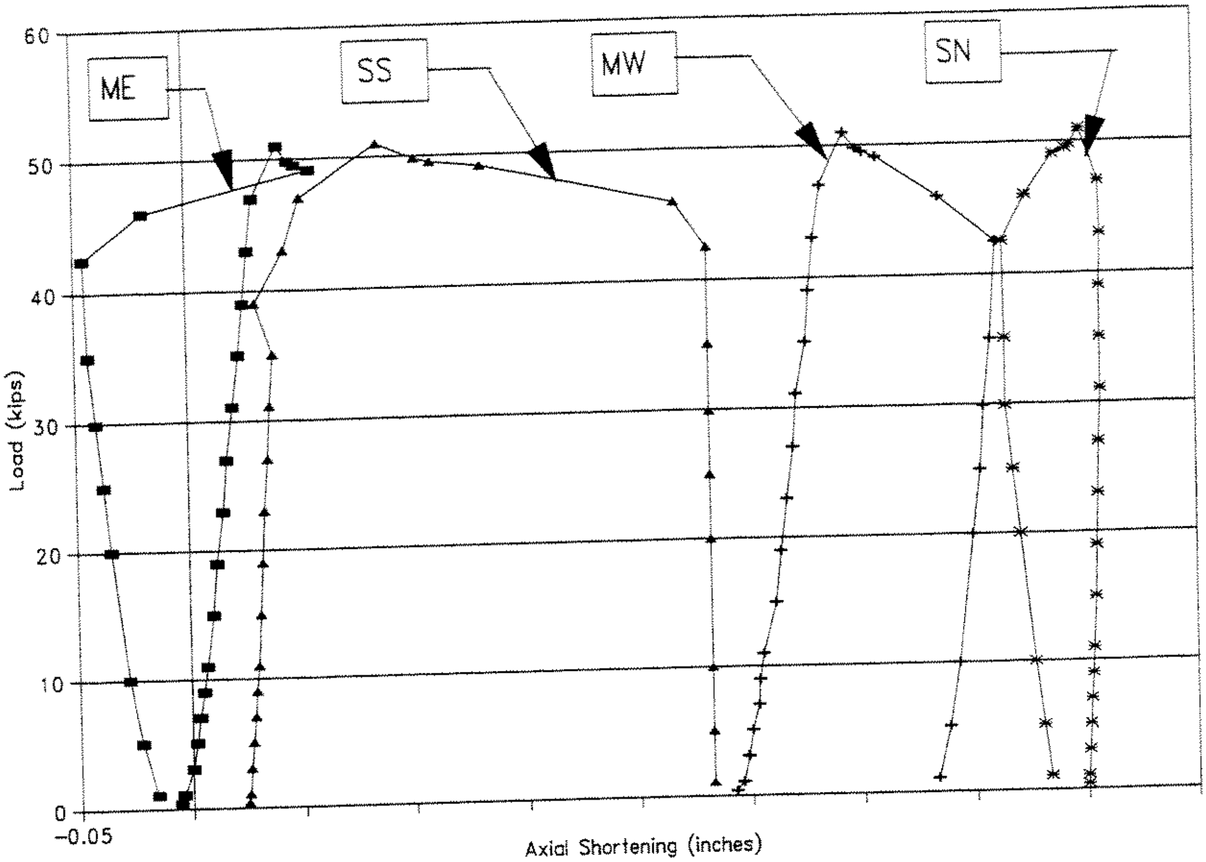

Figure 2-15: Axial Load vs. Axial Shortening for Specimen MP2

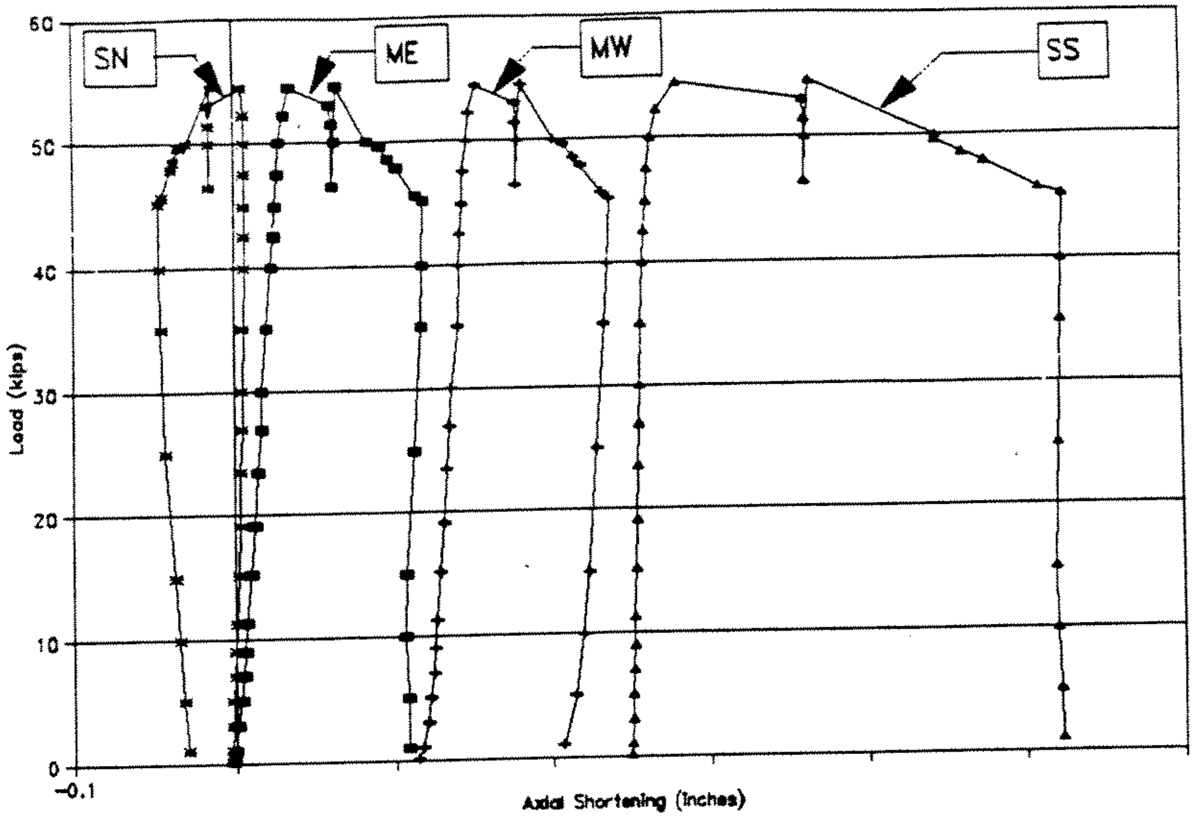

Figure 2-14: Axial Load vs. Axial Shortening for Specimen MP1

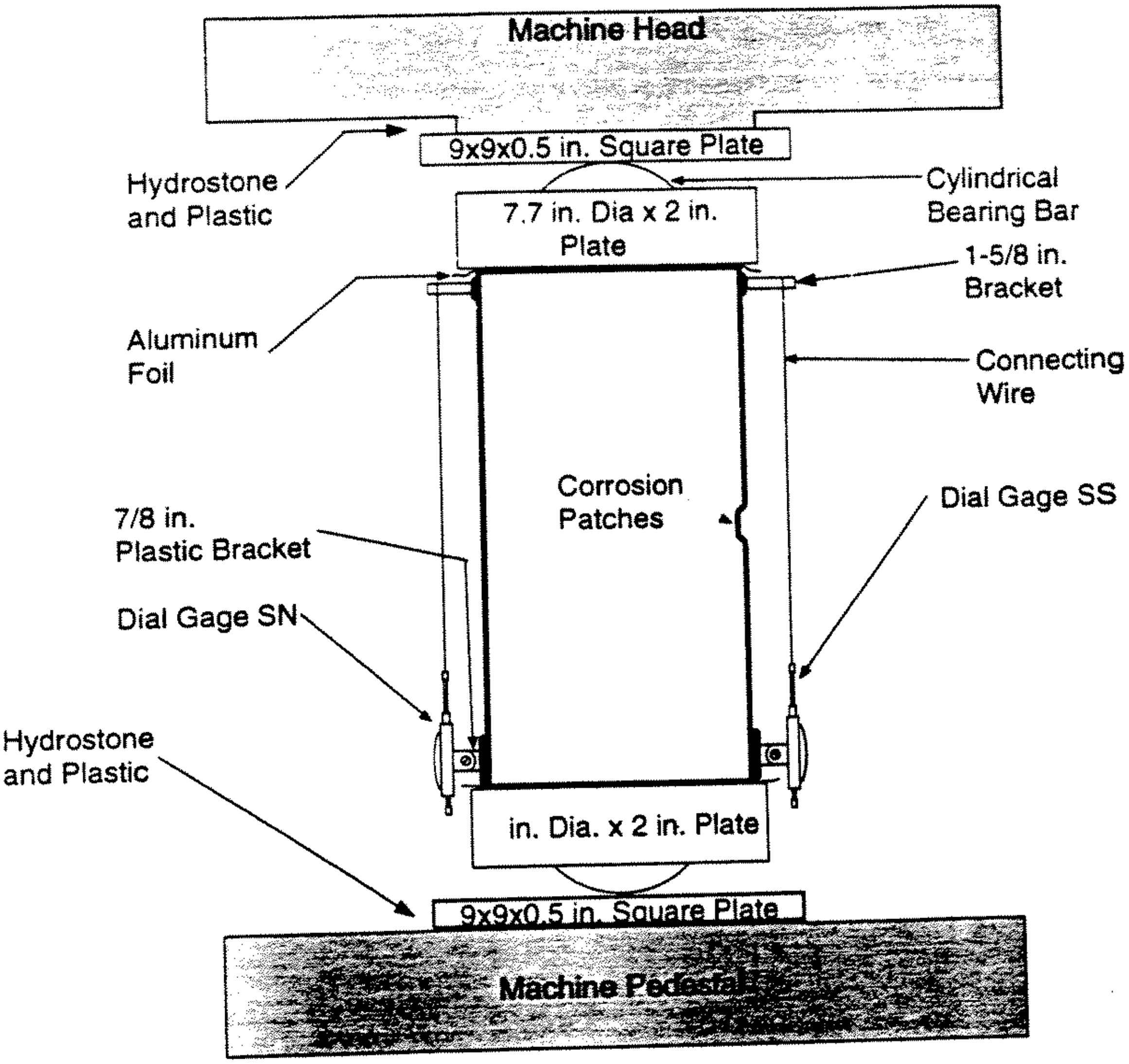

Figure 2-13: Test Setup for Specimens MP1 and MP2
(Cylindrical Bearing Fixtures)

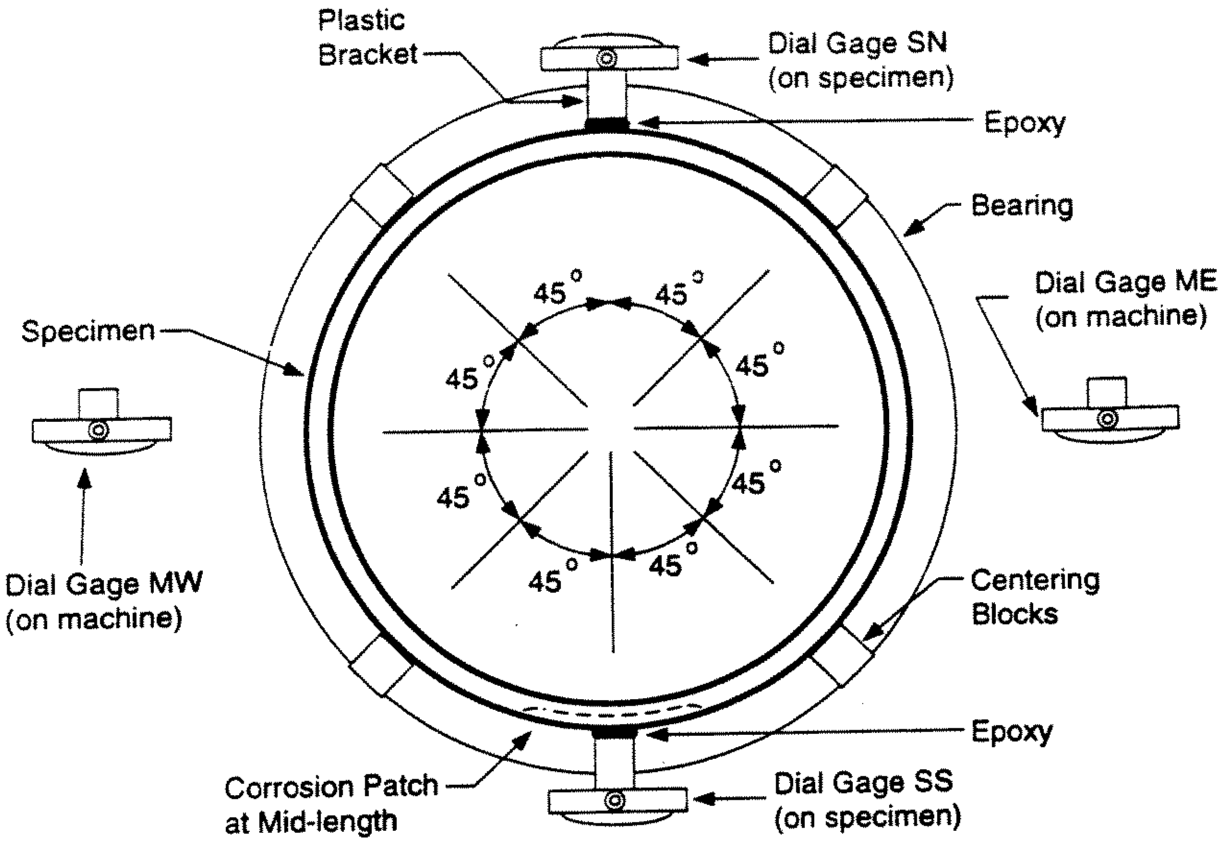

Figure 2-12: Plan View of Dial Gage Arrangement

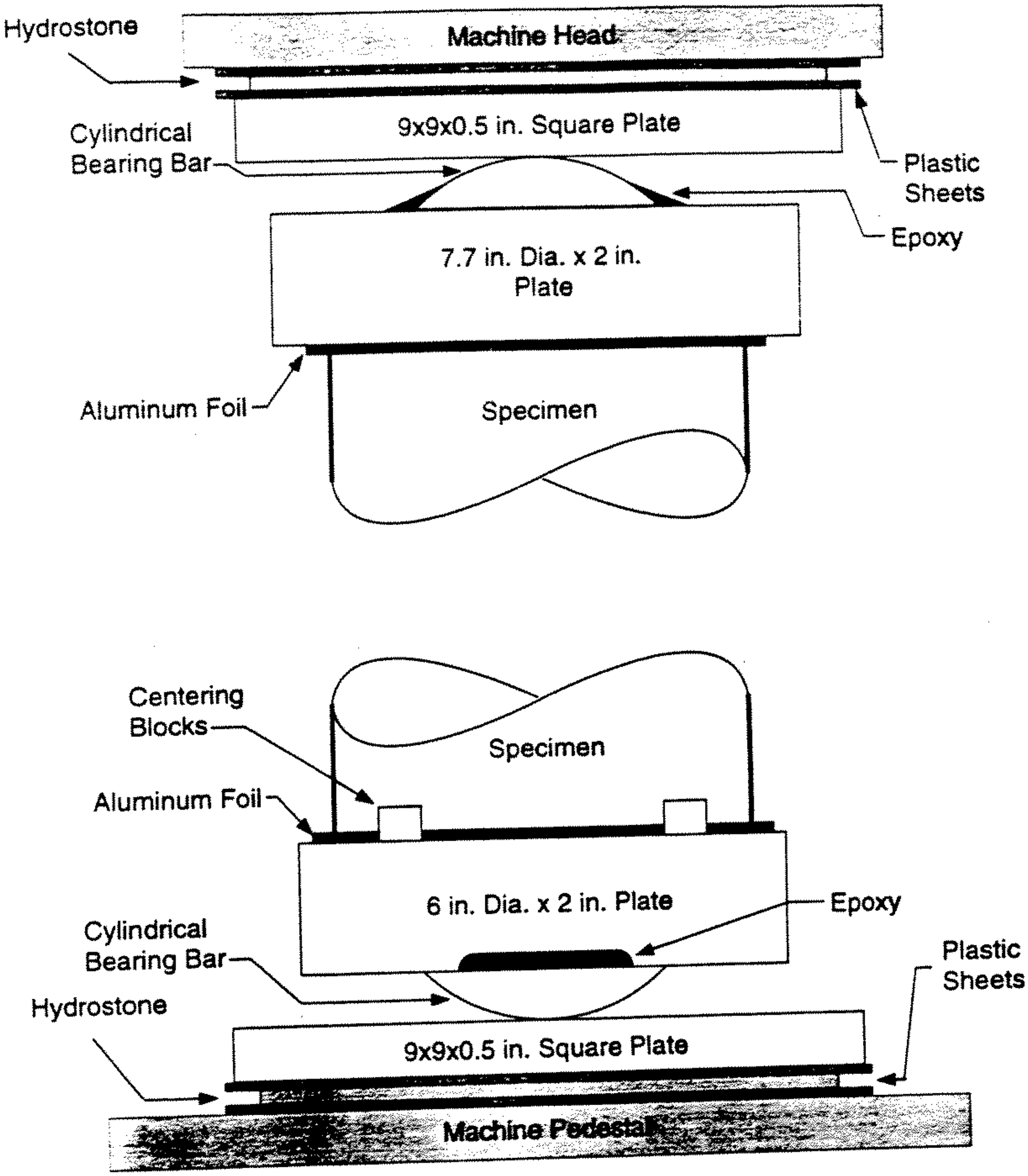

Figure 2-11: Cylindrical Bearing Fixtures

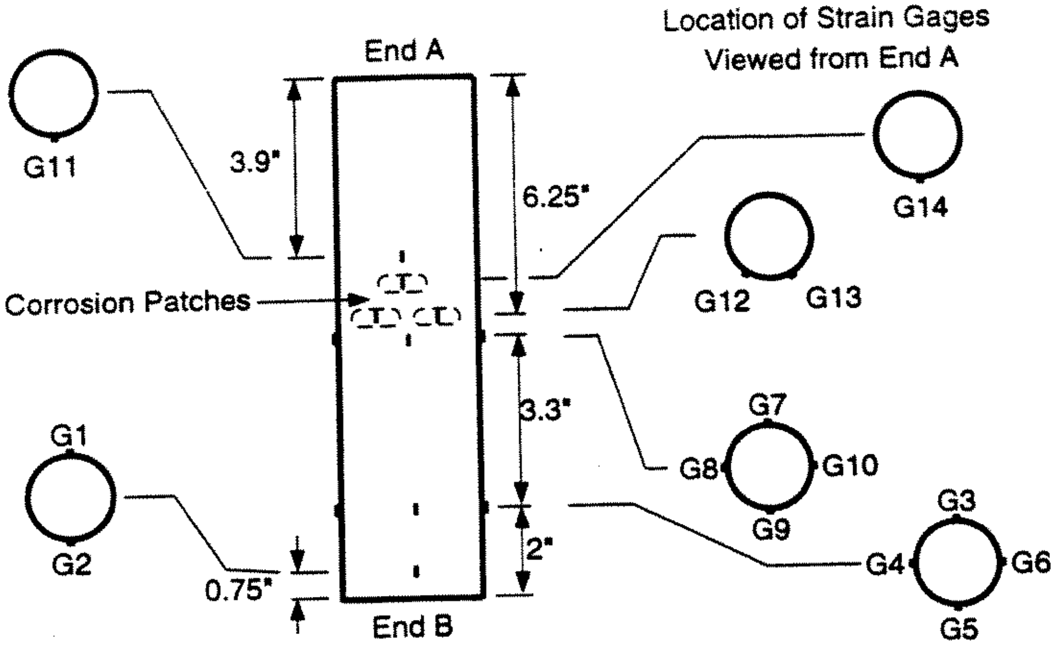

Figure 2-10: Layout of Strain Gages for Specimen MP2

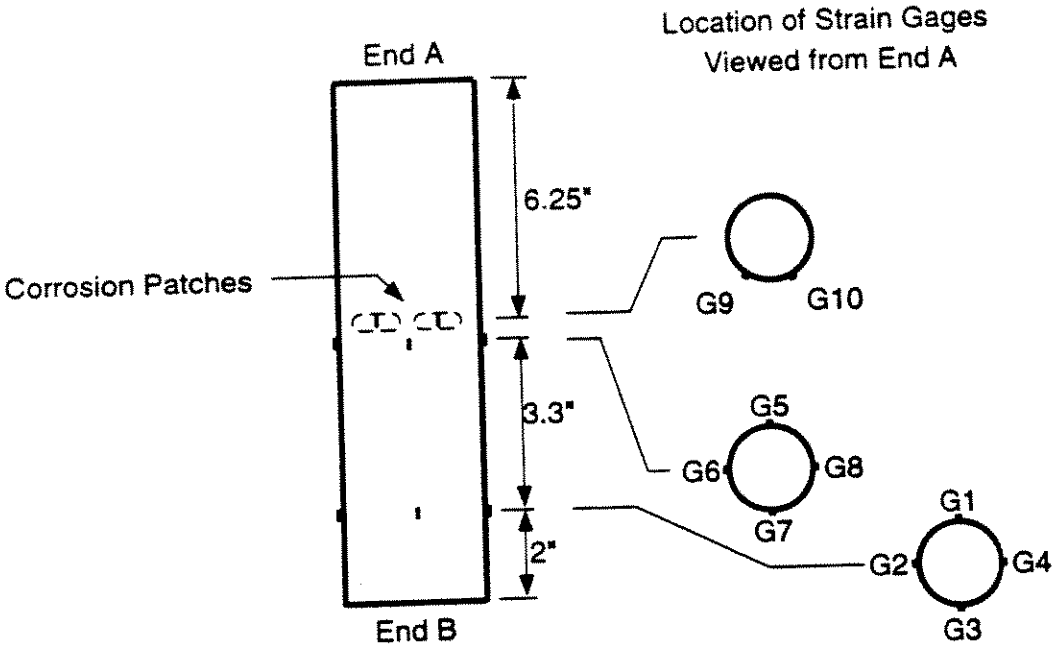

Figure 2-9: Layout of Strain Gages for Specimen MP1

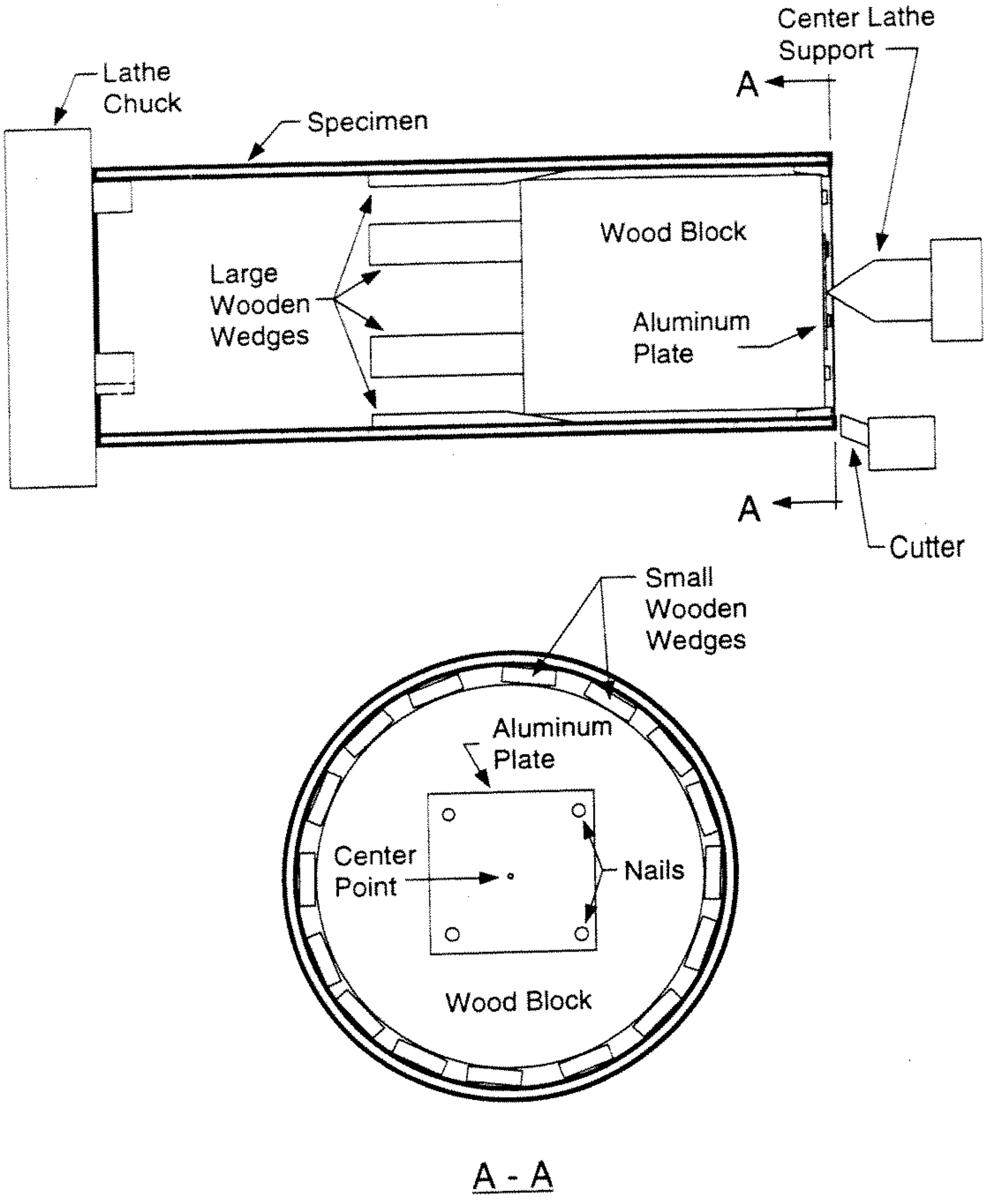

Figure 2-8: Arrangement in Lathe for Milling Specimen Ends

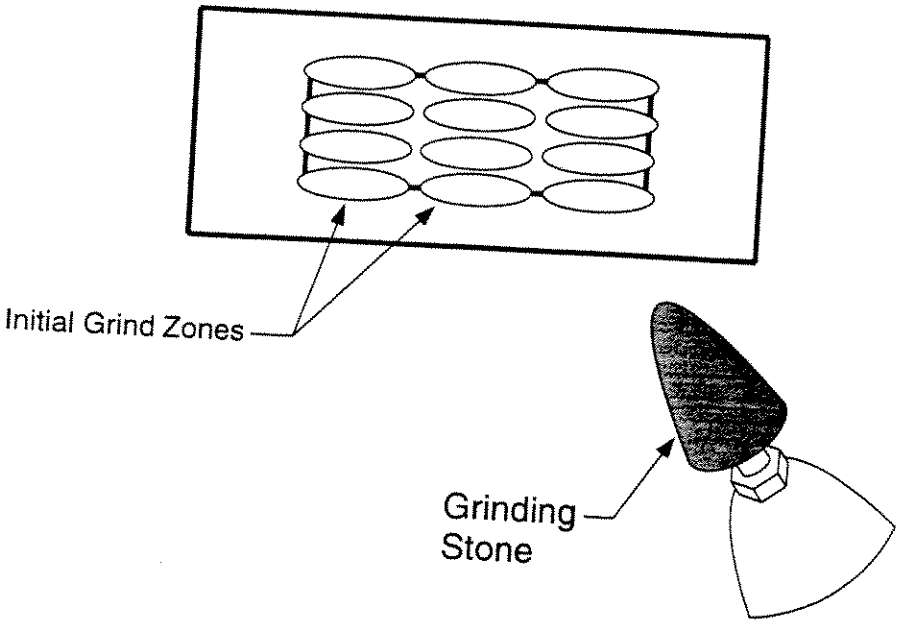

Figure 2-7: Initial Grind Zones and Grinding Stone

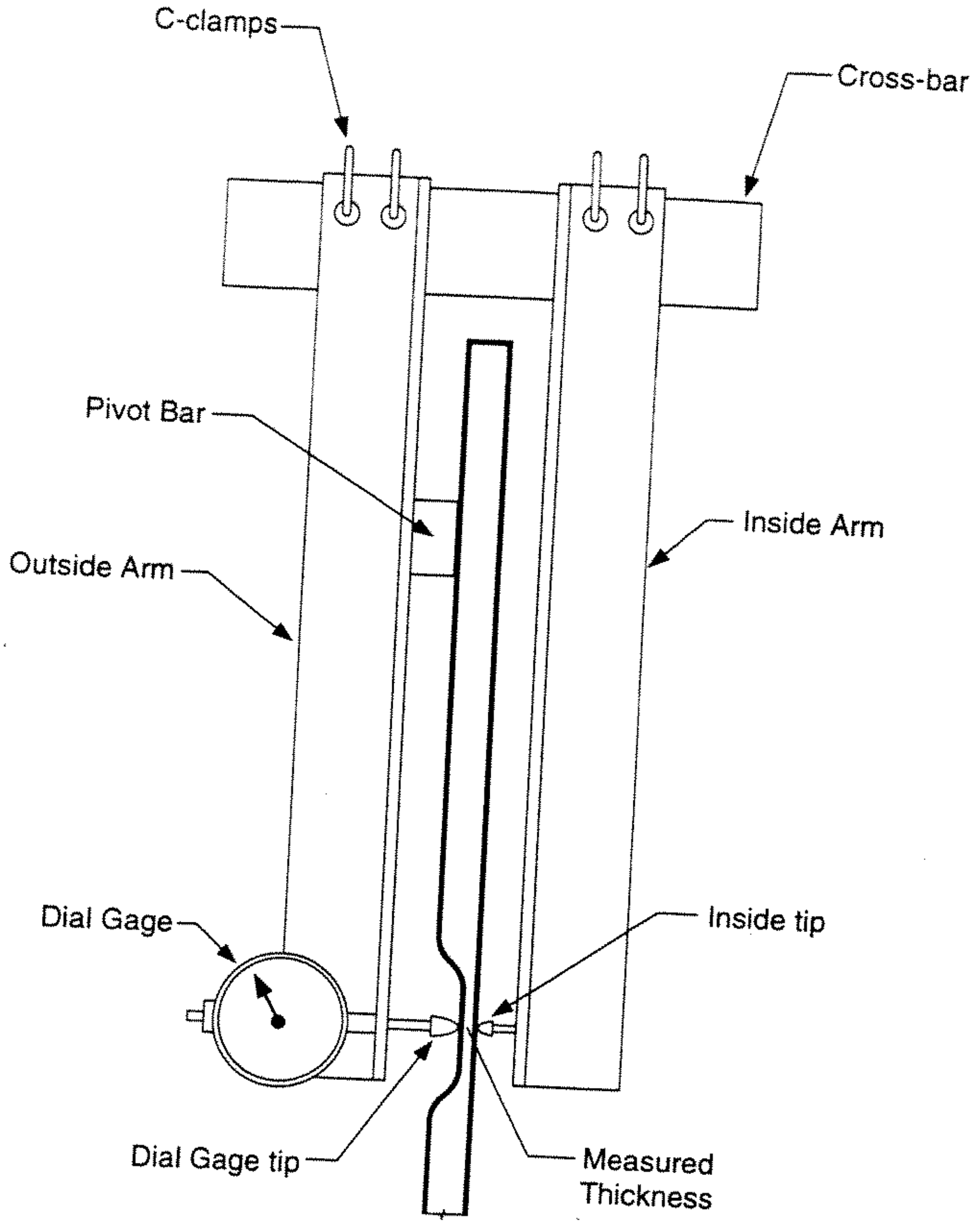

Figure 2-6: Fork Tool

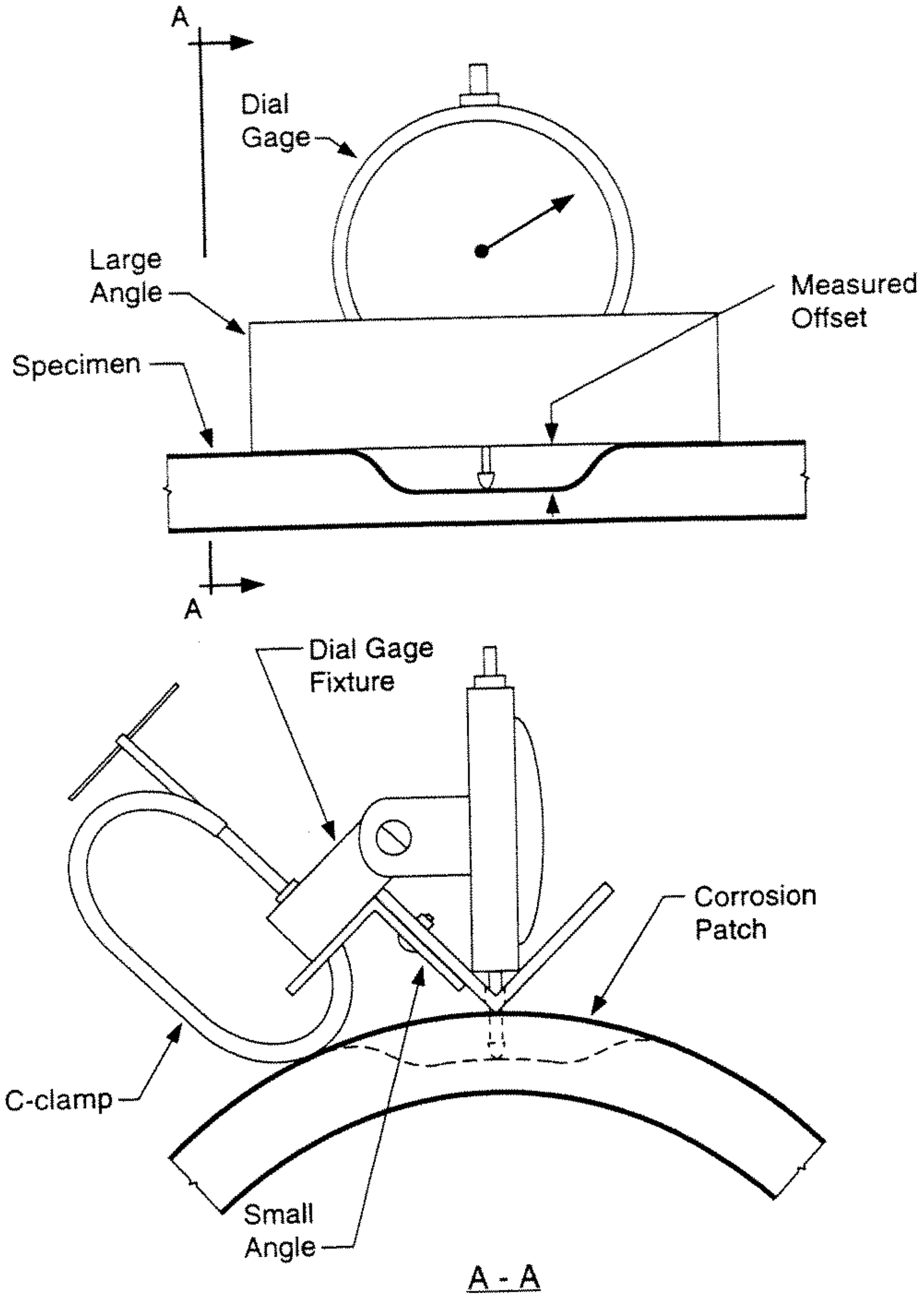

Figure 2-5: Frontal and Cross-Sectional Views of the Angle Tool

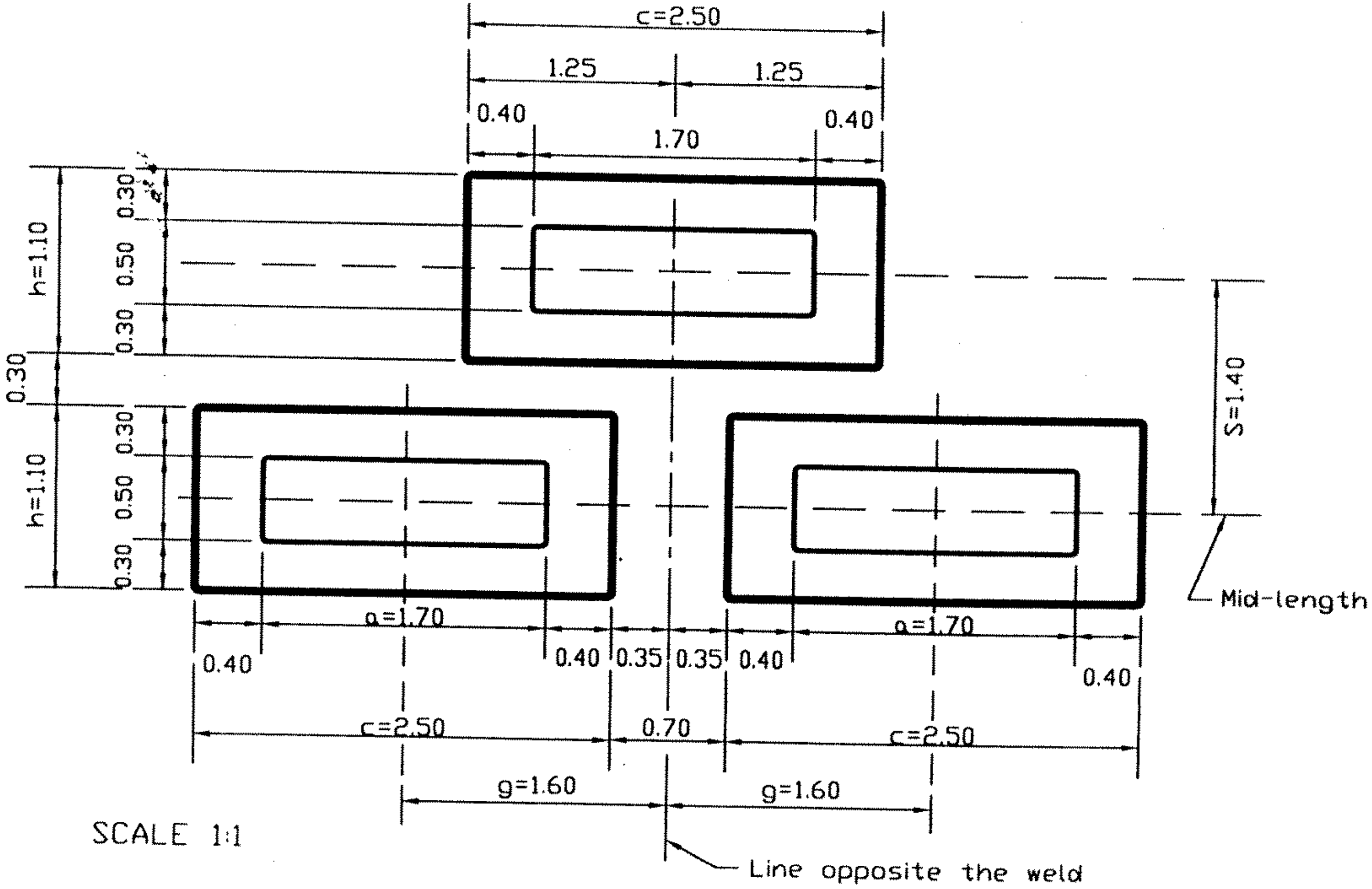

Figure 2-4: Dimensions and Arrangement of Corrosion Patches in Test Specimen MP2

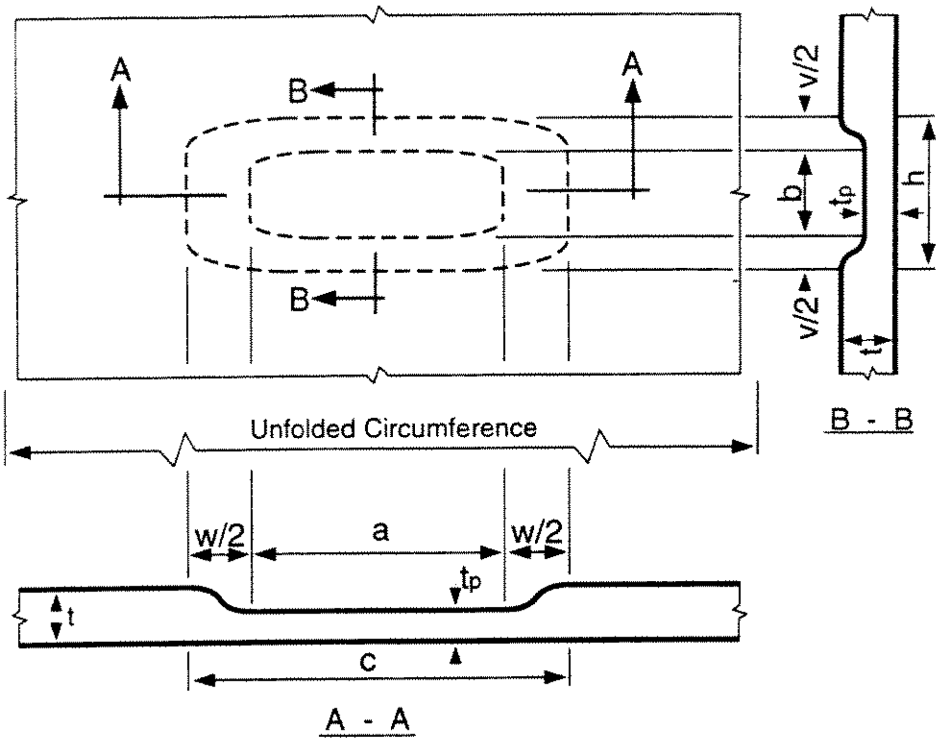

Figure 2-3: Layout of Corrosion Patch and Dimensional Parameters [10]

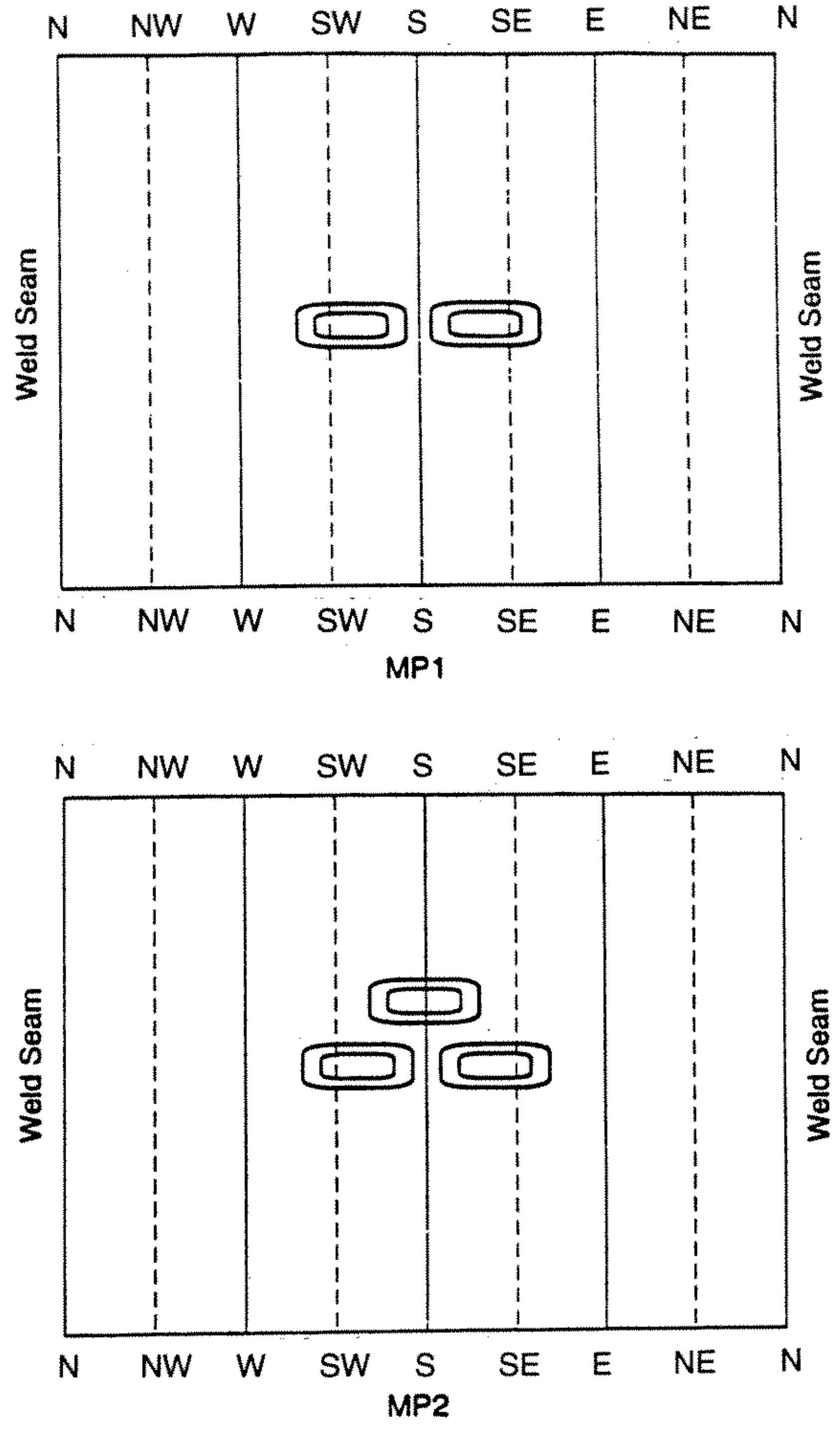

Figure 2-2: Unfolded View of Patch Layout for Test Specimens MP1 and MP2

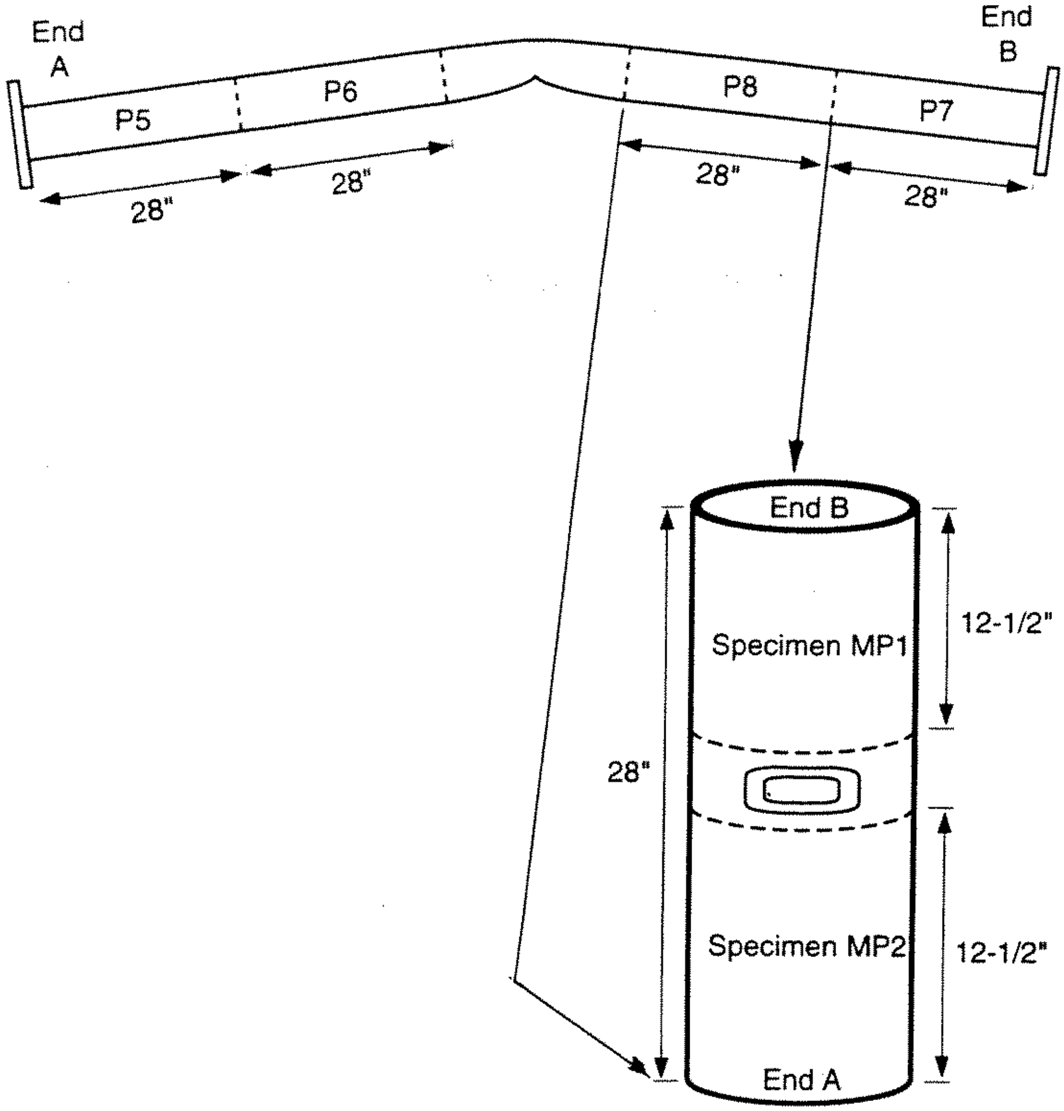

Figure 2-1: Layout of Specimen P8 for Test Specimens MP1 and MP2

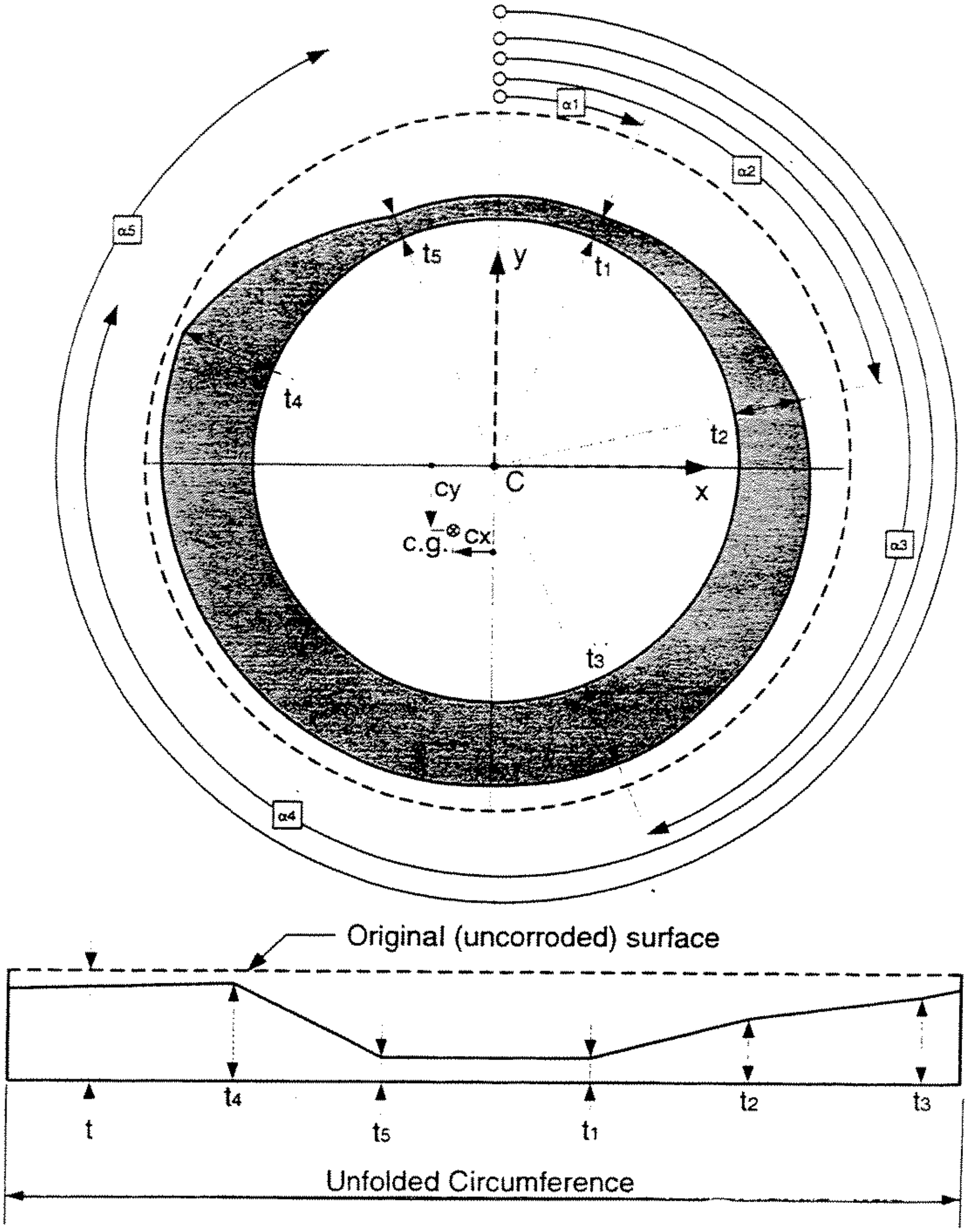

Figure 1-8: "Linear Segments" Model for Approximating Corroded Section [10]

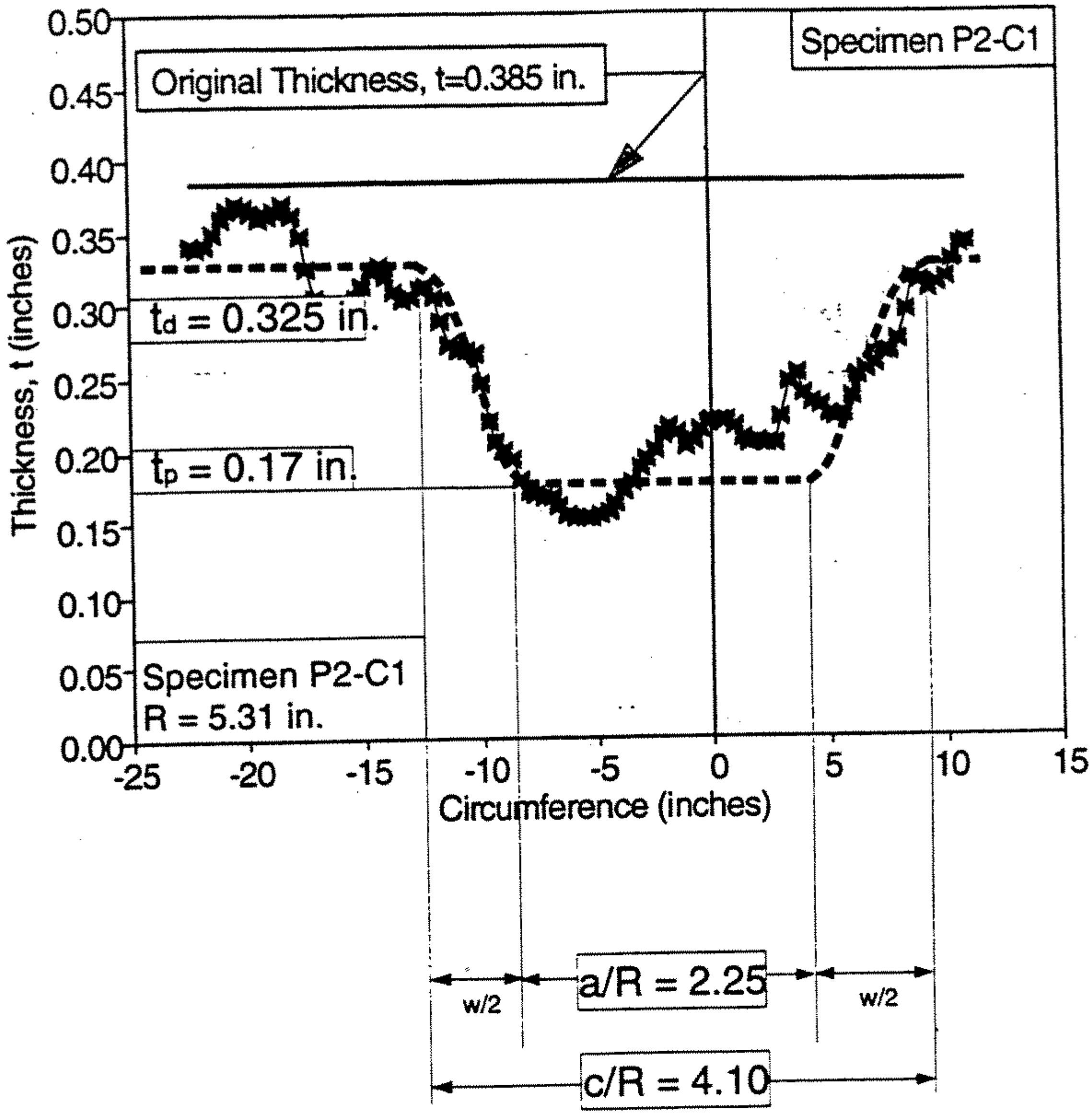

Figure 1-7: "Constant-Thickness Patch" Model of Thickness Variation at Location of Buckle 3 in Fig. 1-2. [10]

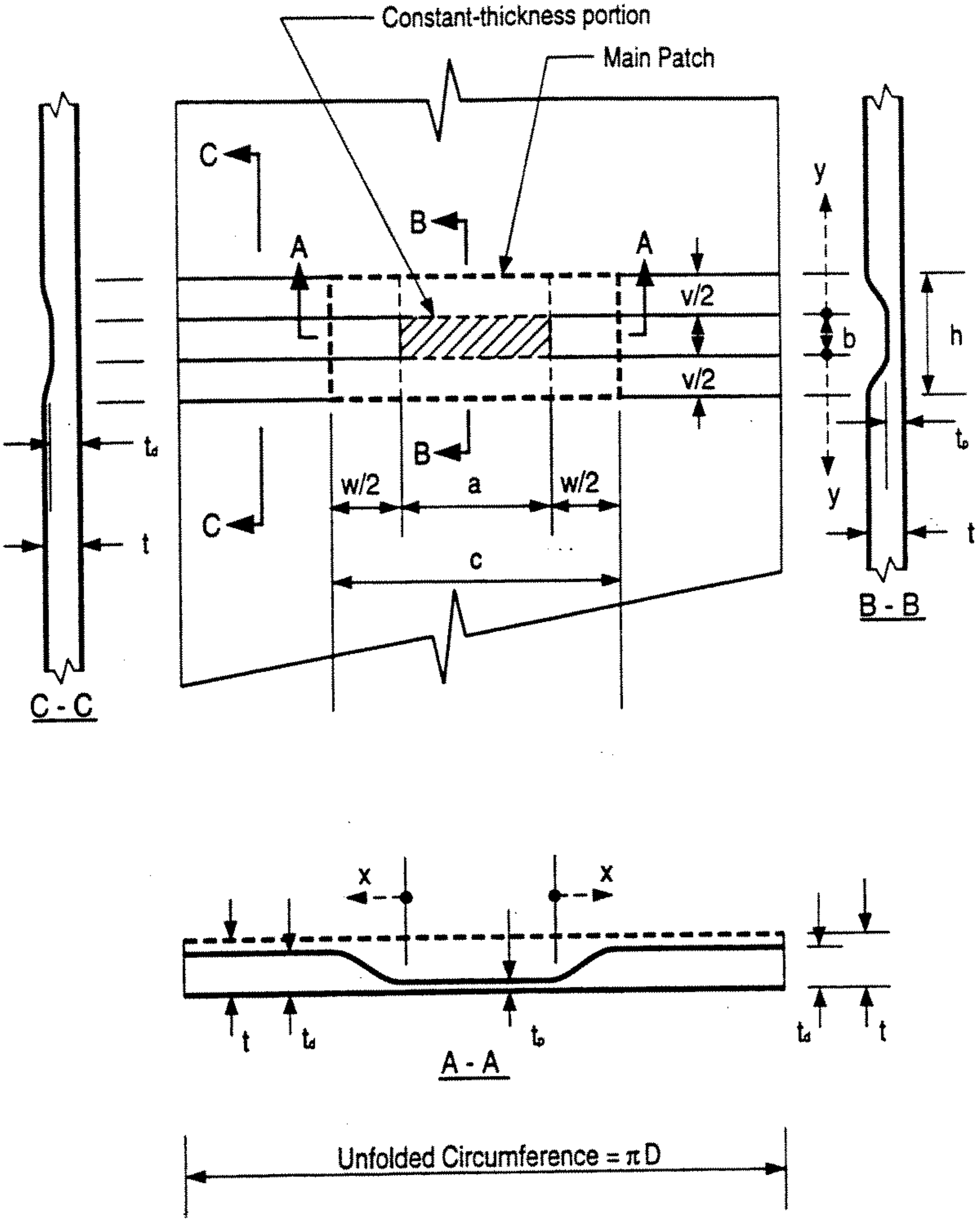

Figure 1-6: "Constant-Thickness Patch" Model of Thickness Variation in Corrosion Patch

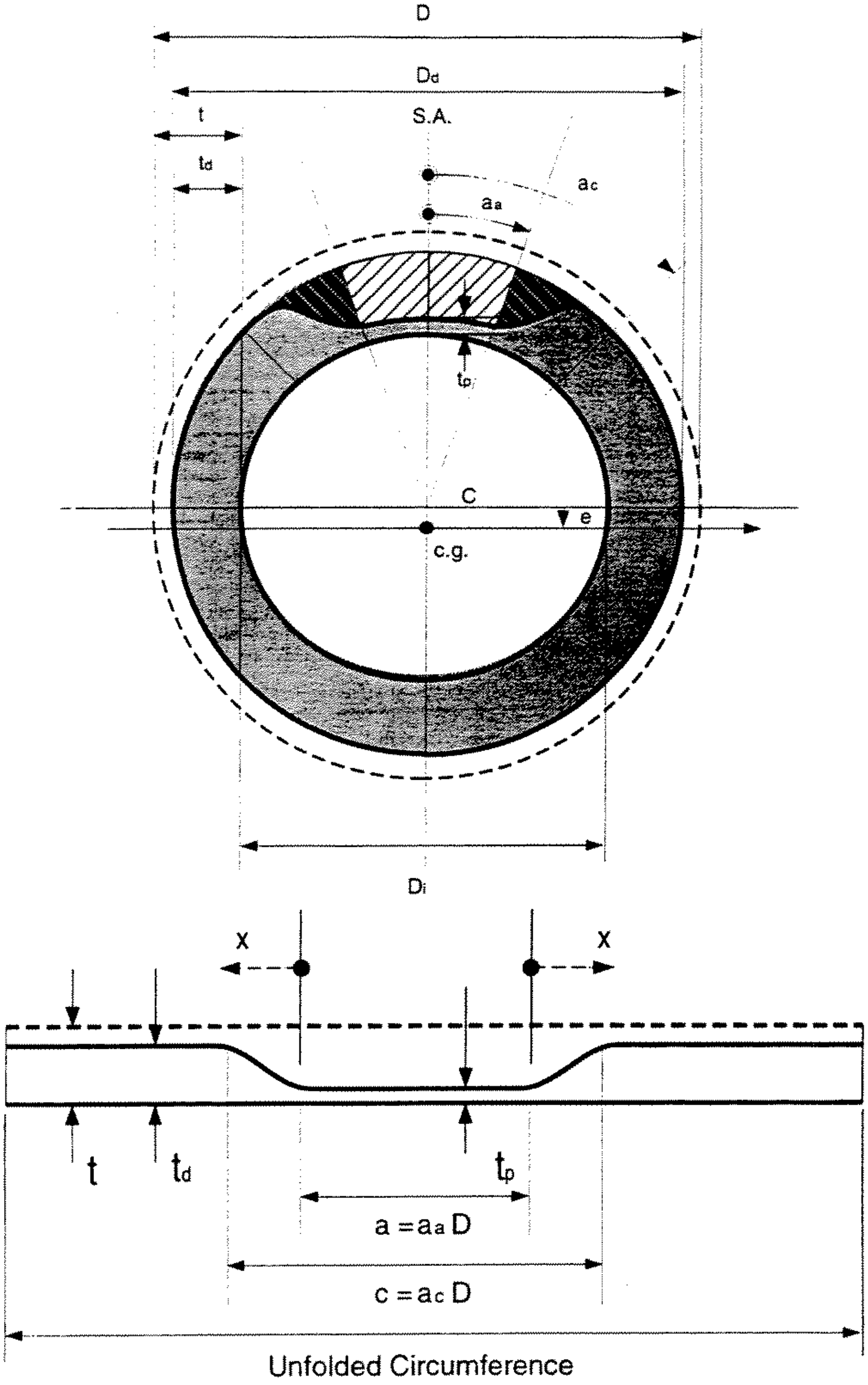

Figure 1-5: "Constant-Thickness Patch" Model of Thickness Variation around Circumference

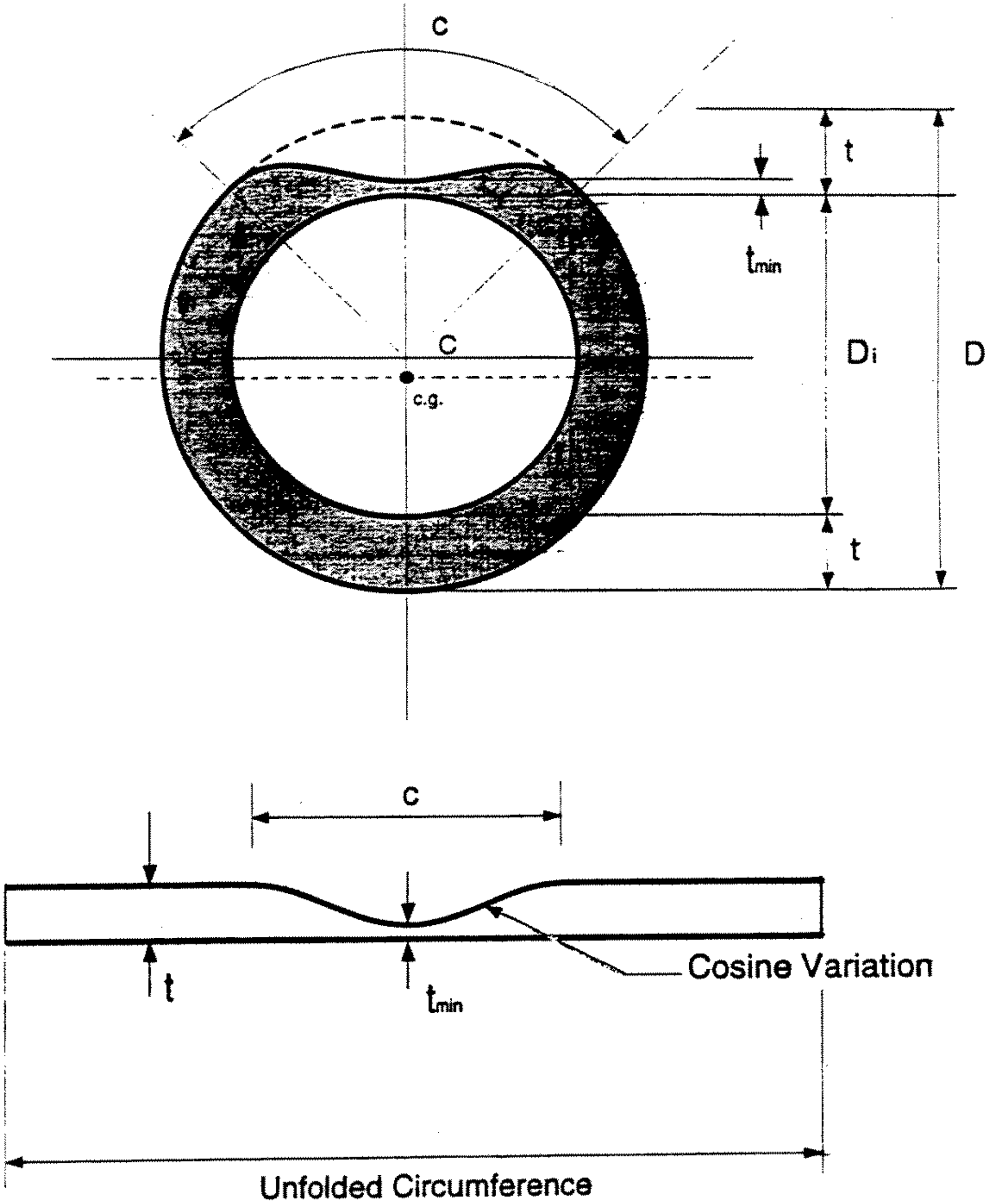

Figure 1-4: "Cosine Patch" Model of Thickness Variation Around Circumference [5,12,13]

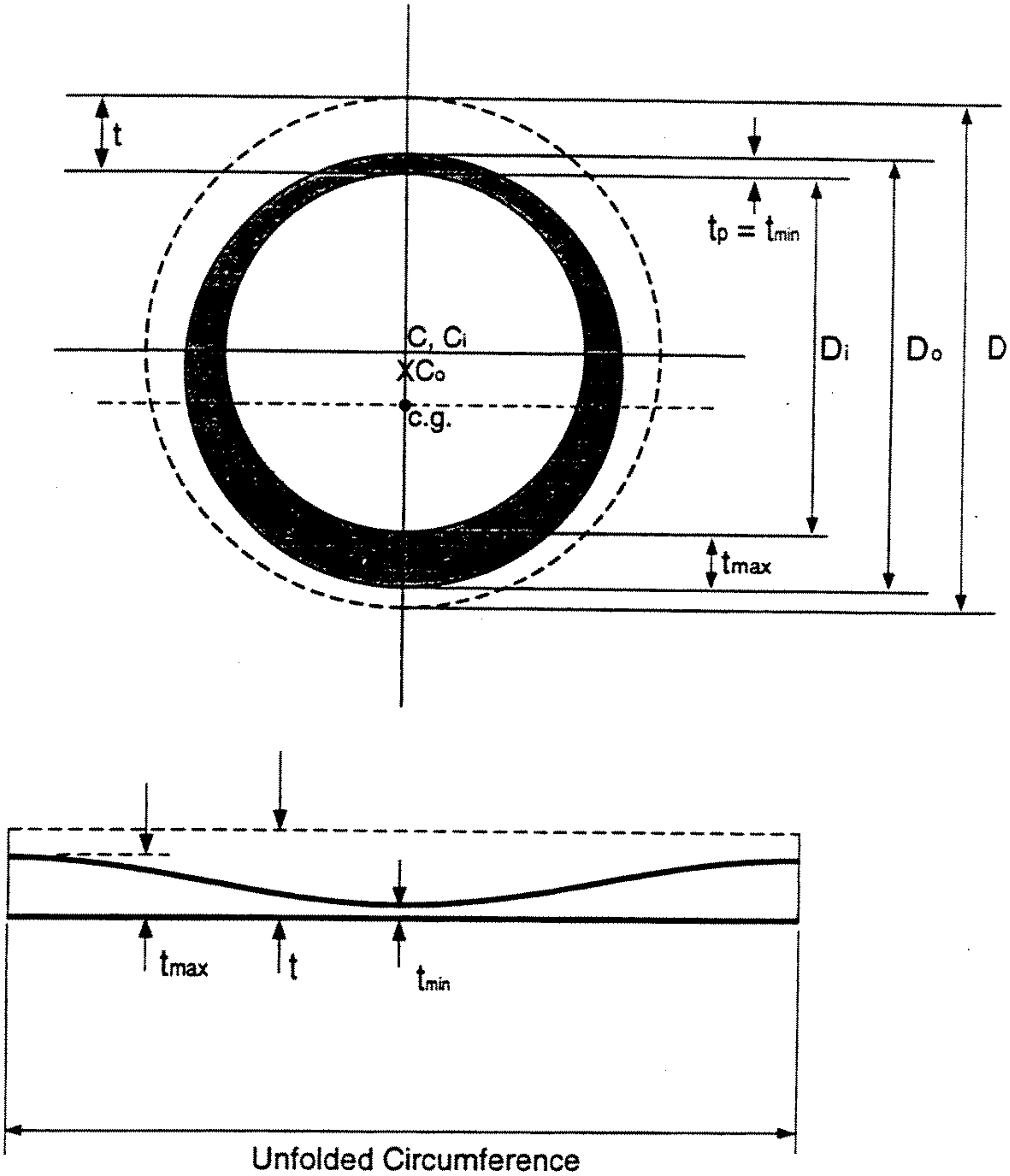

Figure 1-3: “Shifted Circles” Model of Thickness Variation around Circumference

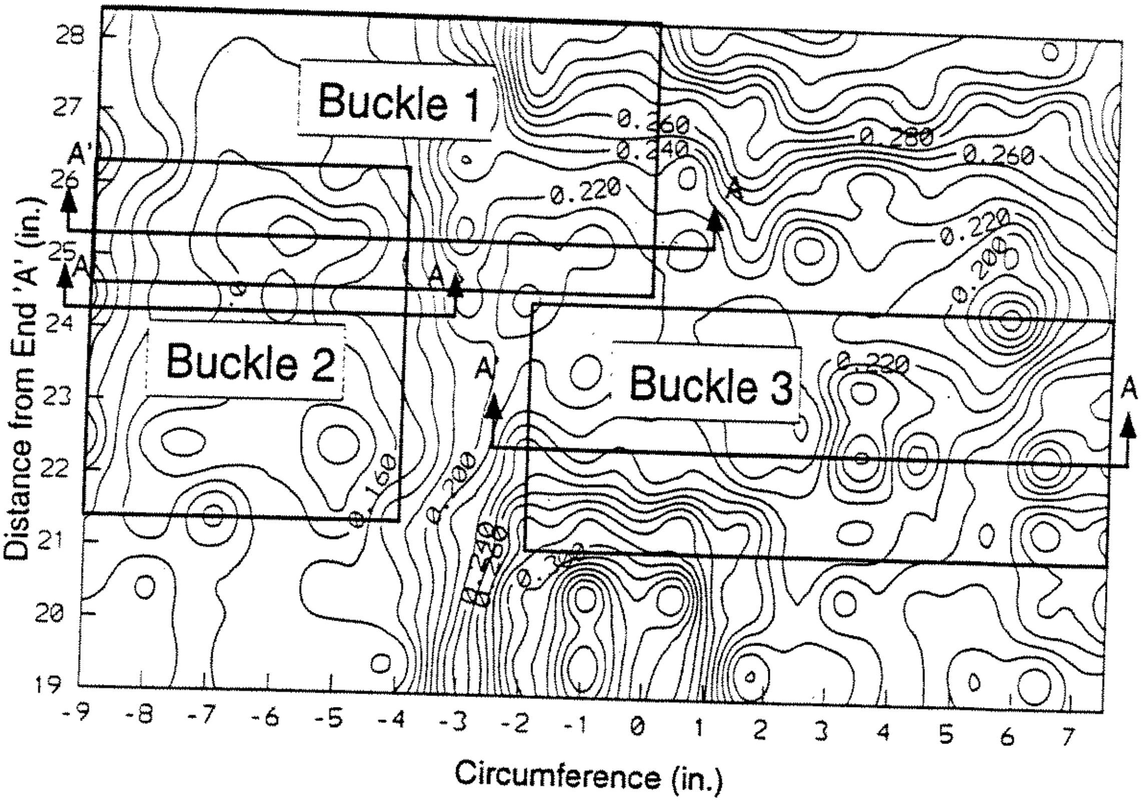

Figure 1-2: A Typical Surface Contour Plot of a Corroded Tube and Location of Possible Buckles

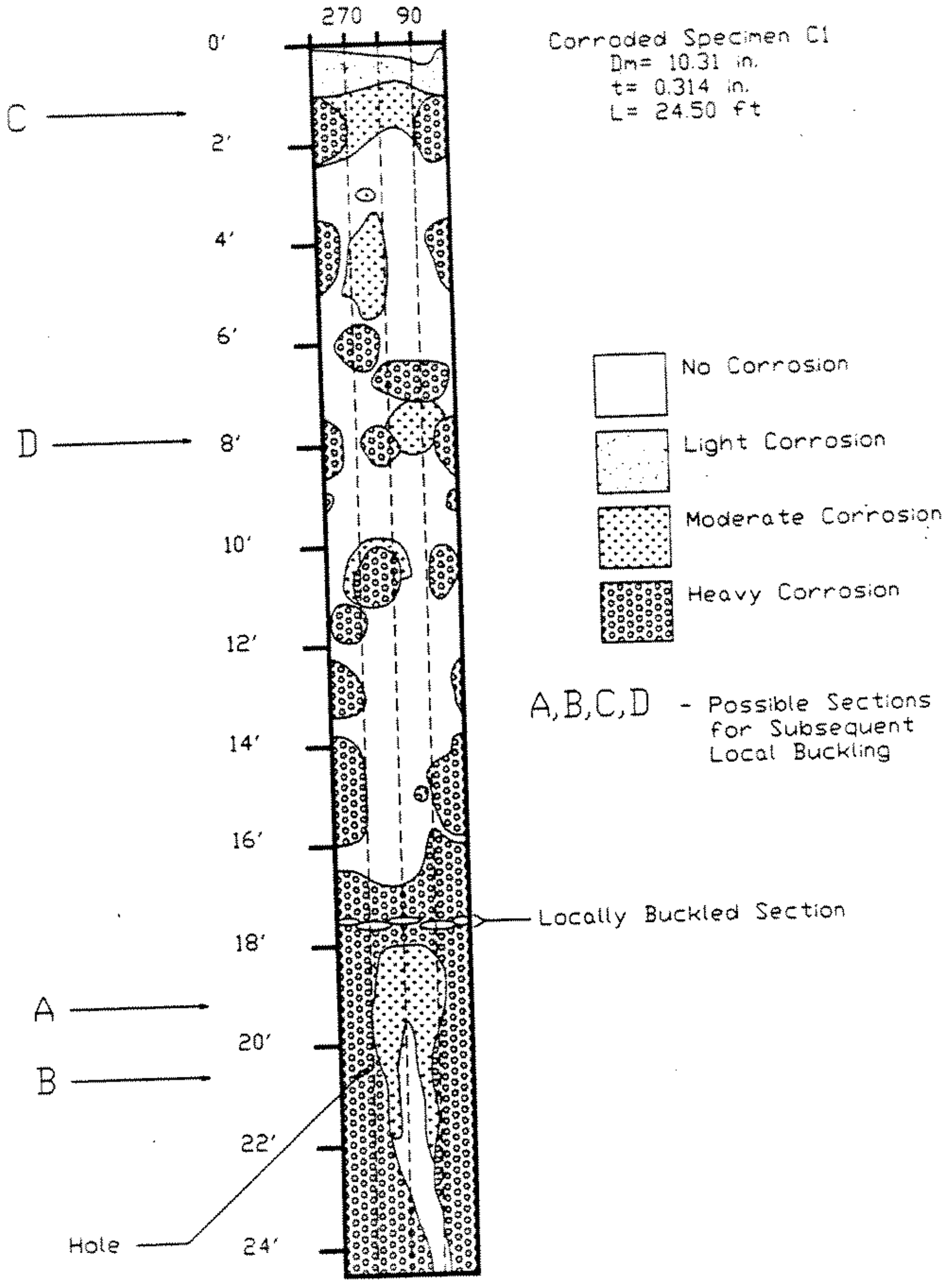

Figure 1-1: Map of Corrosion on Unfolded Surface of Tube [10]

Table 6-1: Geometrical Properties and Ultimate FEM Strength of Specimens with Three Corrosion Patches (CONTINUATION)

| No. | Specim Name | Spr g [in] | Spc s [in] | Lng L [in] | Ptch tp [in] | Yield Fy [ksi] | PuF Fix [kip] | PuP Pin [kip] | pF | pP |
|---|---|---|---|---|---|---|---|---|---|---|
| 206 | 3M211P33 | 2.68 | 1.1 | 136 | 0.03 | 36 | 38.98 | | 0.526 | |
| 207 | 3M222P33 | 2.68 | 2.2 | 136 | 0.03 | 36 | 43.36 | | 0.585 | |
| 208 | 3M233P33 | 2.68 | 3.3 | 136 | 0.03 | 36 | 47.82 | | 0.645 | |
| 209 | 3M244P33 | 2.68 | 4.4 | 136 | 0.03 | 36 | 49.02 | | 0.661 | |
| 210 | 3M299P33 | 2.68 | 9.9 | 136 | 0.03 | 36 | 49.06 | | 0.662 | |
| 211 | 3M200P35 | 2.68 | 0 | 136 | 0.03 | 50 | 45.46 | | 0.441 | |
| 212 | 3M211P35 | 2.68 | 1.1 | 136 | 0.03 | 50 | 47.6 | | 0.462 | |
| 213 | 3M222P35 | 2.68 | 2.2 | 136 | 0.03 | 50 | 56.6 | | 0.55 | |
| 214 | 3M233P35 | 2.68 | 3.3 | 136 | 0.03 | 50 | 62.92 | | 0.611 | |
| 215 | 3M244P35 | 2.68 | 4.4 | 136 | 0.03 | 50 | 65.46 | | 0.636 | |
| 216 | 3M299P35 | 2.68 | 9.9 | 136 | 0.03 | 50 | 66.42 | | 0.645 | |
| 217 | 3M200P37 | 2.68 | 0 | 136 | 0.03 | 75 | 59.92 | | 0.388 | |
| 218 | 3M211P37 | 2.68 | 1.1 | 136 | 0.03 | 75 | 62.06 | | 0.402 | |
| 219 | 3M222P37 | 2.68 | 2.2 | 136 | 0.03 | 75 | 77.82 | | 0.504 | |
| 220 | 3M233P37 | 2.68 | 3.3 | 136 | 0.03 | 75 | 87.48 | | 0.566 | |
| 221 | 3M244P37 | 2.68 | 4.4 | 136 | 0.03 | 75 | 92.86 | | 0.601 | |
| 222 | 3M299P37 | 2.68 | 9.9 | 136 | 0.03 | 75 | 95.46 | | 0.618 | |
| 223 | 3L200P33 | 2.68 | 0 | 200 | 0.03 | 36 | 30.52 | | 0.412 | |
| 224 | 3L211P33 | 2.68 | 1.1 | 200 | 0.03 | 36 | 31.54 | | 0.425 | |
| 225 | 3L222P33 | 2.68 | 2.2 | 200 | 0.03 | 36 | 40.28 | | 0.543 | |
| 226 | 3L233P33 | 2.68 | 3.3 | 200 | 0.03 | 36 | 45.38 | | 0.612 | |
| 227 | 3L244P33 | 2.68 | 4.4 | 200 | 0.03 | 36 | 47.62 | | 0.642 | |
| 228 | 3L299P33 | 2.68 | 9.9 | 200 | 0.03 | 36 | 48.72 | | 0.657 | |
| 229 | 3L200P35 | 2.68 | 0 | 200 | 0.03 | 50 | 41.2 | | 0.4 | |
| 230 | 3L211P35 | 2.68 | 1.1 | 200 | 0.03 | 50 | 42.14 | | 0.409 | |
| 231 | 3L222P35 | 2.68 | 2.2 | 200 | 0.03 | 50 | 52.9 | | 0.514 | |
| 232 | 3L233P35 | 2.68 | 3.3 | 200 | 0.03 | 50 | 59.78 | | 0.58 | |
| 233 | 3L244P35 | 2.68 | 4.4 | 200 | 0.03 | 50 | 53.42 | | 0.519 | |
| 234 | 3L299P35 | 2.68 | 9.9 | 200 | 0.03 | 50 | 65.86 | | 0.639 | |
| 235 | 3L200P37 | 2.68 | 0 | 200 | 0.03 | 75 | 59.32 | | 0.384 | |
| 236 | 3L211P37 | 2.68 | 1.1 | 200 | 0.03 | 75 | 59.4 | | 0.384 | |
| 237 | 3L222P37 | 2.68 | 2.2 | 200 | 0.03 | 75 | 73.26 | | 0.474 | |
| 238 | 3L233P37 | 2.68 | 3.3 | 200 | 0.03 | 75 | 82.54 | | 0.534 | |
| 239 | 3L244P37 | 2.68 | 4.4 | 200 | 0.03 | 75 | 89.04 | | 0.576 | |
| 240 | 3L299P37 | 2.68 | 9.9 | 200 | 0.03 | 75 | 94.48 | | 0.612 | |

## Table 6-1: Geometrical Properties and Ultimate FEM Strength of Specimens with Three Corrosion Patches (CONTINUATION)

| No. | Specim Name | Spr g [in] | Spc s [in] | Lng L [in] | Ptch tp [in] | Yield Fy [ksi] | PuF Fix [kip] | PuP Pin [kip] | pF | pP |
|---|---|---|---|---|---|---|---|---|---|---|
| 167 | 3T322*4 | 3.055 | 2.2 | 12.5 | 0.04 | 42.11 | 64.1 | 50.36 | 0.739 | 0.581 |
| 168 | 3T333*4 | 3.055 | 3.3 | 12.5 | 0.04 | 42.11 | 65.66 | 55.28 | 0.757 | 0.637 |
| 169 | 3T344*4 | 3.055 | 4.4 | 12.5 | 0.04 | 42.11 | 67.5 | 58.9 | 0.778 | 0.679 |
| 170 | 3T399*4 | 3.055 | 9.9 | 12.5 | 0.04 | 42.11 | 69.18 | 62.92 | 0.797 | 0.725 |
| 171 | 3T400*4 | 3.384 | 0 | 12.5 | 0.04 | 42.11 | 61.62 | 49.94 | 0.71 | 0.576 |
| 172 | 3T411*4 | 3.384 | 1.1 | 12.5 | 0.04 | 42.11 | 62.18 | 49.1 | 0.717 | 0.566 |
| 173 | 3T416*4 | 3.384 | 1.65 | 12.5 | 0.04 | 42.11 | 62.26 | 49.14 | 0.718 | 0.566 |
| 174 | 3T427*4 | 3.384 | 2.75 | 12.5 | 0.04 | 42.11 | 64.12 | 53.1 | 0.739 | 0.612 |
| 175 | 3T444*4 | 3.384 | 4.4 | 12.5 | 0.04 | 42.11 | 66.06 | 58.58 | 0.762 | 0.675 |
| 176 | 3T499*4 | 3.384 | 9.9 | 12.5 | 0.04 | 42.11 | 69.14 | 64.96 | 0.797 | 0.749 |
| 177 | 3S200*4 | 2.68 | 0 | 90 | 0.04 | 42.11 | 36.04 |  | 0.415 |  |
| 178 | 3S211*4 | 2.68 | 1.1 | 90 | 0.04 | 42.11 | 42.35 |  | 0.488 |  |
| 179 | 3S222*4 | 2.68 | 2.2 | 90 | 0.04 | 42.11 | 55.14 |  | 0.636 |  |
| 180 | 3S244*4 | 2.68 | 4.4 | 90 | 0.04 | 42.11 | 58.72 |  | 0.677 |  |
| 181 | 3S299*4 | 2.68 | 9.9 | 90 | 0.04 | 42.11 | 57.96 |  | 0.668 |  |
| 182 | 3L200*4 | 2.68 | 0 | 200 | 0.04 | 42.11 | 35.28 |  | 0.407 |  |
| 183 | 3L211*4 | 2.68 | 1.1 | 200 | 0.04 | 42.11 | 36.76 |  | 0.424 |  |
| 184 | 3L222*4 | 2.68 | 2.2 | 200 | 0.04 | 42.11 | 45.9 |  | 0.529 |  |
| 185 | 3L244*4 | 2.68 | 4.4 | 200 | 0.04 | 42.11 | 54.68 |  | 0.63 |  |
| 186 | 3L299*4 | 2.68 | 9.9 | 200 | 0.04 | 42.11 | 56.3 |  | 0.649 |  |
|  | Specimens with tp=0.03 in. but other Fy than Fy=42.11 ksi |  |  |  |  |  |  |  |  |  |
| 187 | 3T200P33 | 2.68 | 0 | 12.5 | 0.03 | 36 | 49.86 |  | 0.672 |  |
| 188 | 3T211P33 | 2.68 | 1.1 | 12.5 | 0.03 | 36 | 50.94 |  | 0.687 |  |
| 189 | 3T222P33 | 2.68 | 2.2 | 12.5 | 0.03 | 36 | 53.78 |  | 0.725 |  |
| 190 | 3T233P33 | 2.68 | 3.3 | 12.5 | 0.03 | 36 | 55.46 |  | 0.748 |  |
| 191 | 3T244P33 | 2.68 | 4.4 | 12.5 | 0.03 | 36 | 56.62 |  | 0.763 |  |
| 192 | 3T299P33 | 2.68 | 9.9 | 12.5 | 0.03 | 36 | 57.68 |  | 0.778 |  |
| 193 | 3T200P35 | 2.68 | 0 | 12.5 | 0.03 | 50 | 67.72 |  | 0.657 |  |
| 194 | 3T211P35 | 2.68 | 1.1 | 12.5 | 0.03 | 50 | 69.36 |  | 0.673 |  |
| 195 | 3T222P35 | 2.68 | 2.2 | 12.5 | 0.03 | 50 | 73.44 |  | 0.713 |  |
| 196 | 3T233P35 | 2.68 | 3.3 | 12.5 | 0.03 | 50 | 75.64 |  | 0.734 |  |
| 197 | 3T244P35 | 2.68 | 4.4 | 12.5 | 0.03 | 50 | 77.32 |  | 0.751 |  |
| 198 | 3T299P35 | 2.68 | 9.9 | 12.5 | 0.03 | 50 | 78.94 |  | 0.766 |  |
| 199 | 3T200P37 | 2.68 | 0 | 12.5 | 0.03 | 75 | 98.42 |  | 0.637 |  |
| 200 | 3T211P37 | 2.68 | 1.1 | 12.5 | 0.03 | 75 | 100.94 |  | 0.653 |  |
| 201 | 3T222P37 | 2.68 | 2.2 | 12.5 | 0.03 | 75 | 107.48 |  | 0.696 |  |
| 202 | 3T233P37 | 2.68 | 3.3 | 12.5 | 0.03 | 75 | 110.5 |  | 0.715 |  |
| 203 | 3T244P37 | 2.68 | 4.4 | 12.5 | 0.03 | 75 | 113.0 |  | 0.731 |  |
| 204 | 3T299P37 | 2.68 | 9.9 | 12.5 | 0.03 | 75 | 115.64 |  | 0.748 |  |
| 205 | 3M200P33 | 2.68 | 0 | 136 | 0.03 | 36 | 36.46 |  | 0.492 |  |

## Table 6-1: Geometrical Properties and Ultimate FEM Strength of Specimens with Three Corrosion Patches (CONTINUATION)

| No. | Specim Name | Spr g [in] | Spc s [in] | Lng L [in] | Ptch tp [in] | Yield Fy [ksi] | PuF Fix [kip] | PuP Pin [kip] | pF | pP |
|---|---|---|---|---|---|---|---|---|---|---|
| 127 | 3L427 | 3.384 | 2.75 | 200 | 0.03 | 42.11 | 49.52 | 42.88 | 0.571 | 0.494 |
| 128 | 3L444 | 3.384 | 4.4 | 200 | 0.03 | 42.11 | 55.7 | 46.48 | 0.642 | 0.536 |
| 129 | 3L471 | 3.384 | 7.15 | 200 | 0.03 | 42.11 | 60.24 | 49.82 | 0.694 | 0.574 |
| 130 | 3L499 | 3.384 | 9.9 | 200 | 0.03 | 42.11 | 61.88 | 54.76 | 0.713 | 0.631 |
| | Specimens with other tp than tp=0.03 in. | | | | | | | | | |
| 131 | 3T200*2 | 2.68 | 0 | 12.5 | 0.02 | 42.11 | 55.32 | 28.58 | 0.638 | 0.329 |
| 132 | 3T211*2 | 2.68 | 1.1 | 12.5 | 0.02 | 42.11 | 56.48 | 31.46 | 0.651 | 0.363 |
| 133 | 3T222*2 | 2.68 | 2.2 | 12.5 | 0.02 | 42.11 | 60 | 42.28 | 0.692 | 0.487 |
| 134 | 3T233*2 | 2.68 | 3.3 | 12.5 | 0.02 | 42.11 | 62.24 | 49.26 | 0.717 | 0.568 |
| 135 | 3T244*2 | 2.68 | 4.4 | 12.5 | 0.02 | 42.11 | 63.86 | 52.04 | 0.736 | 0.6 |
| 136 | 3T299*2 | 2.68 | 9.9 | 12.5 | 0.02 | 42.11 | 65.26 | 53.2 | 0.752 | 0.613 |
| 137 | 3T300*2 | 3.055 | 0 | 12.5 | 0.02 | 42.11 | 55.38 | 34.44 | 0.638 | 0.397 |
| 138 | 3T311*2 | 3.055 | 1.1 | 12.5 | 0.02 | 42.11 | 56.56 | 35.88 | 0.652 | 0.414 |
| 139 | 3T322*2 | 3.055 | 2.2 | 12.5 | 0.02 | 42.11 | 58.74 | 41.62 | 0.677 | 0.48 |
| 140 | 3T333*2 | 3.055 | 3.3 | 12.5 | 0.02 | 42.11 | 61.08 | 49.28 | 0.704 | 0.568 |
| 141 | 3T344*2 | 3.055 | 4.4 | 12.5 | 0.02 | 42.11 | 62.62 | 53.16 | 0.722 | 0.613 |
| 142 | 3T399*2 | 3.055 | 9.9 | 12.5 | 0.02 | 42.11 | 65.2 | 56.7 | 0.752 | 0.654 |
| 143 | 3T400*2 | 3.384 | 0 | 12.5 | 0.02 | 42.11 | 55.5 | 38.26 | 0.64 | 0.441 |
| 144 | 3T411*2 | 3.384 | 1.1 | 12.5 | 0.02 | 42.11 | 56.58 | 38.9 | 0.652 | 0.448 |
| 145 | 3T416*2 | 3.384 | 1.65 | 12.5 | 0.02 | 42.11 | 56.68 | 39.32 | 0.653 | 0.453 |
| 146 | 3T427*2 | 3.384 | 2.75 | 12.5 | 0.02 | 42.11 | 59.2 | 45.78 | 0.682 | 0.528 |
| 147 | 3T444*2 | 3.384 | 4.4 | 12.5 | 0.02 | 42.11 | 61.64 | 53.62 | 0.711 | 0.618 |
| 148 | 3T499*2 | 3.384 | 9.9 | 12.5 | 0.02 | 42.11 | 65.2 | 59.54 | 0.752 | 0.686 |
| 149 | 3S200*2 | 2.68 | 0 | 90 | 0.02 | 42.11 | 35.94 | | 0.414 | |
| 150 | 3S211*2 | 2.68 | 1.1 | 90 | 0.02 | 42.11 | 42.3 | | 0.488 | |
| 151 | 3S222*2 | 2.68 | 2.2 | 90 | 0.02 | 42.11 | 55.04 | | 0.634 | |
| 152 | 3S244*2 | 2.68 | 4.4 | 90 | 0.02 | 42.11 | 58.66 | | 0.676 | |
| 153 | 3S299*2 | 2.68 | 9.9 | 90 | 0.02 | 42.11 | 57.9 | | 0.667 | |
| 154 | 3L200*2 | 2.68 | 0 | 200 | 0.02 | 42.11 | 35.24 | | 0.406 | |
| 155 | 3L211*2 | 2.68 | 1.1 | 200 | 0.02 | 42.11 | 36.7 | | 0.423 | |
| 156 | 3L222*2 | 2.68 | 2.2 | 200 | 0.02 | 42.11 | 45.92 | | 0.529 | |
| 157 | 3L244*2 | 2.68 | 4.4 | 200 | 0.02 | 42.11 | 54.6 | | 0.629 | |
| 158 | 3L299*2 | 2.68 | 9.9 | 200 | 0.02 | 42.11 | 56.3 | | 0.649 | |
| 159 | 3T200*4 | 2.68 | 0 | 12.5 | 0.04 | 42.11 | 61 | 41.88 | 0.703 | 0.483 |
| 160 | 3T211*4 | 2.68 | 1.1 | 12.5 | 0.04 | 42.11 | 62.24 | 42.58 | 0.717 | 0.491 |
| 161 | 3T222*4 | 2.68 | 2.2 | 12.5 | 0.04 | 42.11 | 65.32 | 50.24 | 0.753 | 0.579 |
| 162 | 3T233*4 | 2.68 | 3.3 | 12.5 | 0.04 | 42.11 | 66.98 | 55.48 | 0.772 | 0.64 |
| 163 | 3T244*4 | 2.68 | 4.4 | 12.5 | 0.04 | 42.11 | 68.2 | 58.44 | 0.786 | 0.674 |
| 164 | 3T299*4 | 2.68 | 9.9 | 12.5 | 0.04 | 42.11 | 69.46 | 60.18 | 0.801 | 0.694 |
| 165 | 3T300*4 | 3.055 | 0 | 12.5 | 0.04 | 42.11 | 61.38 | 46.76 | 0.708 | 0.539 |
| 166 | 3T311*4 | 3.055 | 1.1 | 12.5 | 0.04 | 42.11 | 62.26 | 46.46 | 0.718 | 0.536 |

# Table 6-1: Geometrical Properties and Ultimate FEM Strength of Specimens with Three Corrosion Patches (CONTINUATION)

| No. | Specim Name | Spr g [in] | Spc s [in] | Lng L [in] | Ptch tp [in] | Yield Fy [ksi] | PuF Fix [kip] | PuP Pin [kip] | pF | pP |
|---|---|---|---|---|---|---|---|---|---|---|
| 87 | 3L300 | 3.055 | 0 | 200 | 0.03 | 42.11 | 40.56 | 38.84 | 0.468 | 0.448 |
| 88 | 3L305 | 3.055 | 0.55 | 200 | 0.03 | 42.11 | 40.42 | 37.9 | 0.466 | 0.437 |
| 89 | 3L311 | 3.055 | 1.1 | 200 | 0.03 | 42.11 | 40.74 | 38.14 | 0.47 | 0.44 |
| 90 | 3L316 | 3.055 | 1.65 | 200 | 0.03 | 42.11 | 41.48 | 38.58 | 0.478 | 0.445 |
| 91 | 3L322 | 3.055 | 2.2 | 200 | 0.03 | 42.11 | 45.56 | 40.24 | 0.525 | 0.464 |
| 92 | 3L327 | 3.055 | 2.75 | 200 | 0.03 | 42.11 | 49.1 | 41.62 | 0.566 | 0.48 |
| 93 | 3L344 | 3.055 | 4.4 | 200 | 0.03 | 42.11 | 55.38 | 45.8 | 0.638 | 0.528 |
| 94 | 3L371 | 3.055 | 7.15 | 200 | 0.03 | 42.11 | ??? | 49.14 | ??? | 0.56613 |
| 95 | 3L399 | 3.055 | 9.9 | 200 | 0.03 | 42.11 | 59.32 | 52.52 | 0.684 | 0.605 |
| 96 | 3T400 | 3.384 | 0 | 12.5 | 0.03 | 42.11 | 58.08 | 44.18 | 0.67 | 0.509 |
| 97 | 3T411 | 3.384 | 1.1 | 12.5 | 0.03 | 42.11 | 58.94 | 43.52 | 0.679 | 0.502 |
| 98 | 3T416 | 3.384 | 1.65 | 12.5 | 0.03 | 42.11 | 59.16 | 43.8 | 0.682 | 0.505 |
| 99 | 3T427 | 3.384 | 2.75 | 12.5 | 0.03 | 42.11 | 61.22 | 49.44 | 0.706 | 0.57 |
| 100 | 3T444 | 3.384 | 4.4 | 12.5 | 0.03 | 42.11 | 63.46 | 55.88 | 0.732 | 0.644 |
| 101 | 3T471 | 3.384 | 7.15 | 12.5 | 0.03 | 42.11 | 66.58 | 59.94 | 0.76706 | 0.69056 |
| 102 | 3T499 | 3.384 | 9.9 | 12.5 | 0.03 | 42.11 | 66.81 | 61.98 | 0.77 | 0.714 |
| 103 | 3S400 | 3.384 | 0 | 90 | 0.03 | 42.11 | 47.28 | 43.84 | 0.545 | 0.505 |
| 104 | 3S411 | 3.384 | 1.1 | 90 | 0.03 | 42.11 | 47.26 | 43 | 0.545 | 0.496 |
| 105 | 3S416 | 3.384 | 1.65 | 90 | 0.03 | 42.11 | 48.54 | 43.24 | 0.56 | 0.498 |
| 106 | 3S427 | 3.384 | 2.75 | 90 | 0.03 | 42.11 | 55.86 | 47.1 | 0.644 | 0.543 |
| 107 | 3S444 | 3.384 | 4.4 | 90 | 0.03 | 42.11 | 59.78 | 53.12 | 0.689 | 0.612 |
| 108 | 3S471 | 3.384 | 7.15 | 90 | 0.03 | 42.11 | 64.58 | 58.36 | 0.74402 | 0.67236 |
| 109 | 3S499 | 3.384 | 9.9 | 90 | 0.03 | 42.11 | 63.12 | 61.14 | 0.728 | 0.705 |
| 110 | 3M400 | 3.384 | 0 | 136 | 0.03 | 42.11 | 44.7 | 43.5 | 0.515 | 0.501 |
| 111 | 3M411 | 3.384 | 1.1 | 136 | 0.03 | 42.11 | 45.06 | 42.58 | 0.519 | 0.491 |
| 112 | 3M416 | 3.384 | 1.65 | 136 | 0.03 | 42.11 | 45.06 | 42.76 | 0.519 | 0.493 |
| 113 | 3M427 | 3.384 | 2.75 | 136 | 0.03 | 42.11 | 52.54 | 45.98 | 0.606 | 0.53 |
| 114 | 3M444 | 3.384 | 4.4 | 136 | 0.03 | 42.11 | 57.92 | 51.56 | 0.668 | 0.594 |
| 115 | 3M471 | 3.384 | 7.15 | 136 | 0.03 | 42.11 | 62.1 | 56.84 | 0.71544 | 0.65484 |
| 116 | 3M499 | 3.384 | 9.9 | 136 | 0.03 | 42.11 | 62.3 | 60.42 | 0.718 | 0.697 |
| 117 | 3I400 | 3.384 | 0.00 | 168 | 0.03 | 42.11 |  | 43.12 |  | 0.49678 |
| 118 | 3I411 | 3.384 | 1.10 | 168 | 0.03 | 42.11 |  | 42.14 |  | 0.48549 |
| 119 | 3I416 | 3.384 | 1.65 | 168 | 0.03 | 42.11 |  | 42.20 |  | 0.48618 |
| 120 | 3I427 | 3.384 | 2.75 | 168 | 0.03 | 42.11 |  | 44.78 |  | 0.5159 |
| 121 | 3I444 | 3.384 | 4.40 | 168 | 0.03 | 42.11 |  | 49.70 |  | 0.57259 |
| 122 | 3I471 | 3.384 | 7.15 | 168 | 0.03 | 42.11 |  | 54.72 |  | 0.63042 |
| 123 | 3I499 | 3.384 | 9.90 | 168 | 0.03 | 42.11 |  | 59.22 |  | 0.68226 |
| 124 | 3L400 | 3.384 | 0 | 200 | 0.03 | 42.11 | 44.4 | 42.12 | 0.512 | 0.486 |
| 125 | 3L411 | 3.384 | 1.1 | 200 | 0.03 | 42.11 | 43.82 | 41.16 | 0.505 | 0.474 |
| 126 | 3L416 | 3.384 | 1.65 | 200 | 0.03 | 42.11 | 44.18 | 41.14 | 0.509 | 0.474 |

# Table 6-1: Geometrical Properties and Ultimate FEM Strength of Specimens with Three Corrosion Patches (CONTINUATION)

| No. | Specim Name | Spr g [in] | Spc s [in] | Lng L [in] | Ptch tp [in] | Yield Fy [ksi] | PuF Fix [kip] | PuP Pin [kip] | pF | pP |
|---|---|---|---|---|---|---|---|---|---|---|
| 45 | 3L211 | 2.68 | 1.1 | 200 | 0.03 | 42.11 | 36.7 | 33.78 | 0.423 | 0.389 |
| 46 | 3L222 | 2.68 | 2.2 | 200 | 0.03 | 42.11 | 45.9 | 39.06 | 0.529 | 0.45 |
| 47 | 3L227 | 2.68 | 2.75 | 200 | 0.03 | 42.11 | 49.28 | 40.7 | 0.568 | 0.469 |
| 48 | 3L233 | 2.68 | 3.3 | 200 | 0.03 | 42.11 | 51.82 | 42.54 | 0.597 | 0.49 |
| 49 | 3L244 | 2.68 | 4.4 | 200 | 0.03 | 42.11 | 54.64 | 45.42 | 0.63 | 0.524 |
| 50 | 3L271 | 2.68 | 7.15 | 200 | 0.03 | 42.11 | 47.37 | 48.2 |  | 0.5553 |
| 51 | 3L299 | 2.68 | 9.9 | 200 | 0.03 | 42.11 | 56.28 | 50.34 | 0.649 | 0.58 |
| 52 | 3T300 | 3.055 | 0 | 12.5 | 0.03 | 42.11 | 57.9 | 40.6 | 0.667 | 0.468 |
| 53 | 3T305 | 3.055 | 0.55 | 12.5 | 0.03 | 42.11 | 58.7 | 40.66 | 0.677 | 0.469 |
| 54 | 3T311 | 3.055 | 1.1 | 12.5 | 0.03 | 42.11 | 59.02 | 40.44 | 0.68 | 0.466 |
| 55 | 3T316 | 3.055 | 1.65 | 12.5 | 0.03 | 42.11 | 59.44 | 41.62 | 0.685 | 0.48 |
| 56 | 3T322 | 3.055 | 2.2 | 12.5 | 0.03 | 42.11 | 61.02 | 45.38 | 0.703 | 0.523 |
| 57 | 3T327 | 3.055 | 2.75 | 12.5 | 0.03 | 42.11 | 62.06 | 49.01 | 0.715 | 0.565 |
| 58 | 3T333 | 3.055 | 3.3 | 12.5 | 0.03 | 42.11 | 62.96 | 51.74 | 0.726 | 0.596 |
| 59 | 3T344 | 3.055 | 4.4 | 12.5 | 0.03 | 42.11 | 64.46 | 55.56 | 0.743 | 0.64 |
| 60 | 3T371 | 3.055 | 7.15 | 12.5 | 0.03 | 42.11 | 67.02 | 58.38 | 0.77213 | 0.67259 |
| 61 | 3T399 | 3.055 | 9.9 | 12.5 | 0.03 | 42.11 | 66.9 | 59.44 | 0.771 | 0.685 |
| 62 | 3S300 | 3.055 | 0 | 90 | 0.03 | 42.11 | 41.4 | 40.2 | 0.477 | 0.463 |
| 63 | 3S311 | 3.055 | 1.1 | 90 | 0.03 | 42.11 | 45.04 | 39.7 | 0.519 | 0.458 |
| 64 | 3S316 | 3.055 | 1.65 | 90 | 0.03 | 42.11 | 46.06 | 40.54 | 0.531 | 0.467 |
| 65 | 3S322 | 3.055 | 2.2 | 90 | 0.03 | 42.11 | 52.68 | 43.48 | 0.607 | 0.501 |
| 66 | 3S327 | 3.055 | 2.75 | 90 | 0.03 | 42.11 | 56.22 | 46.24 | 0.648 | 0.533 |
| 67 | 3S344 | 3.055 | 4.4 | 90 | 0.03 | 42.11 | 60.34 | 52.8 | 0.696 | 0.609 |
| 68 | 3S371 | 3.055 | 7.15 | 90 | 0.03 | 42.11 | ?? | 56.86 | ?? | 0.65508 |
| 69 | 3S399 | 3.055 | 9.9 | 90 | 0.03 | 42.11 | 60.8 | 58.5 | 0.701 | 0.674 |
| 70 | 3M300 | 3.055 | 0 | 136 | 0.03 | 42.11 | 41.04 | 39.94 | 0.473 | 0.46 |
| 71 | 3M311 | 3.055 | 1.1 | 136 | 0.03 | 42.11 | 41.88 | 39.3 | 0.483 | 0.453 |
| 72 | 3M316 | 3.055 | 1.65 | 136 | 0.03 | 42.11 | 42.86 | 40.04 | 0.494 | 0.462 |
| 73 | 3M322 | 3.055 | 2.2 | 136 | 0.03 | 42.11 | 47.72 | 42.66 | 0.55 | 0.492 |
| 74 | 3M327 | 3.055 | 2.75 | 136 | 0.03 | 42.11 | 52.26 | 44.94 | 0.602 | 0.518 |
| 75 | 3M344 | 3.055 | 4.4 | 136 | 0.03 | 42.11 | 57.7 | 51.08 | 0.665 | 0.589 |
| 76 | 3M371 | 3.055 | 7.15 | 136 | 0.03 | 42.11 | 60.08 | 55.42 | 0.69217 | 0.63849 |
| 77 | 3M399 | 3.055 | 9.9 | 136 | 0.03 | 42.11 | 59.78 | 57.78 | 0.689 | 0.666 |
| 78 | 3I300 | 3.055 | 0.00 | 168 | 0.03 | 42.11 |  | 39.62 |  | 0.45646 |
| 79 | 3I305 | 3.055 | 0.55 | 168 | 0.03 | 42.11 |  | 38.74 |  | 0.44632 |
| 80 | 3I311 | 3.055 | 1.10 | 168 | 0.03 | 42.11 |  | 38.90 |  | 0.44816 |
| 81 | 3I316 | 3.055 | 1.65 | 168 | 0.03 | 42.11 |  | 39.54 |  | 0.45553 |
| 82 | 3I322 | 3.055 | 2.20 | 168 | 0.03 | 42.11 |  | 41.68 |  | 0.48019 |
| 83 | 3I327 | 3.055 | 2.75 | 168 | 0.03 | 42.11 |  | 43.54 |  | 0.50162 |
| 84 | 3I344 | 3.055 | 4.40 | 168 | 0.03 | 42.11 |  | 49.10 |  | 0.56567 |
| 85 | 3I371 | 3.055 | 7.15 | 168 | 0.03 | 42.11 |  | 53.50 |  | 0.61637 |
| 86 | 3I399 | 3.055 | 9.90 | 168 | 0.03 | 42.11 |  | 56.58 |  | 0.65185 |

## Table 6-1: Geometrical Properties and Ultimate FEM Strength of Specimens with Three Corrosion Patches

| No. | Specim Name | Spr g [in] | Spc s [in] | Lng L [in] | Ptch tp [in] | Yield Fy [ksi] | PuF Fix [kip] | PuP Pin [kip] | pF | pP |
|---|---|---|---|---|---|---|---|---|---|---|
| 1 | 3T100 | 1.6 | 0 | 12.5 | 0.03 | 42.11 | 62.24 | 36.28 | 0.717 | 0.418 |
| 2 | 3T111 | 1.6 | 1.12 | 12.5 | 0.03 | 42.11 | 65.12 | 41.82 | 0.751 | 0.482 |
| 3 | 3T112 | 1.6 | 1.2 | 12.5 | 0.03 | 42.11 | 65.54 | 42.68 | 0.756 | 0.492 |
| 4 | 3T113 | 1.6 | 1.3 | 12.5 | 0.03 | 42.11 | 65.98 | 43.78 | 0.761 | 0.505 |
| 5 | 3T114 | 1.6 | 1.4 | 12.5 | 0.03 | 42.11 | 66.38 | 44.8 | 0.765 | 0.516 |
| 6 | 3T116 | 1.6 | 1.6 | 12.5 | 0.03 | 42.11 | 67.04 | 46.52 | 0.773 | 0.536 |
| 7 | 3T118 | 1.6 | 1.8 | 12.5 | 0.03 | 42.11 | 67.52 | 47.26 | 0.778 | 0.545 |
| 8 | 3T120 | 1.6 | 2 | 12.5 | 0.03 | 42.11 | 67.74 | 47.38 | 0.781 | 0.546 |
| 9 | 3T199 | 1.6 | 9.9 | 12.5 | 0.03 | 42.11 | 67.46 | 46.7 | 0.778 | 0.538 |
| 10 | 3T200 | 2.68 | 0 | 12.5 | 0.03 | 42.11 | 57.7 | 35.2 | 0.665 | 0.406 |
| 11 | 3T205 | 2.68 | 0.55 | 12.5 | 0.03 | 42.11 | 58.84 | 35.76 | 0.678 | 0.412 |
| 12 | 3T211 | 2.68 | 1.1 | 12.5 | 0.03 | 42.11 | 59.06 | 36.28 | 0.681 | 0.418 |
| 13 | 3T216 | 2.68 | 1.65 | 12.5 | 0.03 | 42.11 | 60.74 | 40.3 | 0.7 | 0.465 |
| 14 | 3T222 | 2.68 | 2.2 | 12.5 | 0.03 | 42.11 | 62.42 | 45.6 | 0.72 | 0.526 |
| 15 | 3T227 | 2.68 | 2.75 | 12.5 | 0.03 | 42.11 | 63.42 | 49.14 | 0.731 | 0.566 |
| 16 | 3T233 | 2.68 | 3.3 | 12.5 | 0.03 | 42.11 | 64.32 | 51.86 | 0.741 | 0.598 |
| 17 | 3T244 | 2.68 | 4.4 | 12.5 | 0.03 | 42.11 | 65.7 | 54.74 | 0.757 | 0.631 |
| 18 | 3T299 | 2.68 | 9.9 | 12.5 | 0.03 | 42.11 | 67.04 | 56.22 | 0.773 | 0.648 |
| 19 | 3S200 | 2.68 | 0 | 90 | 0.03 | 42.11 | 35.96 | 34.78 | 0.415 | 0.401 |
| 20 | 3S205 | 2.68 | 0.55 | 90 | 0.03 | 42.11 | 40.08 | 35.14 | 0.462 | 0.405 |
| 21 | 3S211 | 2.68 | 1.1 | 90 | 0.03 | 42.11 | 41.88 | 35.16 | 0.483 | 0.405 |
| 22 | 3S216 | 2.68 | 1.65 | 90 | 0.03 | 42.11 | 51.14 | 38.82 | 0.59 | 0.448 |
| 23 | 3S222 | 2.68 | 2.2 | 90 | 0.03 | 42.11 | 55.16 | 43.08 | 0.636 | 0.497 |
| 24 | 3S233 | 2.68 | 3.3 | 90 | 0.03 | 42.11 | 58.58 | 48.7 | 0.675 | 0.561 |
| 25 | 3S244 | 2.68 | 4.4 | 90 | 0.03 | 42.11 | 58.7 | 52.32 | 0.677 | 0.603 |
| 26 | 3S299 | 2.68 | 9.9 | 90 | 0.03 | 42.11 | 57.96 | 55 | 0.668 | 0.634 |
| 27 | 3M200 | 2.68 | 0 | 136 | 0.03 | 42.11 | 35.56 | 34.6 | 0.41 | 0.399 |
| 28 | 3M211 | 2.68 | 1.1 | 136 | 0.03 | 42.11 | 38.4 | 34.72 | 0.443 | 0.4 |
| 29 | 3M222 | 2.68 | 2.2 | 136 | 0.03 | 42.11 | 49.34 | 41.88 | 0.569 | 0.483 |
| 30 | 3M227 | 2.68 | 2.75 | 136 | 0.03 | 42.11 | 52.44 | 44.5 | 0.605 | 0.513 |
| 31 | 3M233 | 2.68 | 3.3 | 136 | 0.03 | 42.11 | 54.56 | 47 | 0.629 | 0.542 |
| 32 | 3M244 | 2.68 | 4.4 | 136 | 0.03 | 42.11 | 56.26 | 50.78 | 0.649 | 0.585 |
| 33 | 3M299 | 2.68 | 9.9 | 136 | 0.03 | 42.11 | 56.8 | 54.68 | 0.655 | 0.63 |
| 34 | 3I200 | 2.68 | 0.00 | 168 | 0.03 | 42.11 |  | 34.40 |  | 0.39632 |
| 35 | 3I205 | 2.68 | 0.55 | 168 | 0.03 | 42.11 |  | 34.54 |  | 0.39793 |
| 36 | 3I211 | 2.68 | 1.10 | 168 | 0.03 | 42.11 |  | 34.36 |  | 0.39586 |
| 37 | 3I216 | 2.68 | 1.65 | 168 | 0.03 | 42.11 |  | 37.56 |  | 0.43272 |
| 38 | 3I222 | 2.68 | 2.20 | 168 | 0.03 | 42.11 |  | 40.72 |  | 0.46913 |
| 39 | 3I233 | 2.68 | 3.30 | 168 | 0.03 | 42.11 |  | 45.24 |  | 0.5212 |
| 40 | 3I244 | 2.68 | 4.40 | 168 | 0.03 | 42.11 |  | 48.88 |  | 0.56314 |
| 41 | 3I271 | 2.68 | 7.15 | 168 | 0.03 | 42.11 |  | 52.00 |  | 0.59908 |
| 42 | 3I299 | 2.68 | 9.90 | 168 | 0.03 | 42.11 |  | 53.34 |  | 0.61452 |
| 43 | 3L200 | 2.68 | 0 | 200 | 0.03 | 42.11 | 35.58 | 33.96 | 0.41 | 0.391 |
| 44 | 3L205 | 2.68 | 0.55 | 200 | 0.03 | 42.11 | 36.12 | 34.05 | 0.416 | 0.393 |

## Table 5-1: Geometrical Properties and Ultimate FEM Strength of Specimens with Two Corrosion Patches (CONTINUATION)

| No. | Specim Name | Spr g [in] | Spc s [in] | Lng L [in] | Ptch tp [in] | Yield Fy [ksi] | PuF Fix [kip] | PuP Pin [kip] | pF | pP |
|---|---|---|---|---|---|---|---|---|---|---|
| 86 | 2M722 | 6.768 | 2.2 | 136 | 0.03 | 42.11 | 63.53 | | 0.732 | |
| 87 | 2M744 | 6.768 | 4.4 | 136 | 0.03 | 42.11 | 66.98 | | 0.772 | |
| 88 | 2M766 | 6.768 | 6.6 | 136 | 0.03 | 42.11 | 70.47 | | 0.812 | |
| Specimens with "infinite" longitudinal spacing s (One-patch failure) | | | | | | | | | | |
| 89 | 2T*99* | * | 9.9 | 12.5 | 0.03 | 42.11 | 76.66 | 63.33 | 0.883188 | 0.72961 |
| 90 | 2S*99* | * | 9.9 | 90 | 0.03 | 42.11 | 69.54 | 59.10 | 0.801159 | 0.6809 |
| 91 | 2M*99* | * | 9.9 | 136 | 0.03 | 42.11 | 65.96 | 56.40 | 0.759915 | 0.6498 |
| 92 | 2L*99* | * | 9.9 | 200 | 0.03 | 42.11 | 64.86 | 47.16 | 0.747242 | 0.5433 |
| Specimens with Load Eccentricity (Last digit in the name is e in 1/10 inches) | | | | | | | | | | |
| 93 | 2S500Pe4 | 5.36 | 0 | 90 | 0.03 | 42.11 | 60.03 | 51.16 | 0.692 | 0.58941 |
| 94 | 2S544Pe4 | 5.36 | 4.4 | 90 | 0.03 | 42.11 | 63.34 | 53.75 | 0.73 | 0.6192 |
| 95 | 2S588Pe4 | 5.36 | 8.8 | 90 | 0.03 | 42.11 | 41.88 | 58.83 | 0.483 | 0.6778 |
| 96 | 2M544Pe4 | 5.36 | 4.4 | 136 | 0.03 | 42.11 | 63.48 | 51.55 | 0.732 | 0.5939 |
| 97 | 2M588Pe4 | 5.36 | 8.8 | 136 | 0.03 | 42.11 | 72.13 | 54.71 | 0.832 | 0.6303 |
| 98 | 2L500Pe3 | 5.36 | 0 | 200 | 0.03 | 42.11 | | 42.38 | | 0.4883 |
| 99 | 2L500Pe4 | 5.36 | 0 | 200 | 0.03 | 42.11 | 56.67 | 40.86 | 0.653 | 0.4707 |
| 100 | 2L500Pe7 | 5.36 | 0 | 200 | 0.03 | 42.11 | | 37.34 | | 0.4302 |
| 101 | 2L522Pe4 | 5.36 | 2.2 | 200 | 0.03 | 42.11 | 56.72 | 41.99 | 0.654 | 0.4838 |
| 102 | 2L544Pe4 | 5.36 | 4.4 | 200 | 0.03 | 42.11 | 59.19 | 41.32 | 0.682 | 0.4760 |
| 103 | 2L566Pe2 | 5.36 | 6.6 | 200 | 0.03 | 42.11 | | 46.18 | | 0.5320 |
| 104 | 2L566Pe4 | 5.36 | 6.6 | 200 | 0.03 | 42.11 | 62.03 | 41.93 | 0.715 | 0.4831 |
| 105 | 2L566Pe7 | 5.36 | 6.6 | 200 | 0.03 | 42.11 | | 38.29 | | 0.4411 |
| 106 | 2L566Pe9 | 5.36 | 6.6 | 200 | 0.03 | 42.11 | | 36.40 | | 0.4194 |
| 107 | 2L588Pe3 | 5.36 | 8.8 | 200 | 0.03 | 42.11 | | 45.03 | | 0.5188 |
| 108 | 2L588Pe4 | 5.36 | 8.8 | 200 | 0.03 | 42.11 | 59.32 | 43.48 | 0.684 | 0.5009 |
| 109 | 2L588Pe7 | 5.36 | 8.8 | 200 | 0.03 | 42.11 | | 39.89 | | 0.4596 |
| 110 | 2S600Pe8 | 6.11 | 0 | 90 | 0.03 | 42.11 | 61.9 | 53.26 | 0.714 | 0.6136 |
| 111 | 2S644Pe8 | 6.11 | 4.4 | 90 | 0.03 | 42.11 | 63.85 | 53.60 | 0.736 | 0.6175 |
| 112 | 2M600Pe8 | 6.11 | 0 | 136 | 0.03 | 42.11 | 60.32 | 51.36 | 0.695 | 0.5917 |
| 113 | 2M644Pe8 | 6.11 | 4.4 | 136 | 0.03 | 42.11 | 62.1 | 51.69 | 0.716 | 0.5955 |
| 114 | 2M688Pe8 | 6.11 | 8.8 | 136 | 0.03 | 42.11 | 64.15 | 56.17 | 0.668 | 0.6471 |
| 115 | 2L600Pe8 | 6.11 | 0 | 200 | 0.03 | 42.11 | 59.66 | 44.77 | 0.718 | 0.5158 |
| 116 | 2L622Pe8 | 6.11 | 2.2 | 200 | 0.03 | 42.11 | 59.71 | 44.70 | 0.688 | 0.5150 |
| 117 | 2L644Pe8 | 6.11 | 4.4 | 200 | 0.03 | 42.11 | 60.91 | 44.85 | 0.701735 | 0.5167 |
| 118 | 2L666Pe8 | 6.11 | 6.6 | 200 | 0.03 | 42.11 | 62.99 | 45.42 | 0.725698 | 0.5233 |
| 119 | 2L688Pe8 | 6.11 | 8.8 | 200 | 0.03 | 42.11 | 63.43 | 48.70 | 0.731 | 0.5611 |

## Table 5-1: Geometrical Properties and Ultimate FEM Strength of Specimens with Two Corrosion Patches (CONTINUATION)

| No. | Specim Name | Spr g [in] | Spc s [in] | Lng L [in] | Ptch tp [in] | Yield Fy [ksi] | PuF Fix [kip] | PuP Pin [kip] | pF | pP |
|---|---|---|---|---|---|---|---|---|---|---|
| 45 | 2T533 | 5.36 | 3.3 | 12.5 | 0.03 | 42.11 | 68.95 | 58.42 | 0.795 | 0.673 |
| 46 | 2T544 | 5.36 | 4.4 | 12.5 | 0.03 | 42.11 | 70.51 | 59.88 | 0.813 | 0.690 |
| 47 | 2T566 | 5.36 | 6.6 | 12.5 | 0.03 | 42.11 | 72.3 | 62.94 | 0.833 | 0.726 |
| 48 | 2S500 | 5.36 | 0 | 90 | 0.03 | 42.11 | 60.03 | 55.92 | 0.692 | 0.645 |
| 49 | 2S511 | 5.36 | 1.1 | 90 | 0.03 | 42.11 | 60.51 | 55.72 | 0.698 | 0.642 |
| 50 | 2S522 | 5.36 | 2.2 | 90 | 0.03 | 42.11 | 61.17 | 55.36 | 0.705 | 0.638 |
| 51 | 2S544 | 5.36 | 4.4 | 90 | 0.03 | 42.11 | 63.34 | 57.17 | 0.73 | 0.659 |
| 52 | 2S566 | 5.36 | 6.6 | 90 | 0.03 | 42.11 | 65.6 | 60.35 | 0.756 | 0.696 |
| 53 | 2M500 | 5.36 | 0 | 136 | 0.03 | 42.11 | 57.22 | 55.13 | 0.66 | 0.636 |
| 54 | 2M511 | 5.36 | 1.1 | 136 | 0.03 | 42.11 | 57.62 | 55.14 | 0.664 | 0.636 |
| 55 | 2M522 | 5.36 | 2.2 | 136 | 0.03 | 42.11 | 58.08 | 54.88 | 0.67 | 0.633 |
| 56 | 2M533 | 5.36 | 3.3 | 136 | 0.03 | 42.11 | 60.55 | 55.88 | 0.698 | 0.644 |
| 57 | 2M544 | 5.36 | 4.4 | 136 | 0.03 | 42.11 | 63.48 | 58.84 | 0.732 | 0.678 |
| 58 | 2M566 | 5.36 | 6.6 | 136 | 0.03 | 42.11 | 72.13 | 57.22 | 0.832 | 0.660 |
| 59 | 2L500 | 5.36 | 0 | 200 | 0.03 | 42.11 | 56.67 | 50.27 | 0.653 | 0.580 |
| 60 | 2L511 | 5.36 | 1.1 | 200 | 0.03 | 42.11 | 56.65 | 50.28 | 0.653 | 0.580 |
| 61 | 2L522 | 5.36 | 2.2 | 200 | 0.03 | 42.11 | 56.72 | 50.13 | 0.654 | 0.578 |
| 62 | 2L544 | 5.36 | 4.4 | 200 | 0.03 | 42.11 | 59.19 | 50.12 | 0.682 | 0.578 |
| 63 | 2L566 | 5.36 | 6.6 | 200 | 0.03 | 42.11 | 62.03 | 51.29 | 0.715 | 0.591 |
| 64 | 2T600 | 6.11 | 0 | 12.5 | 0.03 | 42.11 | 67.13 | 59.61 | 0.774 | 0.687 |
| 65 | 2T611 | 6.11 | 1.1 | 12.5 | 0.03 | 42.11 | 67.26 | 59.92 | 0.775 | 0.691 |
| 66 | 2T622 | 6.11 | 2.2 | 12.5 | 0.03 | 42.11 | 67.75 | 59.75 | 0.781 | 0.689 |
| 67 | 2T644 | 6.11 | 4.4 | 12.5 | 0.03 | 42.11 | 70.33 | 61.75 | 0.811 | 0.712 |
| 68 | 2T666 | 6.11 | 6.6 | 12.5 | 0.03 | 42.11 | 73.56 | 63.73 | 0.848 | 0.735 |
| 69 | 2S600 | 6.11 | 0 | 90 | 0.03 | 42.11 | 61.9 | 58.80 | 0.714 | 0.678 |
| 70 | 2S611 | 6.11 | 1.1 | 90 | 0.03 | 42.11 | 62.35 | 59.01 | 0.719 | 0.680 |
| 71 | 2S622 | 6.11 | 2.2 | 90 | 0.03 | 42.11 | 62.28 | 58.70 | 0.718 | 0.677 |
| 72 | 2S644 | 6.11 | 4.4 | 90 | 0.03 | 42.11 | 63.85 | 60.43 | 0.736 | 0.697 |
| 73 | 2S666 | 6.11 | 6.6 | 90 | 0.03 | 42.11 | 65.73 | 62.55 | 0.758 | 0.721 |
| 74 | 2M600 | 6.11 | 0 | 136 | 0.03 | 42.11 | 60.32 | 58.00 | 0.695 | 0.669 |
| 75 | 2M611 | 6.11 | 1.1 | 136 | 0.03 | 42.11 | 60.56 | 58.23 | 0.698 | 0.671 |
| 76 | 2M622 | 6.11 | 2.2 | 136 | 0.03 | 42.11 | 60.46 | 58.34 | 0.697 | 0.673 |
| 77 | 2M644 | 6.11 | 4.4 | 136 | 0.03 | 42.11 | 62.1 | 59.23 | 0.716 | 0.683 |
| 78 | 2M666 | 6.11 | 6.6 | 136 | 0.03 | 42.11 | 64.15 | 60.83 | 0.74 | 0.701 |
| 79 | 2L600 | 6.11 | 0 | 200 | 0.03 | 42.11 | 59.66 | 52.31 | 0.688 | 0.603 |
| 80 | 2L611 | 6.11 | 1.1 | 200 | 0.03 | 42.11 | 59.82 | 52.65 | 0.69 | 0.607 |
| 81 | 2L622 | 6.11 | 2.2 | 200 | 0.03 | 42.11 | 59.71 | 52.58 | 0.688 | 0.606 |
| 82 | 2L644 | 6.11 | 4.4 | 200 | 0.03 | 42.11 | 61.14 | 52.62 | 0.705 | 0.607 |
| 83 | 2L666 | 6.11 | 6.6 | 200 | 0.03 | 42.11 | 63.43 | 53.07 | 0.731 | 0.612 |
| 84 | 2M700 | 6.768 | 0 | 136 | 0.03 | 42.11 | 62.32 |  | 0.718 |  |
| 85 | 2M711 | 6.768 | 1.1 | 136 | 0.03 | 42.11 | 62.88 |  | 0.725 |  |

Table 5-1: Geometrical Properties and Ultimate FEM Strength of Specimens with Two Corrosion Patches

| No. | Specim Name | Spr g [in] | Spc s [in] | Lng L [in] | Ptch tp [in] | Yield Fy [ksi] | PuF Fix [kip] | PuP Pin [kip] | pF | pP |
|---|---|---|---|---|---|---|---|---|---|---|
| 1 | 2T200 | 2.68 | 0 | 12.5 | 0.03 | 42.11 | 67.37 | 44.22 | 0.777 | 0.510 |
| 2 | 2T211 | 2.68 | 1.1 | 12.5 | 0.03 | 42.11 | 68.11 | 46.00 | 0.785 | 0.530 |
| 3 | 2T222 | 2.68 | 2.2 | 12.5 | 0.03 | 42.11 | 71.26 | 55.57 | 0.821 | 0.641 |
| 4 | 2T244 | 2.68 | 4.4 | 12.5 | 0.03 | 42.11 | 73.91 | 62.00 | 0.852 | 0.715 |
| 5 | 2T266 | 2.68 | 6.6 | 12.5 | 0.03 | 42.11 | 75.61 | 62.68 | 0.872 | 0.723 |
| 6 | 2S200 | 2.68 | 0 | 90 | 0.03 | 42.11 | 55.76 | 41.80 | 0.643 | 0.482 |
| 7 | 2S211 | 2.68 | 1.1 | 90 | 0.03 | 42.11 | 56.49 | 43.65 | 0.651 | 0.503 |
| 8 | 2S222 | 2.68 | 2.2 | 90 | 0.03 | 42.11 | 60.55 | 49.09 | 0.698 | 0.566 |
| 9 | 2S244 | 2.68 | 4.4 | 90 | 0.03 | 42.11 | 65.09 | 56.07 | 0.75 | 0.646 |
| 10 | 2S266 | 2.68 | 6.6 | 90 | 0.03 | 42.11 | 67.74 | 59.78 | 0.781 | 0.689 |
| 11 | 2M200 | 2.68 | 0 | 136 | 0.03 | 42.11 | 49.24 | 40.14 | 0.568 | 0.463 |
| 12 | 2M211 | 2.68 | 1.1 | 136 | 0.03 | 42.11 | 49.66 | 41.95 | 0.572 | 0.484 |
| 13 | 2M222 | 2.68 | 2.2 | 136 | 0.03 | 42.11 | 55.89 | 47.24 | 0.644 | 0.545 |
| 14 | 2M244 | 2.68 | 4.4 | 136 | 0.03 | 42.11 | 61.19 | 53.49 | 0.705 | 0.617 |
| 15 | 2M266 | 2.68 | 6.6 | 136 | 0.03 | 42.11 | 64.43 | 57.61 | 0.743 | 0.664 |
| 16 | 2L200 | 2.68 | 0 | 200 | 0.03 | 42.11 | 45.65 | 36.73 | 0.526 | 0.423 |
| 17 | 2L211 | 2.68 | 1.1 | 200 | 0.03 | 42.11 | 46.32 | 38.17 | 0.534 | 0.440 |
| 18 | 2L222 | 2.68 | 2.2 | 200 | 0.03 | 42.11 | 52.84 | 41.95 | 0.609 | 0.484 |
| 19 | 2L244 | 2.68 | 4.4 | 200 | 0.03 | 42.11 | 59.54 | 46.65 | 0.686 | 0.538 |
| 20 | 2L266 | 2.68 | 6.6 | 200 | 0.03 | 42.11 | 62.76 | 48.24 | 0.723 | 0.556 |
| 21 | 2T300 | 3.055 | 0 | 12.5 | 0.03 | 42.11 | 67.56 | 46.92 | 0.779 | 0.541 |
| 22 | 2T311 | 3.055 | 1.1 | 12.5 | 0.03 | 42.11 | 68.04 | 48.91 | 0.784 | 0.564 |
| 23 | 2T322 | 3.055 | 2.2 | 12.5 | 0.03 | 42.11 | 70.23 | 53.57 | 0.81 | 0.618 |
| 24 | 2T344 | 3.055 | 4.4 | 12.5 | 0.03 | 42.11 | 72.52 | 58.57 | 0.836 | 0.675 |
| 25 | 2T366 | 3.055 | 6.6 | 12.5 | 0.03 | 42.11 | 74.78 | 62.55 | 0.862 | 0.721 |
| 26 | 2S300 | 3.055 | 0 | 90 | 0.03 | 42.11 | 55.78 | 45.52 | 0.643 | 0.525 |
| 27 | 2S311 | 3.055 | 1.1 | 90 | 0.03 | 42.11 | 57.3 | 46.86 | 0.661 | 0.540 |
| 28 | 2S322 | 3.055 | 2.2 | 90 | 0.03 | 42.11 | 61.43 | 50.81 | 0.708 | 0.586 |
| 29 | 2S344 | 3.055 | 4.4 | 90 | 0.03 | 42.11 | 65.08 | 55.95 | 0.75 | 0.645 |
| 30 | 2S366 | 3.055 | 6.6 | 90 | 0.03 | 42.11 | 67.28 | 59.66 | 0.776 | 0.688 |
| 31 | 2M300 | 3.055 | 0 | 136 | 0.03 | 42.11 | 49.86 | 44.74 | 0.575 | 0.516 |
| 32 | 2M311 | 3.055 | 1.1 | 136 | 0.03 | 42.11 | 52.25 | 45.45 | 0.602 | 0.524 |
| 33 | 2M322 | 3.055 | 2.2 | 136 | 0.03 | 42.11 | 56.47 | 48.82 | 0.651 | 0.563 |
| 34 | 2M344 | 3.055 | 4.4 | 136 | 0.03 | 42.11 | 61.11 | 53.00 | 0.704 | 0.611 |
| 35 | 2M366 | 3.055 | 6.6 | 136 | 0.03 | 42.11 | 64.12 | 57.43 | 0.739 | 0.662 |
| 36 | 2L300 | 3.055 | 0 | 200 | 0.03 | 42.11 | 47.62 | 42.70 | 0.549 | 0.492 |
| 37 | 2L311 | 3.055 | 1.1 | 200 | 0.03 | 42.11 | 48.5 | 42.34 | 0.559 | 0.488 |
| 38 | 2L322 | 3.055 | 2.2 | 200 | 0.03 | 42.11 | 54.03 | 43.40 | 0.623 | 0.500 |
| 39 | 2L344 | 3.055 | 4.4 | 200 | 0.03 | 42.11 | 59.19 | 45.60 | 0.682 | 0.526 |
| 40 | 2L366 | 3.055 | 6.6 | 200 | 0.03 | 42.11 | 62.51 | 48.35 | 0.721 | 0.557 |
| 41 | 2T500 | 5.36 | 0 | 12.5 | 0.03 | 42.11 | 67.28 | 56.75 | 0.776 | 0.654 |
| 42 | 2T511 | 5.36 | 1.1 | 12.5 | 0.03 | 42.11 | 67.47 | 56.79 | 0.778 | 0.655 |
| 43 | 2T516 | 5.36 | 1.65 | 12.5 | 0.03 | 42.11 | 67.71 | 56.88 | 0.781 | 0.656 |
| 44 | 2T522 | 5.36 | 2.2 | 12.5 | 0.03 | 42.11 | 67.92 | 56.96 | 0.783 | 0.657 |

## Table 3-5: Types of Elements used in Selection of Elements

| Designation Label | Length, L [in.] | Width, b [in.] | Depth, t [in.] | Number of Segments | Number of Layers | Type of Element | Ultimate Load [kips] | Comments on Post-Ultimate Behavior |
|---|---|---|---|---|---|---|---|---|
| RigidPlastic | 0.66 | 0.10 | 0.022 | 2 | - | Rigid-Plastic Analysis | N.A. | |
| beam | 0.66 | 0.10 | 0.022 | 6 | 1 | Beam Elements | 0.0279 | *Lower value than others* |
| beamref | 0.66 | 0.10 | 0.022 | 10 | 1 | Beam Elements | 0.0282 | *Close to shell model solution* |
| 5sh6thin | 0.66 | 0.10 | 0.022 | 6 | 1 | 9-node shell, 5 DOF/node | 0.0299 | *Comparable to rigid-plastic analysis* |
| 1br8thin | 0.66 | 0.10 | 0.022 | 6 | 1 | 8-node brick | no ultimate | *Irrational* |
| 1br8thra | 0.66 | 0.10 | 0.022 | 10 | 1 | 8-node brick | 0.0347 | *Close to refined 20-node brick results* |
| 2br8thin | 0.66 | 0.10 | 0.022 | 6 | 2 | 8-node brick | 0.0306 | *Bad in post-buckling range* |
| 2br8thra | 0.66 | 0.10 | 0.022 | 10 | 2 | 8-node brick | 1.0306 | *Unrealistic ultimate load* |
| 1br20thin | 0.66 | 0.10 | 0.022 | 6 | 1 | 20-node brick | 0.0329 | *Far from rigid-plastic analysis* |
| 1br20thra | 0.66 | 0.10 | 0.022 | 10 | 1 | 20-node brick | 0.0257 | *Lower value than others* |
| 2br20thin | 0.66 | 0.10 | 0.022 | 6 | 2 | 20-node brick | 0.0325 | *Far from rigid-plastic analysis* |
| 2br20thra | 0.66 | 0.10 | 0.022 | 10 | 2 | 20-node brick | 0.0295 | *Close to shell model solution* |
| 3br20thin | 0.66 | 0.10 | 0.022 | 6 | 3 | 20-node brick | 0.0314 | *Bad jump* |
| 3br20thra | 0.66 | 0.10 | 0.022 | 10 | 3 | 20-node brick | 0.0294 | *Close to shell model solution* |
| 4br20thin | 0.66 | 0.10 | 0.022 | 6 | 4 | 20-node brick | 0.0313 | *Bad jump* |
| 4br20thra | 0.66 | 0.10 | 0.022 | 10 | 4 | 20-node brick | 0.0292 | *Close to shell model solution* |
| RigidPlastic | 0.66 | 0.10 | 0.122 | 2 | - | Rigid-Plastic Analysis | -- | |
| beam | 0.66 | 0.10 | 0.122 | 6 | 1 | Beam Elements | 0.4205 | *Similar behaviour to shell modeling* |
| 5sh6ori | 0.66 | 0.10 | 0.122 | 6 | 1 | 9-node shell, 5 DOF/ node | 0.4351 | *Comparable to rigid-plastic analysis* |
| 6sh6ori | 0.66 | 0.10 | 0.122 | 6 | 1 | 8-node shell, 6 DOF/ node | 0.4413 | *Very close to shell model with 5 DOF/node* |
| 1br8ori | 0.66 | 0.10 | 0.122 | 6 | 1 | 8-node brick | 0.4482 | *Bad representation of elastic range* |
| 2br8ori | 0.66 | 0.10 | 0.122 | 6 | 2 | 8-node brick | 0.4127 | *Bad representation of ultimate load* |
| 1br20ori | 0.66 | 0.10 | 0.122 | 6 | 1 | 20-node brick | 0.4138 | *Conflicts with other multi-layered bricks* |
| 2br20ori | 0.66 | 0.10 | 0.122 | 6 | 2 | 20-node brick | 0.4394 | |
| 3br20ori | 0.66 | 0.10 | 0.122 | 6 | 3 | 20-node brick | 0.4432 | *Improved behavior but doubled CPU time* |
| 4br20ori | 0.66 | 0.10 | 0.122 | 6 | 4 | 20-node brick | 0.4443 | *Small difference in results but in CPU time* |
| 8br20ori | 0.66 | 0.10 | 0.122 | 6 | 8 | 20-node brick | 0.4418 | *Horrendously increased CPU time* |

Table 3-2: Comparison of Quarter-Tube Model with Full-Tube Model
for Specimens with One Corrosion Patch

| **Model Type** | **Length, ℓ[inch]** | **$P_{ult}$ (fixed) [kips]** | **$P_{ult}$ (pinned) [kips]** |
|---|---|---|---|
| Quarter-Tube | 28 | 74.88 | 62.02 |
| Full-Tube | 12.5 | 76.66 | 63.33 |
| *% Difference* | | ***2.32*** | ***2.07*** |

Table 3-3: Comparison of Half-Tube Model with Full-Tube Model
for Specimens with Multiple Corrosion Patches

| **Specimen** | **Model Type** | **$P_{ult}$ (fixed) [kips]** | **$P_{ult}$ (pinned) [kips]** |
|---|---|---|---|
| 3T299*3 | Half-Tube | 67.04 | 56.75 |
| 2T200*3 | Full-Tube | 67.28 | 56.22 |
| | *% Difference* | ***+0.36*** | ***-0.93*** |
| 3L299*3 | Half-Tube | 56.28 | 50.27 |
| 2L200*3 | Full-Tube | 56.67 | 50.34 |
| | *% Difference* | ***+0.69*** | ***+0.14*** |

Table 3-4: Comparison of FE Specimens with Test Specimens

| | TEST | ABAQUS | | CXS.for (formula) | | |
|---|---|---|---|---|---|---|
| | $P_{test}$ | $P_u$(fix) | $P_u$(pin) | $P_f$(fix) | $P_f$(pin) | $P_y$(1$^{st}$ yield) |
| MP1 | 57.00 | 67.46 | 46.70 | 65.03 | 43.57 | 45.76 |
| MP2 | 51.10 | 66.38 | 44.80 | N.A. | N.A. | N.A. |

N.A.= Not Available

## Table 3-1: Specimen Names and Labeling

| Character Position in Specimen Name, its Label and Meaning | | | | | | | | | | | | | | | |
|---|---|---|---|---|---|---|---|---|---|---|---|---|---|---|---|
| 1 | | 2 | | 3 | | 4 and 5 | | 6 | | 7 | | 8 | | | |
| **Number of Patches** | | **Column Length, $\ell$** | | **Circumferential Spread, g** | | **Longitudinal Spacing, s** | | **End Conditions** | | **Patch Thickness, $t_p$** | | **Misc. * ($F_y$)** | | | |
| **1** | One | **T** | 12.5 in | **1** | 1.60 in. | **00** | 0.00 in. | **F** | Fixed | **2** | 0.02 in. | | 42.11 ksi | | |
| **2** | Two | **S** | 90 in. | **2** | 2.68 in. | **05** | 0.55 in. | **P** | Pinned | **3** | 0.03 in. | **3** | 36 ksi | | |
| **3** | Three | **M** | 136 in. | **3** | 3.055 in. | **11** | 1.10 in. | | | **4** | 0.04 in. | **5** | 50 ksi | | |
| | | **I** | 168 in. | **4** | 3.384 in. | **14** | 1.40 in. | | | | | **7** | 75 ksi | | |
| | | **L** | 200 in. | **5** | 5.36 in. | **16** | 1.65 in. | | | | | | | | |
| | | | | **6** | 6.11 in. | **22** | 2.20 in. | | | | | | | | |
| | | | | **7** | 6.768 in. | **27** | 2.75 in. | | | | | | | | |
| | | | | | | **33** | 3.30 in. | | | | | | | | |
| | | | | | | **44** | 4.40 in. | | | | | | | | |
| | | | | | | **66** | 6.60 in. | | | | | | | | |
| | | | | | | **71** | 7.15 in. | | | | | | | | |
| | | | | | | **99** | 9.9 (Inf.) | | | | | | | | |

***Examples of Specimen Names:***

**2T500P2:** Two patches, $\ell$=12.5 in., g=5.36 in., s=0.00 in., pinned ends, $t_p$=0.02 in.

**3L344F3:** Three patches, $\ell$=200 in., g=3.055 in., s=4.40 in., fixed ends, $t_p$=0.03 in.

**3S399F45:** Three patches, $\ell$=90 in., g=3.055 in., s=Infinity, fixed ends, $t_p$=0.04 in., $F_y$=50 ksi

**2M588Pe4:** Two patches, $\ell$=136 in., g=5.36 in., s=8.80 in., pinned ends, (tp=0.03 in.), Load eccentricity e=0.4 in.

* The 8th character in the name is optionally used for supplementary information, for example, digits (3,5,7) are used for the yield stress other than the default $F_y$=42.11 ksi.

| | |
|---|---|
| v | (v/2) = longitudinal width of the cosine variation of wall thickness within the patch. [in.] |
| w | (w/2) = circumferential width of the cosine variation of wall thickness within the patch. [in.] |
| x, y, z | Coordinate axes. |
| $x_1^n$ | Distance of the n-th node from the x-axis. |
| $x_2^n$ | Distance of the $n^{th}$ node from the y-axis. |
| $\nu$ | Poisson's ratio. |

| | | |
|---|---|---|
| $d_1, d_2, \ldots$ | Constants used in approximation formulas. | |
| D | Outside tube diameter. [in.] | |
| E | Modulus of elasticity. [ksi] | |
| $F_y$ | Yield stress.. [ksi] | |
| g | Circumferential spread of patches. [in.] | |
| G | Relative circumferential spread of patches. | $(G = g/D)$ |
| H | Longitudinal height (length) of corrosion patch. [in.] | |
| $\ell$ | Column (Specimen) length. [in.] | |
| L | Column slenderness variable.<br>(In some tables, L = the actual length of the column $\ell$)<br>Designator for "Long" specimens ($\ell = 200$ in.). | $(L = \ell/100r)$ |
| p | Non-dimensionalized ultimate axial load. | $(p = P_u/P_y)$ |
| P | Axial load. [kips] | |
| $P_u$ | Ultimate load. [kips] | |
| $P_{uP}, P_{uF}$ | Ultimate load from FE analysis for pinned and fixed-end conditions. [kips] | |
| $P_y$ | Axial load causing yielding of the gross cross section. [kips] | $(P_y = AF_y)$ |
| r | Radius of gyration of gross (undamaged) cross section. [in.] | |
| $r_i^n$ | Rotation of the n-th node in direction i. | |
| R | Outside radius. [in.] | |
| $R_i$ | Inside radius. [in.] | |
| $R_m$ | Average (mean) radius. [in.] | |
| t | Uncorroded (original) thickness of the tube wall. [in.] | |
| $T_p$ | Wall thickness in the constant-thickness portion of corrosion patch. [in.] | |
| $u_i^n$ | Displacement of the n-th node in direction i. | |

# 13. NOMENCLATURE

## MEANING OF SUBSCRIPTS

| | |
|---|---|
| a | actual patch size |
| d | design load |
| f | fixed end supports |
| n | nominal patch size used in the parametric analysis |
| p | pinned end supports |
| r | reduction of cross-sectional area due to a corrosion patch |
| u | ultimate load |
| 1 | Column damaged by only 'one' corrosion patch |

| | |
|---|---|
| $a$ | Circumferential width of the constant minimum thickness in the patch. [in.] |
| $a_n$ | Relative net area. ($a_n = A_n/A$) |
| $a_r$ | Relative area reduction due to corrosion damage. ($a_r = A_r/A$) |
| $a_1, a_2, \ldots$ | Constants or parameters used in approximation formulas. |
| $A$ | Uncorroded (Gross) cross-sectional area. [in.$^2$] ($A = \pi (D - t)t$ ) |
| $A_n$ | Net area of corroded tube cross section. [in.$^2$] |
| $A_r$ | Area reduction of the cross section due to corrosion. [in.$^2$] |
| $b$ | Longitudinal width of the constant-thickness portion in the patch. [in.] |
| $b_1, b_2 \ldots$ | Constants used in approximation formulas. |
| $c$ | Full circumferential width of the corrosion patch.. [in.] |
| $c_1, c_2, \ldots$ | Constants used in approximation formulas. |
| $C_f, C_p$ | Correction factor for the actual size of corrosion patches (fixed or pinned ends). |

[10] Ostapenko, A., Berger T.W., Chambers, S.L., and Hebor, M.F.

"Corrosion Damage - Effect on Strength of Tubular Columns with Patch Corrosion", ATLSS Report No. 96-01, Lehigh University, Bethlehem, PA, August 1996.

[11] PMB/TX A&M

"Testing and Evaluation of Damaged Jacket Braces", PMB Engineering, Inc., and Texas A&M University, *Final Report*, PMB Engineering Inc., Houston, May 1990,

[12] Ricles, J.M., Bruin, W.M., Sooi, T.K., Hebor, M.F., and Schönwetter, P.C.

"Residual Strength Assessment and Repair of Damaged Offshore Tubulars", *Proceedings of the 27th Annual Offshore Technology Conference*, Houston, May, 1995, (OTC 7807), pp. 6-12.

[13] Ricles, J.M., and Hebor, M.F.

"Residual Strength and Epoxy-Based Grout Repair of Corroded Offshore Tubulars", *Proceedings of the 7th International Conference on Behavior of Offshore Structures (BOSS'94)*, Volume 3: Structures, Pergamon Press, 1994, pp. 307-322.

[14] Riehle

"Rockwell Hardness Table"
in "Instruction Manual, Riehle Portable Hardness Tester Model PHT-2"
Riehle Testing Machines, Division of Ametek, Inc., East Moline, IL, 1963.

[15] Searle, S.R.

"Matrix Algebra Useful for Statistics", John Wiley & Sons, New York, 1982.

# 12. REFERENCES

[1] ABAQUS

"ABAQUS User's Manual" (Versions 5.4 to 5.8) Copyright: Hibbitt, Karlsson and Sorensen, Inc., Pawtucket, Rhode Island, 02860-4847, 1994-98.

[2] API

"Recommended Practice for Planning, Designing, and Constructing Fixed Offshore Platforms, API, RP2A", American Petroleum Institute, Washington, D.C., 1989.

[3] API

"Recommended Practice for Fabricated Structural Steel Pipe in Fixed Offshore Platforms, API, RP2B", American Petroleum Institute, Washington, D.C., 1993?.

[4] DnV (Det Norske Veritas)

"Rules for the Design, Construction and Inspection of Fixed Offshore Structures", Det Norske Veritas (DnV), Oslo, 1974.

[5] Hebor, M.F., and Ricles, J.M.

"Residual Strength and Repair of Corrosion Damaged Steel Tubular Bracing", *Proceedings of the Structural Stability Research Council*, 1994; Annual Task Group Technical Session, June 20, 1994, Lehigh University, Bethlehem, PA, (ISBN 1-879749-57-2).

[6] Kim, Woobum

"Behavior and Strength of Damaged Tubular Columns with End Restraints", Ph.D. Dissertation, Lehigh University, Bethlehem, PA, September 1992. (Supervised by A. Ostapenko)

[7] Ostapenko, A.

"Local Buckling of Welded Tubular Columns", *Proceedings of the International Colloquium on Stability of Structures under Static and Dynamic Loads*, Washington, D.C., May, 1977, American Society of Civil Engineers, New York, 1977, pp. 367-374.

[8] Ostapenko, A., and Surahman, A.

"Structural Element Models for Hull Strength Analysis", FEL Report No. 480.6, Lehigh University, Bethlehem, PA (Prepared for U.S. Coast Guard), September 1982.

[9] Ostapenko, A., Wood, B.A., Chowdhury, A., and Hebor, M.F.

"Residual Strength of Damaged and Deteriorated Tubular Members in Offshore Structures", ATLSS Report No. 93-03, Lehigh University, Bethlehem, PA, January 1993.

# 11. ACKNOWLEDGMENTS

This report describes the work performed on the project "Residual Strength and Repair of Damaged and Deteriorated Offshore Structures" at Lehigh University, Department of Civil and Environmental Engineering (Le-Wu Lu and Arup SenGupta, consecutive Chairmen). The project was within the managerial structure of ATLSS (Advanced Technology for Large Structural Systems, John W. Fisher, Director) and represents a continuation of the previous subproject titled "Corrosion Damage -- Effect on Strength".

The project was sponsored as a Joint Industry Project by the following: EXXON Production Research Company (Contract: PR-14257), Minerals Management Service (DOI) (Contract: 14-35-0001-30719), and Mobil Technology Company (Contract: 055-20-017). We are most grateful for the financial support provided by these organizations. We are also indebted for the advice and guidance of the following Representatives of these organizations: Jaime Buitrago (EXXON); Douglas R. Angevine, V.V.D. Nair and James A. Volker (Mobil); and Charles E. Smith (MMS/DOI).

We are grateful to the undergraduate student Christopher S. Blechschmidt who conducted the tests on damaged specimens that are described in Chapter 2.

Thanks are also due to Eugene P. Matlock and John A. Pinter of Fritz Engineering Laboratory who helped with the tests, and to Peter Y. Bryan who helped with computer operations.

- The effect of end conditions on the ultimate strength was more pronounced for short columns than for long columns. Also, the pinned-end specimens had a greater reduction of the ultimate strength than the specimens with fixed ends.
- The patch thickness did not seem to have any direct effect on the ultimate strength within the range of the study.
- The yield stress was found to have a linear effect on the ultimate load.

## 10.3 Recommendations for Future Research

The following studies are recommended for future work on the ultimate strength of tubular members with multiple corrosion patches.

i. Tests are needed for a more thorough verification of the FE analysis results, especially, for two-patch patterns.
ii. Extension of the database for columns with two corrosion patches, a parametric study, and the development of "engineering" formulas for computing the ultimate load.
iii. Computational (analytical) and experimental results are needed to verify and improve consideration of corrosion patches of variable size when they are all the same in a pattern and when they differ from each other. This should include a study of columns with three patches having non-equal circumferential spread.

The parametric study of the project included the effects of the number of corrosion patches, the relative longitudinal and circumferential position of the patches, the column length, the thickness of the constant-thickness portion of the patches, and yield stress, for both fixed and pinned end conditions. All of the specimens had a diameter to patch thickness ratio of $D/t=45$ and the same patch geometry. Also, the position of the patches on the specimen followed a specific pattern. The ratio of column length to radius of gyration ($\ell/r$) ranged from 6.5 to 105, the ratio of diameter to patch thickness ($D/t_p$) from 137.5 to 275, and the yield stress from 36 ksi to 75 ksi.

A multi-variable regression analysis was performed to obtain simple "engineering"-type formulas for computing the ultimate strength of columns with three corrosion patches as affected by the parameters listed above. In the formulas, the ultimate strength was non-dimensionalized with respect to the full yield load ($p=P_u/P_y$), and the parameters with respect to the appropriate dimensions ($\ell/r$, $g/D$ and $s/D$).

To compensate for the limitation of the strength formulas to the size of the corrosion patches of the database, an approximate method was proposed for adjusting the solutions to the actual size of the patches.

## 10.2 Conclusions

The following conclusions were drawn from this study:

- The member strength is directly limited by local buckling and/or yielding of the wall within the corrosion patches. Yielding starts in the patch area and continues spreading over the cross section until the ultimate load is reached.
- Interaction between the patches had an important effect on the ultimate strength. When the patches were positioned sufficiently far from each other, the interaction diminished and the column behaved as if it had one less patch.
- For the patches spaced very closely in the longitudinal direction ($s<R/2$), the circumferential spread was found to be a very critical parameter for the ultimate strength.

# 10. SUMMARY, CONCLUSIONS AND RECOMMENDATIONS

## 10.1 Summary

Ultimate strength behavior of a tubular column damaged by irregular corrosion patches is a very complex three-dimensional phenomenon involving large deformations, non-linear material response and residual stresses. Conceptually, an analysis of this problem can be carried out by using modern finite element programs once all the information on the initial geometry and material properties is available and an optimum discretization scheme is determined. However, the FE method, requiring specialized knowledge and trial-and-error procedure idealizations, is hardly suitable for the irregular corrosion patch patterns of corrosion damage in actual structures.

In this project, the principal objective was to formulate a simplified "engineering" procedure for evaluating the ultimate load of tubular columns damaged by multiple corrosion patches. The work performed consisted of experimental and analytical studies and eventually resulted in approximate formulas for columns with three corrosion patches.

The report describes the tests on two short specimens with multiple corrosion patches: one (MP1) with two and the other (MP2) with three patches. The first specimen had two corrosion patches positioned at the mid-length in the same circumference, and the second had three patches, two at the mid-length as in the first specimen and the third straddling between the two and offset longitudinally. The third patch significantly reduced the strength of the two-patch specimen, and both specimens showed noticeably lower strength than specimens with a single corrosion patch that were tested in a previous project. Good correlation was found between the analytical and experimental results, and this verified the validity of using analytical results in a parametric study.

More than 500 different combinations of the parameters were analyzed by the finite element program -- ABAQUS. The finite element modeling techniques of tubular columns, the analysis methodology of the FE software and the comparison and selection of different element types were discussed.

The ultimate load is then $P_{up} = p_{ap} P_y = p_{ap} \{\pi(D\text{-}t)(t)(F_y)\} =$

$$= 0.36444 \{\pi(5.5 - 0.122)(0.122)(42.11)\} = \quad \underline{\mathbf{31.6296}} \text{ kips}$$

These results mean that for this case the doubling of the size of the patches reduced the capacity by

$$p_{ap}/p_{np} = 0.36444/0.536407 = 0.679, \text{ that is, by } 32.1\%$$

Application of this procedure to the same column but with variable values of $a_r$ and to a column with fixed ends (3M427F), as well as, to a column with $\ell$ = 200 in., g = 3.055 in. and s = 2.75 in., and with pinned and fixed ends resulted in Fig. 9-2. The example computation for 3M427P20 is marked in this figure with a circle. The labels for the second column are 3L327F and 3L327P.

## 9.4 Design Recommendation

Since the members in real offshore platforms are neither fully fixed nor fully pinned, it would be over-conservative to assume pinned ends and may be unsafe to assume fixed ends. Thus, it is proposed here to use the **design ultimate load** equal to the load for pinned ends increased by one-third of the difference between the loads for fixed and pinned ends, that is,

$$p_d = p_p + \frac{1}{3}(p_f - p_p) = \frac{1}{3}(2p_p + p_f) \tag{9-13}$$

For example, the sample columns analyzed in the previous section (3M427) has $p_p = 0.36444$ (3M427P20) and $p_f = 0.52512$ (3M427F20). Then, the relative design load $p_d$ would be

$$p_d = \frac{1}{3}(2*0.36444 + 0.52512) = \mathbf{0.418} \tag{9-14}$$

The design load for this column (3M427) is then $P_d = p_d P_y =$ **36.282** kips (9-15)

### 9.2.3 Computation of $p_a$ ($p_{af}$ and $p_{ap}$)

Formulas for computing the relative ultimate load for different end conditions are obtained by incorporating Eqs. 9-8 and 9-9 into Eq. 9-2.

Then, for **fixed ends**,
$$p_{af} = \frac{p_{laf}}{p_{lnf}} p_{nf} = C_f p_{nf} \tag{9-10}$$

and for **pinned ends**,
$$p_{ap} = \frac{p_{lap}}{p_{lnp}} p_{np} = C_p p_{np} \tag{9-11}$$

## 9.3 Sample Application

**Problem**:

Compute the ultimate load $P_u$ (and $p_u$) for the following pinned-end column with three corrosion patches:

$\ell = 136$ in., $g = 3.384$ in., $s = 2.75$ in., and the patch size such that the relative area reduction for one patch is twice the nominal size, that is,

$$a_{ra} = 2\, a_{rn} = 0.18746 \tag{9-12}$$

Note that, except for the patch size, the previously accepted designation for this column would be 3M427P. In fact, it may be convenient to extend the name by two digits designating the ratio of $a_{ra}/a_{rn}$, that is, the name would be 3M427P20.

**Solution Procedure**:

The non-dimensionalized parameters needed for using relevant formulas are:

$$L = \ell/100r = 0.7158, \quad G = g/D = 0.62, \quad \text{and} \quad x = s/D = 0.50$$

With these values, Eqs 8-3, 8-5, 8-6, and 8-1 give $p_{np} = 0.536407$

The <u>actual</u> $a_{ra} = 0.18746$ in Eq. 9-9 gives $C_p = 0.679405$

Then, the relative ultimate load is from Eq. 9-11 $p_{ap} = C_p p_{np} = \mathbf{0.36444}$

Equation 15-18 of Ref. 10 for **pinned ends** is

$$p_{lap} = 1.0 - 2.8876\, a_r + 6.1095\, a_r^3 \tag{9-5}$$

Since the $p_{ln}$ values for use in Eq. 9-2 can be readily computed from these equations in advance because the nominal area reduction is the same for all cases, Eqs. 9-4 and 9-5 can be modified as shown next.

The relative area reduction for one nominal patch is, according to Eq. 9-3 and using the dimensions of the patch,

$$a_m = \frac{A_m}{A} = \frac{a+c}{2A}(t-t_p) = 0.09373 \tag{9-6}$$

Then the values computed from Eqs. 9-4 and 9-5 equations are

$$p_{lnf} = 0.8877337 \quad \text{and} \quad p_{lnp} = 0.734377 \tag{9-7a,b}$$

These values remain constant in application of Eq. 9-2. It is then convenient to divide Eqs. 9-4 and 9-5 by these $p_{ln}$, respectively, to produce the **correction factors** $C_f$ and $C_p$ for direct use in Eq. 9-2 as described in the next Subsection.

For **fixed ends**,

$$C_f = C_f(a_r) = \frac{p_{laf}}{p_{lnf}} = 1.13977 - 1.50222\, a_r + 1.28532\, a_r^3 \tag{9-8}$$

For **pinned ends**,

$$C_p = C_p(a_r) = \frac{p_{lap}}{p_{lnp}} = 1.36170 - 3.93204\, a_r + 8.31930\, a_r^3 \tag{9-9}$$

Figure 9-1 shows the plots of $C_f$ and $C_p$ against $a_r$ according to these equations. It is notable that increasing the value of $a_r$ leads to a much more dramatic reduction in strength for pinned end conditions than for fixed, and, as should be expected, the curves intersect at $a_r = a_m$. A more general presentation of these relationships is given in Fig. 9-2 where the abscissa is nondimensionalized with respect to $a_m$ and thus stands for the ratio of the actual area reduction to the nominal ($a_{ra}/a_m$).

## 9.2 Methodology for Considering Patch Size

Formulation of the procedure for considering the effect of patch size and the details of application are described next.

### 9.2.1 Computation of $p_n$ ($p_{nf}$ and $p_{np}$)

Assume that the patches are of the nominal size and compute the relative ultimate load $p_n$ according to the formulas in Chapters 7 or 8 as follows.

For fixed end conditions, compute $p_{nf}$ by using Eqs. 7-10, 7-12 and 7-11 of Chapter 7.

For pinned end conditions, compute $p_{np}$ by using Eqs. 8-3 to 8-8 and 8-1 of Chapter 8.

### 9.2.2 Computation of $p_l$ ($p_{laf}$, $p_{lnf}$ and $p_{lap}$, $p_{lnp}$)

The effect of the size of one corrosion patch was studied in a previous project.[10] It was found that the most dominant parameter affecting the strength was the area reduction of the cross section by the corrosion patch $A_r$. For the "Constant-Thickness Patch" model used in this project, the area reduction can be computed from Eq. 9-3.

$$A_r = \frac{a+c}{2}(t-t_p) \qquad (9\text{-}3)$$

For a general case, $A_r$ can be computed by using the "Linear Segments" model described in Paragraph 1.2.2.4.

Then, with the relative area reduction $a_r$ defined by Eq. 9-1, the formulas of Ref. 10 can be used for computing the $p_l$ values.* For convenience, these equations are repeated here.

Equation 15-19 of Ref. 10 for **fixed ends** is

$$p_{laf} = 1.0 - 1.3186\, a_r + 1.1277\, a_r^3 \qquad (9\text{-}4)$$

---

* An alternative formulation of the effect of patch size can be made by using the net (remaining) area $A_n$=A-$A_r$ (or $a_n$=1-$a_r$), instead of the area reduction, and formulas from Ref.10.

# 9. EFFECT OF PATCH SIZE

## 9.1 Introduction

Since the emphasis in this project was mainly on the effect of the column length ($\ell$) and of the position of the patches relative to each other (**g** and **s**), the test and FE specimens had the patches of the same dimensions except for very few that had their patch thickness different from $t_p$=0.03 in. An approximate method is proposed in this Chapter for considering the effect of patches of other sizes, that is, the same among themselves but different from the size researched so far.

To facilitate further discussion, the following terminology is introduced:

Word '<u>size</u>' indicates the reduction of the cross-sectional area due to one corrosion patch, $A_r$, or the relative area reduction, $a_r$.

$$a_r = \frac{A_r}{A} \tag{9-1}$$

Word '<u>nominal</u>' designates the size analyzed in this report and '<u>actual</u>' a different size. Letters 'n' and 'a' are used as subscripts when needed to indicate these meanings.

It is proposed that the ultimate load of columns with three corrosion patches be computed by assuming the patches to be of <u>nominal</u> size, and, then, the computed value adjusted by the ratio of the ultimate loads of columns with a <u>single</u> patch (the numerator for the <u>actual</u> patch size and the denominator for the <u>nominal</u> patch size).

$$p_a = p_n \frac{p_{1a}}{p_{1n}} \tag{9-2}$$

Where $p_a = P_{ua}/P_y$ is the nondimensionalized ultimate load for <u>three</u> patches of <u>actual</u> size.

$p_n = P_{un}/P_y$ is the nondimensionalized ultimate load for <u>three</u> patches of <u>nominal</u> size.

$p_{1a}$ is the nondimensionalized ultimate load for <u>one</u> patch of <u>actual</u> size.

$p_{1n}$ is the nondimensionalized ultimate load for <u>one</u> patch of <u>nominal</u> size.

Subscript 'f' or 'p' would be added to the items in Eq. 9-2 to differentiate between the columns with fixed or pinned ends, respectively.

$G = G4 = \frac{g}{D} = 0.61527$ $\qquad$ $L = (\ell/100r) = 0.71526$ $\qquad$ $s/D = 0.5$

Substitution of these G and L into Eqs 8-3, 8-5 and 8-6 results in the following values of a1 to a3:

$a1 = 0.72207$ $\qquad$ $a2 = -0.23567$ $\qquad$ $a3 = 0.69602$

For s/D=0.5, the computed ultimate load from Eq. 8-1 is then

$$p_c = P_{uc}/P_y = 0.53640$$

Compared to the original value (from ABAQUS) of $p_g = 0.532$, this gives a ratio $p_c/p_g = 1.01$, that is, an error of only 1.0%.

## 8.4 Accuracy of Approximation

### 8.4.1 Graphical Comparison

An illustration of the accuracy of the proposed formulas is shown in Fig.8-8. As in Fig. 7-4, plotted are the ratios **($p_c/p_g$)** of the ultimate loads **$p_c$** computed from the formulas and the loads given in the database **$p_g$**. The points are arranged in groups according to the values of the circumferential spread in non-dimensionalized form as marked by G1, G2, G3 and G4 for **g** = 1.60, 2.68, 3.055, 3.384 in., respectively. All the points clearly fall within 10% of the reference line for perfect fit, **($p_c/p_g$)**=1.0, and only a few exceed 5%.

### 8.4.2 Numerical Accuracy

The numerical indicators of accuracy according to Eqs. 7-13 to 7-16 are listed next, and they confirm the good correlation shown in the figure.

Root-Mean-Square (Eq. 7-13) RMS = 0.0109
Coefficient of Variation (Eq. 7-14) COV% = 2.080%
Relative-Error-Average (Eq. 7-15) REA% = 1.715% (8-9)
Coefficient of Determination (Eq. 7-16) $R^2$ = 1.0008

## 8.5 Strength Computation for a Pinned-End Column

Once the values of parameters a1, a2 and a3 are obtained from Eqs. 8-3, 8-5 and 8-6 for a given set of G and L, the ultimate load can be computed from Eq. 8-1 for the desired longitudinal patch spacing s (x=s/D). A sample illustration of the approximations is shown in Fig. 8-9 for Specimens 3M4**P3 [3 patches, length $\ell$=136 in., g=3.384 in., s=0 to 11.0 in.(x=s/D=0 to 2.0), Pinned ends].

For example, for s=2.75 in. (x=0.5), the specimen designation becomes 3M427P, and the controlling non-dimensionalized values are

## 8.3 Approximation of Parameters a2 and a3

The 4-term format of Eq. 8-3 was also found to be suitable for parameters a2 and a3 as shown by Eqs. 8-5 and 8-6 in terms of constants $c_i$ and $d_i$.

$$a2 = c1 + c2*G + c3*L + c4*G^{c5}*L^{c6} \tag{8-5}$$

$$a3 = d1 + d2*G + d3*L + d4*G^{d5}*L^{d6} \tag{8-6}$$

Separate regression analyses of the values of a2 and a3 computed in Section 8.1 resulted in the sets of constants for $c_i$ and $d_i$ given in Eqs 8-7 and 8-8, respectively.

$$c = \begin{Bmatrix} c_1 \\ c_2 \\ c_3 \\ c_4 \\ c_5 \\ c_6 \end{Bmatrix} = \begin{Bmatrix} -0.31373 \\ 0.11653 \\ 0.006215 \\ 0.032152 \\ -0.20 \\ 8.70 \end{Bmatrix} \tag{8-7}$$

$$d = \begin{Bmatrix} d_1 \\ d_2 \\ d_3 \\ d_4 \\ d_5 \\ d_6 \end{Bmatrix} = \begin{Bmatrix} -0.55364 \\ 1.71793 \\ -0.03734 \\ 1.11807 \\ 2.590 \\ 1.106 \end{Bmatrix} \tag{8-8}$$

Figures 8-4 and 8-5 are the plots of the effect of G and L on parameter a2. These figures are analogous to Figs. 8-2 and 8-3 for a1, and Figs. 8-6 and 8-7 for parameter a3.

A four-stage procedure was followed to implement this approximation. In the first stage, parameters a1, a2 and a3 were determined by nonlinear regression analysis of Eq.8-1 for each combination of G and L. This process resulted in three sets of 15 values of constants, one set for each parameter. The next three stages were to determine a suitable approximation for each of the three parameters (a1, a2 and a3) as a function of G and L.

## 8.2 Approximation of Parameter a1

Figures 8-2 and 8-3 show typical plots of the parametric study of the effects of G and L on parameter **a1**. Figure 8-2 gives the effect of variable G for the following five values of length: T($\ell$/100r=0.0658), S($\ell$/100r=0.4737), M($\ell$/100r=0.7158), I($\ell$/100r=0.8836) and L($\ell$/100r=1.0526). Figure 8-3 has the length ($\ell$/100r) as the variable and the plots are for three specific values of G: G2, G3 and G4 (**g** = 2.68, 3.055 and 3.384 in.).

From the appearance of these plots and after many trials, it was concluded that a suitable short approximation would be of a hyperbolic-paraboloidal type, and the 4-term nonlinear function of Eq. 8-3 with six $b_i$ constants was selected.

$$a1 = b1 + b2*G + b3*L + b4*G^{b5}*L^{b6} \tag{8-3}$$

Nonlinear regression analysis of the 15 **a1** values from the previous section gave the values of constants **b**(b1 to b6) listed in Eq. 8-4.

$$b = \begin{Bmatrix} b_1 \\ b_2 \\ b_3 \\ b_4 \\ b_5 \\ b_6 \end{Bmatrix} = \begin{Bmatrix} 0.32210 \\ 0.67162 \\ -0.01513 \\ -0.06785 \\ 0.91 \\ 8.61 \end{Bmatrix} \tag{8-4}$$

Figures 8-2 and 8-3 indicate the original data with markers and solid lines and the approximations of **a1** computed from Eqs. 8-3 and 8-4 with dashed curves.

# 8. STRENGTH OF PINNED-END COLUMNS WITH THREE CORROSION PATCHES

In Chapter 7, the strength formula for columns with fixed ends (Eq. 7-9) was obtained by linear regression analysis using a coordinate function from a combination (via direct product) of the coordinate functions for the variables affecting column strength. Nonlinear analysis was used only for the denominator of the second regressor of the coordinate function for column length (the **tanh** function in Eq. 7-8). A quite different approach was used for columns with pinned ends. Four stages of nonlinear regression analysis were used to arrive at the strength formula as discussed in the following sections.

## 8.1 Effect of Longitudinal Patch Spacing s

Figure 8-1 illustrates a typical relationship between **p** (Pu/Py) and x (s/D) for pinned-end columns with three corrosion patches and a particular set of values for G and L (g=2.68 in., $\ell$=200 in.). The relationship is characterized by an initial short portion of positive curvature, which climbs up and changes to a long climbing portion of negative curvature that asymptotically approaches a horizontal line.

A number of different approximation models (coordinate functions) were tried out in the search for a short yet accurate model. The two-term approximation of Eq. 8-1 was found to be the most suitable although it is linear only in two parameters (a1 and a2) with the third parameter (a3) embedded as a denominator in the argument of **sech**.*

$$p = \frac{P_u}{P_y} = a1 + a2 * \mathbf{sech}\left(\frac{s/D}{a3}\right) \tag{8-1}$$

Where **sech** is a hyperbolic cosecant defined by Eq. 8-2 as a function of an argument, say, of y.

$$\mathbf{sech}(y) = \frac{2}{(e^{y} + e^{-y})} \tag{8-2}$$

Parameters a1, a2 and a3 are functions of both G and L, and they become constants for a particular set of G and L.

---

*a1, a2 and a3 are used for the subscripted $a_1$, $a_2$ and $a_3$ in order to have the same notation in text, tables and figures.

These values are in good agreement with the plot in Fig. 7-4. In fact, one can almost guess the value of REA% from the figure to be about 2.5%.

## 7.5 Strength Computation for a Fixed-End Column

The procedure formulated above is illustrated here by applying it to Specimen 3M416F3 of the database (Table 6-2). The specimen designation means the following data:

3 patches
M (“medium” length $\ell$ =136 in., $L = \ell/100r = 0.715259.$)
4 (circumferential spread g=3.384 in., $G = G4 = g/D = 0.62$)
16 (longitudinal spacing $s=1.65$ in., $x=s/D=0.30$ ) (7-18)
F (fixed ends)
3 ($t_p$=0.03 in.)

Introduction of the above values of s/D, G and L into Eq. 7-10 gives the one-row combined **coordinate function** listed in Eq. 7-19.

$$\mathbf{H}_{sgL} = \left[ \begin{array}{cccccc} 1.0 & 0.82171 & 0.62 & 0.50946 & 0.58779 & 0.48291 \\ 0.36443 & 0.29945 & -0.30902 & -0.25392 & -0.19159 & -0.15743 \end{array} \right] \qquad (7\text{-}19)$$

The matrix product of this coordinate function and of the constants **C** of Eq.7-12 gives the non-dimensionalized ultimate load **p** of the specimen.

$$p = [\mathbf{H}_{sgL}] \{\mathbf{C}\} = 0.52828$$

The ultimate load is, then,

$$P_u = p\,P_y = (0.52828)(86.799) = 45.854 \text{ kips}$$

This $P_u$, compared with the ABAQUS value $P_g = 45.06$ kips, shows the relative percentage error to be only **re%** = 1.76%.

respectively. All the points clearly fall within 10% of the reference line for perfect fit, **($p_c/p_g$)**=1.0, and only a few exceed 5%.

### 7.4.2 Numerical Accuracy

Root-Mean-Square **RMS** (the same as Standard Deviation $\sigma_n$) is a commonly used indicator of the accuracy of an approximation.

$$\text{RMS} = (\sigma_n) = \sqrt{\frac{\sum_{i=1}^{n}(p_{ci}-p_{gi})^2}{n}} \tag{7-13}$$

However, since RMS has a meaning only when compared with the approximated values, a better intuitively graspable indicator of the accuracy is the Coefficient of Variation in percent, that is, RMS given as a percentage of the average of the approximated values.

$$\text{COV\%} = \frac{\text{RMS}}{\left(\frac{1}{n}\sum_{i=1}^{n} p_{g_i}\right)} * 100 \tag{7-14}$$

Another, even more intuitively meaningful, indicator is the average of the relative errors in percent, the Relative-Error-Average REA%.

$$\text{REA\%} = \frac{1}{n}\sum_{i=1}^{n} \text{abs}\left(\frac{p_c - p_g}{p_g}\right)_i * 100 = \frac{1}{n}\sum_{i=1}^{n}\left|\frac{p_c}{p_g} - 1.0\right|_i * 100 \tag{7-15}$$

The Coefficient of Determination $R^2$ also indicates how closely the approximation model is to the given data.

$$R^2 = \frac{\sum_{i=1}^{n} p_{ci} p_{gi}}{\sum_{i=1}^{n} p_{gi}^2} \tag{7-16}$$

The values of these indicators of accuracy for the approximation formulas of fixed-end columns with three corrosion patches are the following:

| | | |
|---|---|---|
| Root-Mean-Square | RMS | = 0.0182 |
| Coefficient of Variation | COV% | = 2.892% |
| Relative-Error-Average | REA% | = 2.411% |
| Coefficient of Determination | $R^2$ | = 0.999 |

(7-17)

$$G\cos\left(2\pi\frac{s}{D}\right) \qquad G\cos\left(2\pi\frac{s}{D}\right)\tanh\left(\frac{L}{0.13+2.20\left(0.17+{}^{s}\!/\!_{D}\right)^{2}}\right)\Big] \tag{7-10}$$

With this coordinate function, the formula for the ultimate strength of fixed-end tubular columns with three corrosion patches is defined by Eq. 7-11.

$$\mathbf{p} = \frac{\mathbf{P_u}}{\mathbf{P_y}} = \mathbf{H_{sgL}}\,\{\mathbf{C}\} \tag{7-11}$$

where C is the column matrix of constants listed in Eq. 7-12.

$$C = \begin{Bmatrix} 0.8546 \\ -0.6120 \\ -0.2100 \\ 0.6455 \\ 0.1190 \\ -0.0456 \\ -0.2346 \\ 0.0769 \\ 0.0210 \\ -0.3400 \\ -0.0217 \\ 0.5820 \end{Bmatrix} \tag{7-12}$$

These constants were computed by using linear regression analysis of the whole database for fixed-end specimens with three corrosion patches.

## 7.4 Accuracy of Approximation

### 7.4.1 Graphical Comparison

An illustration of the accuracy of the proposed formulas is shown in Fig.7-4. Plotted are the ratios ($\mathbf{p_c}/\mathbf{p_g}$) of the ultimate loads $\mathbf{p_c}$ computed from the formulas and the loads given in the database $\mathbf{p_g}$. The points are arranged in groups according to the values of the circumferential spread in non-dimensionalized form as marked by G1, G2, G3 and G4 for **g** = 1.60, 2.68, 3.055, 3.384 in.,

### 7.2.5 Effect of Yield Stress $F_y$

Yield stress $F_y$ had a linear effect on the ultimate capacity as shown in Figs. 6-16 and 6-17. This parameter was also not included in the regression analysis since it is implicitly (and linearly) incorporated into the non-dimensionalized definition of the ultimate load ($\mathbf{p}=P_u/P_y$).

## 7.3 Strength Formula for Fixed-End Columns with Three Corrosion Patches

The strength formula for fixed-end columns was developed by conducting multi-variable regression analysis for the three independent parameters G=g/D, x=s/D and L=ℓ/100r.

The coordinate functions of Eqs. 7-8, 7-7 and 7-9 for the three parameters were combined by performing the **direct product** operation as discussed in Section 7.1, and the one-row 12-term (3x2x2=12) **combined coordinate function** $\mathbf{H_{sgL}}$ of Eq. 7-10 was obtained.

$$\mathbf{H_{sgL} = h_s \# h_g \# h_L =}$$

$$= \Big[ \begin{array}{ll}
1 & \tanh\left(\dfrac{L}{0.13+2.20\left(0.17+{}^{s}\!/_{D}\right)^{2}}\right) \\[2ex]
G & G\tanh\left(\dfrac{L}{0.13+2.20\left(0.17+{}^{s}\!/_{D}\right)^{2}}\right) \\[2ex]
\cos\left(\pi\dfrac{s}{D}\right) & \cos\left(\pi\dfrac{s}{D}\right)\tanh\left(\dfrac{L}{0.13+2.20\left(0.17+{}^{s}\!/_{D}\right)^{2}}\right) \\[2ex]
G\cos\left(\pi\dfrac{s}{D}\right) & G\cos\left(\pi\dfrac{s}{D}\right)\tanh\left(\dfrac{L}{0.13+2.20\left(0.17+{}^{s}\!/_{D}\right)^{2}}\right) \\[2ex]
\cos\left(2\pi\dfrac{s}{D}\right) & \cos\left(2\pi\dfrac{s}{D}\right)\tanh\left(\dfrac{L}{0.13+2.20\left(0.17+{}^{s}\!/_{D}\right)^{2}}\right)
\end{array} \qquad \frac{(7-10)}{[nxtpg]}$$

small number of terms, yet sufficiently accurately. The following 3-term coordinate function was found to adequately represent the relationship:

$$h_s = [\, h_{s1} \quad h_{s2} \quad h_{s3} \,] = \left[ 1 \qquad \cos\left(\pi \frac{s}{D}\right) \qquad \cos\left(2\pi \frac{s}{D}\right) \right] \tag{7-8}$$

### 7.2.3 Effect of Column Slenderness (Length) $L=\ell/100r$

From the plots for fixed-end specimens with various lengths, as shown in Figs. 6-8a and 6-8b, it was observed that a parabolic-type coordinate function might be suitable to approximate the curves. Several coordinate functions were tried, including 3-term parabolic functions, cosine functions and hyperbolic functions, and the closest approximation was found to be the hyperbolic tangent function. As can be seen in Fig. 7-2 for the most severe case when s=0.0 (Specimen 3M200F3), the **[1 tanh(L)]** coordinate function was very promising. However, a modification was necessary to include the effect of s within the **tanh** term. A separate nonlinear side study was performed to make this adjustment. Finally, the following 2-term coordinate function of length was obtained:

$$h_L = [\, h_{L1} \quad h_{L2} \,] = \left[ 1 \quad \tanh\left( \frac{L = \ell/100\,r}{0.13 + 2.20\left(0.17 + s/D\right)^2} \right) \right] \tag{7-9}$$

Figure 7-3 shows the application of this coordinate function to the specimens of the same **g** distance but variable **s** distances. The relative percentage error was calculated to be ~1.5%, supporting the suitability of this 2-term coordinate function.

### 7.2.4 Effect of Patch Thickness $t_p$

As discussed in Subsections 6.2.4 and 6.3.4, the thickness of the constant-thickness portion $t_p$ has no noticeable effect on the ultimate load for the specimens with either fixed or pinned ends. Since the effect was found to be constant, this parameter was not included in the regression analysis.

$$F(x,y,z) = \left[H_{xyz}\right]\begin{Bmatrix} c_1 \\ c_2 \\ \vdots \\ c_{12} \end{Bmatrix} = \left[H_{xyz}\right]\{C\} \tag{7-6}$$

Constants {**C**} are computed by the linear regression analysis of the approximation function F(x,y,z) for the values of F in a given database.

## 7.2 Parametric Study for Fixed-End Columns with Three Corrosion Patches

In the parametric study for the specimens with three corrosion patches, coordinate functions were determined for the independent variables. The non-dimensionalized ultimate load $p=P_u/P_y$ was the dependent variable and the non-dimensionalized independent variables were the circumferential spread G=g/D, the longitudinal spacing x=s/D, and the column slenderness $L=\ell/100r$. D is the outside diameter and r is the radius of gyration of the gross column cross section. To obtain the coordinate functions, the relationship between the ultimate load and each individual independent variable was investigated while the values of all other variables were kept constant.

### 7.2.1 Effect of Circumferential Spread G=g/D

As can be observed in Figs. 6-1 and 6-10, a straight-line approximation was sufficient for representing the relationship between the circumferential spread g and the ultimate capacity of the specimens with three corrosion patches. The selected coordinate function for both fixed and pinned end conditions is then

$$h_g = [\ h_{g1} \quad h_{g2}\ ] = [\ 1 \quad G\ ] \tag{7-7}$$

### 7.2.2 Effect of Longitudinal Spacing x=s/D

As discussed in Subsections 6.2.3 and 6.3.3, an S-shaped cosine-type curve appeared to be an appropriate approximation for the effect of longitudinal spacing s on the ultimate strength as shown in Fig. 7-1. Several coordinate functions were tried to approximate this relationship with a

or
$$f(x) = [\, h_1 \quad h_2 \quad h_3 \,] \begin{bmatrix} a_1 \\ a_2 \\ a_3 \end{bmatrix} \tag{7-2b}$$

where the row matrix is the **coordinate function** $h_x$ and the column matrix contains the **constants**. In this example, the elements (regressors) of the coordinate function are: $h_1(x)= 1$, $h_2(x)= x$, and $h_3(x)=\cos(x)$, that is,

$$h_x = h(x) = [\, 1 \quad x \quad \cos(x) \,] \tag{7-2c}$$

After obtaining a suitable coordinate function for each independent variable (parameter), the functions for all variables are combined into one coordinate function H obtained by using the **direct product** matrix operation.[8, 15] As an illustration, the operation of the direct product is defined by Eq. 7-3 for two matrices, e.g., $\mathbf{A}=[a_1 \quad a_2 \quad a_3]$ and $\mathbf{B}=[b_1 \quad b_2]$. Here, symbol "#" denotes the **direct product** operation, and the result is a (1 by 6) row matrix.

$$[\mathbf{A}] \# [\mathbf{B}] = [a_1\mathbf{B} \quad a_2\mathbf{B} \quad a_3\mathbf{B}] = [a_1b_1 \quad a_1b_2 \quad a_2b_1 \quad a_2b_2 \quad a_3b_1, \quad a_3b_2] \tag{7-3}$$

For example, consider three independent variables x, y and z with the corresponding coordinate functions, such as,

$$\mathbf{h}_x = h(x) = [\, hx_1 \quad h_{x2} \quad h_{x3} \,] \tag{7-4a}$$

$$\mathbf{h}_{y.} =.h(y).= [\, h_{y1} \quad h_{y2} \,] \tag{7-4b}$$

$$\mathbf{h}_z = h(z) = [\, h_{z1} \quad h_{z2} \,] \tag{7-4c}$$

The **direct product** of these coordinate functions results in a combined coordinate function which is a row matrix with 12 terms (3x2x2 =12) as illustrated below.

$$\mathbf{H}_{xyz} = \mathbf{h}_x \# \mathbf{h}_y \# \mathbf{h}_z = [h_{x1} \quad h_{x2} \quad h_{z3}] \# [h_{y1} \quad h_{y2}] \# [h_{z1} \quad h_{z2}] =$$

$$\begin{aligned} = [\, & h_{x1} h_{y1} h_{z1} \quad h_{x1} h_{y1} h_{z2} \quad h_{x1} h_{y2} h_{z1} \quad h_{x1} h_{y2} h_{z2} \\ & h_{x2} h_{y1} h_{z1} \quad h_{x2} h_{y1} h_{z2} \quad h_{x2} h_{y2} h_{z1} \quad h_{x2} h_{y2} h_{z2} \\ & h_{x3} h_{y1} h_{z1} \quad h_{x3} h_{y1} h_{z2} \quad h_{x3} h_{y2} h_{z1} \quad h_{x3} h_{y2} h_{z2} \,] \end{aligned} \tag{7-5}$$

The dependent variable $\mathbf{F}(x,y,z)$ is then given as a matrix product of $[\mathbf{H}_{xyz}]$ and a column matrix of 12 constants $c_i$.

# 7. STRENGTH OF FIXED-END COLUMNS WITH THREE CORROSION PATCHES

## 7.1 Multi-Variable Regression Analysis

A multi-variable regression analysis was performed to obtain approximation formulas for the ultimate strength of columns with patch corrosion damage as affected by the following parameters: the number of corrosion patches, the circumferential spread **g**, the longitudinal spacing **s**, the column length $\ell$, the patch thickness $\mathbf{t_p}$, and the yield stress $F_y$ for both fixed and pinned end conditions. The database generated in this project was used as the numerical source for this analysis.

In order to express the ultimate strength in terms of these parameters, the non-dimensionalized ultimate load, $\mathbf{p}=P_u/P_y$, was chosen to be the dependent variable, while the other parameters were used as the independent variables. In general, the results of regression analysis are usually reliable within the range of the database and may be less accurate outside the range.

As the first step in the multi-variable regression analysis, an appropriate approximation function is selected for the effect of each individual independent variable (while other variables are kept constant). The major objective of this selection is to define the effect with as few terms as possible, yet to represent the behavior accurately.

For the convenience of further operations, each approximation function is defined as a matrix product of the **coordinate function** and the column matrix of constants. For example,

$$f(x) = a_1 + a_2 x + a_3 \cos(x) \tag{7-1}$$

would become

$$f(x) = [\ 1 \ \ x \ \ \cos(x)\ ] \begin{bmatrix} a_1 \\ a_2 \\ a_3 \end{bmatrix} \tag{7-2a}$$

The rate of reduction was particularly pronounced for **s** less than the radius of the tube, that is, $s \leq R=2.75$ in. After that, the interaction gradually diminished. The interaction has an **S-shape** type pattern.

For pinned-end columns (Figs. 6-13a and 6-13b), the effect of longitudinal spacing on the ultimate load was of the same pattern as for the fixed-end columns but more pronounced.

### 6.2.5 Effect of Patch Thickness $t_p$

The effect of patch thickness $t_p$ on the ultimate load is illustrated in Figs. 6-14 and 6-15 for long ($\ell$=200 in.) columns with **g**=2.68 in., and fixed and pinned ends, respectively. The following values of $\mathbf{t_p}$ were used: 0.02, 0.03 and 0.04 inches. The variation of the thickness of the constant-thickness portion of patches, $\mathbf{t_p}$, appeared to have no noticeable effect on the ultimate load of the columns. However, this may be the logical consequence of the rather narrow range of the relative area reduction of 0.06 ($a_r$=0.25 to 0.31).

## 6.3 Effect of Yield Stress $F_y$

The effect of the yield stress on the ultimate load was investigated by using the $F_y$ values of 36, 42.11, 50 and 75 ksi. (Note that, the effects of **g**, s, $\ell$ and $\mathbf{t_p}$ were all studied on specimens with the yield stress of $F_y$=42.11 ksi.) Two sets of fixed-end columns with $\ell$=12.5 in. and $\ell$=136 in. and variable longitudinal spacing **s** are plotted in Figs. 6-16 and 6-17, respectively. For both sets, the effect is seen to be directly **linear**. If the plots had been made for the non-dimensionalized load $\mathbf{p}=P_u/P_y$, the curves would have become horizontal lines.

A comparison of Figs. 6-6a and 6-7b, which are for the same specimen of the same length but with different end conditions, shows a sharper drop-down in the post-ultimate range for the pinned-end specimens (Fig. 6-7b) than for the fixed-end specimens (Fig. 6-6b).

### 6.2.2 Effect of Column Length $\ell$

The effect of column length on the ultimate load is plotted in Figs 6-8a and 6-8b for columns with fixed ends. The steady concave type of the relationship is more pronounced for the smaller value of s=0.00 in Fig. 6-8a than for the larger s=3.30 in. in Fig. 6-8b. The effect of column length for specimens with pinned ends is shown in Figs. 6-9a and 6-9b. In this case, the relationship is of a **slightly convex type.**

### 6.2.3 Effect of Circumferential Spread g

As shown in Figs. 6-10 and 6-11, the circumferential spread g had an essentially **linear** effect on the ultimate load for both end conditions. The interaction between the patches due to changes in the **g** spread was more pronounced for **s** values of less than 1.65 inches. However, for the **s** value of 2.75 inches and larger, the interaction between the patches was already insignificant. Therefore, it can be concluded that when the longitudinal spacing **s** is greater than approximately 40% of the diameter, the circumferential spread had relatively small effect on the ultimate load of specimens with three corrosion patches.

### 6.2.4 Effect of Longitudinal Spacing s

The study of the effect of longitudinal spacing for stub-columns (as discussed in Subsection 6.2.3) was extended to longer columns, and only 5 or 6 values of **s** were found to be adequate to represent the behavior sufficiently accurately.

In Figures 6-12a and 6-12b, the ultimate load vs. longitudinal spacing is plotted for the fixed-end columns of different lengths, and values of **g**=3.055 in. and **g**=3.384 in, respectively. The ultimate strength was reduced significantly with the reduction of **s**, especially, for longer columns.

## 6.2 Long Columns with Three Corrosion Patches

### 6.2.1 General Behavior

In order to model long tubular columns for FE analysis, the middle damaged portion was supplemented with beam elements, as described in Subsection 3.3.7 and shown in Fig. 3-16a.

Figures 6-6a and 6-6b show the axial load vs. axial shortening plots for the 200-inch long specimens (3L2*F3 and 3L4*F3) with fixed ends and the patch spread **g** of 2.68 and 3.384 inches, respectively. In these figures, the numbers on the curves stand for the different values of longitudinal spacing. Both groups of specimens exhibit a straight-line initial elastic response and a more or less rapid attainment of the ultimate load after deviation from this initial straight line. The behavior in the post-ultimate range, however, shows considerable variation among the specimens; the commonly encountered gradual reduction in strength for specimen with **s**=2.20 to 3.30 or 4.40 inches, and a rapid drop-off or even reversal for specimens with **s**=4.40 (**g**=2.68 in.) and **s**=Infinity.

Very unusual behavior was exhibited by the specimens with **s**=0, 1.10 and 1.65 inches, for which, after reaching a peak, the load gradually increased to a second peak in some of the cases, e.g. 3L211F3 in Fig. 6-6a, to a higher level than the first peak. To understand this unexpected behavior, a study of using different types of elements was made as described in Section 3.5. A plausible explanation for this behavior appears to be the mathematical (rather than physical) over-constraining by Multi-Point Constraints under large post-ultimate deformations in the high in-plane shear areas between the patches where a very refined shell mesh was used. In any case, the ultimate load value for such specimens was taken to be the first peak after which the drop-down was observed.

Figures 6-7a and 6-7b show the axial load vs. axial shortening behavior of specimens with pinned ends for two different lengths, 90 and 200 inches, respectively. It can be seen that there was a sharper drop-down in the post-ultimate range as the column length was increased, in particular, for the 200-inch long columns. The long specimens ($\ell$=200 in.) even show a reversal behavior of the curves (e.g., 3L244P3 in Fig. 6-7b).

As shown in Fig. 6-2 for the pinned-end specimens, the ultimate load increased with an increasing **g**. This increase was more pronounced for the lower values of the longitudinal spacing s. Similarly to the pinned-end specimens, the effect of **g** on the ultimate load was also **linear**.

### 6.1.3 Effect of Longitudinal Spacing s

The relationship between the longitudinal spacing of patches and the ultimate load for specimens with three patches is plotted in Figs. 6-3 and 6-4 for two different **g** values, $g_1$=1.60 and $g_2$=2.68 inches, respectively. When the longitudinal spacing **s** was equal to 2.00 inches with the spread of $g_1$=1.60 inches as shown in Fig. 6-3, the interaction between the patches was minimal, and the specimens behaved as is if there were only two patches. However, as shown in Fig. 6-4, for the specimens with **g** greater than 2.68 inches, the ultimate load curves approached asymptotically the results of the two-patch specimens as **s** grew to 4.40 inches and beyond.

For the pinned-end specimens, the ultimate strength was significantly reduced (by ~40%) when the third patch was introduced. On the other hand, this reduction was only ~15% for the fixed-end specimens.

The specimens with both fixed and pinned end conditions showed similar **S-shaped** behavior.

### 6.1.4 Effect of Patch Thickness $t_p$

To investigate the effect of the reduction of area, which was found to be the most dominant parameter on the strength in the previous study [10], the discretization models for specimens with $t_{p3}$=0.03 inches were modified to have the patch thickness of $t_{p2}$=0.02 and $t_{p4}$=0.04 inches. The results are plotted in Fig. 6-5a for the specimens with fixed ends, and in Fig. 6-5b for the specimens with pinned ends. It can be seen that the effect of the patch thickness on the ultimate load is essentially **linear** with a slight convex curvature.

# 6. TUBULAR COLUMNS WITH THREE CORROSION PATCHES

As shown in Fig. 3-12, the specimens with three corrosion patches were modeled by having two corrosion patches at the mid-length and the third patch straddling them and offset longitudinally. Similarly to the columns with two corrosion patches, the effect of the following parameters on the ultimate load was investigated: the circumferential spread **g**, the longitudinal spacing **s**, the length of the column $\ell$, the patch thickness $\mathbf{t_p}$, the yield stress $F_y$, and the fixed and pinned end conditions. ABAQUS was used to compute the ultimate loads of the specimens with various combinations of these parameters.

Table 6-1 lists the properties and ultimate loads of all the specimens with three corrosion patches contained in the database. The table has three parts. The first contains the specimens of the database used in the development of the formulas in Chapters 7 and 8. The second part contains the specimens with the patch thickness different from the nominal $\mathbf{t_p}$=0.03 inch used in part one. Part three has the specimens that had the yield stress different from the value of $F_y$=42.11 ksi used in the first and second parts.

## 6.1 Stub-Columns with Three Corrosion Patches

### 6.1.1 General

To examine the effect of the circumferential spread **g** on the ultimate strength of the columns with three corrosion patches, the middle corrosion patch was placed between the outer two patches at the center-to-center distances of $g_1$=1.60, $g_2$=2.68, $g_3$=3.055 and $g_4$=3.368 inches as illustrated in Fig. 3-13. As described in Subsection 3.3.6, the longitudinal spacing was set to vary between 0.00 to 4.40 inches. The effect of the patch thickness was also studied.

### 6.1.2 Effect of Circumferential Spread g

Figure 6-1 illustrates that circumferential spread **g** had very small effect on the ultimate load of fixed-end specimens and that the effect was **linear**.

In Figure 5-15, the corresponding eccentricity is given in the right top corner as **e**=0.209 in. For this value, the plotted curves approximately correspond or are below the load value for one-patch damage.

It is planned for future work to use the eccentricity defined by Eq. 5-1 in re-analyzing and amplifying the database for two-patch corrosion damage needed in the parametric study for developing design formulas.

alternate deformation patterns of equilibrium that may develop under a lower load. This way, the point halfway between the patches is subjected to higher average stresses than at the patches with the result that the ultimate load is more directly limited by failure (full yielding or local buckling) in this undamaged area rather than the strength at the corrosion patches. This effect becomes more pronounced as the circumferential spread **g** is increased and the difference between the strains/stresses at the mid-point and the patches grows in significance. Unfortunately, this deficiency of program ABAQUS was not recognized at the time the bulk of finite-element analysis was performed.

On the other hand, real columns are not geometrically perfect, and the overall deformation of the column would be controlled by the weaker patch forcing the column to deform in a generally unsymmetrical pattern leading to an ultimate load which definitely cannot be higher than the ultimate load of a column with a single corrosion patch.* A common technique to simulate this situation and force the computer program away from the skew-symmetric deformation pattern is to introduce either initial imperfections or a small lateral load.

The question is how much such initial out-of-straightness or lateral load should be? As indicated earlier in Fig. 5-15, the ultimate load strongly depends on the value of **e**, and a parallel study using a lateral load resulted in similar plots.

Since the purpose of this work is to develop a procedure for practical application by engineers, a conservative value of out-of-straightness can be taken to be the maximum permitted by the API specification for fabrication of offshore structures.[3] The simplified value of this limitation is given by Eq. 5-1.

$$\frac{e}{\ell} = \frac{1}{960} \text{ or } \approx \frac{1}{1000} \tag{5-1}$$

Where, $e$ is the out-of-straightness (or the load eccentricity in the damaged area),

and $\ell$ is the member length.

---

* Strictly speaking, these observations fully apply only if the ends have 'ball' bearings, that is, rotation of the ends is not prevented in ANY direction. These are actually the end conditions that were used as more conservative in the FE analysis of this research. The effect of 'pinned' end conditions, when the rotation about the y-axis is free but inhibited about the x-axis, needs further investigation.

## 5.5 Effect of Patch Thickness $t_p$

The effect of the thickness of the constant-thickness portion of a patch $\mathbf{t_p}$ on the ultimate load is shown in Fig. 5-14 for a short pinned-end specimen ($\ell$=90 in.) with. The change in the patch thickness did not seem to have any significant effect. This behavior was somehow unexpected since the ultimate load was anticipated to be higher when the patch thickness was increased. However, this behavior is apparently the result of the relatively narrow range of the relative area reduction for the variation in $\mathbf{t_p}$ studied here. ($0.084 \leq \mathbf{a_r} \leq 0.10$ for one patch or $0.17 \leq \mathbf{a_r} \leq 0.21$ for two patches in a cross section)

## 5.6 Effect of Initial Out-of-Straightness (Load Eccentricity e in Damaged Area)

It should be noted that the specimens with one corrosion patch damage represent a special case of the columns with two corrosion patches when the two patches are far enough from each other not to interact. Normally, it would be expected that the ultimate load for this case should be higher than when there are two patches. Yet, paradoxically, many ultimate loads listed in Table 5-1 are higher than for the one-patch solutions, especially, for larger values of **g**.

An example of the variation of the ultimate load with an increasing load eccentricity **e** (in the direction of one of the patches) is shown in Fig. 5-15 for pinned-end columns with $\ell$=200 in., g=5.36 in.(G5), and three values of **s** (0.0, 6.6 and 8.8 in.) (specimen series 2L5**Pe). The maximum load at zero eccentricity rapidly drops off with the growth in eccentricity. For example, Specimen 2L566Pe (s=6.6 in.) loses 29% of its capacity (from **p**=0.591 to 0.419) as **e** increases from 0.0 to 0.9 in. The horizontal line at **p**=0.549 gives the capacity of a straight column with one patch. This value is clearly below the capacities of the two-patch columns when **e**=0. This paradoxical result is the consequence of the inability of ABAQUS to properly analyze such columns with skew-symmetric pattern of damage.

A short explanation for this phenomenon is that the perfectly skew-symmetrical damage pattern leads to perfectly skew-symmetrical deformations under an increasing load so that the stresses in the two patches are skew-symmetrically identical since the program does not search for

When the spacing was equal to 6.60 inches, the interaction between the two patches almost completely disappeared, and the specimens were expected to behave as if they had only one patch.

Figure 5-9 shows the contour plot of longitudinal stresses on the outside surface of a specimen with strong interaction between the individual patches. The areas of surface yielding in tension due to large wall distortions near and within the corrosion patches are clearly indicated by the lighter colors and are labeled with "Tension". The compressive stresses are darker and are labeled with "Compression".

It can be observed that an **S-shaped** curve with a small slope at the beginning and asymptotically becoming horizontal at the end would be convenient to approximate the effect of longitudinal spacing.

## 5.4 Effect of Column Length $\ell$

The effect of column length on the ultimate strength of tubular columns with two corrosion patches with different longitudinal spacing **s** and circumferential spread **g** is examined in this Section. Figures 5-1 and 5-2 show that there is practically no effect of the patches on the behavior of the columns in the elastic range for the same column length; they all fall onto essentially the same straight line for different **s** and **g** distances. However, as the loads are increased, large deformations are more pronounced, and there is a sharper drop-down in the post-ultimate range.

The ultimate load vs. column length is plotted in Figs. 5-10 and 5-11 for the fixed-end specimens with different values of **g** and the longitudinal spacing values of s=1.10 in. and s=6.60 in., respectively. It appears that a concave hyperbolic-type curve would be appropriate for approximating the behavior. On the other hand, a convex parabolic function appears to be more suitable to represent the effect of column length on ultimate capacity of specimens with pinned ends as shown in Figs. 5-12 and 5-13.

fect of this omission (briefly discussed in Section 5.6) showed that the errors were of the order of 15% and may be accepted for the initial parametric study presented in this chapter.

Figure 5-1 shows the plots for the axial load vs. axial shortening relationships of the two-patch stub-column specimens with fixed ends and **g** distance of 2.68 inches for different values of longitudinal spacing s (2T2*P3). Figure 5-2 shows the same information for the pinned-ended specimens. It can be seen that the curves for the pinned-end specimens had a steeper drop-down in the post-ultimate range than for the fixed-ended specimens.

## 5.2 Effect of Circumferential Spread g

The effect of the circumferential spread **g** on the ultimate strength of specimens with pinned ends and various longitudinal spacing values for sTub ($\ell$=12.5 in.) and Short ($\ell$=90 in.) specimens is shown in Figs. 5-3 and 5-4, respectively. Figures 5-5 and 5-6 show the effect of the **g** distance on the ultimate capacity of specimens with fixed ends, respectively. The plots for all cases for both end conditions have significant similarity in being essentially straight lines.

As the patches were moved closer to each other over the circumference, the interaction between the two patches was more pronounced. Correspondingly, earlier yielding or local buckling occurred in high stress areas, resulting in a reduced ultimate load. The types of the curves for both end conditions were quite similar.

For the specimens with two corrosion patches, the effect of circumferential spread **g** on the ultimate capacity was found to be quite linear for smaller longitudinal spacing ($s<R$) and slightly parabolic for larger s values.

## 5.3 Effect of Longitudinal Spacing s

Figures 5-7 and 5-8 illustrate the effect of the longitudinal spacing s on the ultimate capacity for the specimens with **g**=3.055 in. of different lengths for fixed and pinned ends, respectively.

# 5. TUBULAR COLUMNS WITH TWO CORROSION PATCHES

## 5.1 General

This chapter presents an initial study of the effect of the longitudinal spacing **s**, the circumferential spread **g**, the column length $\ell$ and of the patch thickness $\mathbf{t_p}$ on the ultimate capacity of columns with two corrosion patches for both fixed and pinned end conditions. The specimens were modeled by having the two patches straddle the mid-length point of the column as shown in Figs. 3-10 and 3-11. Information on the FE modeling is given in Subsection 3.3.5.

The properties and ultimate strengths of the specimens used in this study are listed in Table 5-1. The table has three parts. The first part lists the specimens used in the principal parametric study. The second part gives the strengths of the specimens with the longitudinal spacing s large enough ("infinite") so that there is no interaction between the two patches and the column fails as if it had only one patch. Thus, the capacity is controlled only by the length and the end conditions (fixed or pinned) and independent of the circumferential spread g. Therefore, in a parametric study, these cases would be inserted into the first part of the table for each set of length and circumferential spread g. In both of these parts, the load is applied concentrically (zero load eccentricity). Part three of the table lists the cases in which the load eccentricity 'e' in the damaged area ('out-of-straightness') is not zero. The magnitude of the eccentricity is indicated by 'eN' in the 7th and 8th places in the specimen name. Here, 'N' is equal to the eccentricity in 1/10 of an inch, e.g., 'e3' means e=0.3 in.

It was later realized that many results were not as accurate as they would have been had a more refined modeling, more accurate internal constraint conditions and initial geometry been used. Although the data in Table 5-1 are adequately accurate for the general discussion given in this chapter, the results need rerunning under improved conditions and the table significantly amplified for a proper parametric study and the development of design formulas. Specifically, there is a need to impose initial load eccentricity for all cases in order to overcome the limitations of the computer program in handling the skew-symmetric nature of the damage geometry. A sample study of the ef-

# 4. TUBULAR COLUMNS WITH ONE CORROSION PATCH

In the preceding research on the ultimate capacity of tubular columns with one corrosion patch, only the effect of the size of the patch was investigated.[10] There was no specific consideration of the column length. The effect of length seemingly contributed to the scatter of the results, whereas the most dominant parameter was found to be the **relative reduction of the area,** $\mathbf{a_r} = A_r / A$ (or the relative net area $\mathbf{a_n} = A_n/A$). (This is discussed in Subsection 1.2.1.3.) In the current project, the scope was extended to examine the effect of column length for both fixed and pinned ends.

The FE analysis of columns with one corrosion patch was performed by using full-tube rather than one-quarter-tube models, as was done previously. (The reasons for this are stated in Section 3.3.4.) Figure 4-1 shows a sample contour plot of longitudinal stresses on the outside surface for the patch area of a specimen with one patch.

The axial load vs. axial shortening relationships for different lengths are plotted in Figs. 4-2 and 4-3 for fixed and pinned end conditions, respectively. Notable is that the curves of the post-ultimate behavior for the specimens with fixed ends were significantly flatter than for the specimens with pinned ends.

In Figs. 4-2 and 4-3, the reduction of the ultimate capacity with increasing length is less significant for the fixed-ended specimens than for the pin-ended. This is more clearly illustrated in Fig. 4-4 where the ultimate load is plotted against the length. For example, when the length of the fixed-end column was increased 16 times, the reduction in strength was only ~8%, but it was ~25% for the pinned-end column.

For the 20-node brick element with one layer, the stress distribution within the column was meaningless. For the purpose of improving this behavior, the specimens with 2,3,4 and 8 layers were also generated. Figure 3-28e shows the specimen with 6 longitudinal segments and 4 layers.

Except for the 20-node brick element with 2 layers, the multi-layering analysis resulted in the curves lumped together in the post-ultimate range and having essentially the same ultimate load values but falling way above the shell elements and the rigid-plastic analysis results as shown in Fig. 3-31. The ultimate load values of specimens with multiple layering were very close to the shell and rigid-plastic results as listed in Table 3-5. However, when compared to the shell elements, the computer time increased greatly due to the increase in the total number of degrees of freedom in the specimens modeled with brick elements.

### 3.5.6 Summary and Conclusions

The summary of the characteristics and ultimate loads of the beam-columns with fixed ends is given in Table 3-5. The application of the 8-node brick elements was limited, and could only be used with a high refinement of the mesh at critical locations. The brick elements with 20 nodes and two layers might be used together with a refined mesh. However, the computational/modeling effort would increase significantly without giving any real benefit in comparison with the shell elements. It was concluded that the 9-node shell elements, used in the original specimens with multiple corrosion patch damage, provided sufficiently accurate results. Thus, the 9-node shell element was kept through the study.

It can be surmised that the ambiguous behavior of the long specimens with three corrosion patches in the post-ultimate range was not caused by the selection of element types. However, it was noticed that in some large deformation patterns in the post-ultimate range there were nodes *moving through each other*. Such behavior, although physically impossible, is mathematically possible in ABAQUS. This may be the logical explanation for the appearance of the second peak observed in Fig. 3-27.

The final conclusion is that the first peak should be considered as the ultimate load.

the relative thickness of the segments with respect to the surface size decreased dramatically and ABAQUS produced unrealistic jumps and drop-downs, as shown in Fig. 3-32 (curves labeled as *3br20thin* and *4br20thin*). Once again, this showed that mesh refinement does not always lead to more accurate results.

The next step was to refine the lengths of the thin segments by putting sets of very short elements at the locations of the expected plastic hinges at the ends and middle portion in order to have the smaller elements better handle the rapid changes of the moments and deformations there. This type of discretization is shown in Fig. 3-28d for 2-layer 20-node brick elements. When coarser elements were used in these regions instead of the refined ones, the constraining moments kept the element flatter at the ends and resulted in higher loads. This refinement resulted in a significant improvement for the 20-node brick elements with two and three layers, and the results agreed with the shell element and the rigid-plastic analysis solutions as shown in Fig. 3-32 by the Δ,    and o symbols with solid lines. In fact, some improvement was achieved by refining the 8-node brick elements modeled with one layer (*1br8thra*) as shown in Fig. 3-32 by "•" symbol.

Thus, a refinement of the discretization in anticipation of the actual deformation pattern resulted in a closer agreement either with the solutions using shell elements or 2-layer 20-node brick elements with refinements. However, when the computational effort is considered, the shell elements appear to be more cost effective. This localized refinement technique was not practical for the existing shell elements in the corrosion patch models. However, the results could be improved if the brick elements were used in the models.

#### *3.5.5.2 Thick Columns*

The thick beam-columns were composed of brick elements having the same dimensions as the elements in the undamaged transition mesh in the actual tube between the corrosion patches. The brick elements with 8-nodes again showed a very irrational overall behavior as shown in Fig 3-31 (hollow triangles). The 8-node brick elements with 2 layers still behaved erratically in the post-ultimate range (hollow squares in Fig. 3-31). Therefore, further study of using the 8-node brick elements was abandoned.

### 3.5.4 Beam Element Analysis

The beam-columns were modeled with three-dimensional linear beam elements, which include plastification of the cross-section in the formulation of the element.

For the thick beam-columns (t=0.122 in.), the ultimate capacity was close to the shell elements but higher in the post-ultimate range as shown in Fig. 3-31. The behavior of the thin beam-columns (t=0.022 in.) was quite close to that of the shell elements and of the rigid-plastic analysis as shown in Fig. 3-32. However, the ultimate loads were lower than for other models as given in Table 3-5. On the other hand, when the end and middle portions of the thin beam-columns were refined (labeled *beamref)*, the ultimate loads fell into the range of the ultimate loads of other models.

### 3.5.5 Brick Element Analysis

#### *3.5.5.1 Thin Columns*

The 8-node brick elements with a single layer (labeled *1br8thin* in Fig. 3-28c) exhibited an extremely irrational behavior both in the elastic and the post-ultimate ranges and did not even give a peak load as expected in a real structure as shown in Fig. 3-32. When the beam-columns were modeled with two layers of 8-node brick elements in anticipation of obtaining a more realistic behavior, the general appearance of the deformation curve was improved as shown in Fig. 3-32 and labeled *2br8thin*. However, the curve still did not behave as expected since it showed no reduction of the capacity in the post-ultimate range.

The most sophisticated brick element available in ABAQUS with 20 nodes and using one layer resulted in a curve (shown in Fig. 3-32 and labeled *1br20thin*), which, in the post-ultimate range, fell far above the results for the rigid-plastic and shell analyses. This puzzling behavior could have been due to either a limitation of the element type in ABAQUS or insufficient layering. Therefore, the specimen was modeled with two layers (labeled as *2br20thin)* and plotted in Fig. 3-32. This attempt improved the abnormal behavior in the post-ultimate range, but still was not realistic. Modeling the column with three and four layers was also tried. However, after 3-layers

$$\delta = \sqrt{L \times \frac{\Delta}{2} \times \left(1 - \frac{\Delta}{2L}\right)} \tag{3-5}$$

The effect of the elastic axial shortening $\Delta_a$ is given by Eq. 3-6.

$$\Delta_a = \frac{PL}{AE} \tag{3-6}$$

The effect of the elastic curvature shortening $\Delta_c$ is the additional shortening due to curvature in the segments, and is given by Eq. 3-7.

$$\Delta_c = P^2 \times L^2 \times \frac{\delta}{4} \times \frac{1}{1440\left(E \times \frac{bh^3}{12}\right)^2}\left(\frac{L}{L-\Delta}\right) \tag{3-7}$$

Then, the total axial shortening is given by Eq. 3-8 as the sum of individual contributions.

$$\Delta_T = \Delta + \Delta_a + \Delta_c \tag{3-8}$$

However, the last two effects were found to have very minor influence on the results, and therefore the portions between the hinges can be considered to be rigid. Figure 3-30 gives an illustration of the relationship between the axial force P and the shortening Δ for three different depths (thicknesses) **t**.

Generally, the rigid-plastic analysis is good for an approximate analysis of slender columns. For stubby columns, the results are less reliable since the assumption of infinitesimally short plastic hinges introduces a much greater inaccuracy.

### 3.5.3 Shell Element Analysis

ABAQUS provides two types of shell elements, one with 9 nodes and 5 DOF and the other with 8 nodes and 6 DOF per node. Thus, the total number of degrees of freedom in a 9-node and 8 node shell element is 45 and 48, respectively. To check the consequences of this small difference in the total number of degrees of freedom, the beam-columns were modeled using both types. Various models with small and larger segment lengths with the same thickness were used. The difference between the patterns of the curves for these types of elements (*5sh6ori* and *6sh6ori*) was insignificant as shown in Fig. 3-31. The ultimate loads were also very close to each other as given in Table 3-5.

Since the principal source of the irregular behavior was expected to be the constant-thickness portion of the corrosion patch, a simple constant-width fixed-end column was used to investigate the effect of different patterns of discretization, sizes and types of elements. Thus, basically, a test on the patch was conducted by using the shell, beam and brick elements. The post-ultimate behavior was also compared with the behavior from the theoretical rigid-plastic analysis. Two types of shell elements were used, one with 9 nodes and 5 degrees of freedom (5 DOF) per node, and the other with 8 nodes and 6 DOF per node. The two brick elements used were: the 8-node brick element with 6 DOF per node at eight corners of the element, and the 20-node brick element with eight nodes each on the top and bottom surfaces and four at the intermediate layer.

The dimensions of the beam-column were chosen to represent a typical strip in the longitudinal direction of the corrosion patch area (length=0.66 in., width=0.10 in.). The two values of thickness **t** studied were 0.122 in., the wall thickness of the undamaged specimens, and 0.022 in. To simulate the load eccentricity in the patch and, thereby, exclude the bifurcation type instability, the shape of the beam-column was assumed to have an initial imperfection of a cosine shape with a 0.025-inch offset at mid-length. The basic discretization models are shown in Fig. 3-28, and their descriptions and properties are listed in Table 3-5.

### 3.5.2 Rigid-Plastic Analysis

The rigid-plastic analysis is a theoretical approach for predicting the deformation of frame structures considering the P-Delta effect and assuming full plastification at the hinges of the mechanism. It gives an upper-bound solution to the actual behavior. The length of the plastic hinges is assumed to be infinitesimal. Figure 3-29 shows the deformation configuration of a typical column assumed in the rigid-plastic analysis. In this study, the cross-section is rectangular with width b and depth h.

Axial load P due to an axial shortening Δ is given by the following formula:

$$P = P(\Delta) = bF_y\delta\left[\sqrt{1+\left(\frac{h}{\delta}\right)^2}-1\right] \qquad (3\text{-}4)$$

Where $\delta$, the lateral deflection at mid-length, is related to the axial shortening Δ by Eq. 3-5.

### 3.4.3 Additional Comments

Both test specimens, MP1 and MP2, were intended to have pinned-end conditions. However, their ultimate loads were higher than for the FE models with pinned ends by 22% and 14%, respectively. This increase in ultimate capacity can be explained by two considerations. First, there was some rotational restraint in the cylindrical bearing fixtures. Second, as described in Chapter 1, the yield stress used in the analysis ($F_y$=42.11 ksi) was determined from the coupons cut from the original tube (Specimen P2PS). [9,10] However, a somewhat higher yield stress may have developed due to work-hardening as the material of Specimen MP2 had undergone straining during the previous tests.

Test Specimen MP1 was also analyzed by using the FORTRAN program (CXS.for). [10] The computed ultimate load-carrying capacity was 65.03 kips for fixed- ended specimen and 46.70 kips for the pinned-ended specimen as shown in Table 3-4. The comparison of the computed results with the FE results was promising and the difference was only 4% and 6%, respectively.

On the basis of these comparisons, it was concluded that the finite element program ABAQUS and the method of discretization could be relied upon to provide acceptably accurate results in generating the database for parametric studies.

## 3.5 Comparison and Selection of Element Types for Corrosion Patches

### 3.5.1 General

In the early stages of the FE analysis of long fixed-end columns with three patches, it was observed that some of the columns exhibited axial deformation curves that had unexpected and illogical behavior. As shown in Fig. 3-27, a two-peak pattern for the ultimate load developed for some cases, that is, after reaching the first peak, the load dropped off and then started climbing again to a second peak that in some cases was higher than the first. This unusual response prompted an investigation of the suitability of the 9-node shell elements used in the analysis.

The analysis was carried out to reach the axial deformation of 3 to 4 times the deformation at the ultimate load. The axial load vs. axial shortening plots of the FE Specimens 3T199P3 and 3T199F3 (pinned and fixed end conditions) and of the test specimen MP1 are plotted in Fig. 3-20. As shown in Table 3-4, the ultimate loads from the FE analysis were 46.70 kips for pinned ends and 67.46 kips for fixed ends, and the load from the test was 57.00 kips.

The deformation pattern of the wall of Specimen 3T199P3 is shown in Fig. 3-21, and it is almost the same as for the tested Specimen MP1 in Photo 2-1. The contour plot of the longitudinal stress on the outside surface of the specimen is given in Fig. 3-22 for the axial shortening equal to the twice the axial shortening at the ultimate load. The areas of surface yielding in tension due to large wall distortions near and within the corrosion patches are clearly indicated by the lighter colors and are labeled with letter "Tension". The compressive stresses are darker and labeled with letter "Compression".

### 3.4.2 Comparison of Test Specimen MP2 with its FE Model

Test specimen MP2 (3 patches) was discretized as a half-tube and labeled as 3T114P3. The FE model is shown in Fig. 3-23. The third (middle) patch is s=1.40 inches away from the other two patches.

The computed axial load vs. axial deformation relationships of the FE models, Specimen 3T114P3 (pinned) and 3T114F3 (fixed), are plotted together with the test Specimen MP2 in Fig. 3-24. The computed load-deformation curves were very close to the test results. Most rewarding were the almost parallel patterns in the post-ultimate range where, most commonly, the curves computed by an FE program tend to show a more rapid loss of strength than the test curves. The ultimate loads from the FE analysis specimens were 66.38 kips for fixed ends and 44.80 kips for pinned ends, and the test load was 51.10 kips.

The deformation pattern of the FE model in the patch area is shown in Fig. 3-25. It agreed well with the actual deformations shown in Photo 2-2. The contour plot of the longitudinal stress on the outside surface of the specimen is given in Fig. 3-26 for the axial shortening equal to the twice the axial shortening at the ultimate load.

refined there. Figure 3-17c shows the longitudinal stress contour plot on the outer surface of the end portions of a specimen distorted by local buckling.

The beam elements were analytically connected to the ends of the shell segments by using the *EQUATION tool provided by ABAQUS, so that the displacements and rotations of the nodes of the shell elements at the ends of the shell segments were all in the same plane controlled by the displacements and rotations of the central node that was connected to the adjoining beam elements. The end nodes of the shell elements were also constrained to maintain a constant distance from the central node in the radial direction. Figure 3-18 illustrates the geometric relationships at the beam-to-shell junction. With the rotations of all shell nodes being the same as the rotations of the central node (Node 0), the following three equations give the linear displacements of the shell nodes with respect to the coordinate axes x (1), y (2) and z (3):

$$u_1^B = u_1^0 - r_3^0 * x_2^B \tag{3-1}$$

$$u_2^B = u_2^0 + r_3^0 * x_1^B \tag{3-2}$$

$$u_3^B = u_3^0 + r_1^0 * x_2^B - r_2^0 * x_1^B \tag{3-3}$$

Where u's are the displacements and r's are the rotations of a node. The subscripts stand for the DOF number, and the superscripts represent the node (Node B in the figure) for which the equations are written.

## 3.4 Comparison of FE Analysis with Test Results

The FE analysis procedure described in Section 3.3 was checked by analyzing the test specimens MP1 and MP2 of Chapter 2.

### 3.4.1 Comparison of Test Specimen MP1 with its FE Model

Test Specimen MP1 (2 patches) was modeled as a half-tube by taking a 3-patch model and setting the middle patch at infinite distance as shown in Fig. 3-19. The FE label for this model was 3T199P3.*

---

*A more laborious process would have been to analyze MP1 as a 2-patch model with g=3.2 in. and s =0.0.

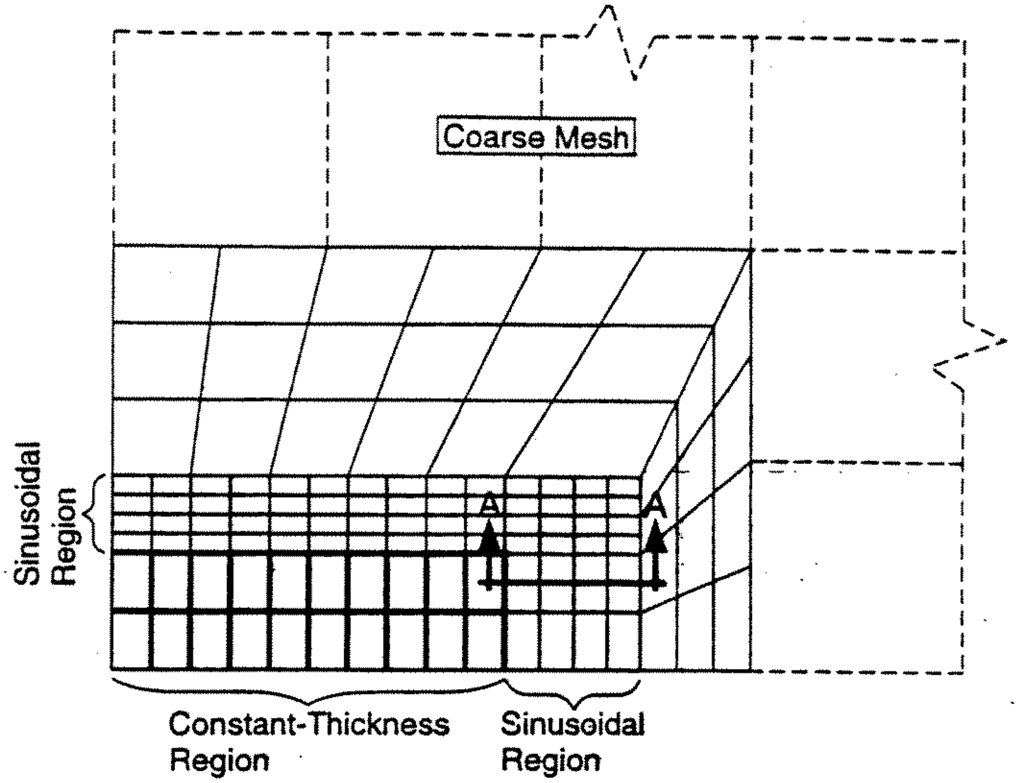

Figure 3-4: Unfolded View of Corrosion Patch Mesh (Quarter-Model)

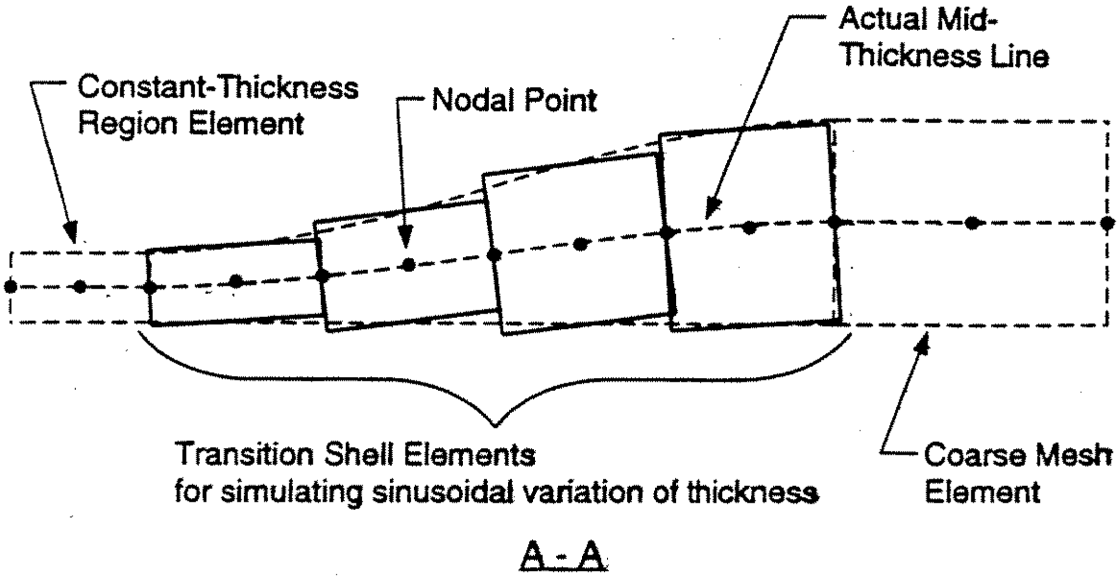

Figure 3-5: Modeling of the Sinusoidal Transition Region

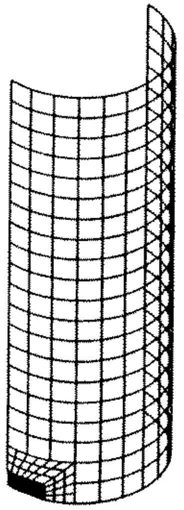

Figure 3-6: Quarter-Tube Model of
Specimens with One Patch

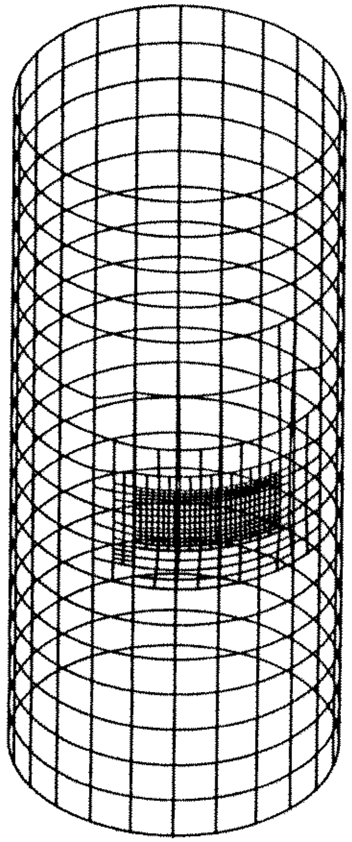

Figure 3-7: Full-Tube Model of
Specimens with One Patch

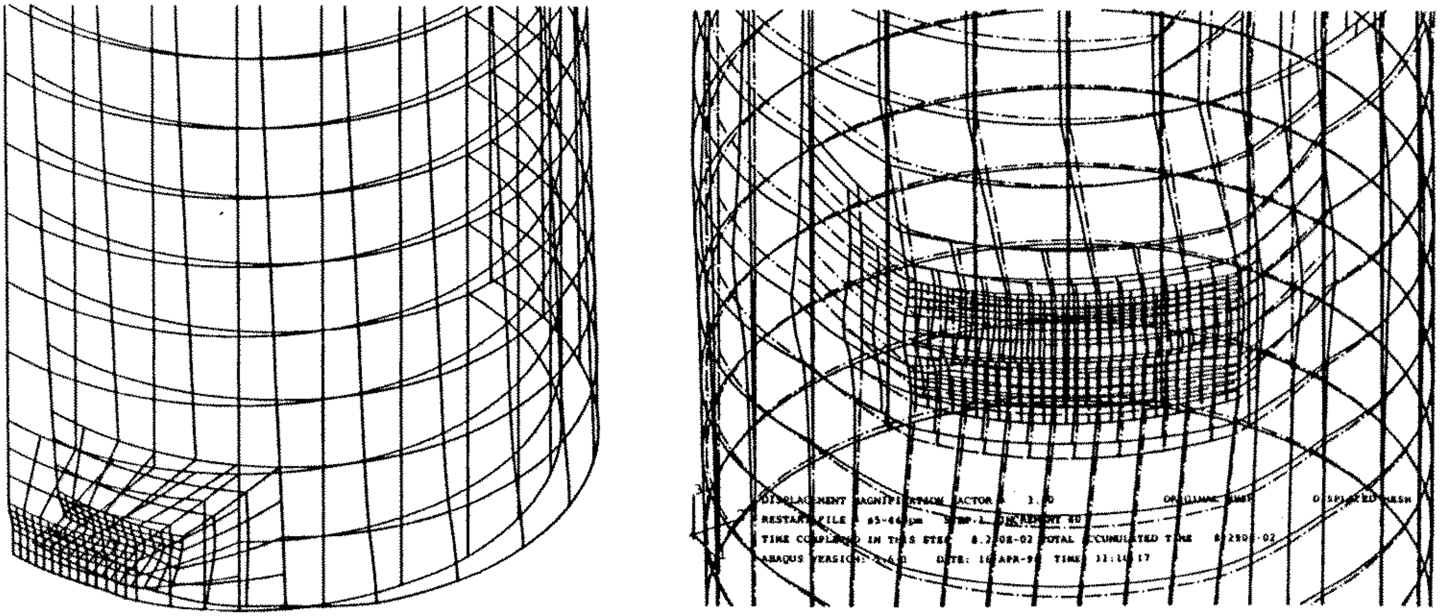

Deformation in the Quarter-Tube Model

Deformation in the Full-Tube Model

Figure 3-8: Comparison of Deformation Patterns in Specimens with One Patch

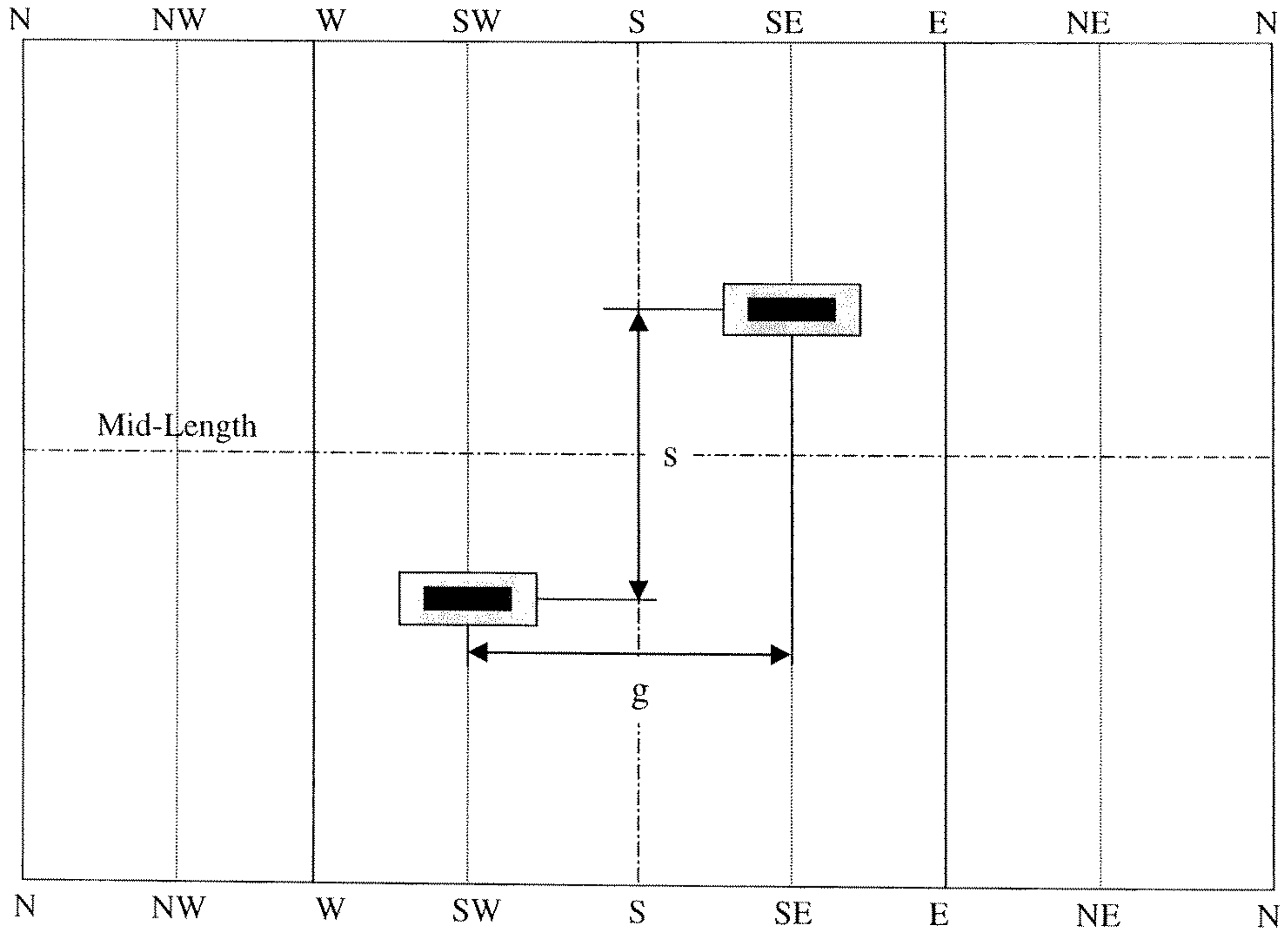

Figure 3-9: Unfolded View of Patch Layout of Specimens with Two Corrosion Patches

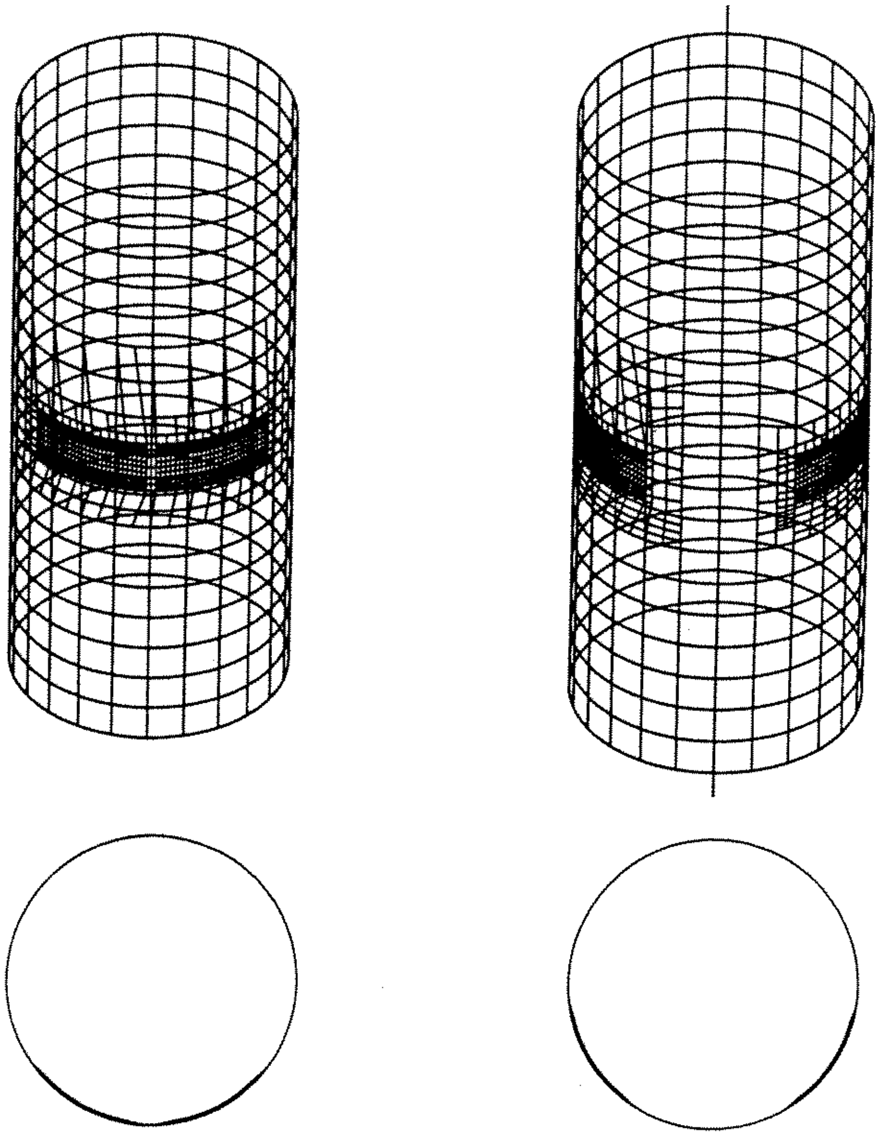

g=2.68 in. (2T200F3)
Front and Top Views

g=5.36 in. (2T500F3)
Front and Top Views

Figure 3-10: Specimens with Two Patches with Different Circumferential Spread g (s=0.00 in.)

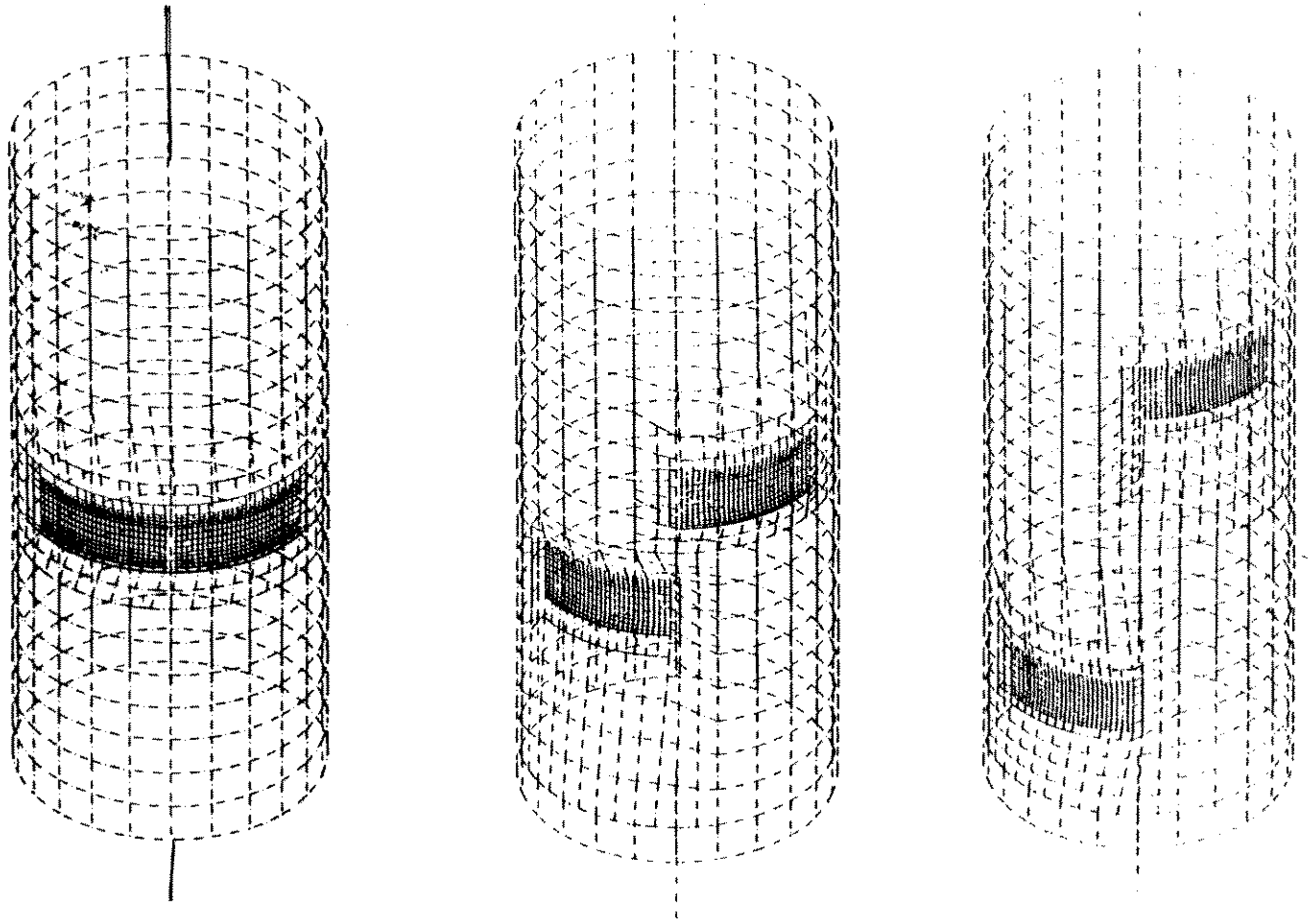

s=0.00 in. (2T200P3)

s=2.20 in. (2T222P3)

s=6.60 in. (2T266P3)

Figure 3-11: Specimens with Two Patches with Different Longitudinal Spacing s (g=2.68 in.)

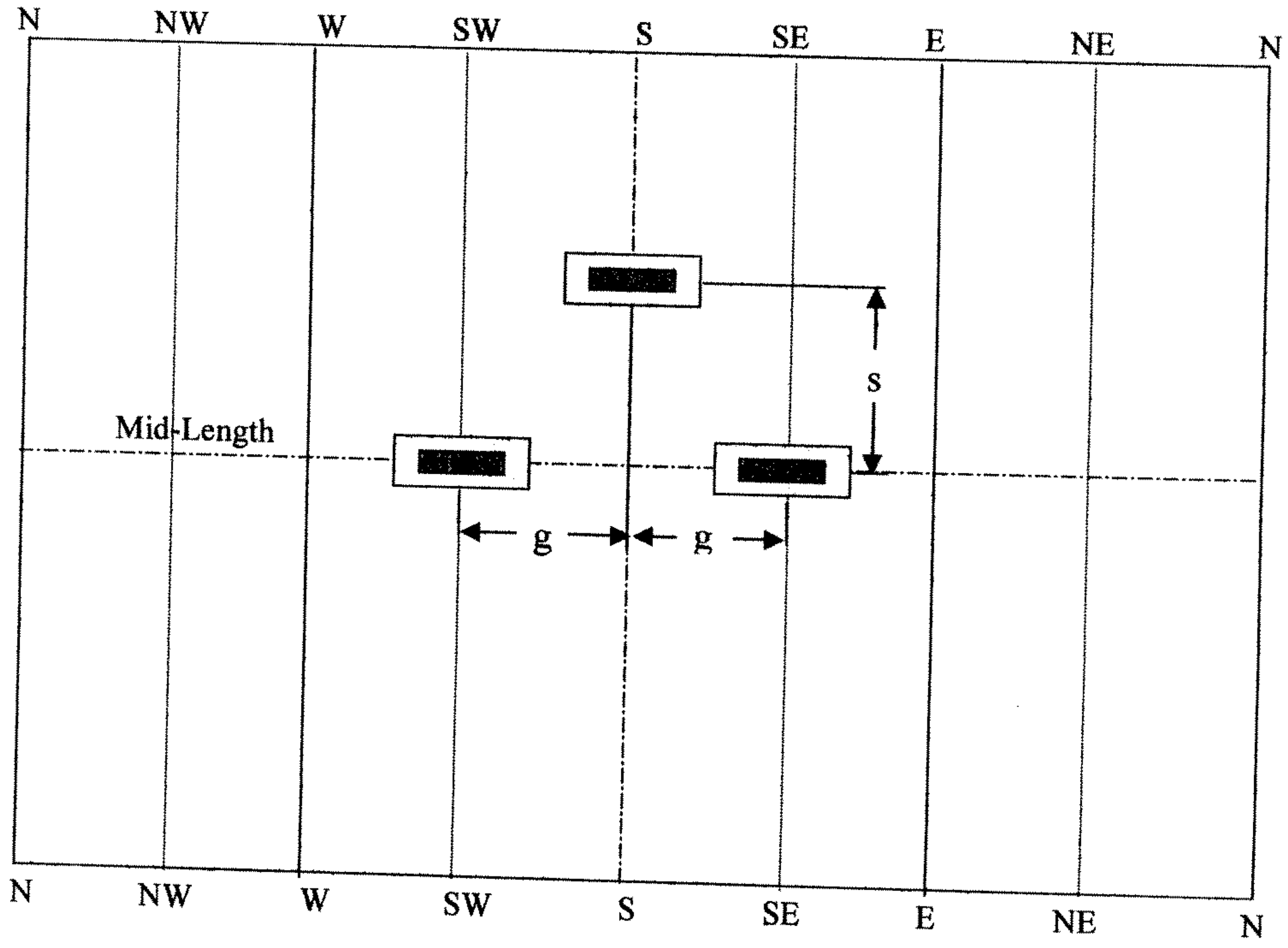

Figure 3-12: Unfolded View of Patch Layout of Specimens with Three Corrosion Patches

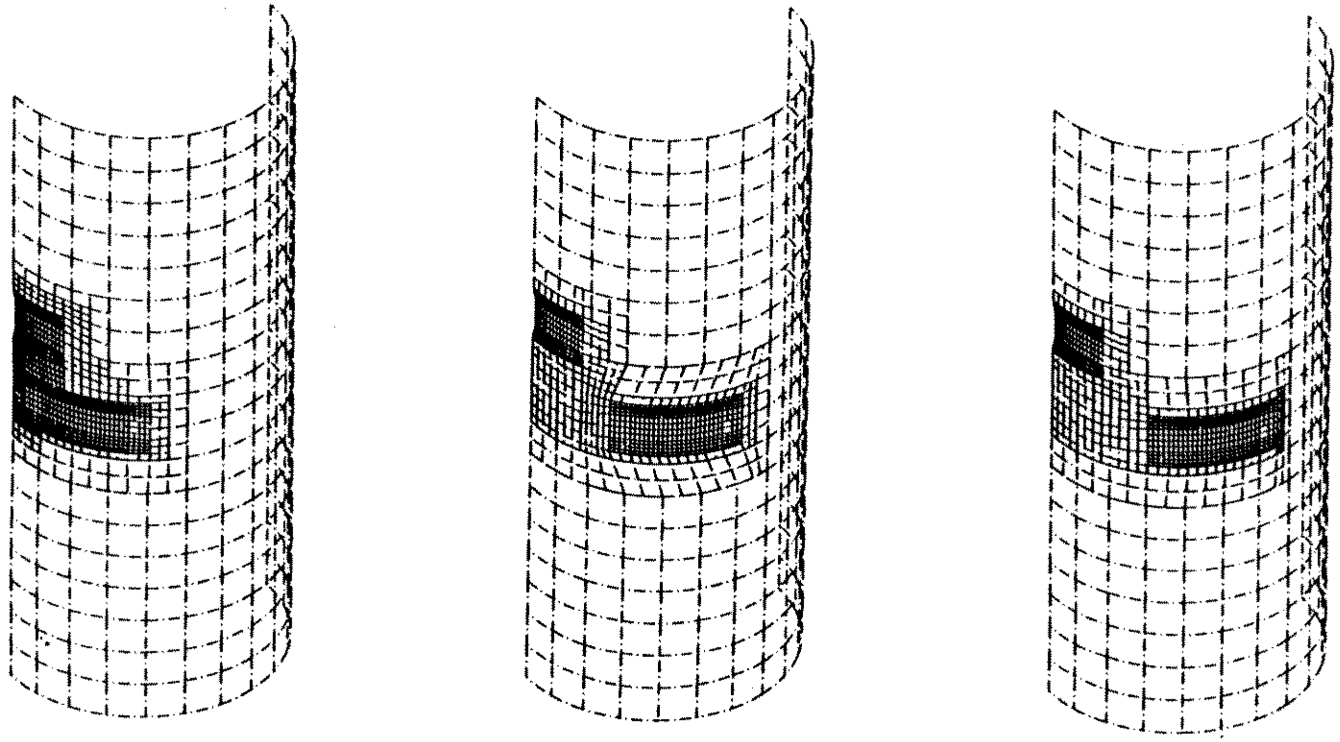

g=1.60 in. (3T116F3)    g=3.055 in. (3T316F3)    g=3.384 in. (3T416F3)

Figure 3-13: Specimens with Three Patches with Different Circumferential Spread g (s=1.65 in.)

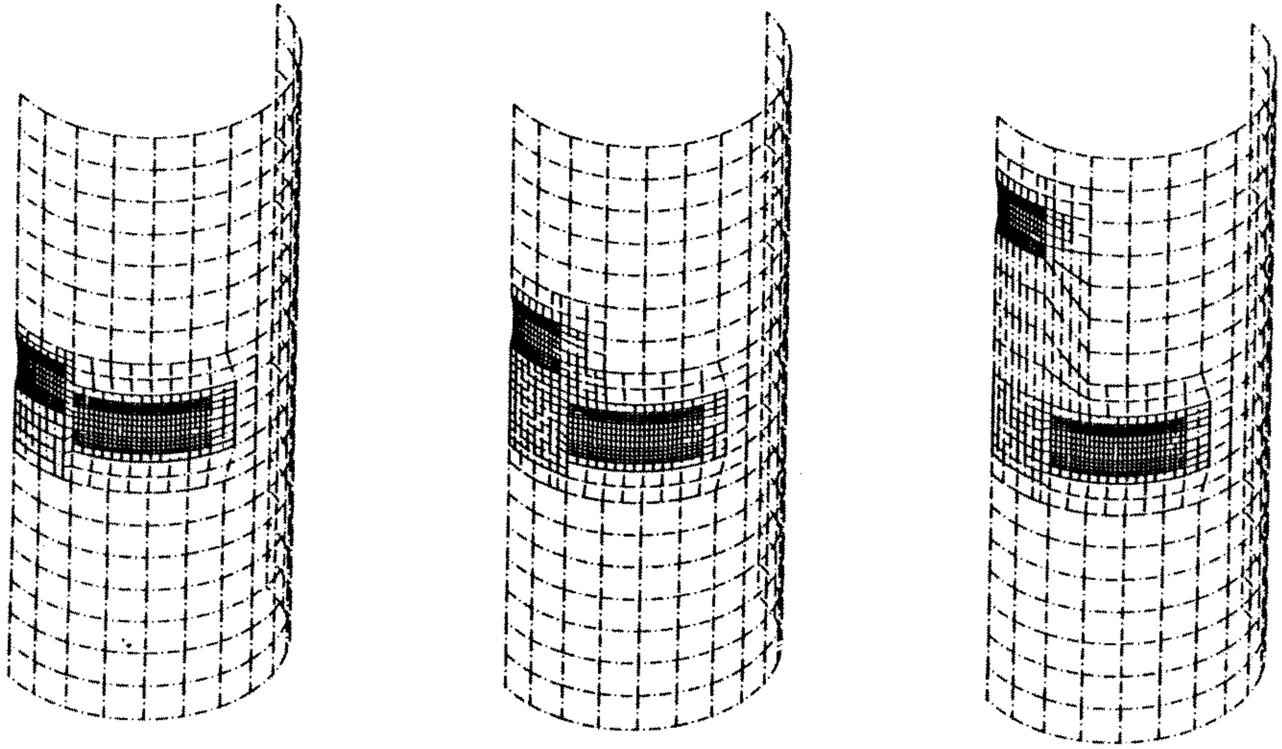

s=0.55 in. (3T205P3)

s=1.65 in. (3T216P3)

s=4.40 in. (3T244P3)

Figure 3-14: Specimens with Three Patches with Different Longitudinal Spacing s (g=2.68 in.)

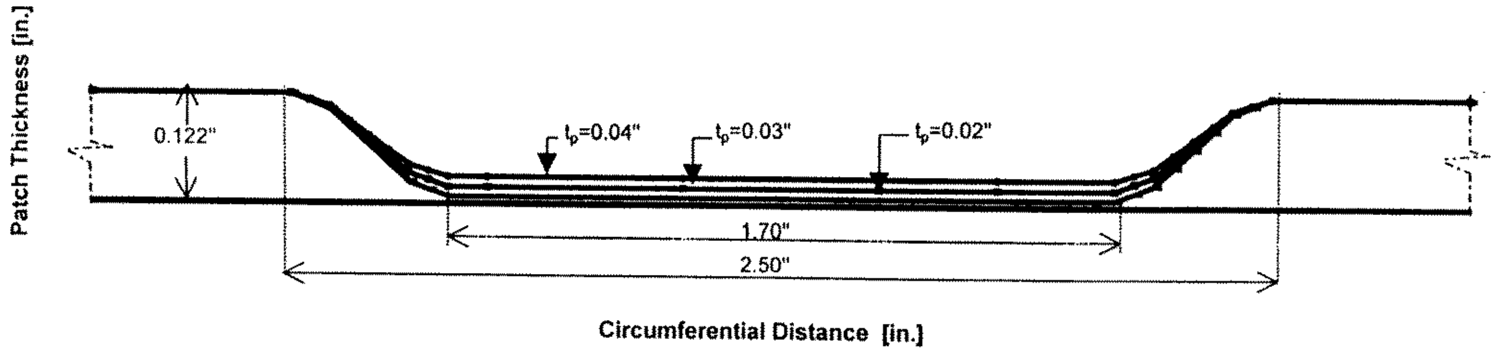

Figure 3-15: Patch Profile for Different Thicknesses

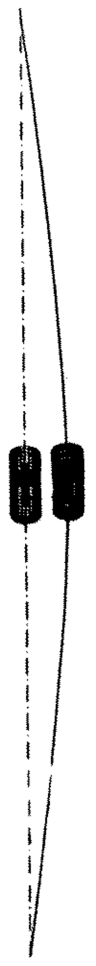

Figure 3-16a: Deformation of a Long Column with Pinned Ends

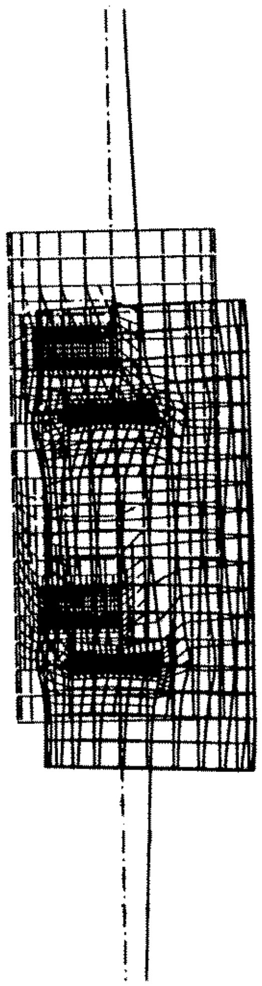

Figure 3-16b: Deformation of Middle Portion (Side View)

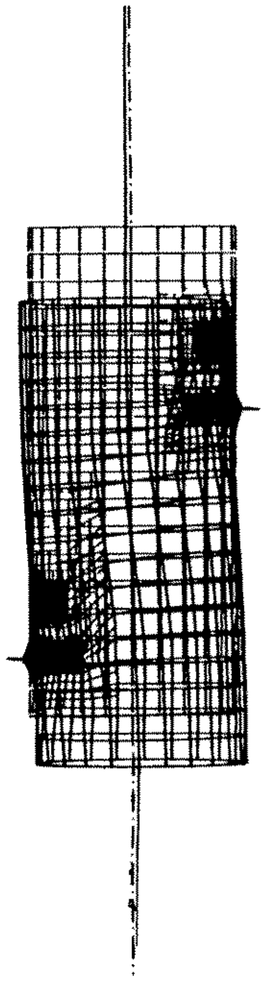

Figure 3-16c: Deformation of Middle Portion (Front View)

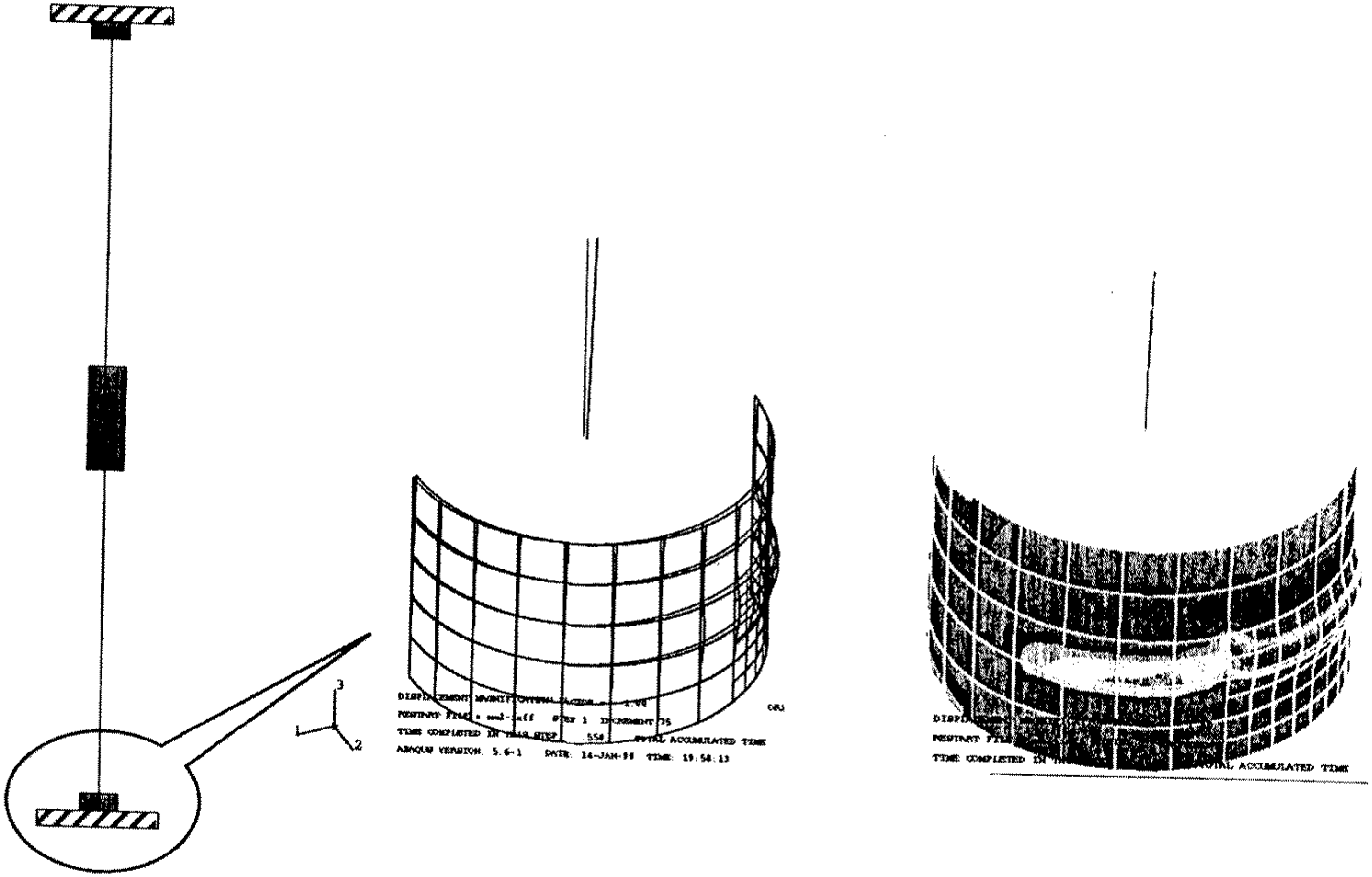

Figure 3-17a: A Typical Long Column with Fixed Ends

Figure 3-17b: End Segment Local Buckles at the Opposite Side of the Patches

Figure 3-17c: Longitudinal Stress Contour Plot on the Outer Surface of the End Segment

Figure 3-17: Modeling of Long Specimens with Fixed Ends and Discretization of End Segments

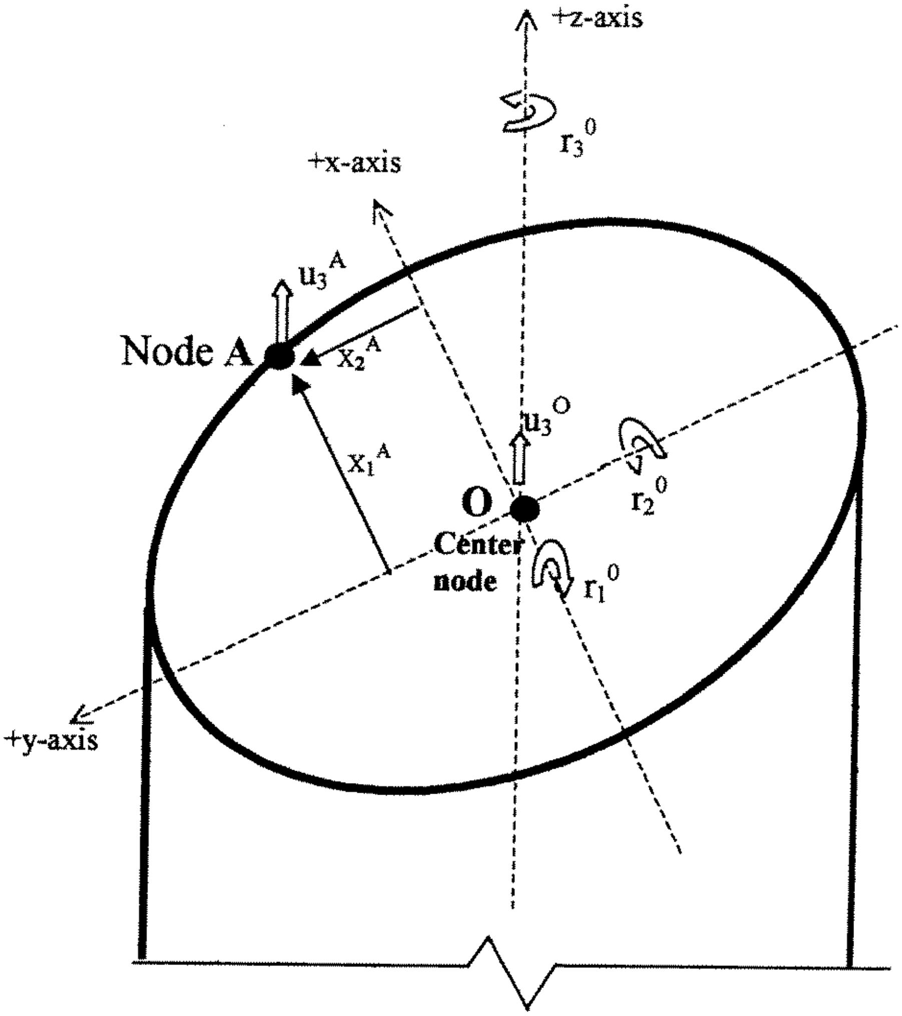

Figure 3-18: The Node and Degree of Freedom Designations for Beam-Shell Element Junction in Long Columns

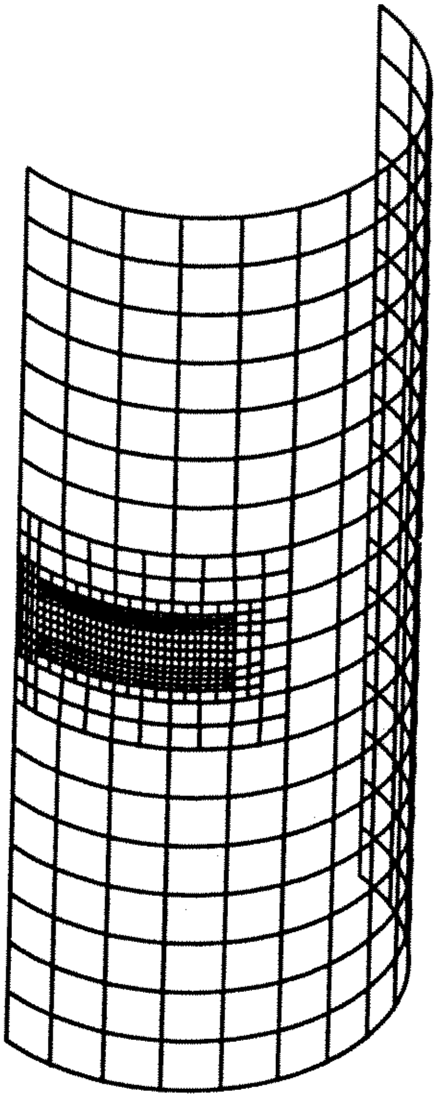

Figure 3-19: FE Discretization of Test Specimen MP1 (3T1IP3)

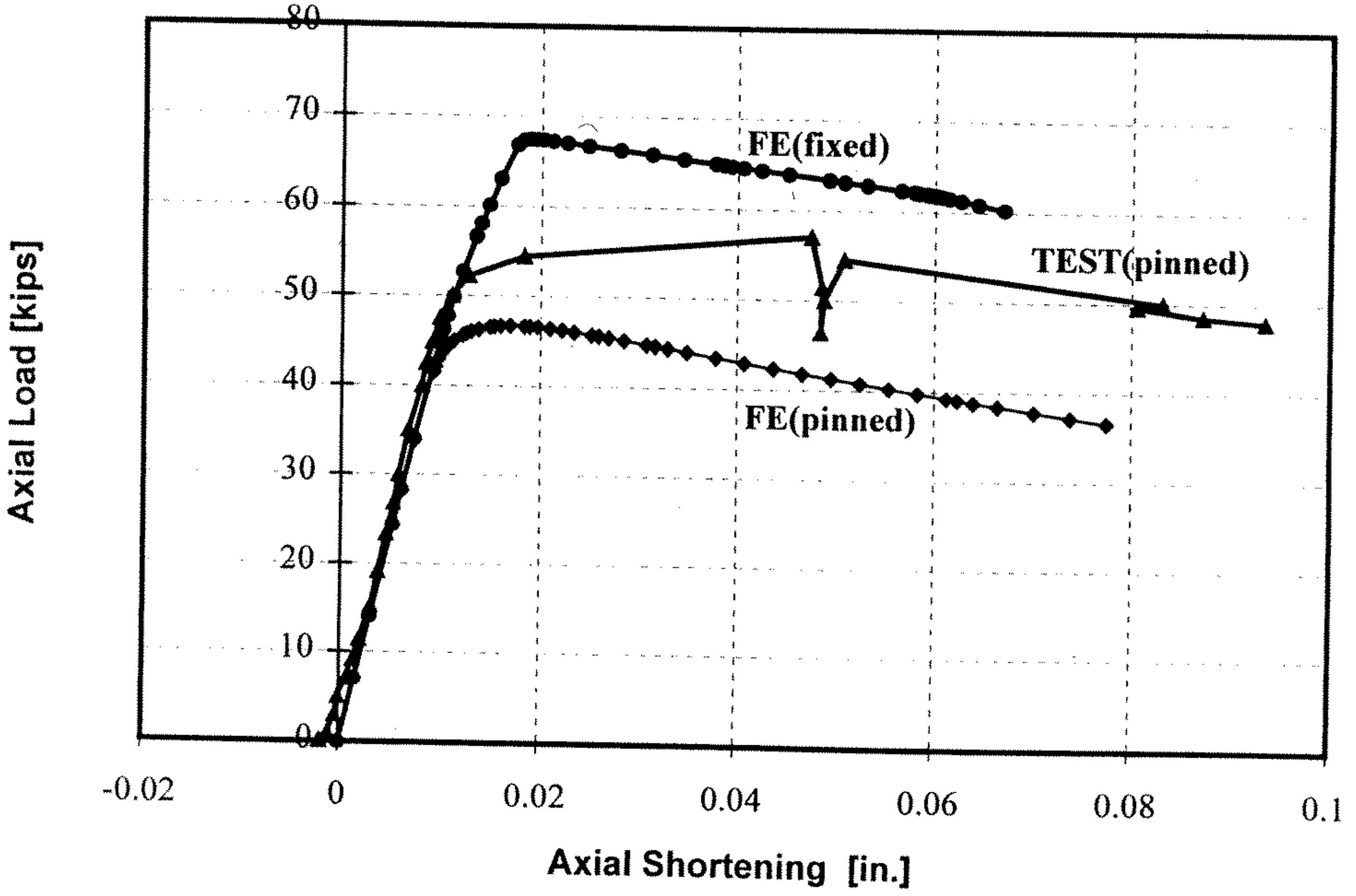

Figure 3-20: Comparison of Axial Load vs. Axial Shortening of FE Specimens 3T199F3 and 3T199P3 with Test Specimen MP1 (3 Patches, s=Infinity)

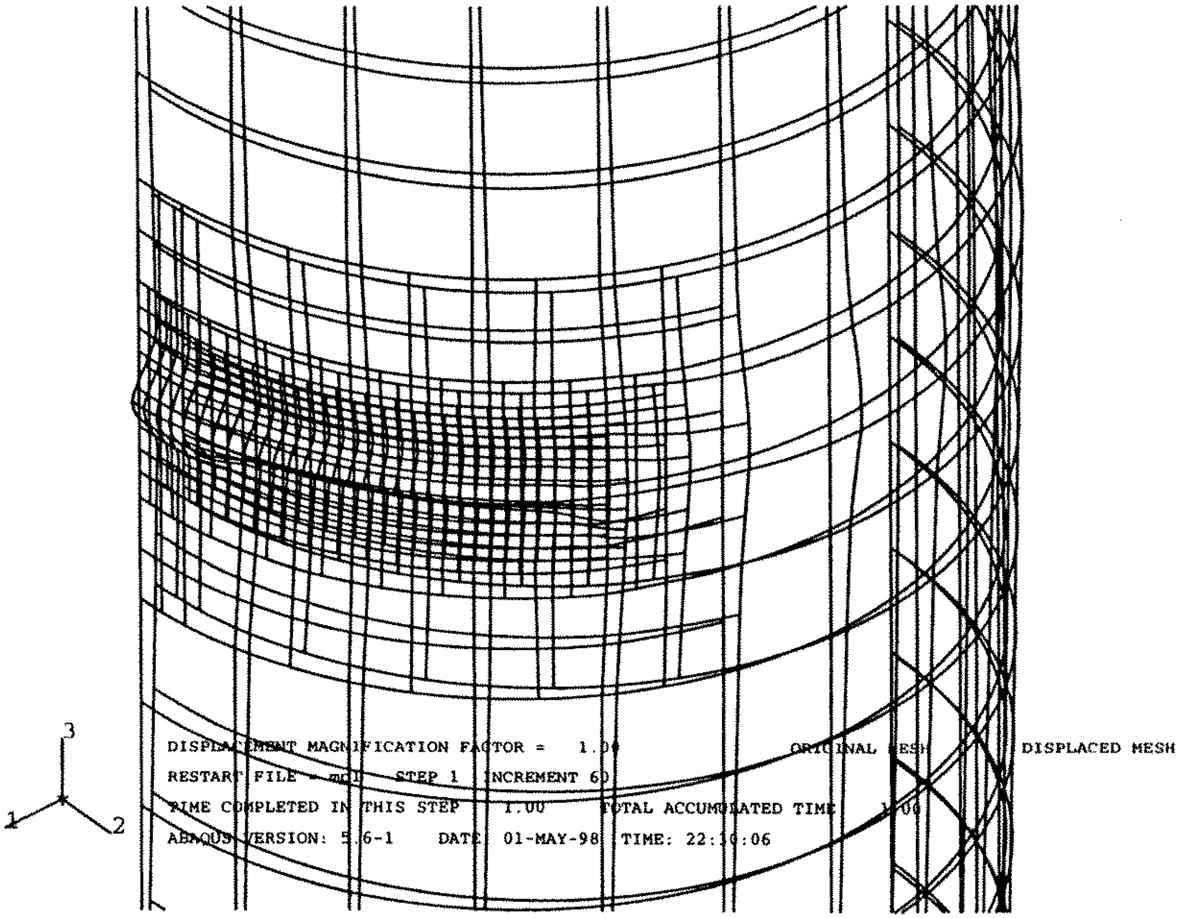

Figure 3-21: Deformation Pattern of FE Specimen 3T199P3

(FE Discretization of Test Specimen MP1)

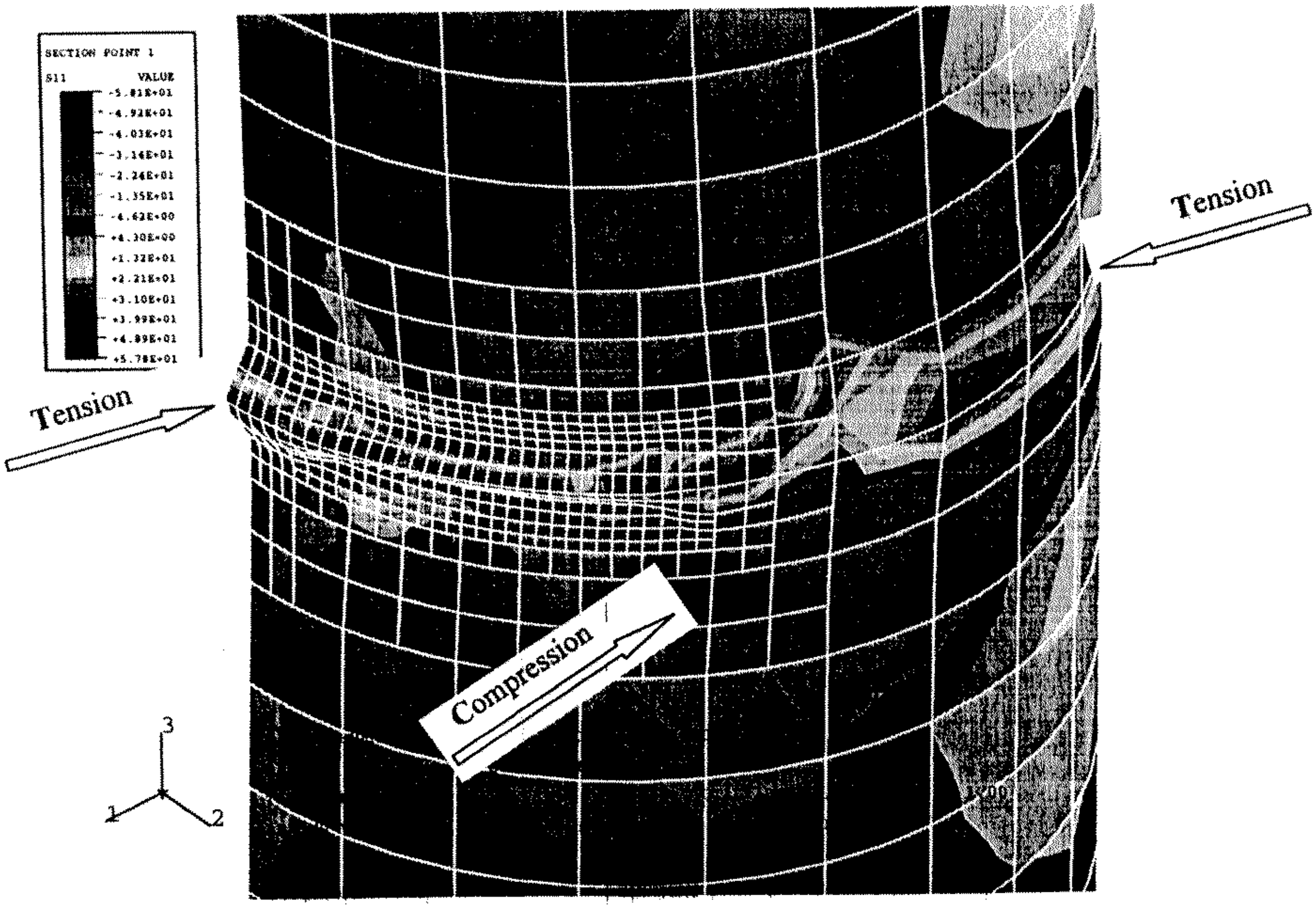

Figure 3-22: Contour Plot of Longitudinal Stresses on Outside Surface of Specimen 3T199P3

(Test Specimen MP1)

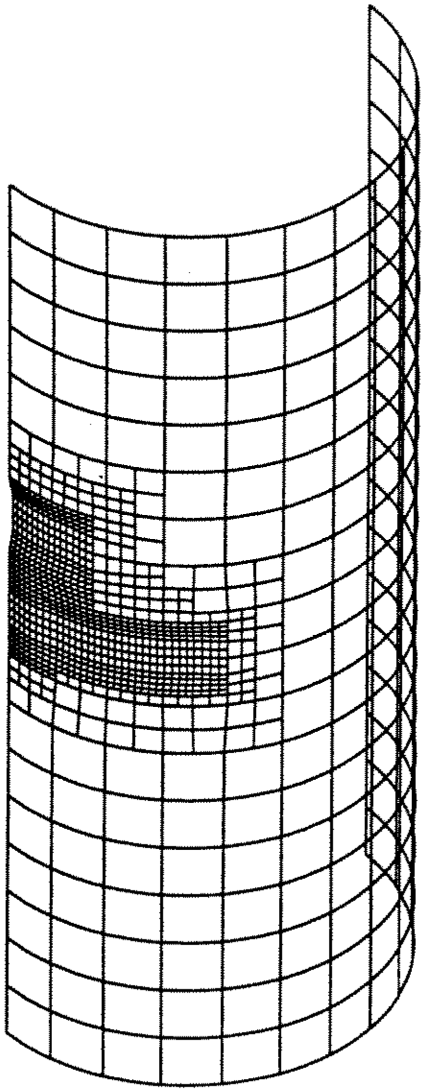

Figure 3-23: FE Discretization of Test Specimen MP2 (3T114P3)

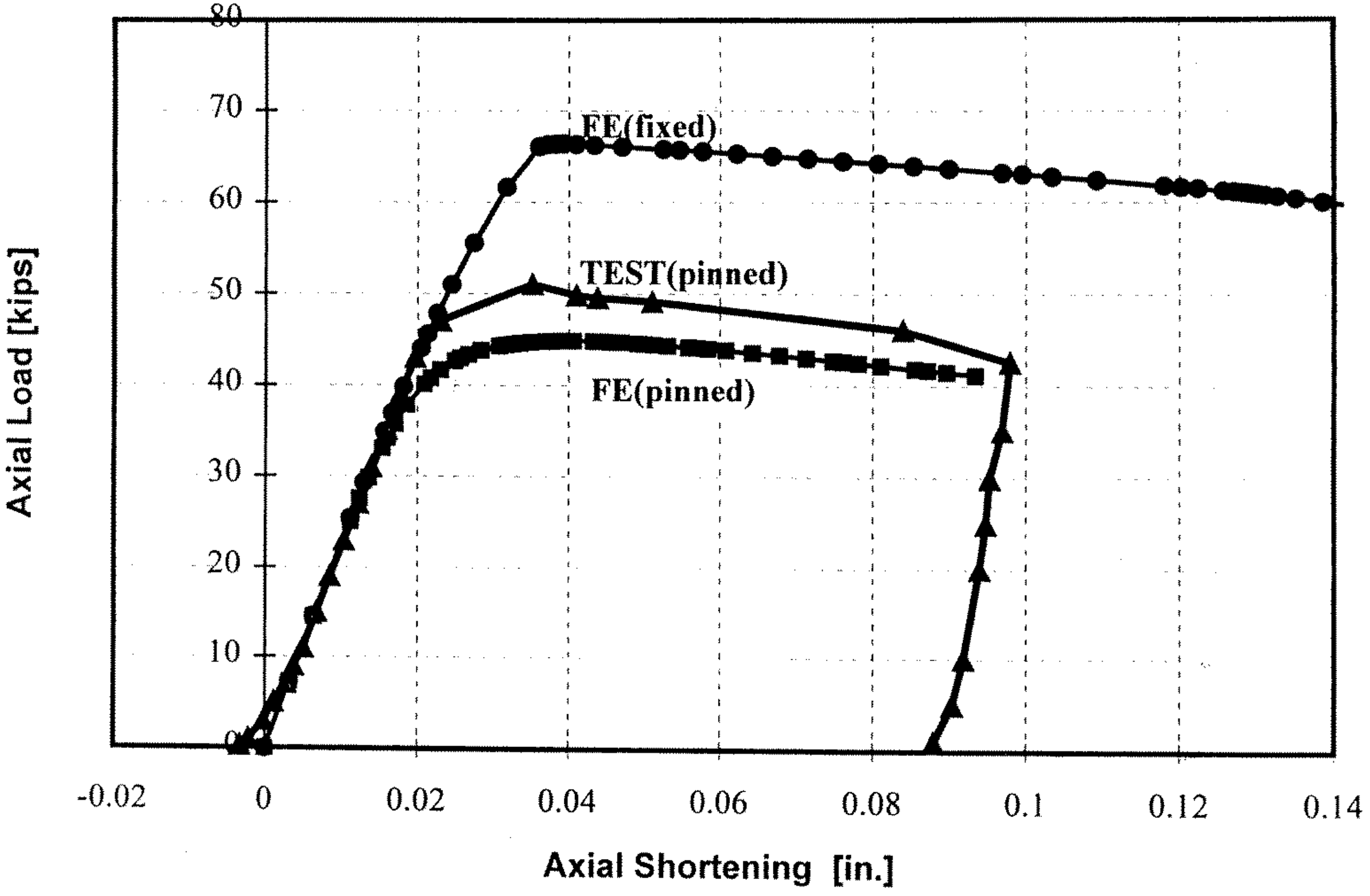

Figure 3-24: Comparison of Axial Load vs. Axial Shortening of FE Specimens 3T114F3 and 3T114P3 with Test Specimen MP2 (3 Patches)

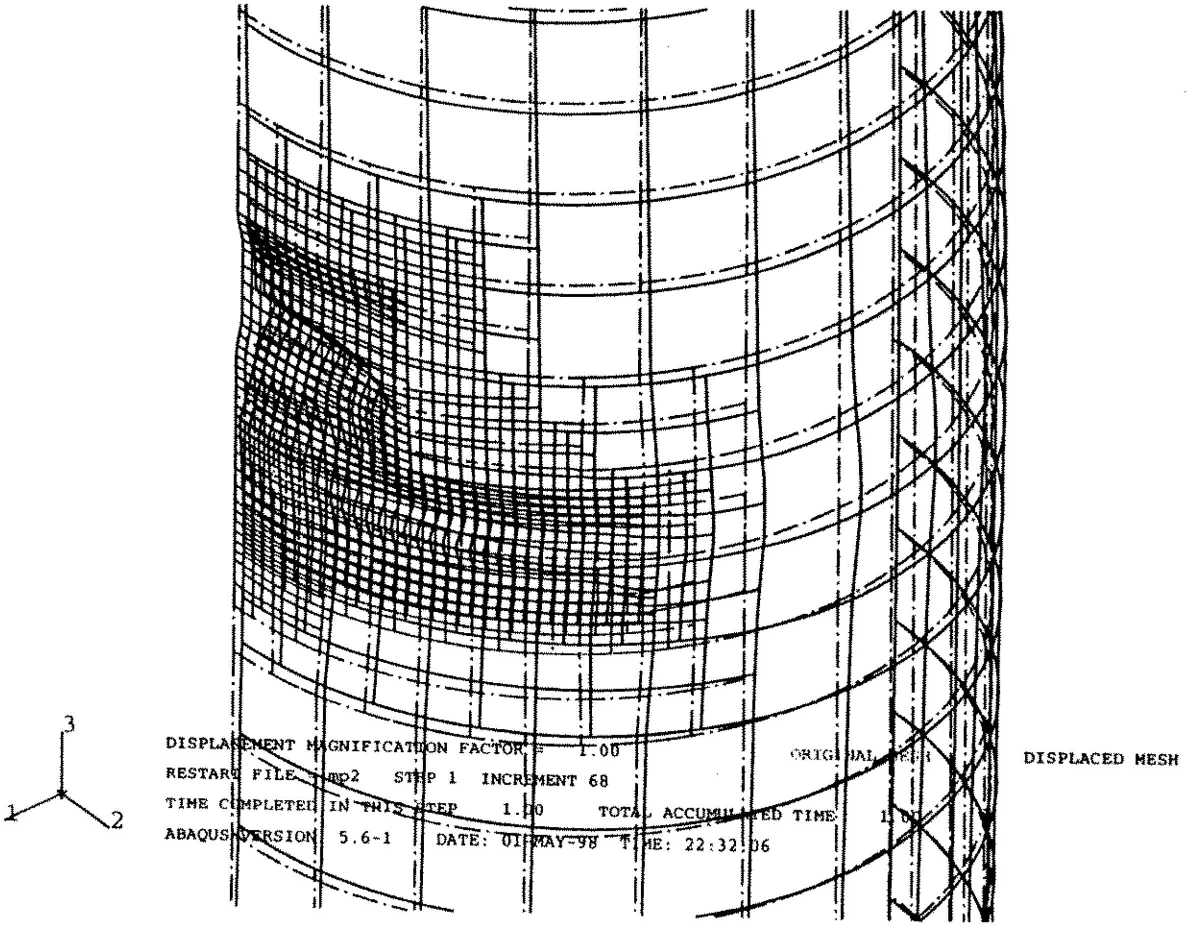

Figure 3-25: Deformation Pattern of FE Specimen 3T114P3 (FE Discretization of Test Specimen MP2)

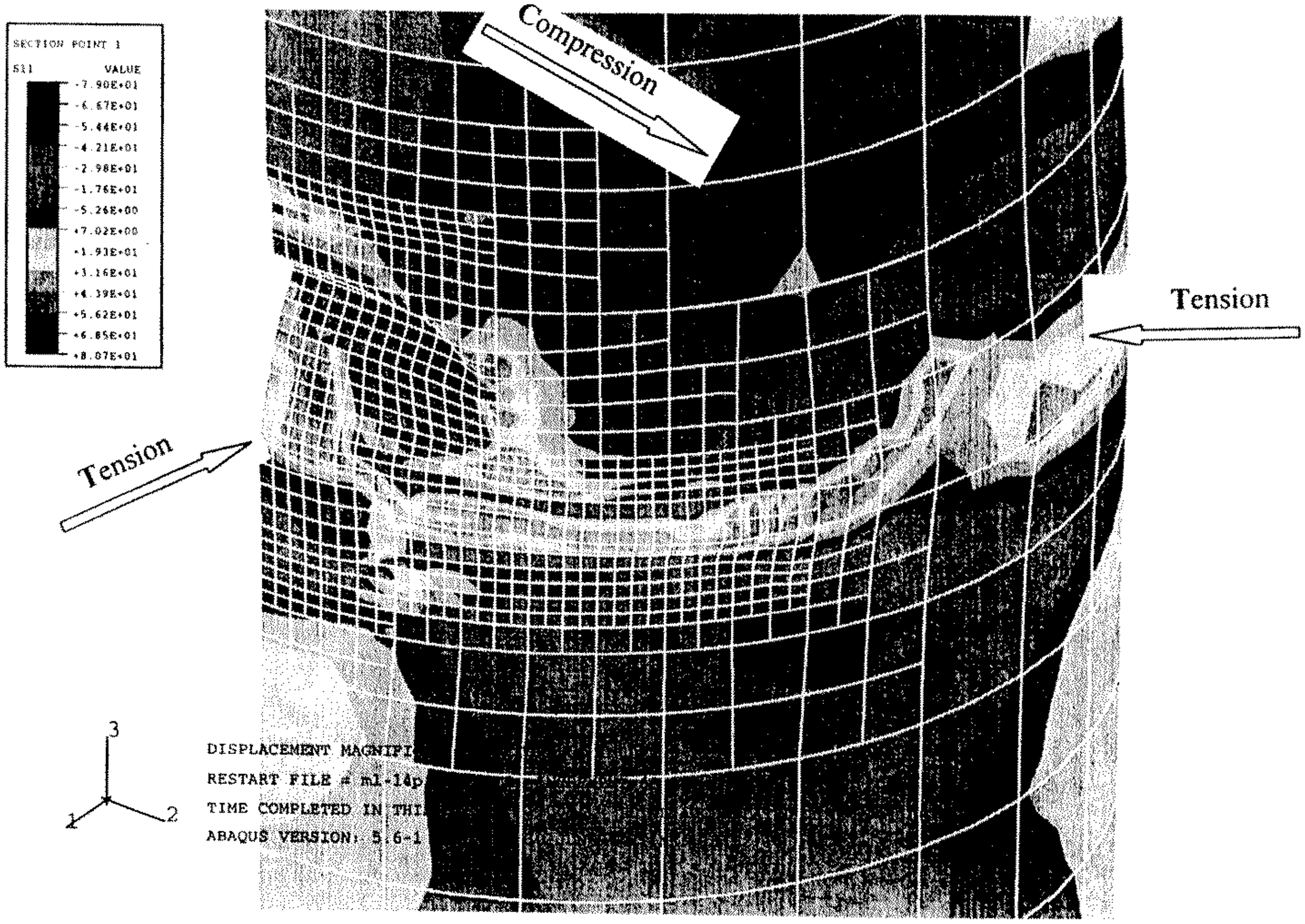

Figure 3-26: Contour Plot for Longitudinal Stress on the Outside Surface of Specimen 3T114P3 (Test Specimen MP2)

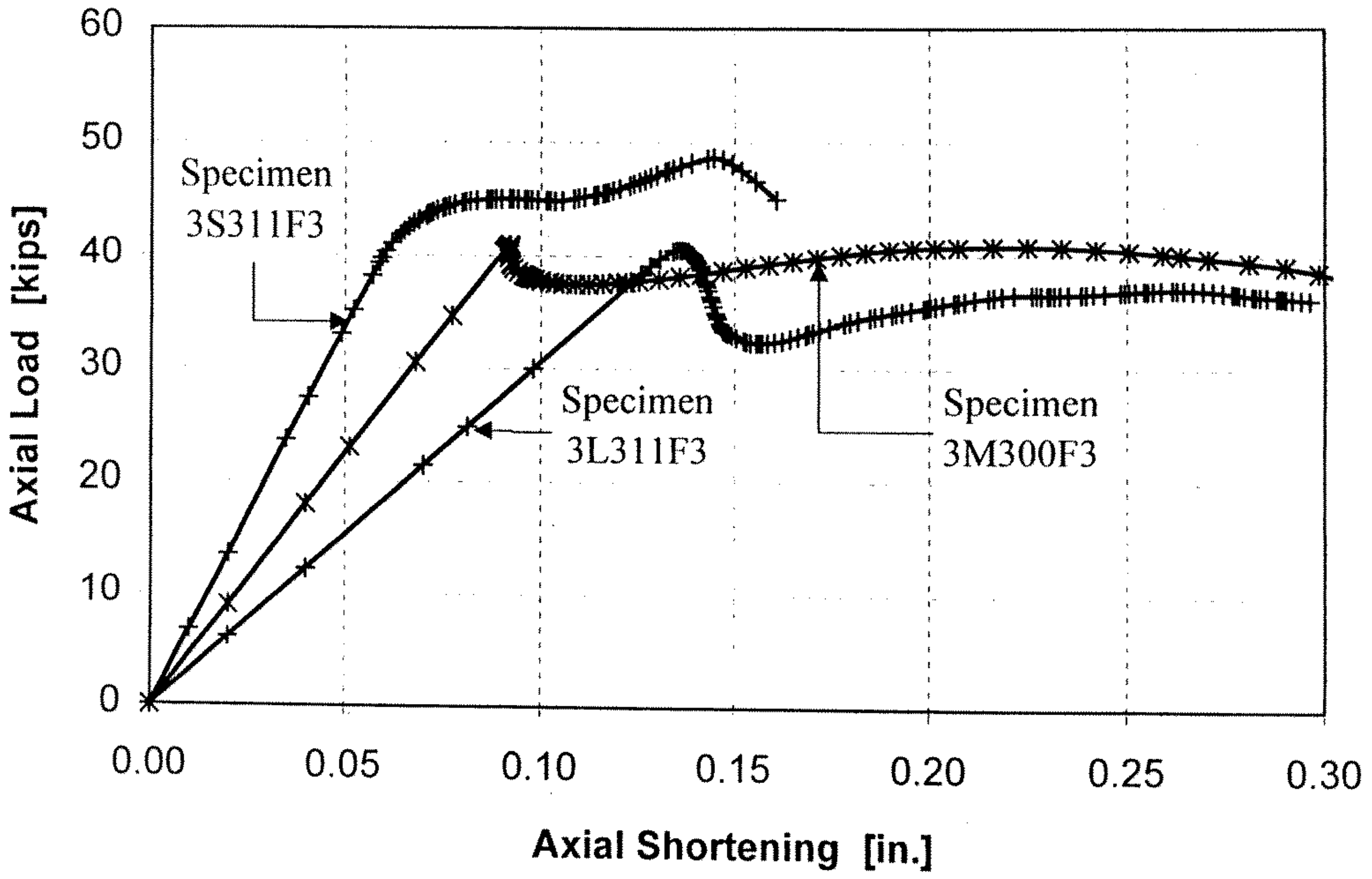

Figure 3-27: Axial Load vs. Shortening for Specimens with Abnormal Behavior in the Post-Ultimate range

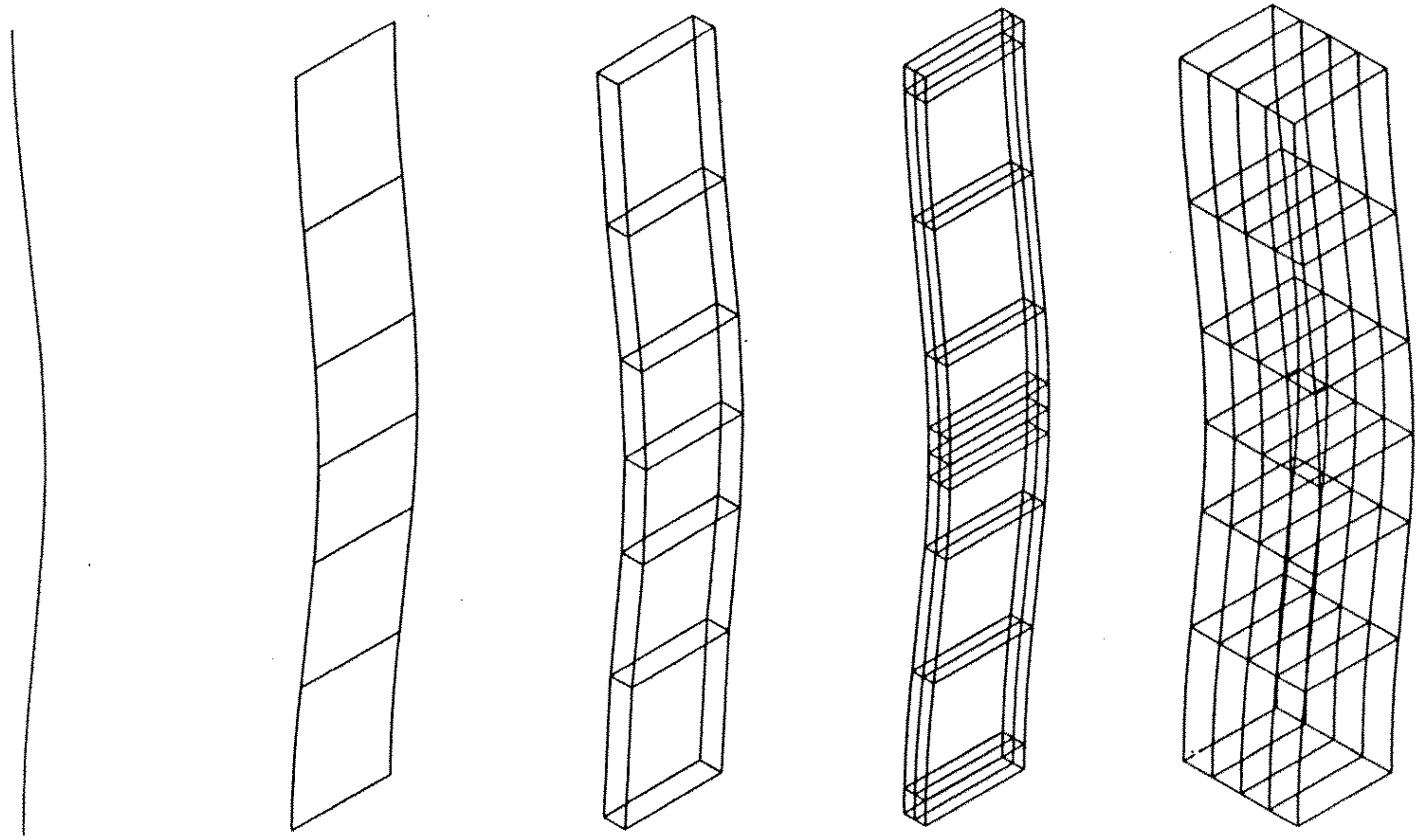

**Figure 3-28a:**
Beam-Column
Elements (refined)
*(beamref)*

**Figure 3-28b:**
Shell Elements
6 Longitudinal Segments
*(5sh6ori)*

**Figure 3-28c:**
6 Longitudinal Segments
1 layer (t=0.022 in.)
*(1br8thin)*

**Figure 3-28d:**
10 Longitudinal Segments
2 layers (refined)
*(2br20thra)*

**Figure 3-28e:**
6 Longitudinal Segments
4 layers (t=0.122 in.)
*(4br20ori)*

Figure 3-28: Basic Discretization Models for the Comparison of Elements

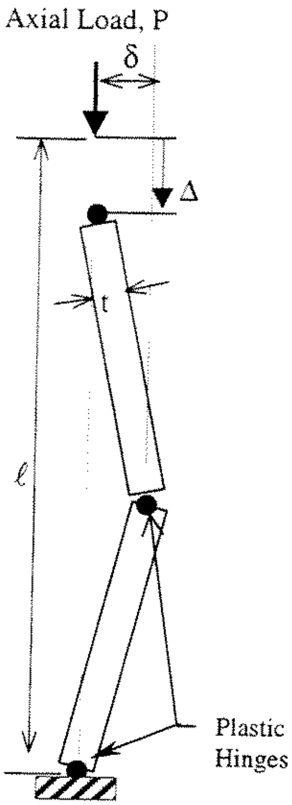

Figure 3-29: Typical Assumption for Rigid-Plastic Analysis Deformation Pattern

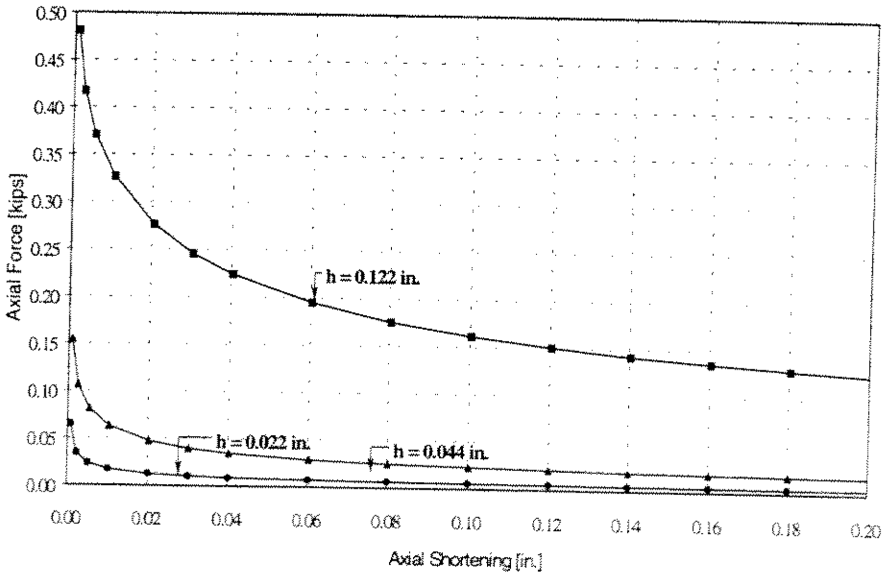

Figure 3-30: Rigid-Plastic Analysis for Beam-Columns with Different Thickness t

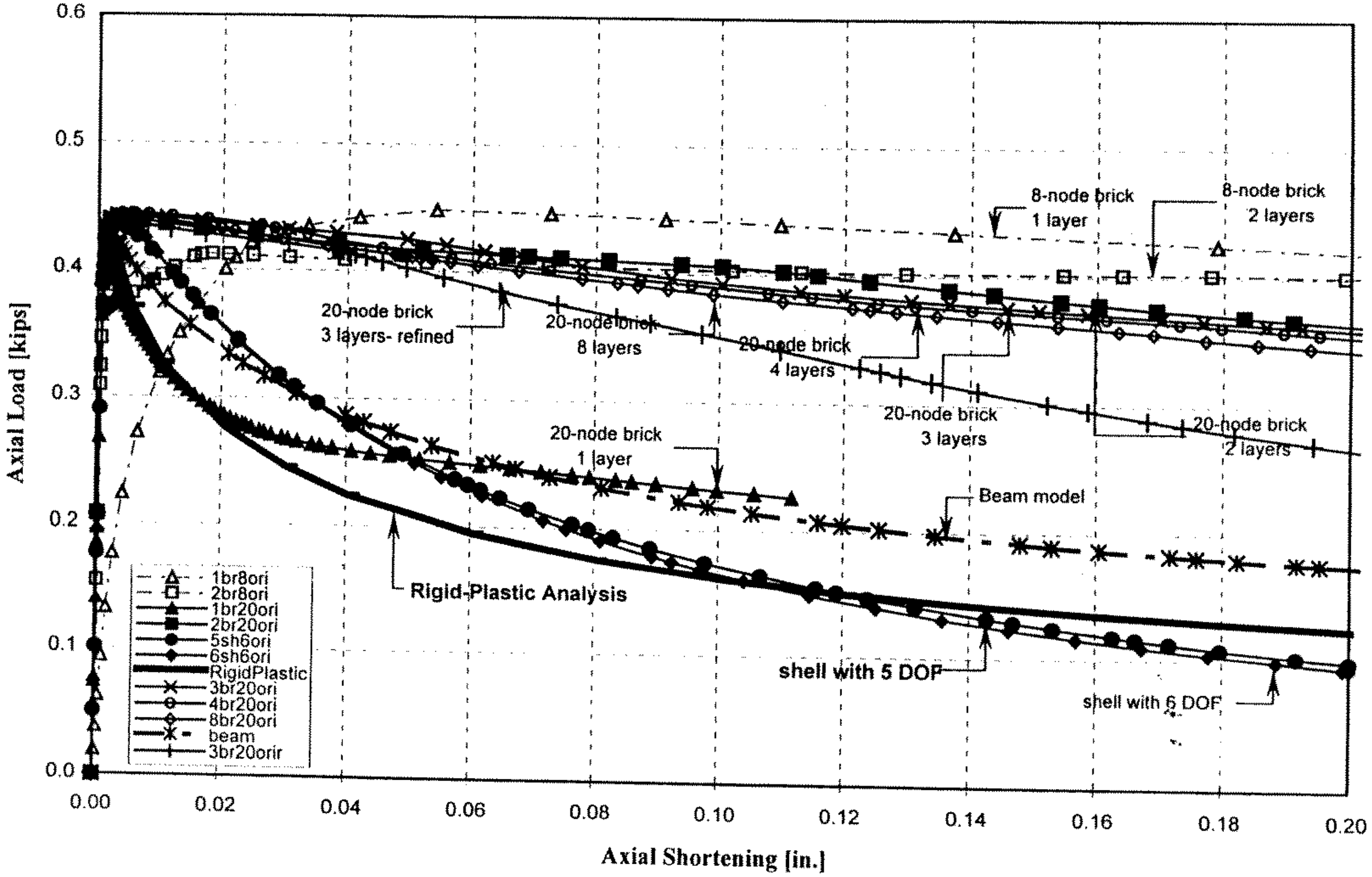

Figure 3-31 : Axial Load vs. Axial Deformation Relationships for Various Types of Elements and Discretization Schemes for Thick Beam-Columns (t=0.122 in.) - with fixed ends

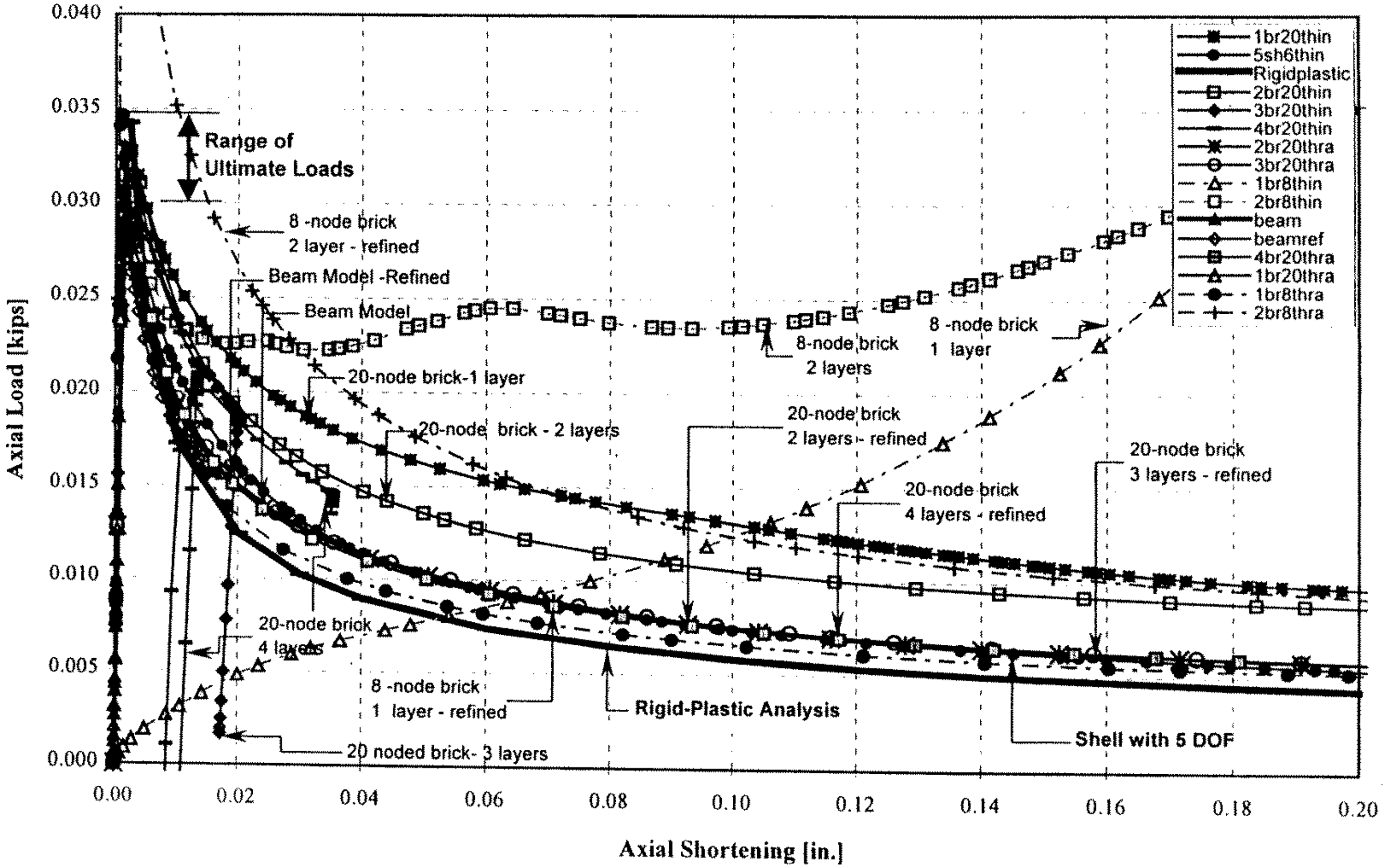

Figure 3-32 : Axial Load vs. Axial Deformation Relationships for Various Types of Elements and Discretization Schemes for Thin Beam-Columns (t=0.022 in.) - with fixed ends

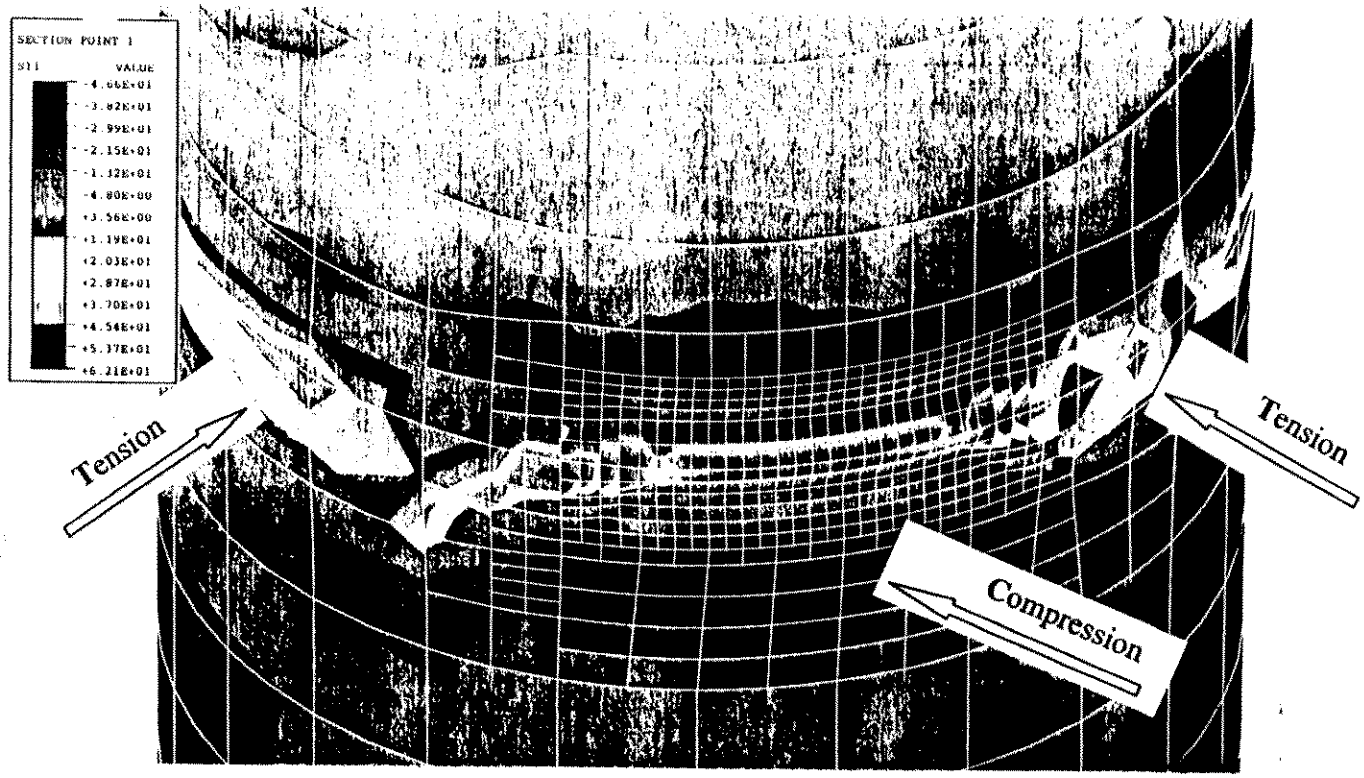

Figure 4-1: Contour Plot of Longitudinal Stresses on the Outside Surface of Specimen with One Corrosion Patch (Full-Tube Model)

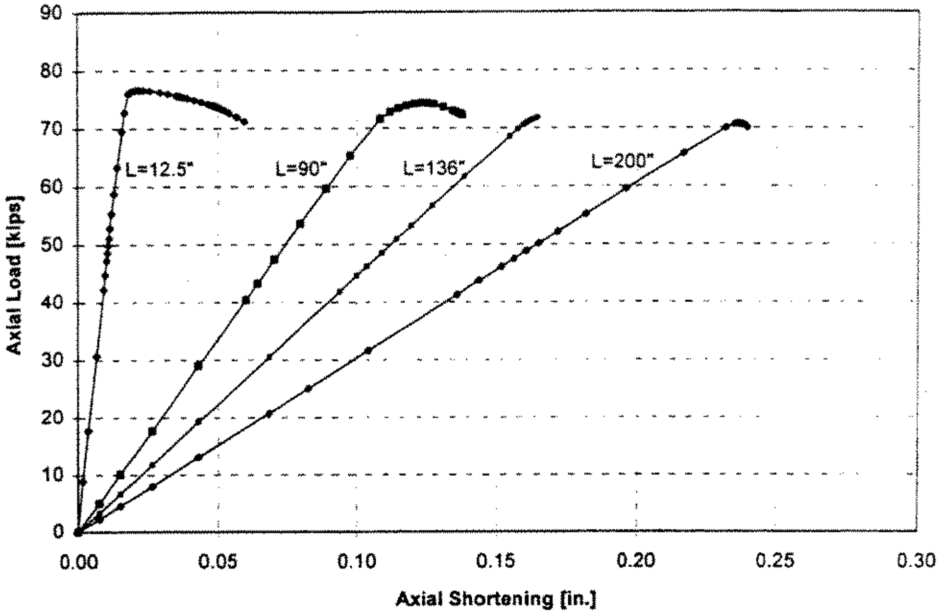

Figure 4-2: Axial Load vs. Axial Shortening for Fixed-End Specimens with One Corrosion Patch and Different Lengths (1*000F3)

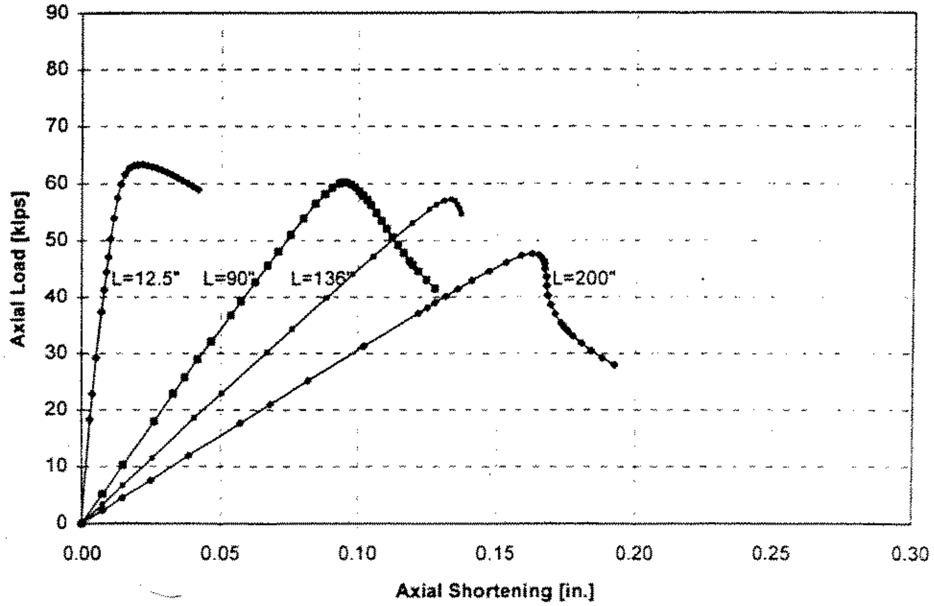

Figure 4-3: Axial Load vs. Axial Shortening for Pinned-End Specimens with One Corrosion Patch and Different Lengths (1*000P3)

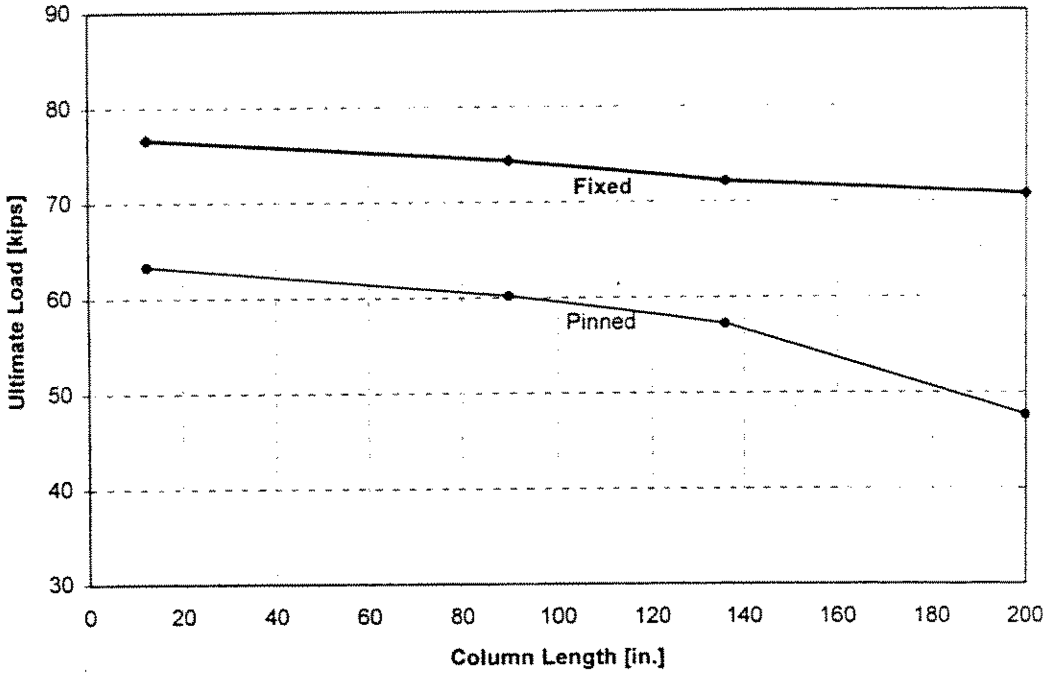

Figure 4-4: Effect of Column Length on $P_u$ for Specimens with One Corrosion Patch and Fixed or Pinned Ends (1*000*3)

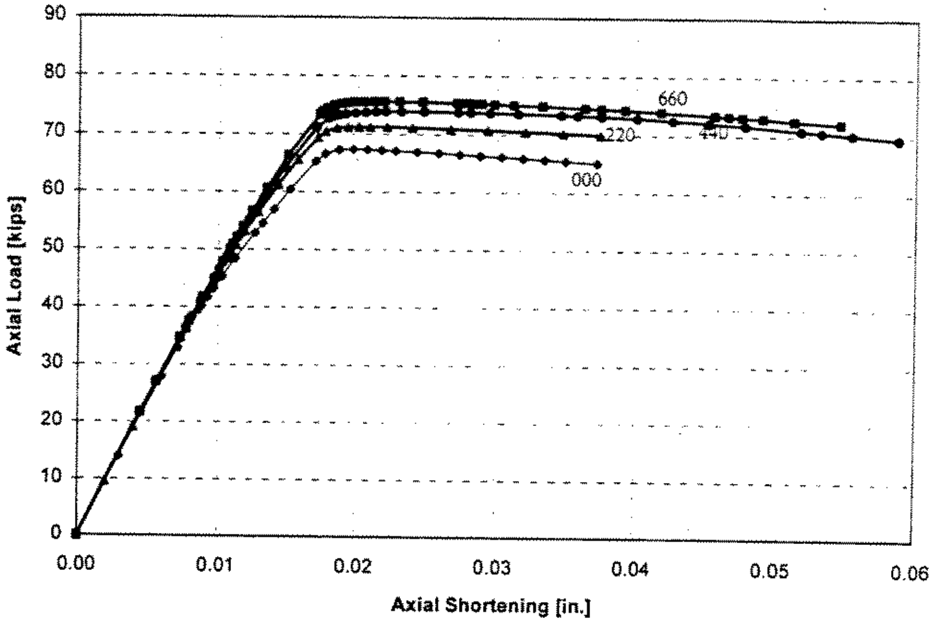

Figure 5-1: Axial Load vs. Axial Shortening Behavior of 2-Patch Stub-Column Specimens with Fixed Ends and g=2.68 in. for Different Values of Longitudinal Spacing s (2T2**F3)

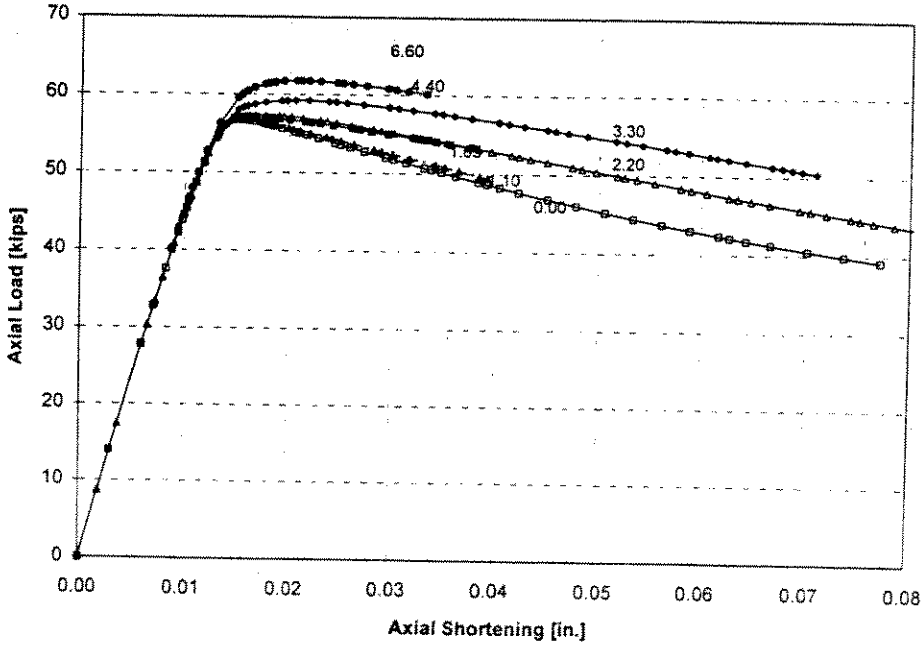

Figure 5-2: Axial Load vs. Axial Shortening Behavior of 2-Patch Stub-Column Specimens with Pinned Ends and g=2.68 in. for Different Values of Longitudinal Spacing s (2T2**P3)

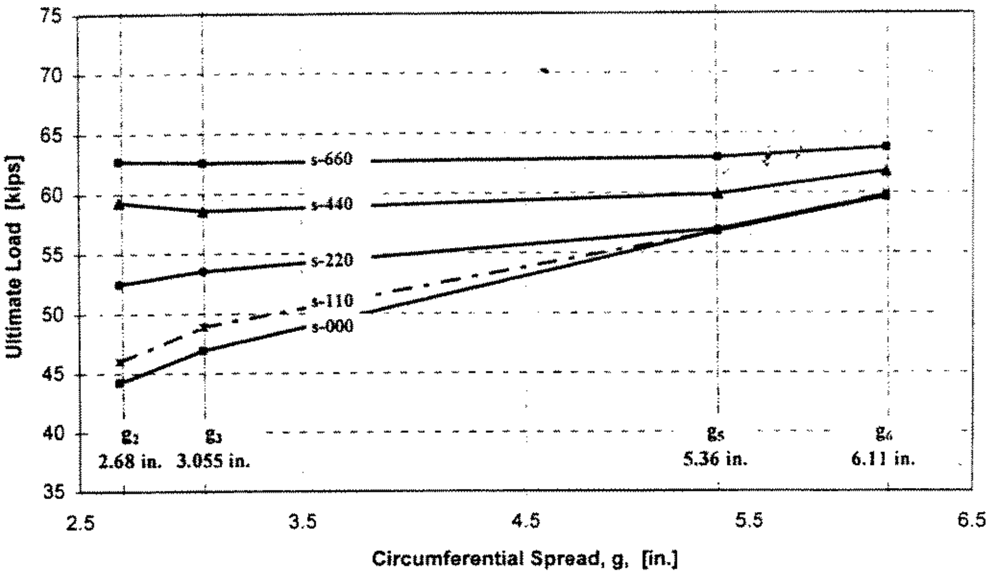

Figure 5-3: Effect of Circumferential Spread on $P_{ult}$ for Stub-Column Specimens with Two Patches with Pinned Ends for variable s distance (2T***P3)

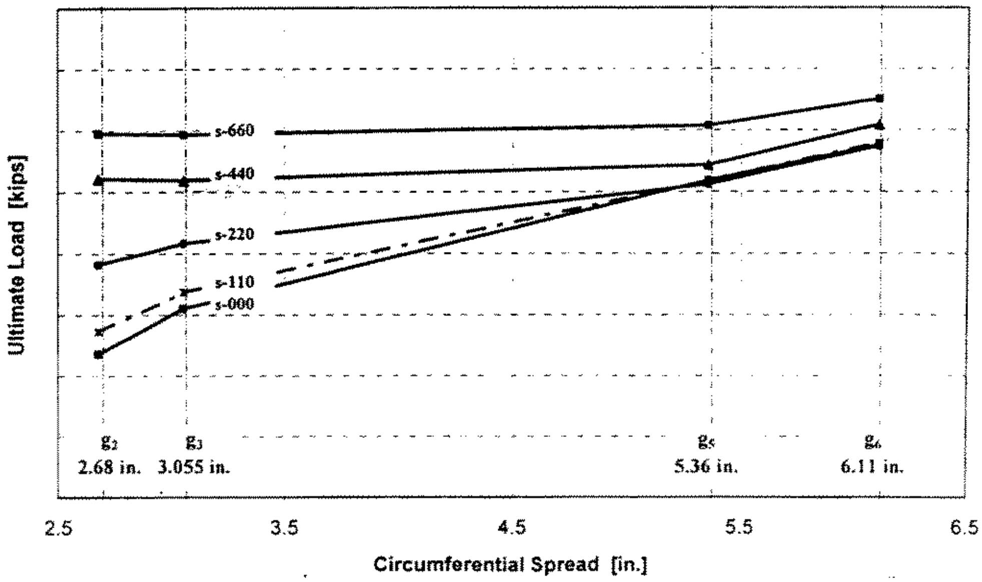

Figure 5-4: Effect of Circumferential Spread g on $P_u$ of Short Specimens ($\ell$=90 in.) with Two Patches and Pinned Ends for Variable Spacing s (2S***P3)

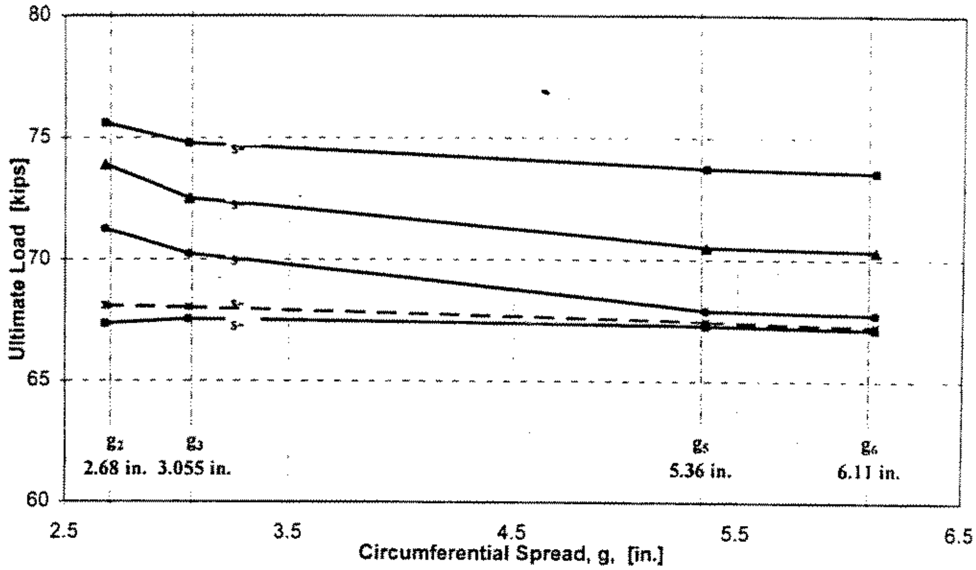

Figure 5-5: Effect of Circumferential Spread **g** on $P_u$ of Stub-Column Specimens ($\ell$=12.5 in.) with Two Patches and Fixed Ends for Variable Spacing s (2S***F3)

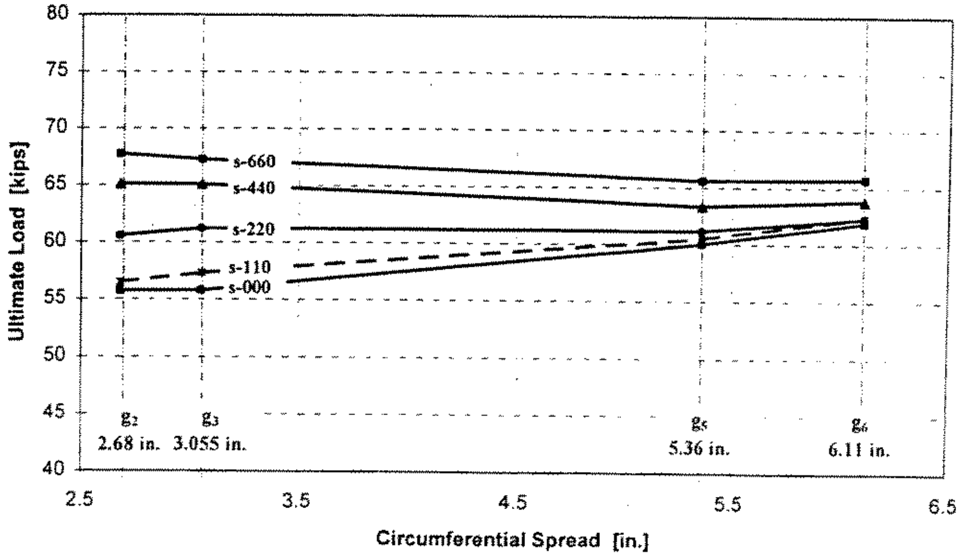

Figure 5-6: Effect of Circumferential Spread **g** on $P_u$ for Fixed-End Short Specimens ($\ell$ = 90 in.) with Two Corrosion Patches for Variable Longitudinal Spacing s (2S***F3)

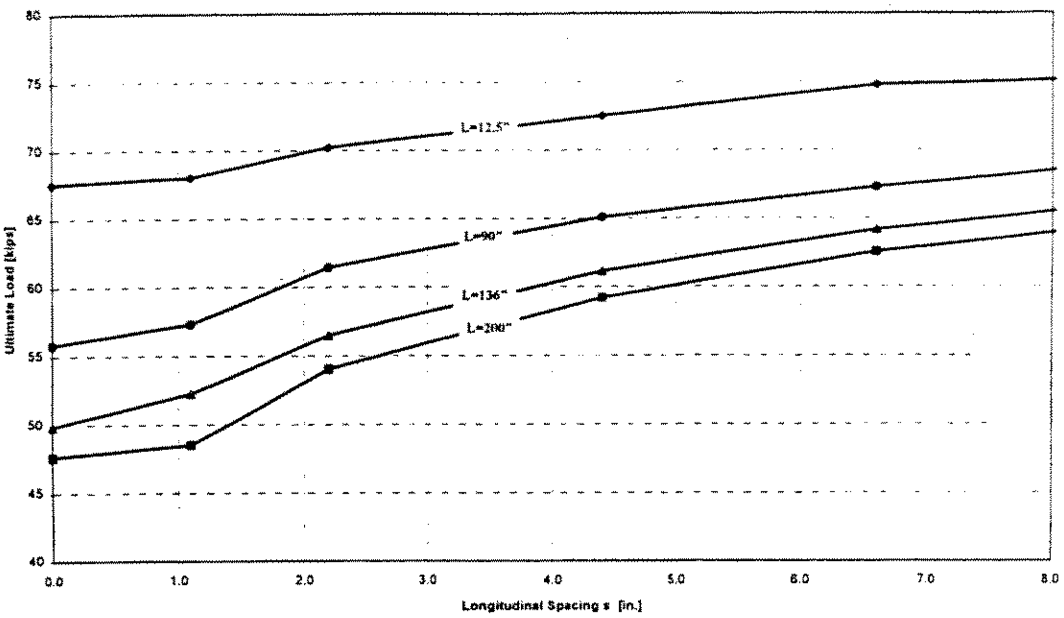

Figure 5-7: Effect of Longitudinal Spacing s on $P_{ult}$ for Specimens of Different Lengths with Two Patches and Fixed Ends for g=3.055 in. (2*3**F3)

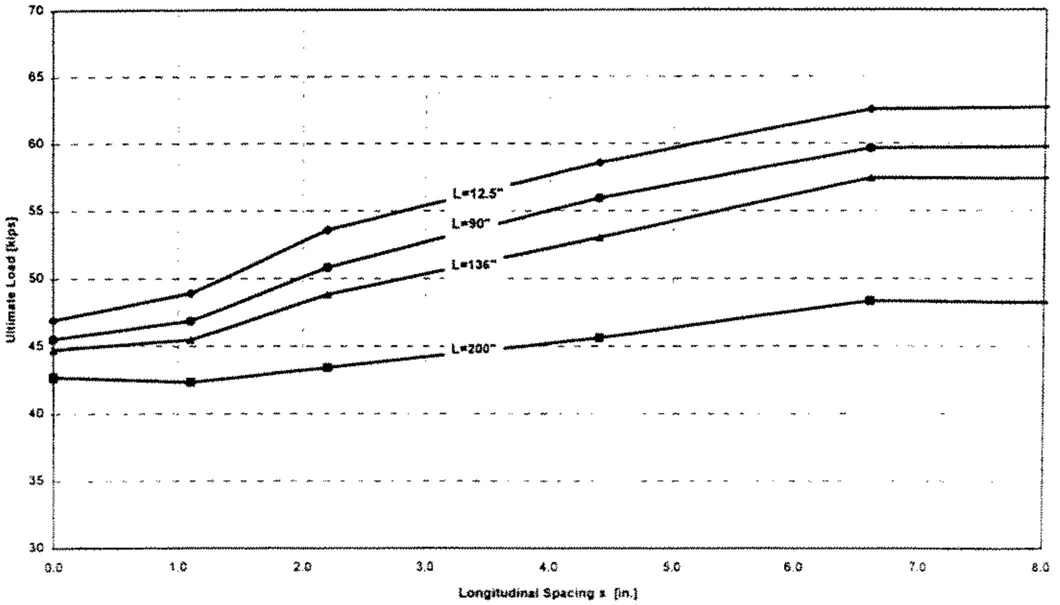

Figure 5-8: Effect of Longitudinal Spacing s on $P_{ult}$ for Specimens of Different Lengths with Two Patches and Pinned Ends for g=3.055 in. (2*3**P3)

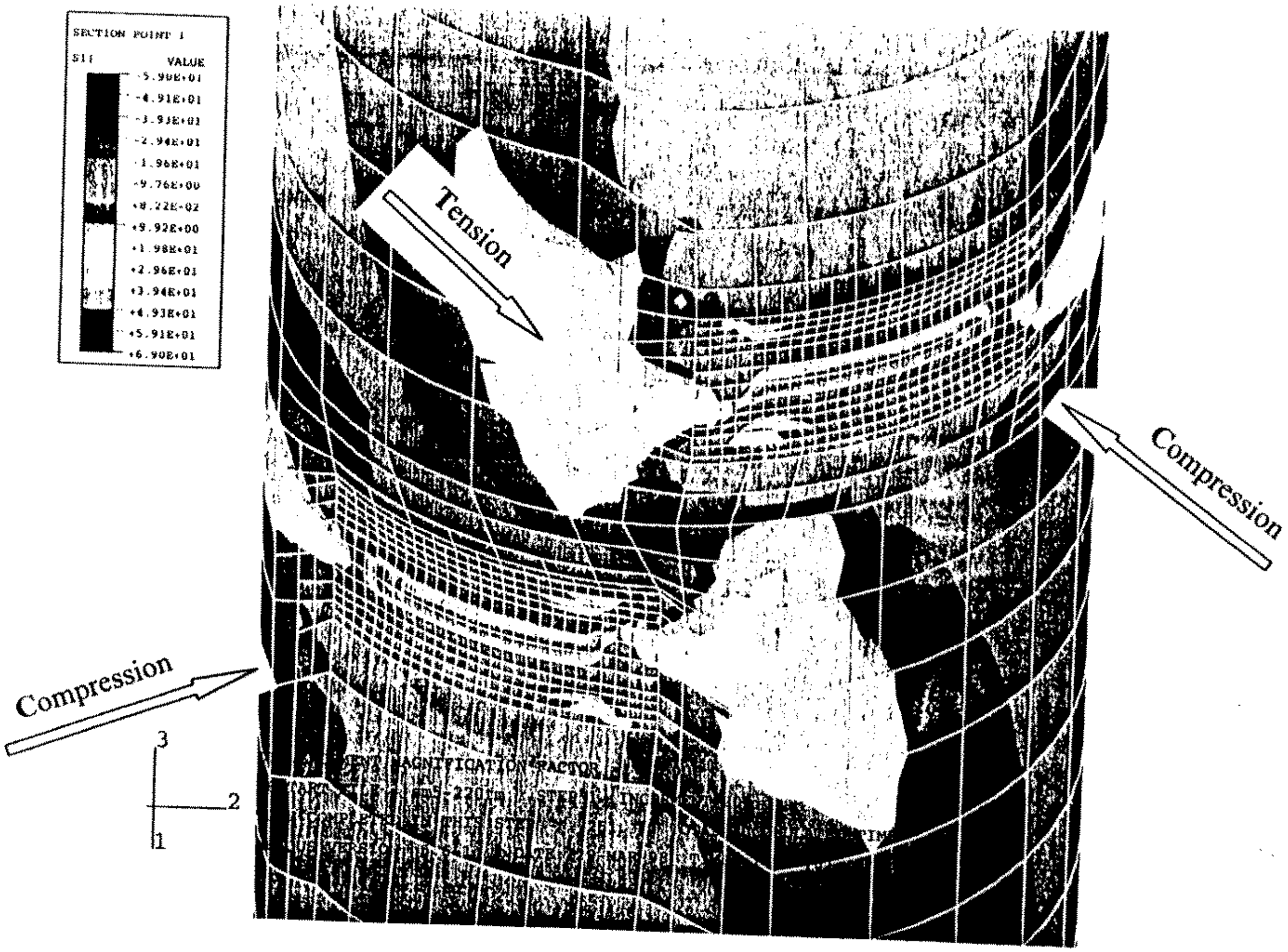

Figure 5-9: Contour Plot for Longitudinal Stress on the Outside Surface of Specimen 2M522F3 and the Interaction Between the Two Patches

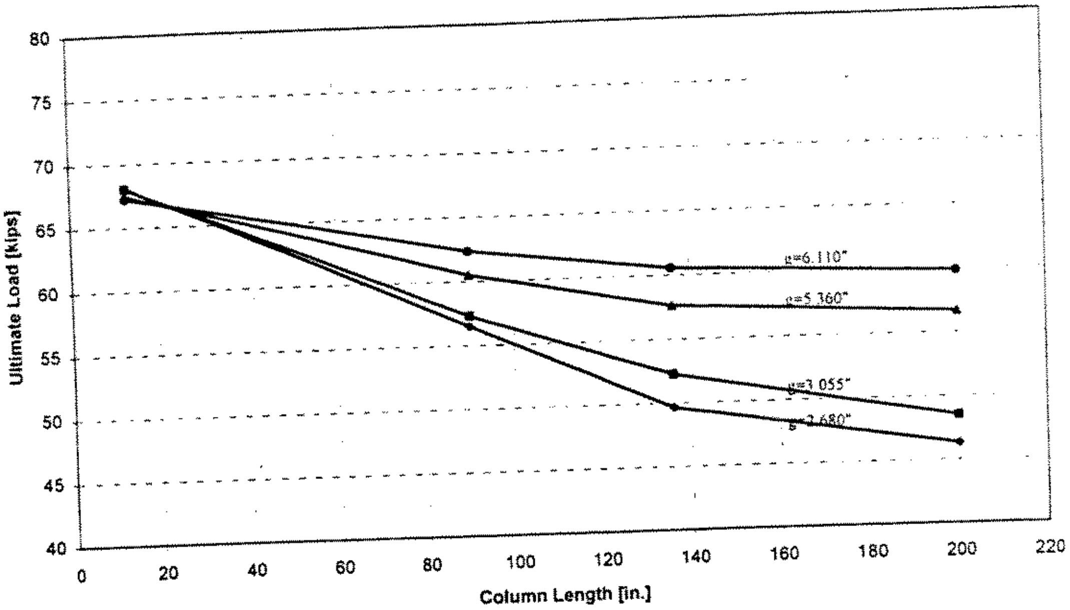

Figure 5-10: Effect of Column Length on $P_{ult}$ for Specimens with Two Patches with Fixed Ends and s=1.10 for variable g distance (2**11F3)

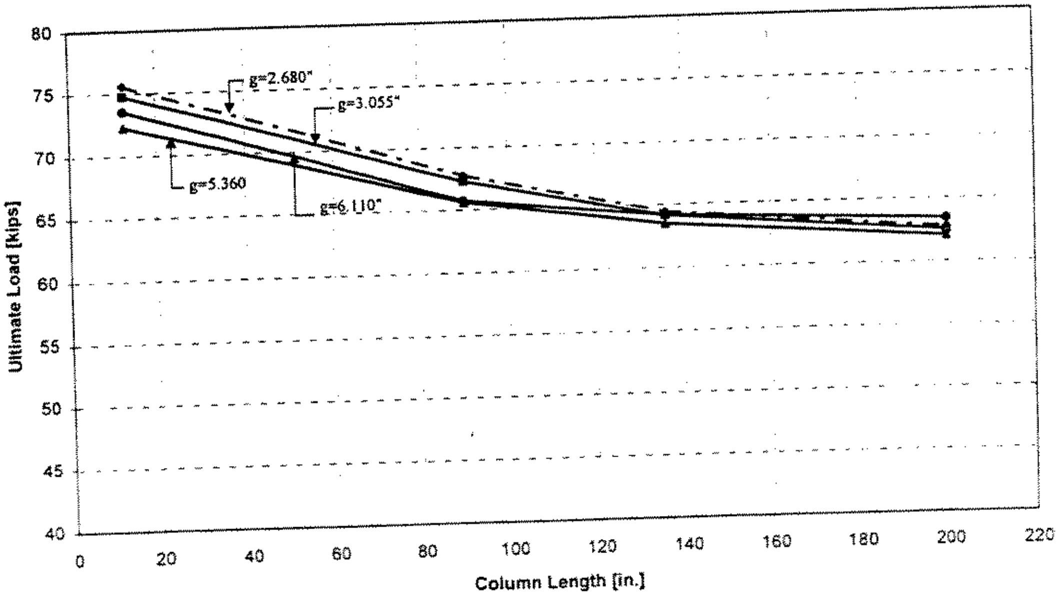

Figure 5-11: Effect of Column Length on $P_{ult}$ for Specimens with Two Patches with Fixed Ends and s=6.60 for variable g distance (2**66F3)

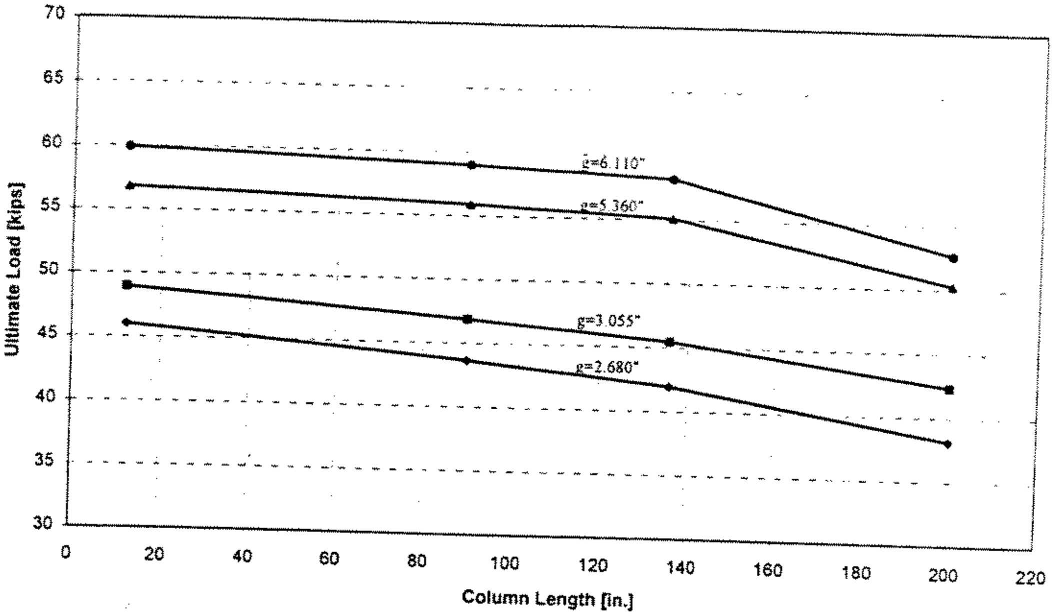

Figure 5-12: Effect of Column Length L on $P_{ult}$ for Specimens with Two Patches with Pinned Ends and s=1.10 for variable g distance (2**11P3)

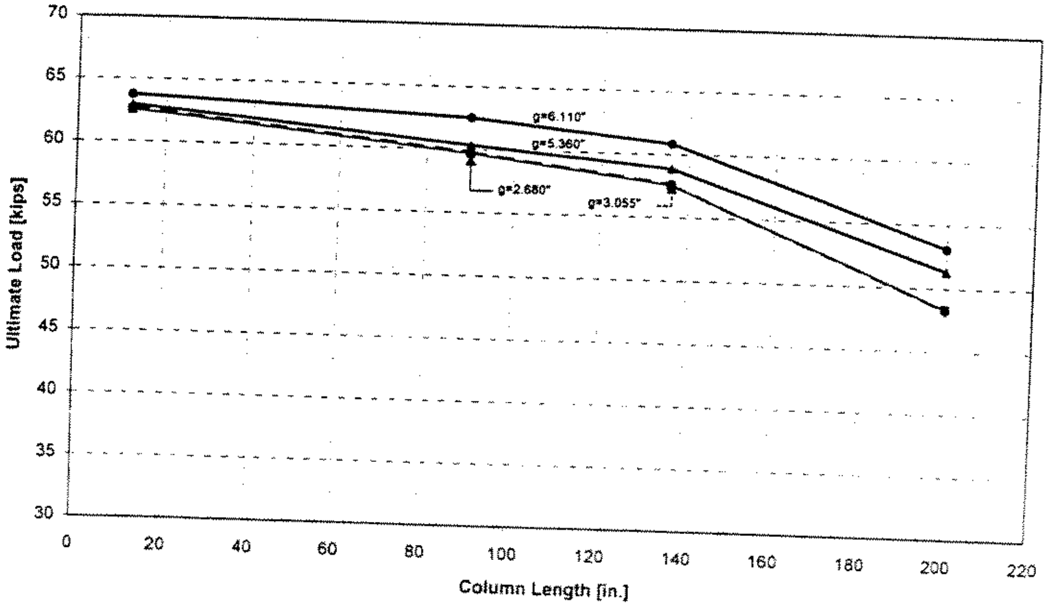

Figure 5-13: Effect of Column Length L on $P_{ult}$ for Specimens with Two Patches with Pinned Ends and s=6.60 for variable g distance (2**66P3)

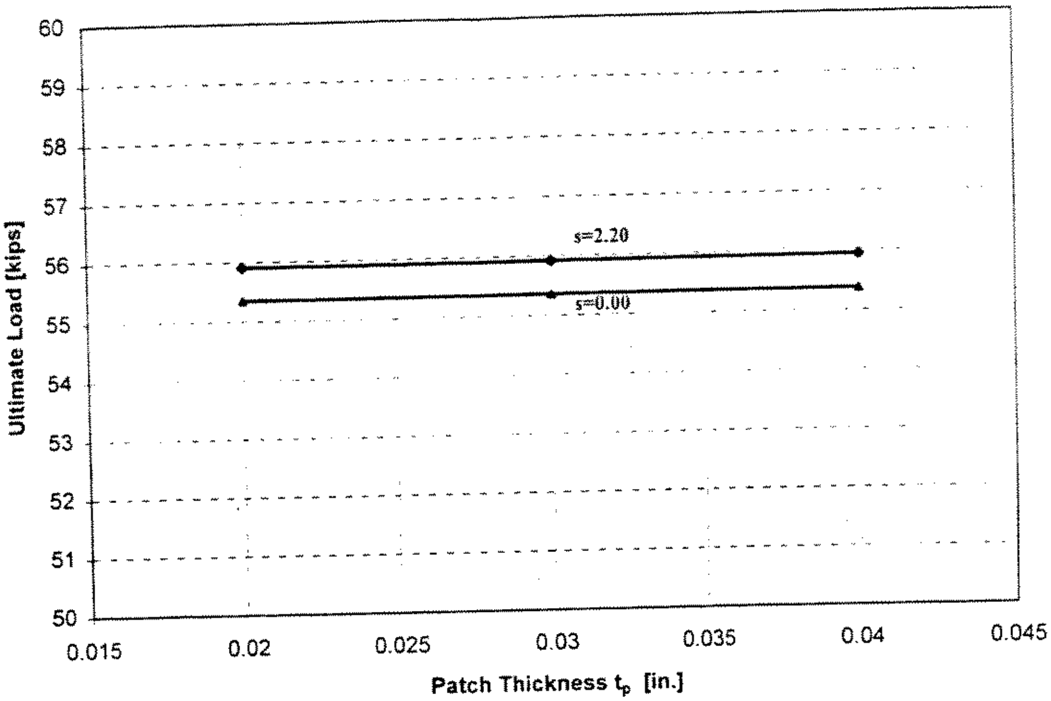

Figure 5-14: Effect of Patch Thickness $\mathbf{t_p}$ on $P_u$ of Short Specimens ($\ell$=90 in.) with Two Patches, Fixed Ends and g=5.36 in. for Variable Spacing s (2S5**F*)

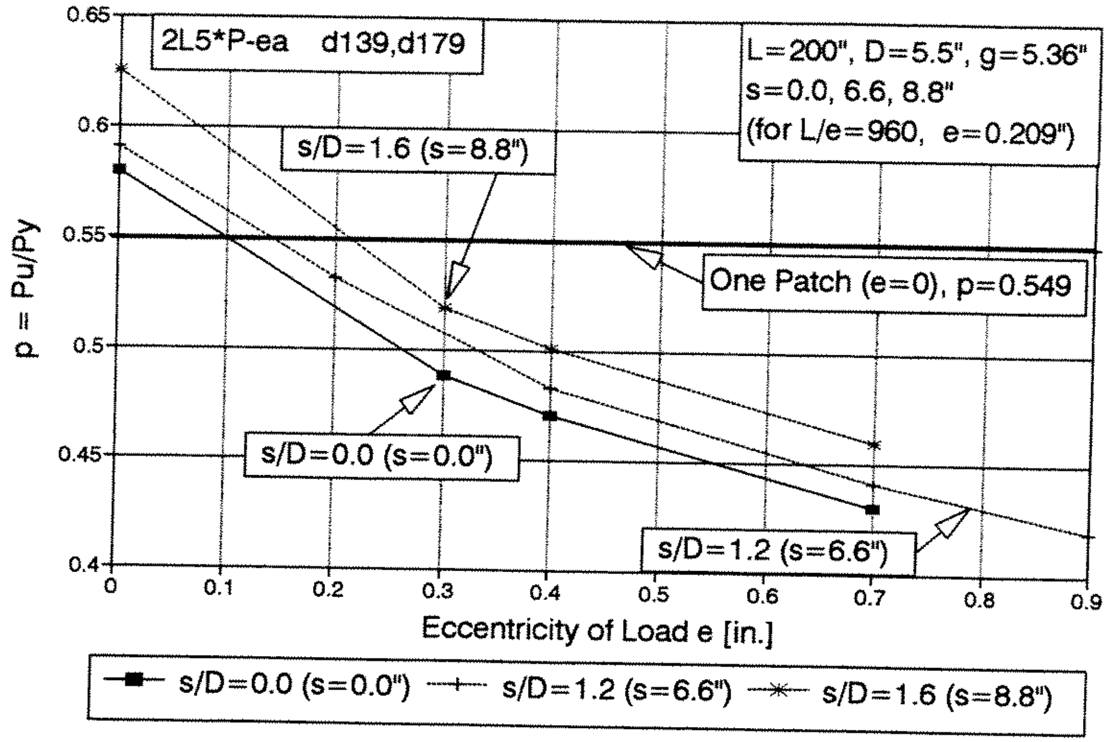

Figure 5-15: Effect of Load Eccentricity e on Capacity of Pinned-End Tubular Columns with Two Corrosion Patches

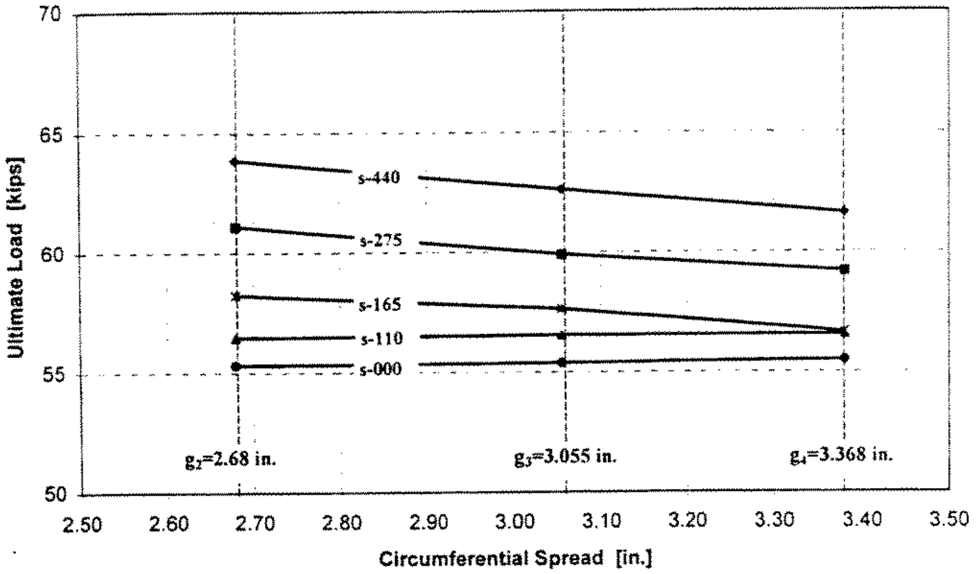

Figure 6-1: Effect of Circumferential Spread **g** on $P_u$ of Stub-Column Specimens ($\ell$=12.5 in.) with Three Corrosion Patches and Fixed Ends (3T***F2)

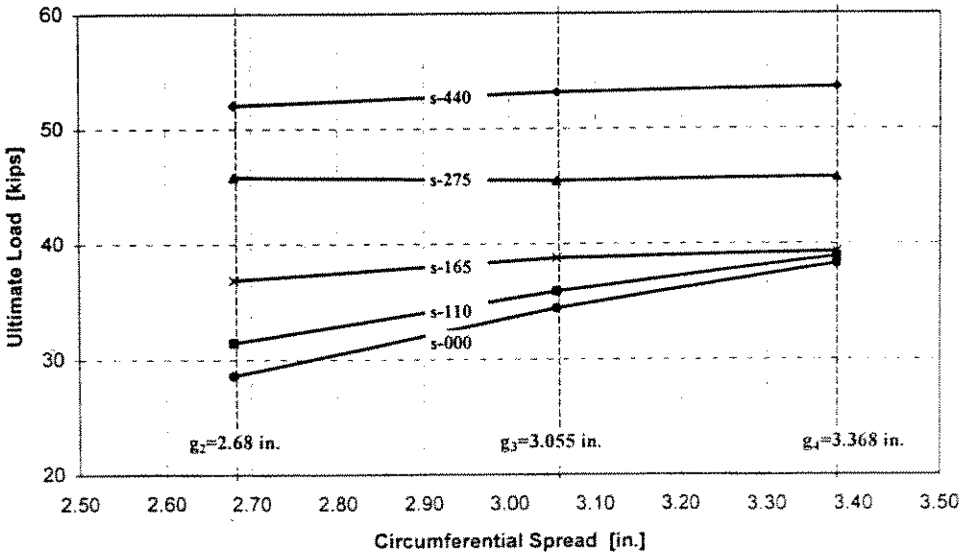

Figure 6-2: Effect of Circumferential Spread **g** on $P_u$ for Pinned-End Stub-Column Specimens with Three Corrosion Patches for Different Values of Longitudinal Spacing **s** (3T***P2)

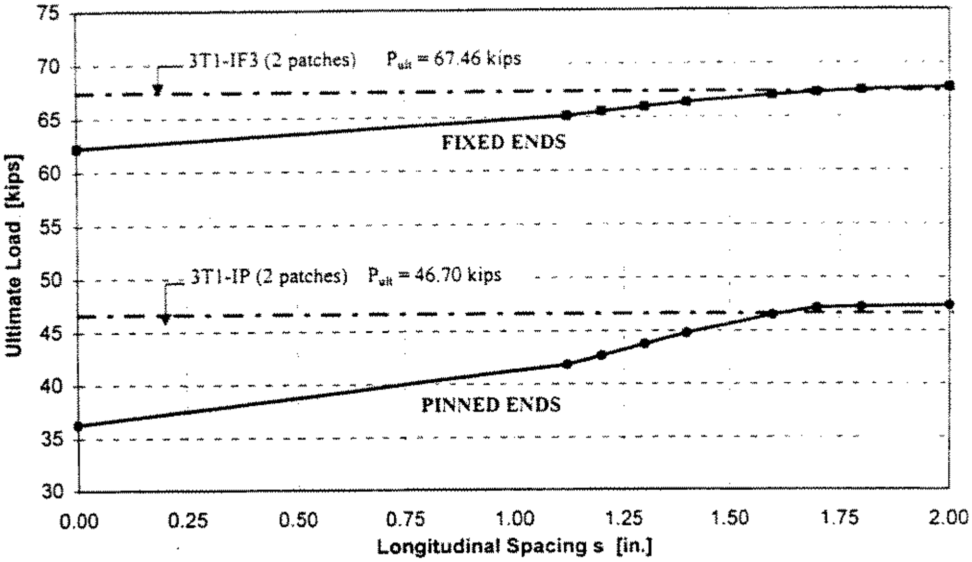

Figure 6-3: Effect of Longitudinal Spacing s on $P_u$ for Stub-Column Specimens with Three Corrosion Patches and Fixed or Pinned Ends and g=1.60 in. (3T1***3)

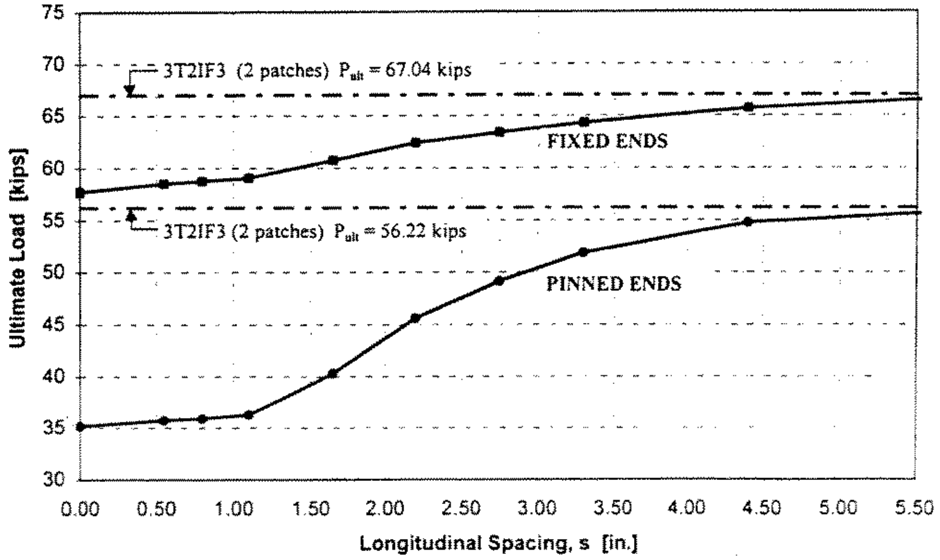

Figure 6-4: Effect of Longitudinal Spacing s on $P_u$ for Stub-Column Specimens with Three Corrosion Patches and Fixed or Pinned Ends and g=2.68 in. (3T2***3)

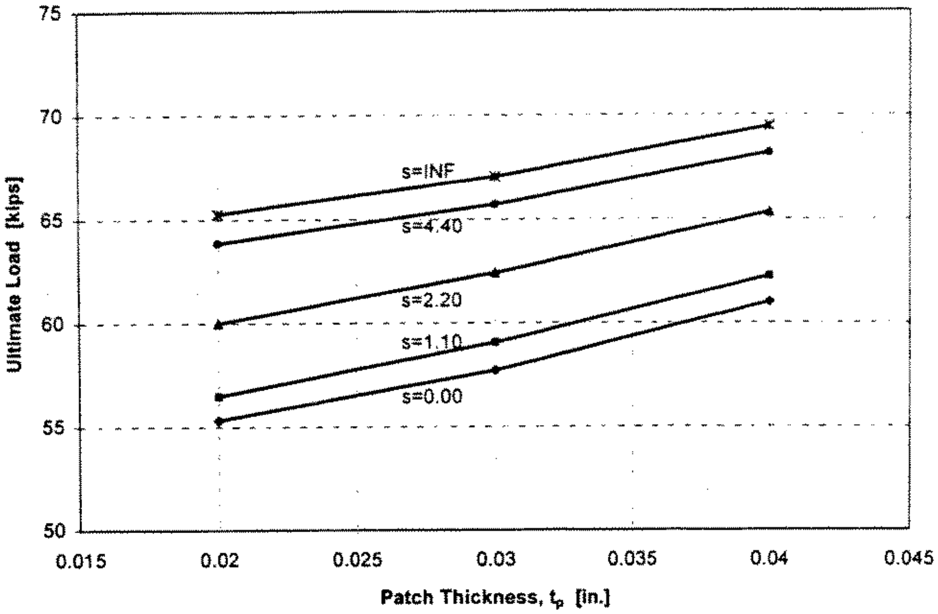

Figure 6-5a: Effect of Patch Thickness $\mathbf{t_p}$ on $P_u$ of Short Specimens ($\ell$=90 in.) with Three Patches, Fixed Ends and g=2.68 in. for Variable Spacing s (3T2**F*)

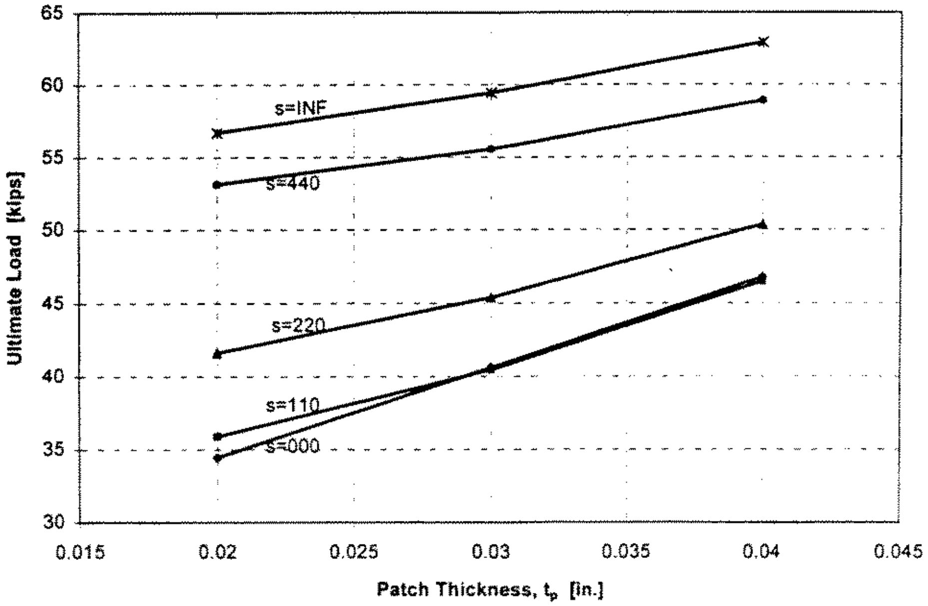

Figure 6-5b: Effect of Patch Thickness $\mathbf{t_p}$ on $P_u$ for Pinned-End Stub-Column Specimens with Three Corrosion Patches and g=3.055 in. (3T3**P*)

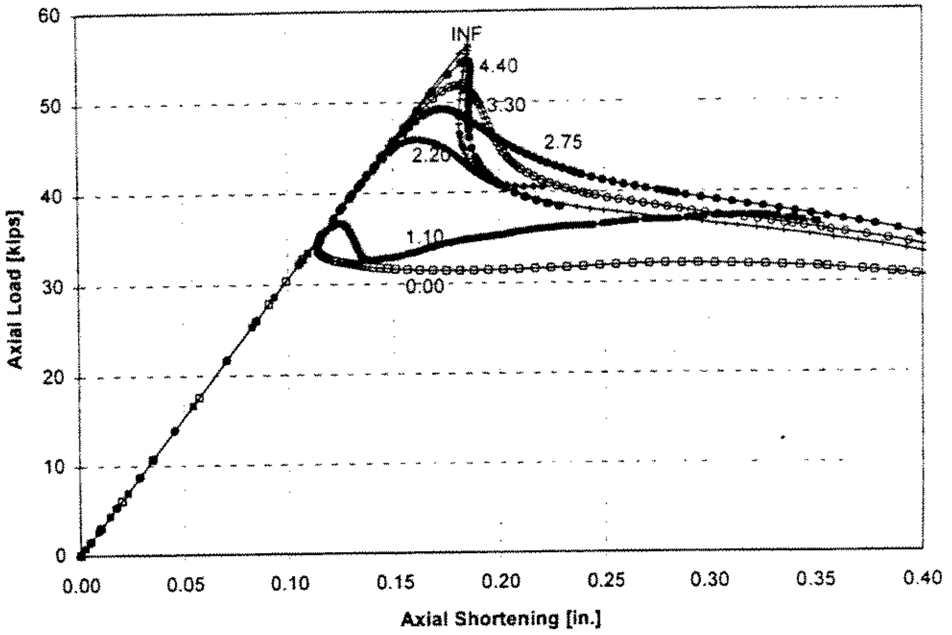

Figure 6-6a: Axial Load vs. Axial Shortening Behavior of 3-Patch Long (200 in.) Specimens with Fixed Ends and g=2.68 in. for Different Values of Longitudinal Spacing s (3L2**F3)

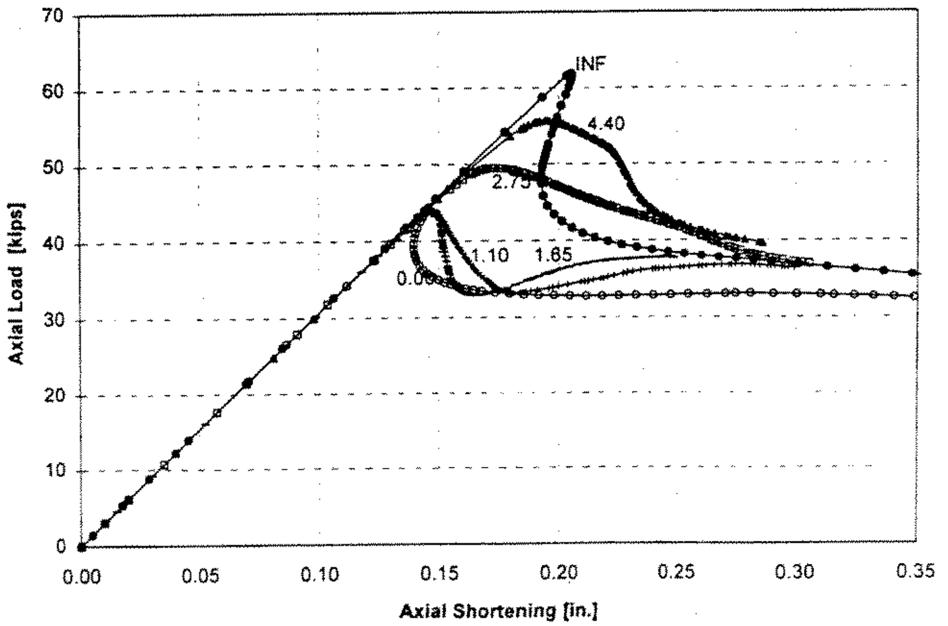

Figure 6-6b: Axial Load vs. Axial Shortening Behavior of 3-Patch Long (200 in.) Specimens with Fixed Ends and g=3.384 in. for Different Values of Longitudinal Spacing s (3L4**F3)

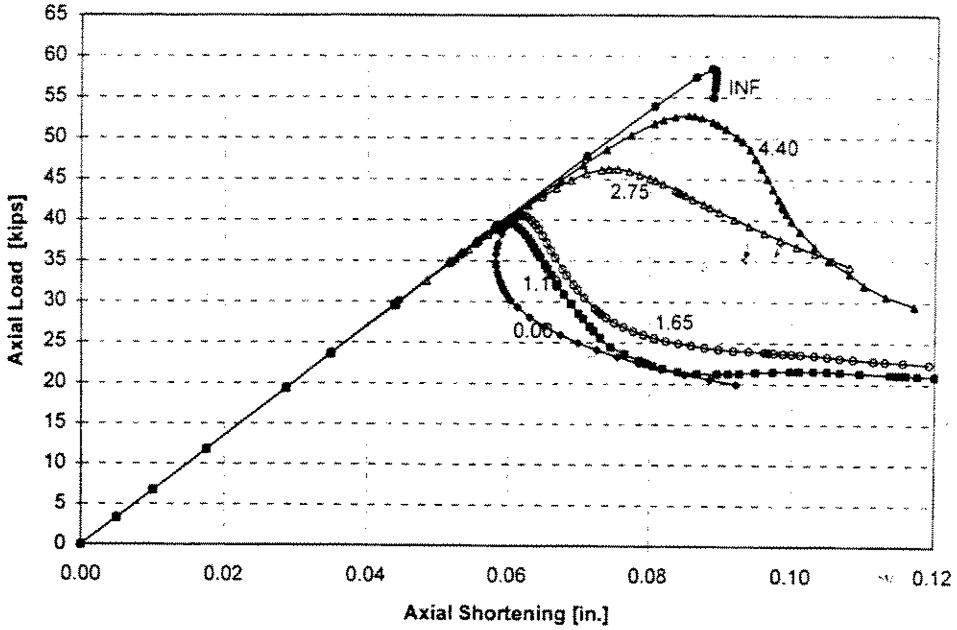

Figure 6-7a: Axial Load vs. Axial Shortening Behavior of 3-Patch Short (90 in.) Specimens with Pinned Ends and g=3.055 in. for Different Values of Longitudinal Spacing s (3S3**P3)

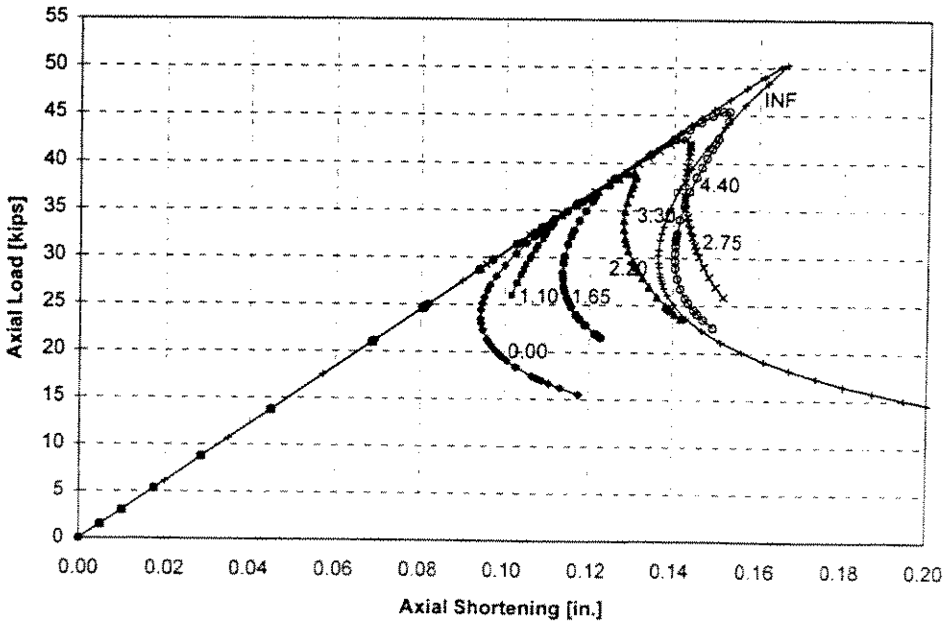

Figure 6-7b: Axial Load vs. Axial Shortening Behavior of 3-Patch Long (200 in.) Specimens with Pinned Ends and g=2.68 in. for Different Values of Longitudinal Spacing s (3L2**P3)

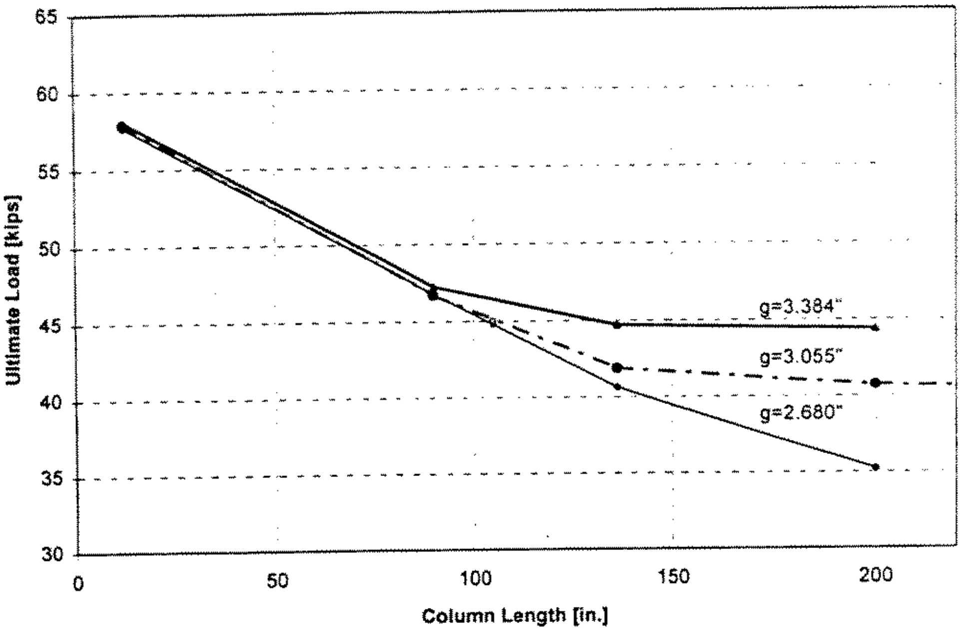

Figure 6-8a: Effect of Column Length on $P_{ult}$ for Specimens with Three Patches with Fixed Ends and s=0.00 for variable g distance (3**00F3)

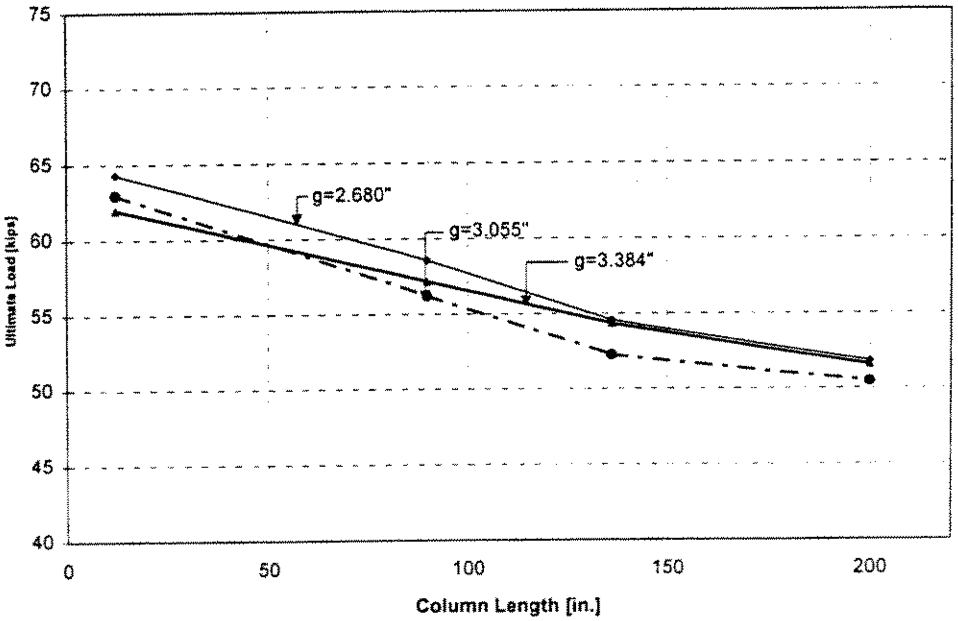

Figure 6-8b: Effect of Column Length on $P_{ult}$ for Specimens with Three Patches with Fixed Ends and s=3.30 for variable g distance (3**33F3)

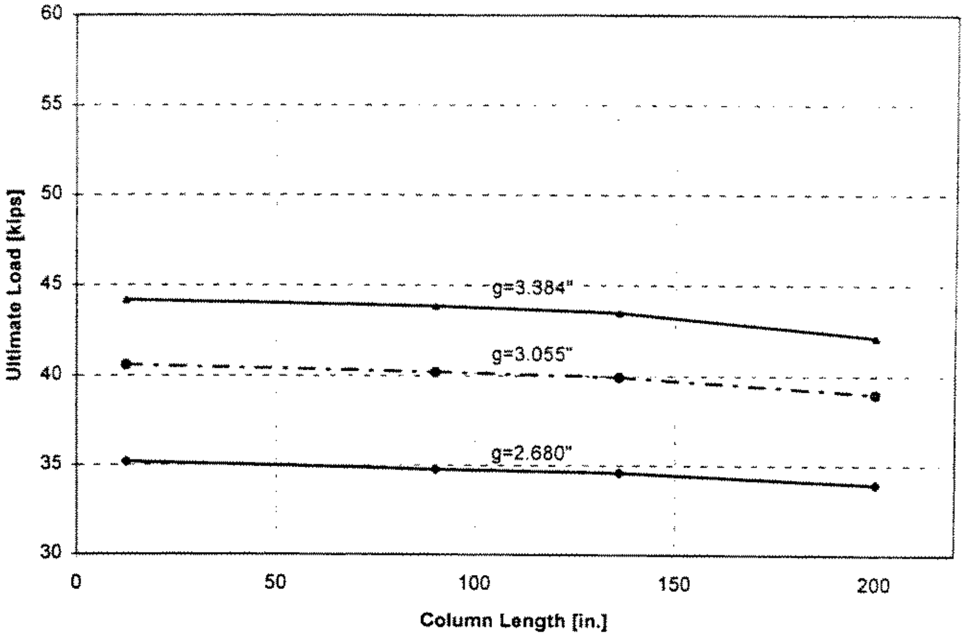

Figure 6-9a: Effect of Column Length on $P_{ult}$ for Specimens with Three Patches with Pinned Ends and s=0.00 for variable g distance (3**00P3)

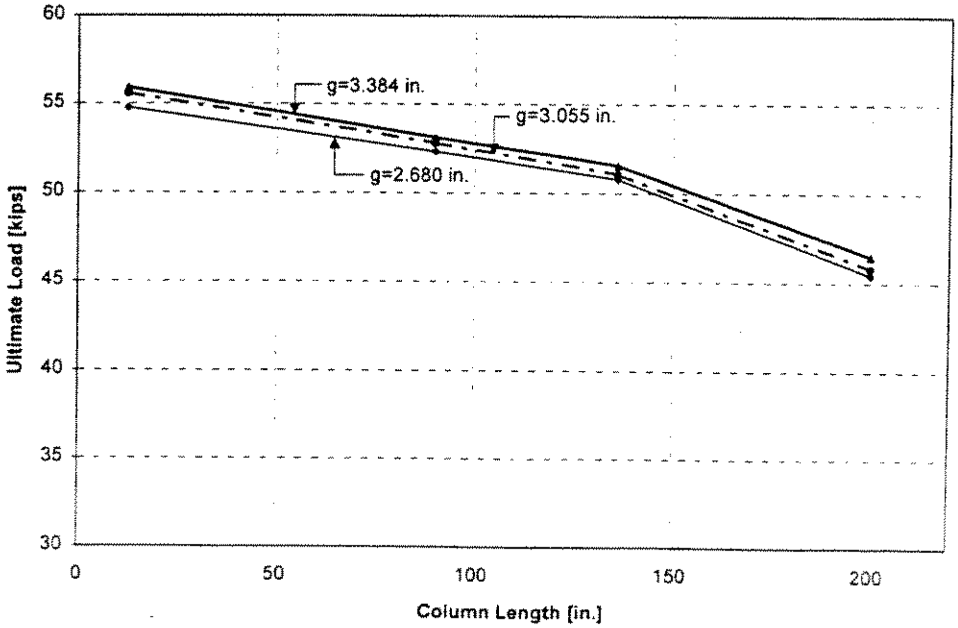

Figure 6-9b: Effect of Column Length on $P_{ult}$ for Specimens with Three Patches with Pinned Ends and s=4.40 for variable g distance (3**44P3)

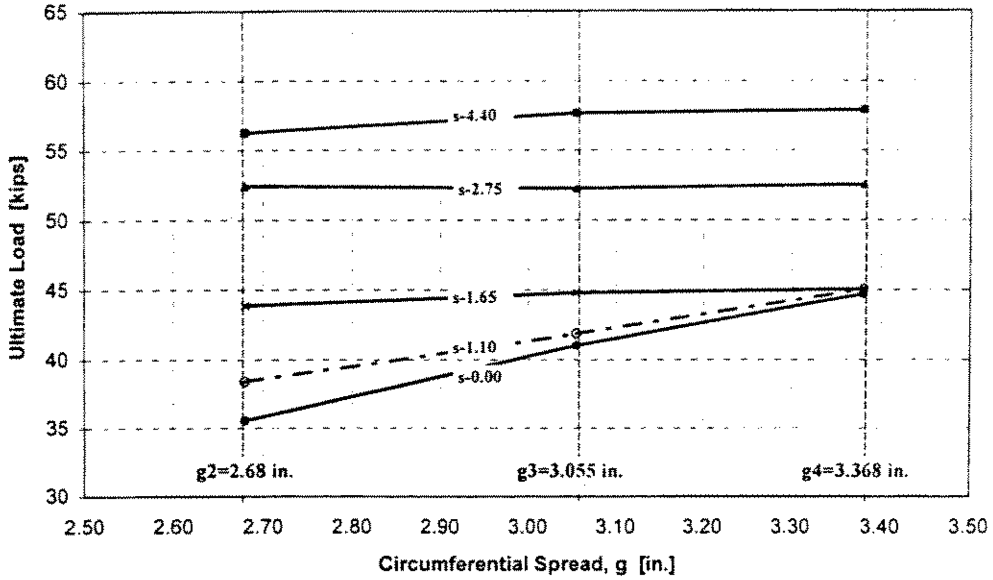

Figure 6-10: Effect of Circumferential Spread **g** on $P_u$ for Fixed-End Median Specimens ($\ell$ = 136 in.) with Three Corrosion Patches for Different Values of **s** (3M***F3)

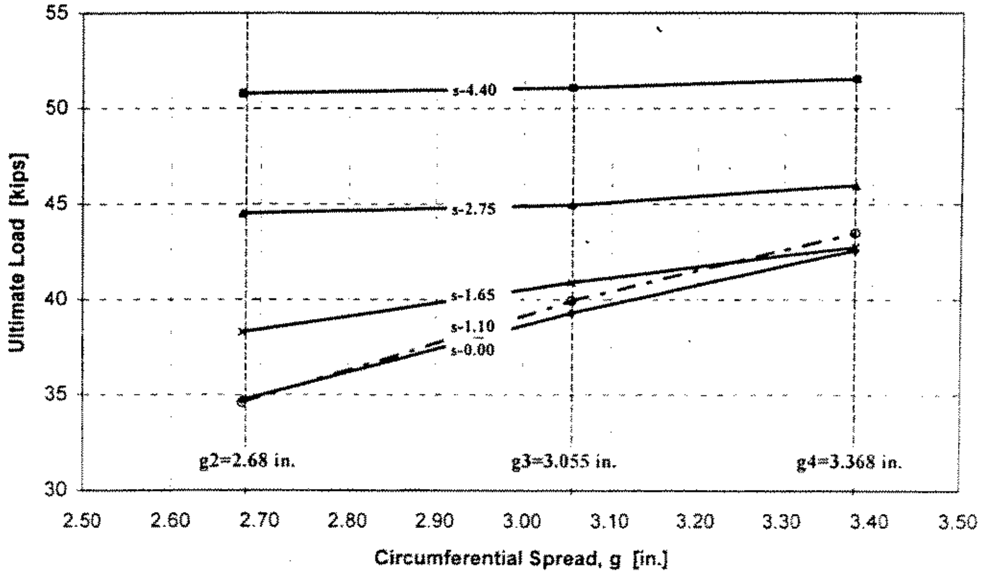

Figure 6-11: Effect of Circumferential Spread **g** on $P_u$ for Pinned-End Median Specimens ($\ell$ = 136 in.) with Three Corrosion Patches for Different Values of **s** (3M***P3)

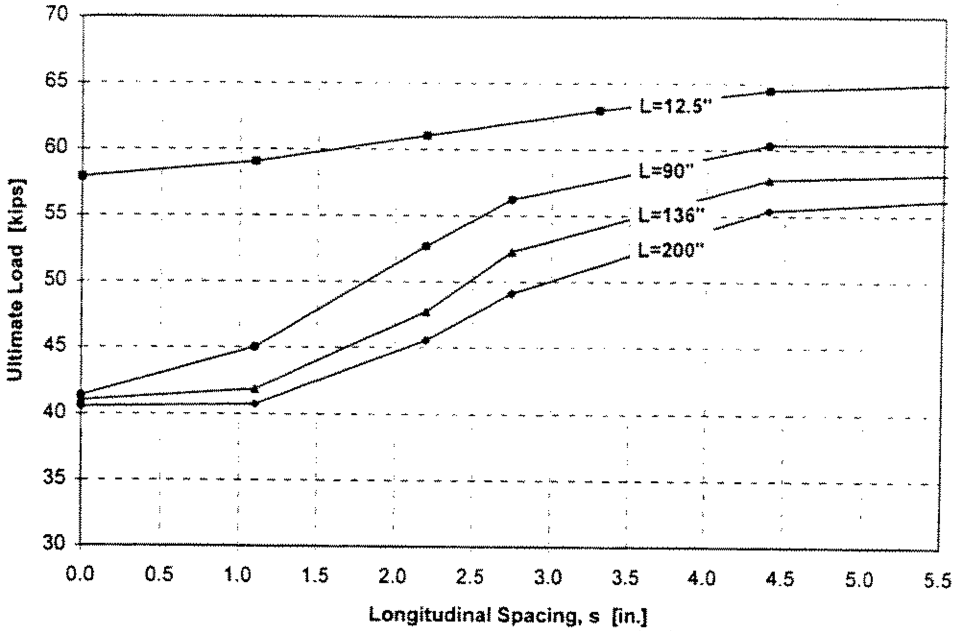

Figure 6-12a: Effect of Longitudinal Spacing **s** on $P_u$ for Fixed-End Specimens with Three Corrosion Patches, g=3.055 in. and Different Lengths (3*3**F3)

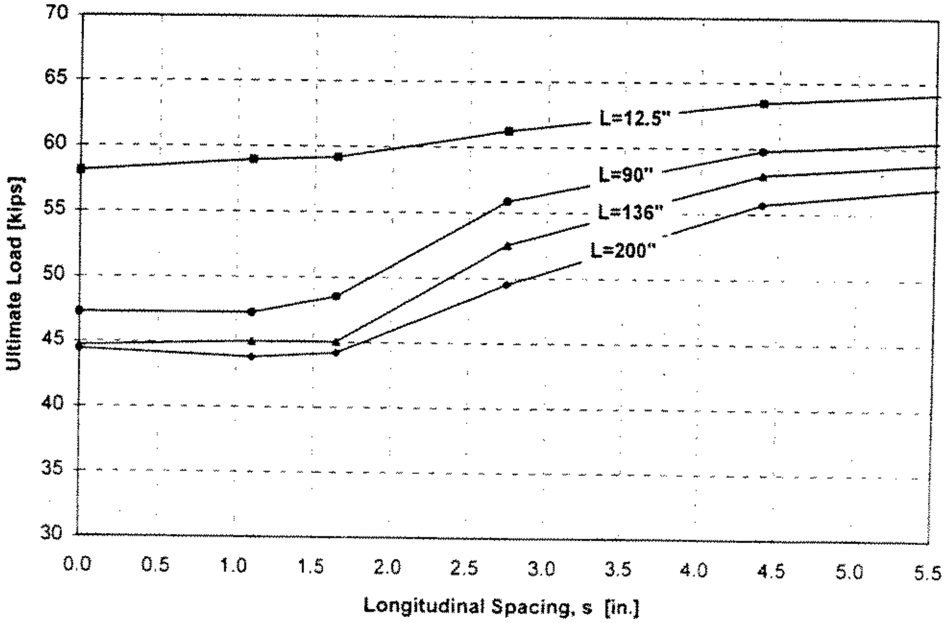

Figure 6-12b: Effect of Longitudinal Spacing s on $P_u$ for Fixed-End Specimens with Three Corrosion Patches, **g**=3.384 in. and Different Lengths (3*4**F3)

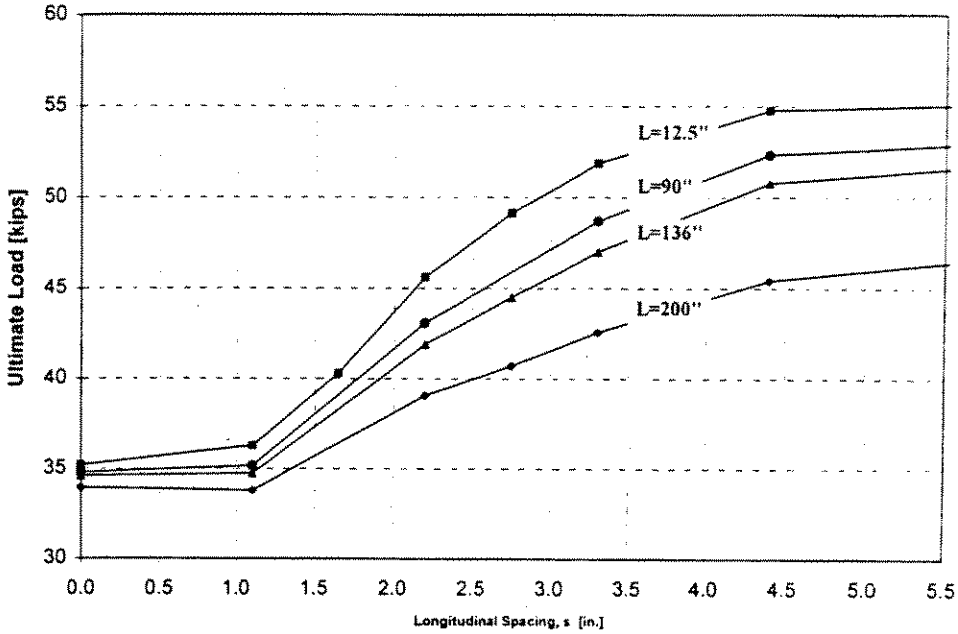

Figure 6-13a: Effect of Longitudinal Spacing s on $P_u$ of specimens with Three Patches, Pinned Ends and g=2.68 in. for Variable Lengths (3*2**P3)

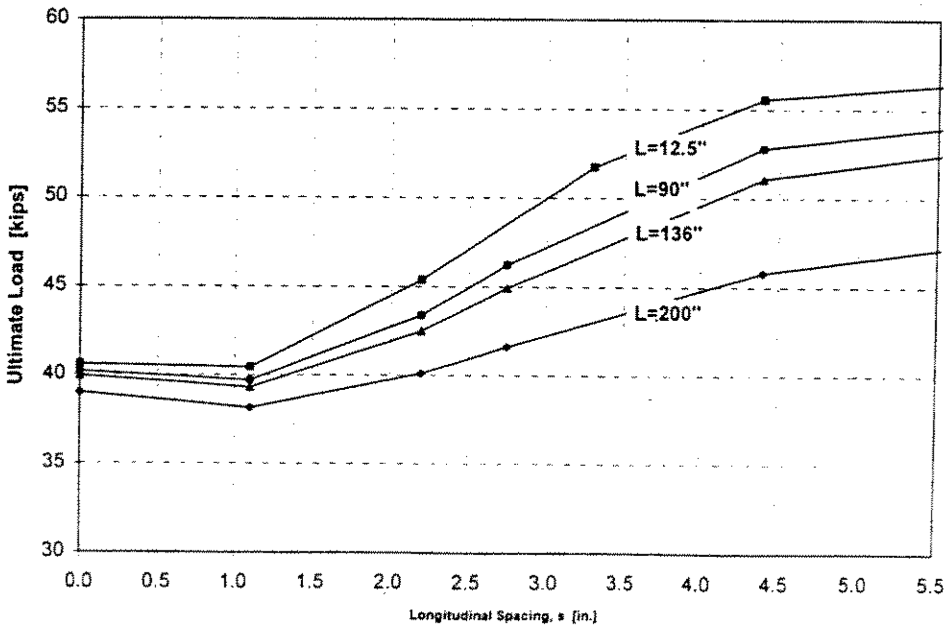

Figure 6-13b: Effect of Longitudinal Spacing s on $P_u$ of specimens with Three Patches, Pinned Ends and g=3.055 in. for Variable Lengths (3*3**P3)

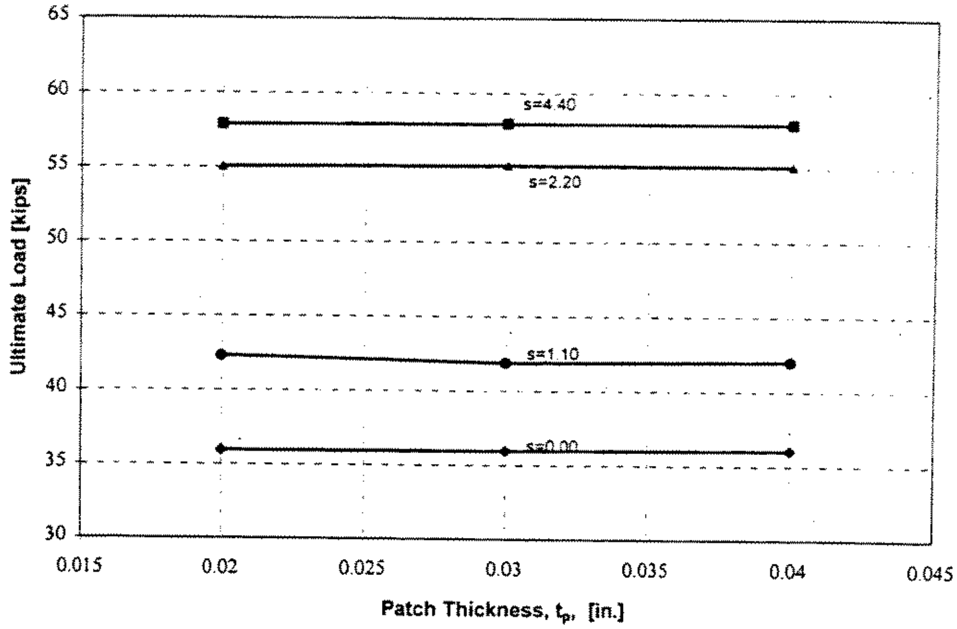

Figure 6-14: Effect of Patch Thickness $t_p$ on $P_u$ of Long Specimens ($\ell$=200 in.) with Three Patches, Fixed Ends and g=2.68 in. for Variable Spacing s (3L2**F*)

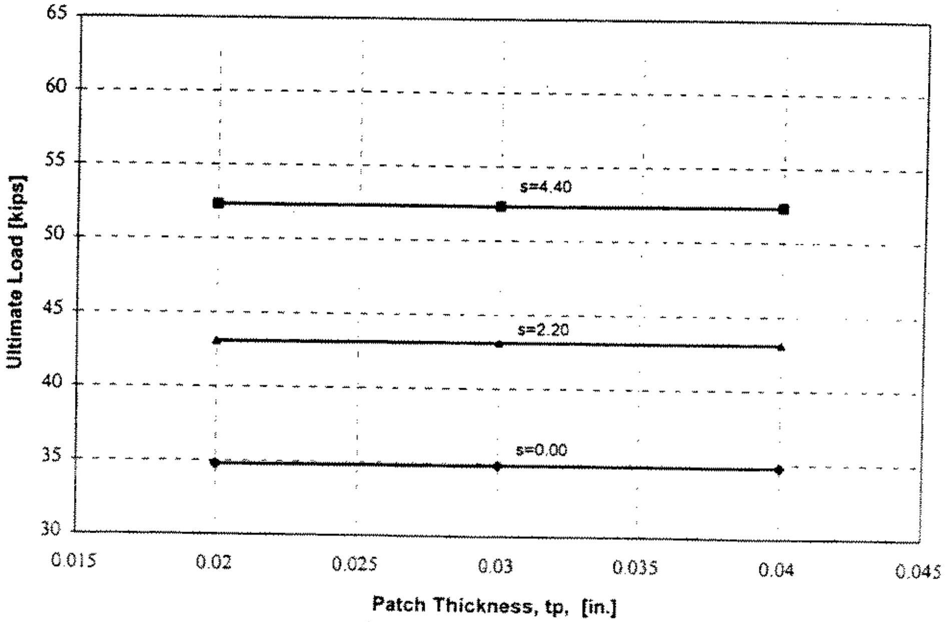

Figure 6-15: Effect of Patch Thickness $t_p$ on $P_u$ of Long Specimens ($\ell$=200 in.) with Three Patches, Pinned Ends and g=2.68 in. for Variable Spacing s (3L2**P*)

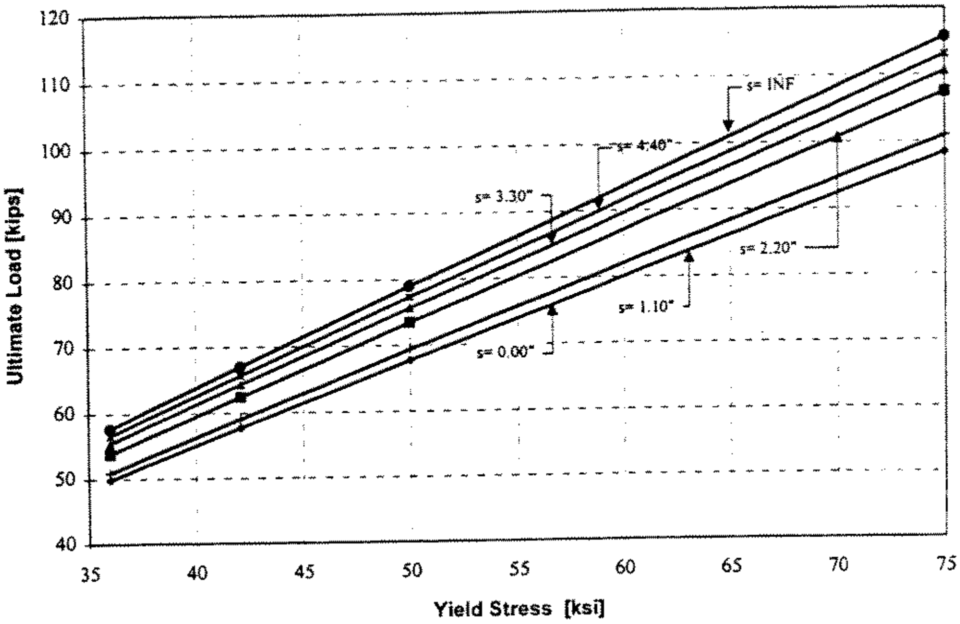

Figure 6-16: Effect of Yield Stress $F_y$ on $P_u$ of Stub-Column Specimens ($\ell$=12.5 in.) with Three Patches, Fixed Ends and g=2.68 in. for Variable Spacing s (3T2**F3)

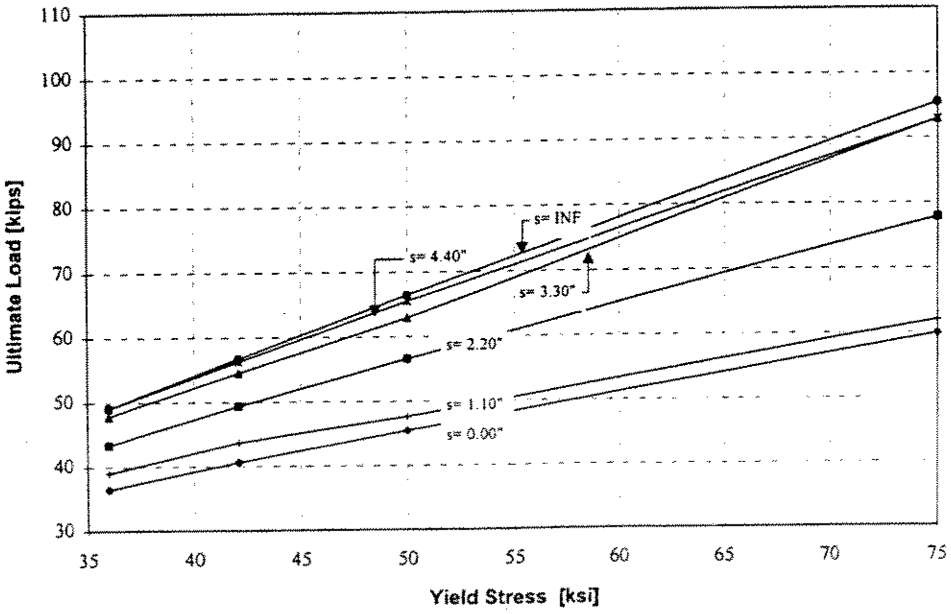

Figure 6-17: Effect of Yield Stress $F_y$ on $P_u$ of Median Specimens ($\ell$=136 in.) with Three Patches, Fixed Ends and g=2.68 in. for Variable Spacing s (3M2**F3)

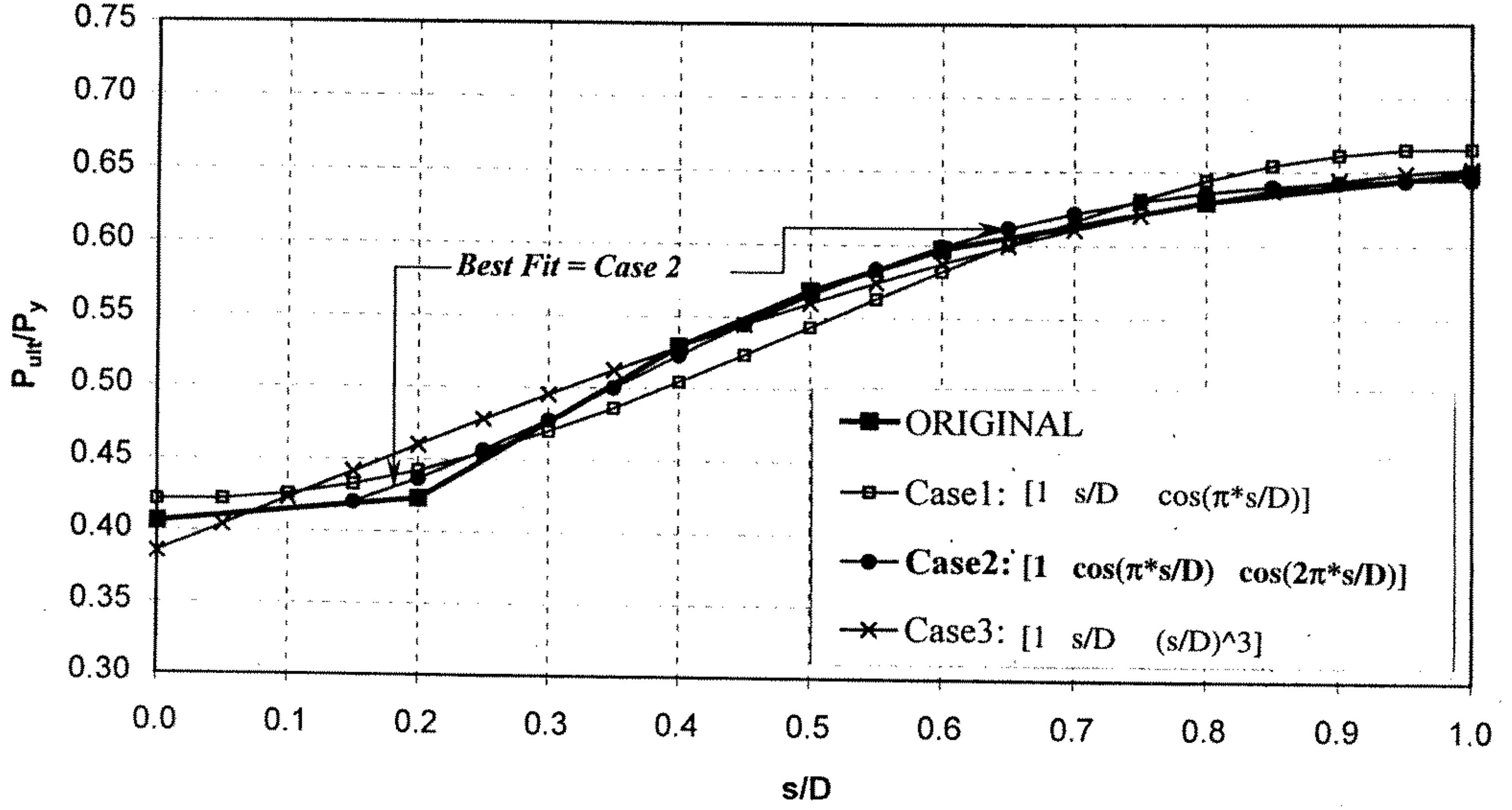

Figure 7-1: Selection of Coordinate Function for Longitudinal Spacing s in Long (200 in.) Fixed-End Specimens with Three Patches and g=2.68 in. (3L2**F3)

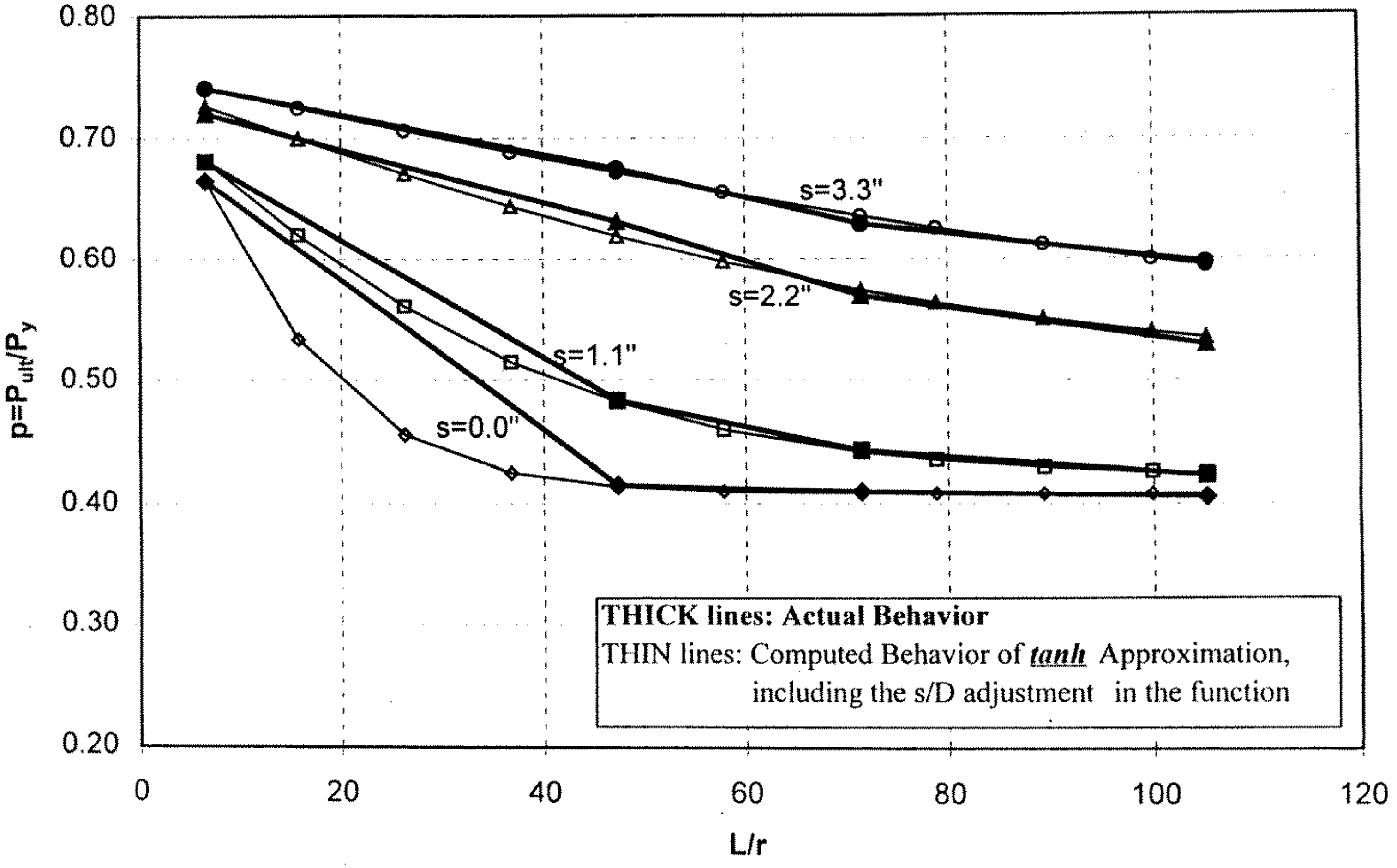

Figure 7-2: Selection of Coordinate Function for Column Length of Fixed-End Specimens with Three Patches and **g**=2.68 in. (3*2**F3)

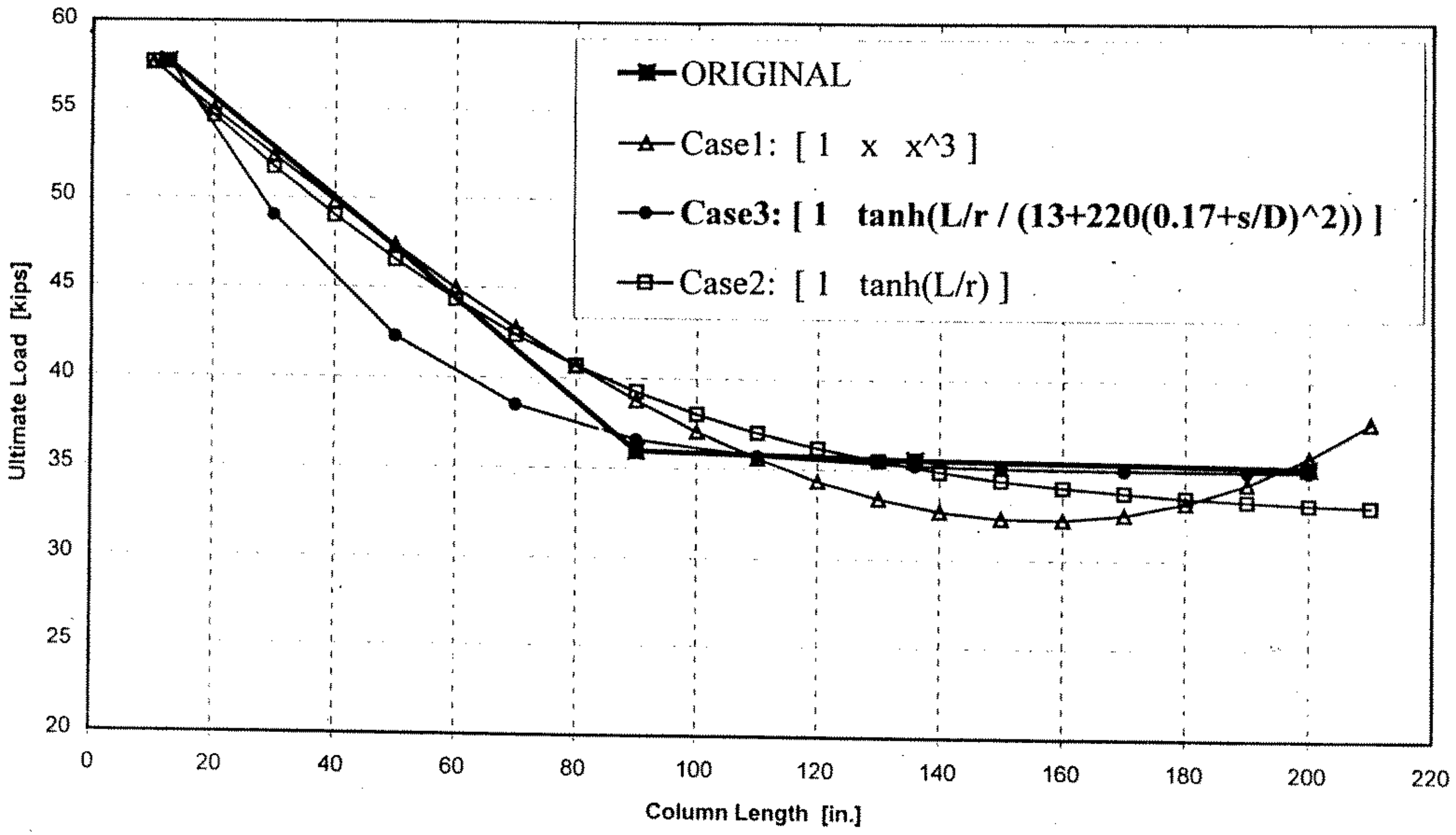

Figure 7-3: Application of "**tanh**" Approximation to Fixed-End Specimens with Three Patches and **g**=2.68 in. for Different s Values (3*288F3)

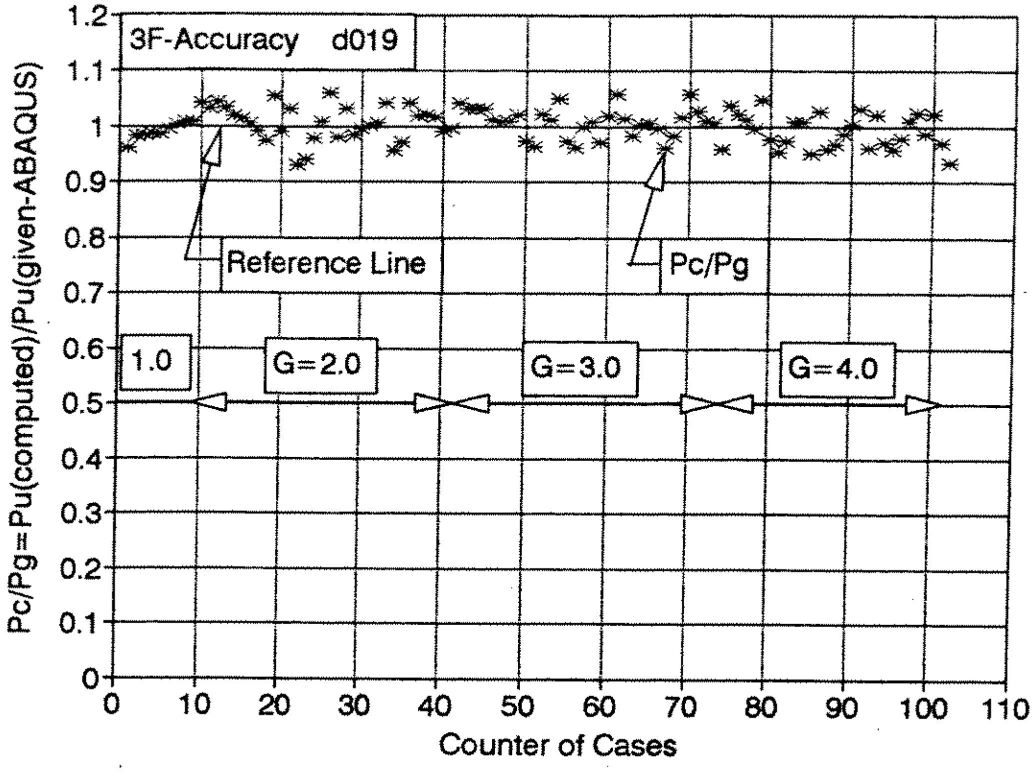

Figure 7-4: Accuracy of Proposed Formulas for Fixed-End Tubular Columns with Three Corrosion Patches

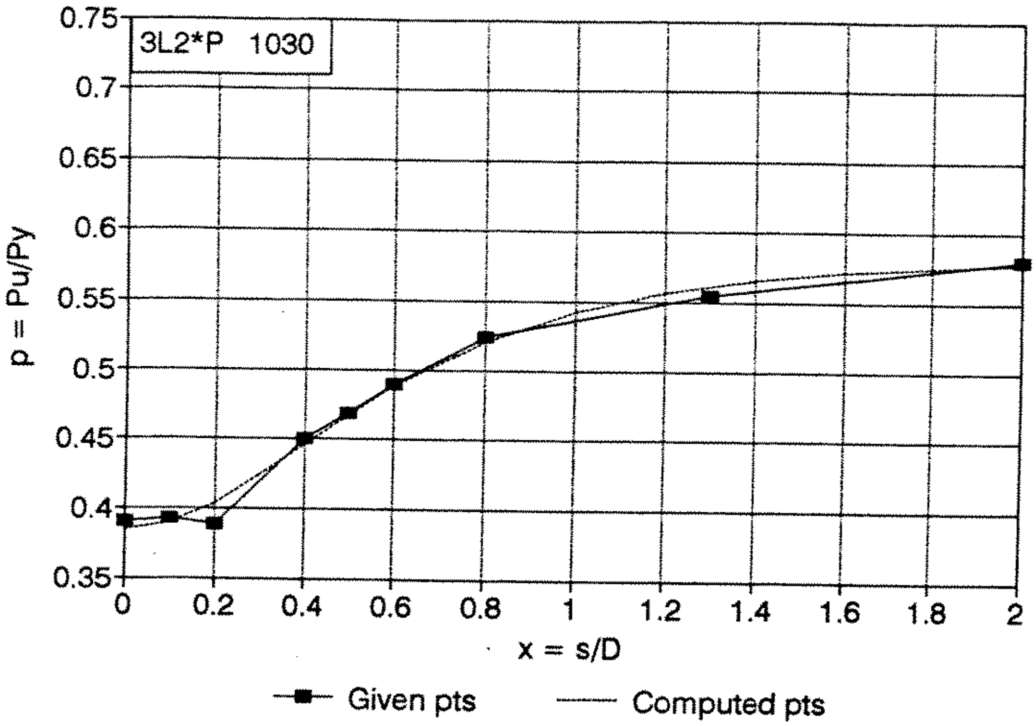

Figure 8-1: Typical Relationship between Ultimate Load ($p=P_u/P_y$) and Longitudinal Patch Spacing ($x=s/D$) for Pinned-End Tubular Columns with Three Patches (3L2**P3)

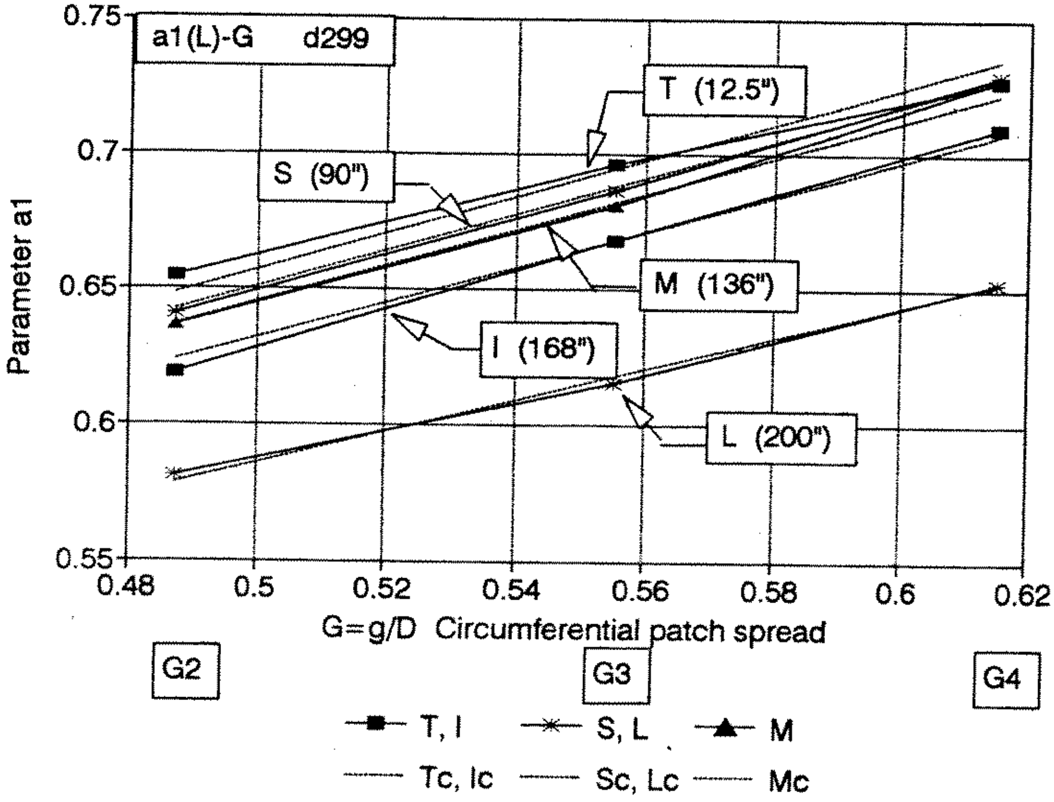

Figure 8-2: Parameter a1 as Function of Circumferential Spread g for Different Column Lengths $\ell$

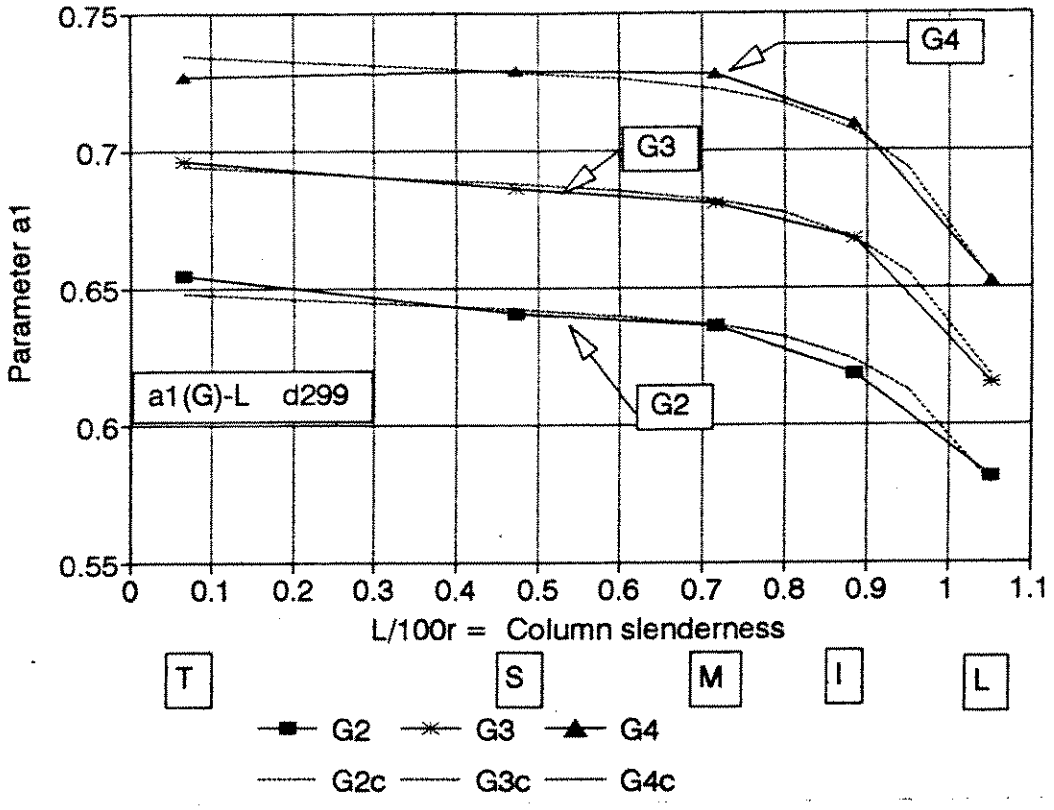

Figure 8-3: Parameter a1 as Function of Column Length (Slenderness) for Different Values of Circumferential Spread **g**

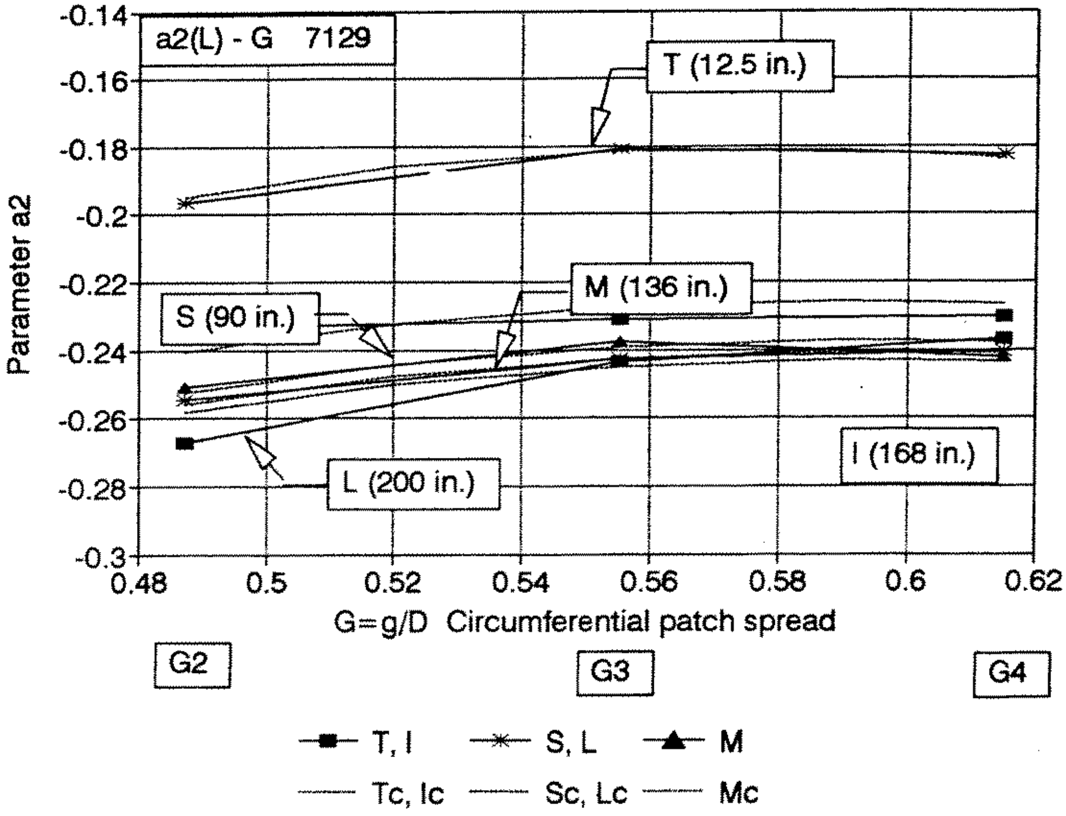

Figure 8-4: Parameter a2 as Function of Circumferential Spread **g** for Different Column Lengths *ℓ*

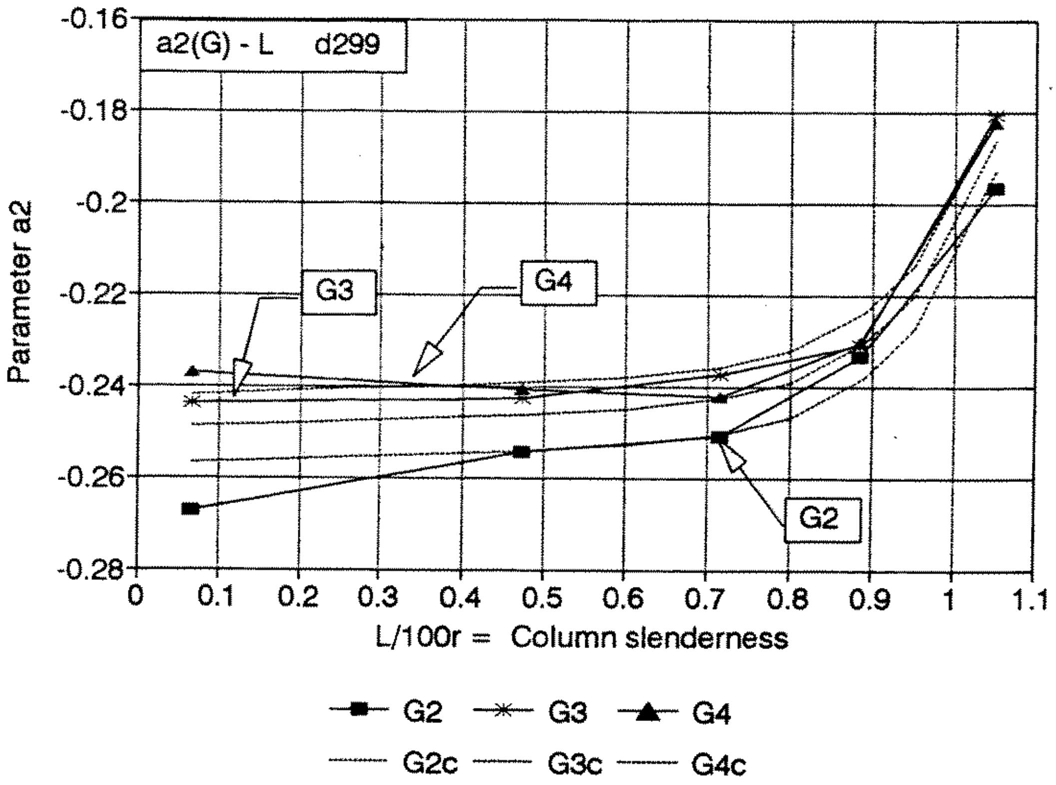

Figure 8-5: Parameter a2 as Function of Column Length (Slenderness) for Different Values of Circumferential Spread **g**

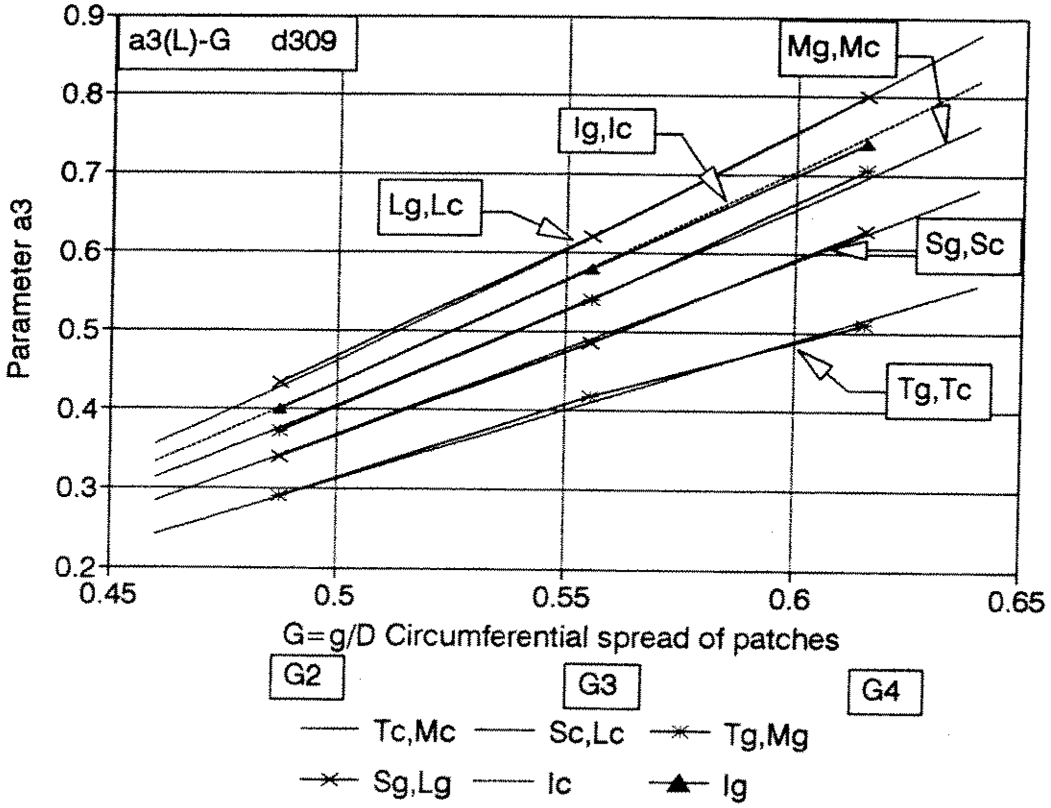

Figure 8-6: Parameter a3 as Function of Circumferential Spread **g** for Different Column Lengths $\ell$

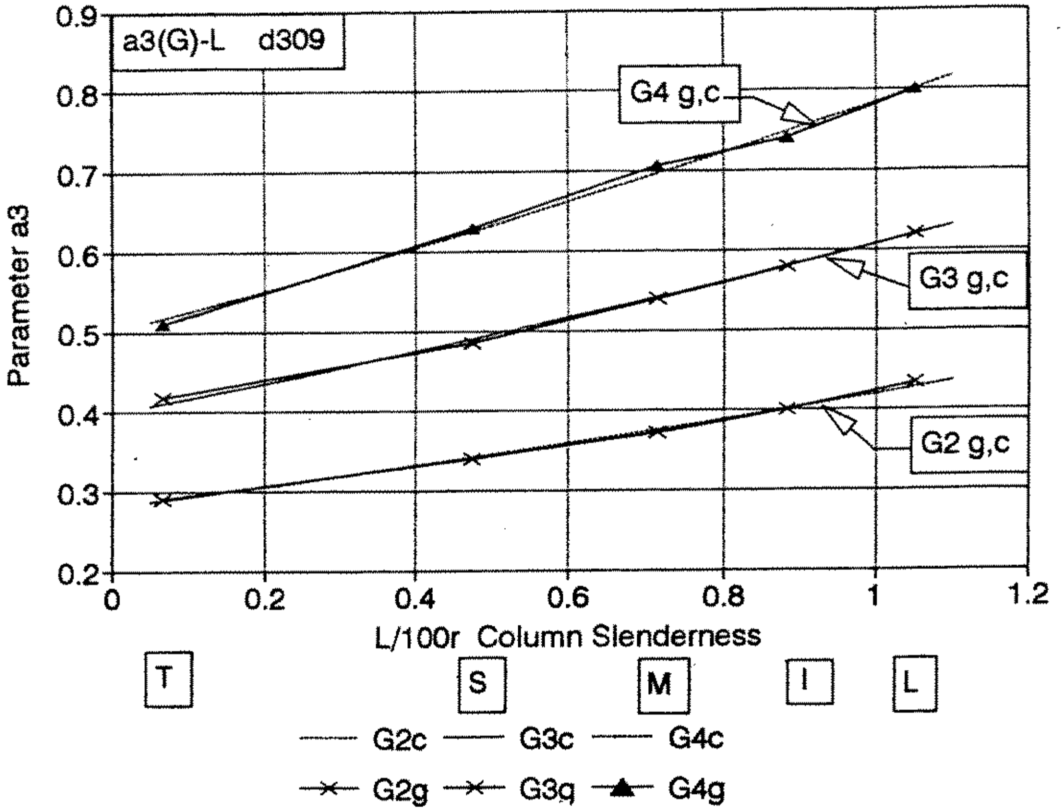

Figure 8-7: Parameter a3 as Function of Column Length (Slenderness) for Different Values of Circumferential Spread **g**

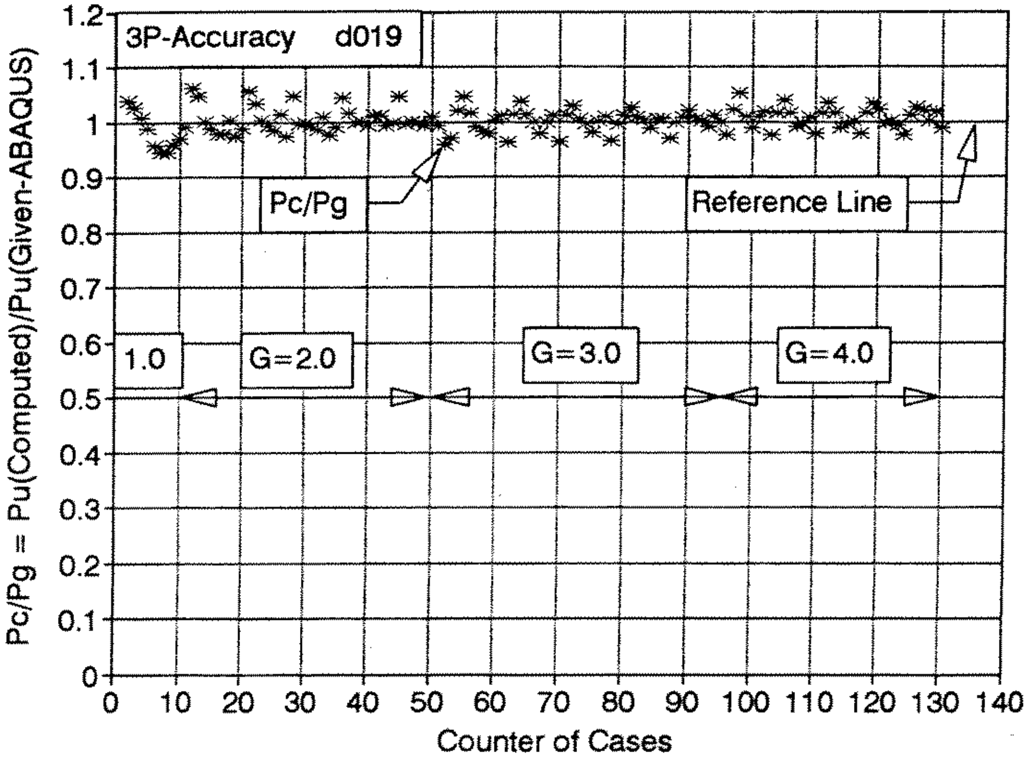

Figure 8-8: Accuracy of Proposed Formulas for Pinned-End Tubular Columns with Three Corrosion Patches

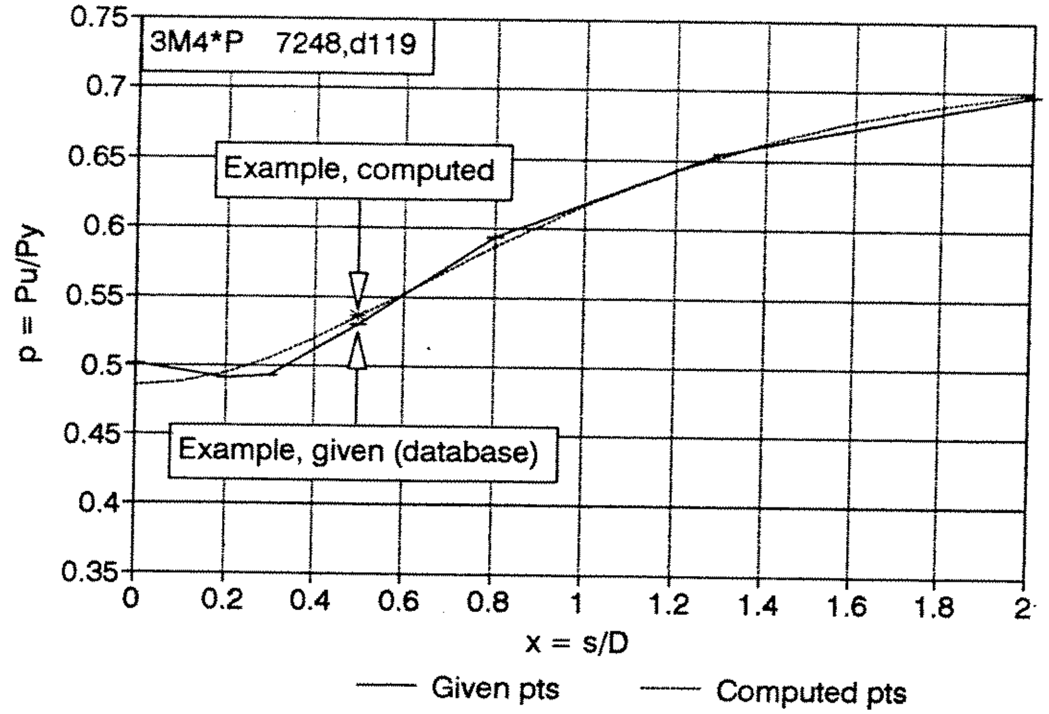

Figure 8-9: Example Solution for a Pinned-End Tubular Column with Three Corrosion Patches

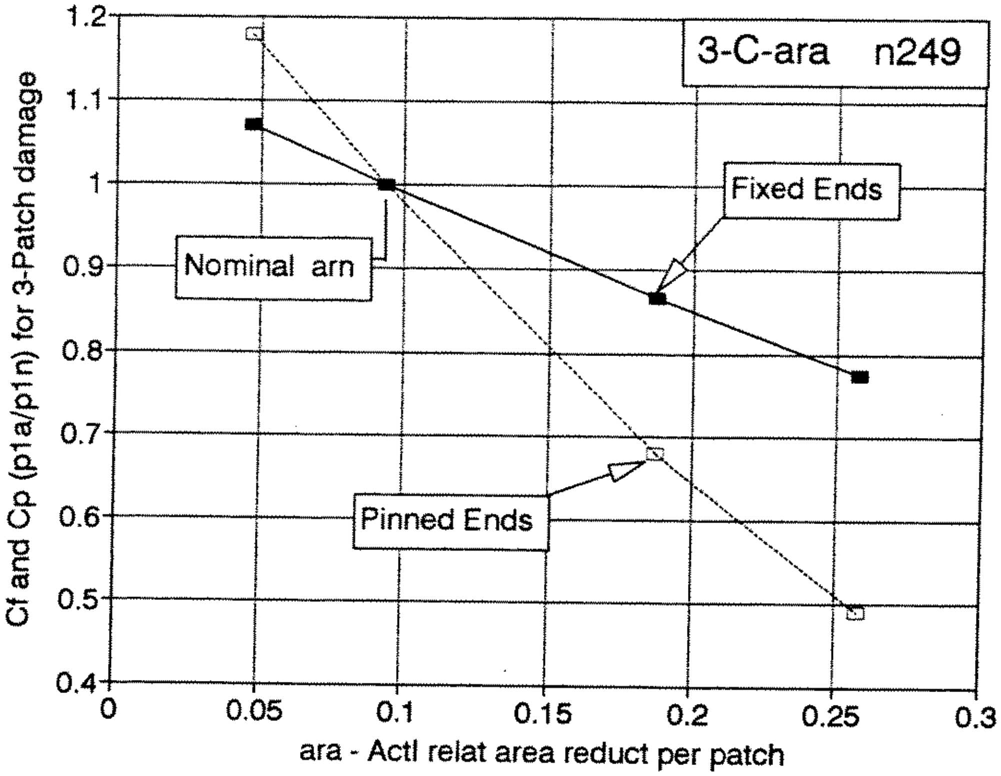

Figure 9-1: Correction Factors $C_f$ and $C_p$ vs. Relative Area Reduction per Patch, **ara**

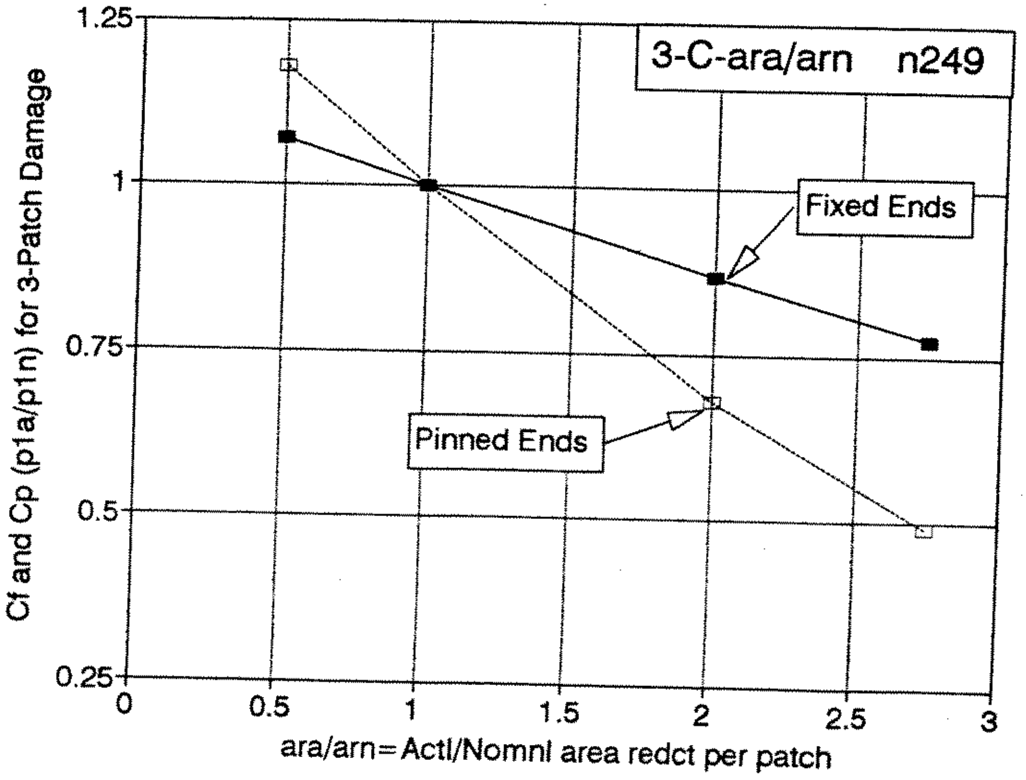

Figure 9-2: Correction Factors $C_f$ and $C_p$ vs. **ara/arn**

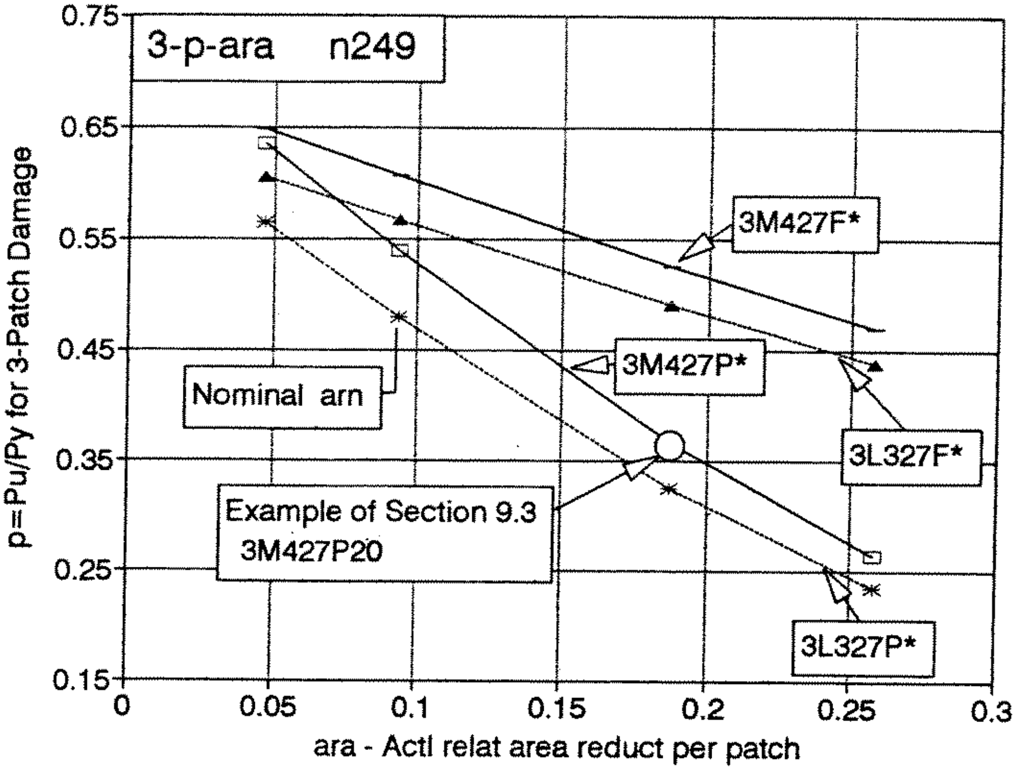

Figure 9-3: Relative Ultimate Load **$p = P_u/P_y$** vs. Variable Patch Size **ara** for Two Specimens with Fixed or Pinned Ends (3M427** and 3L327**)

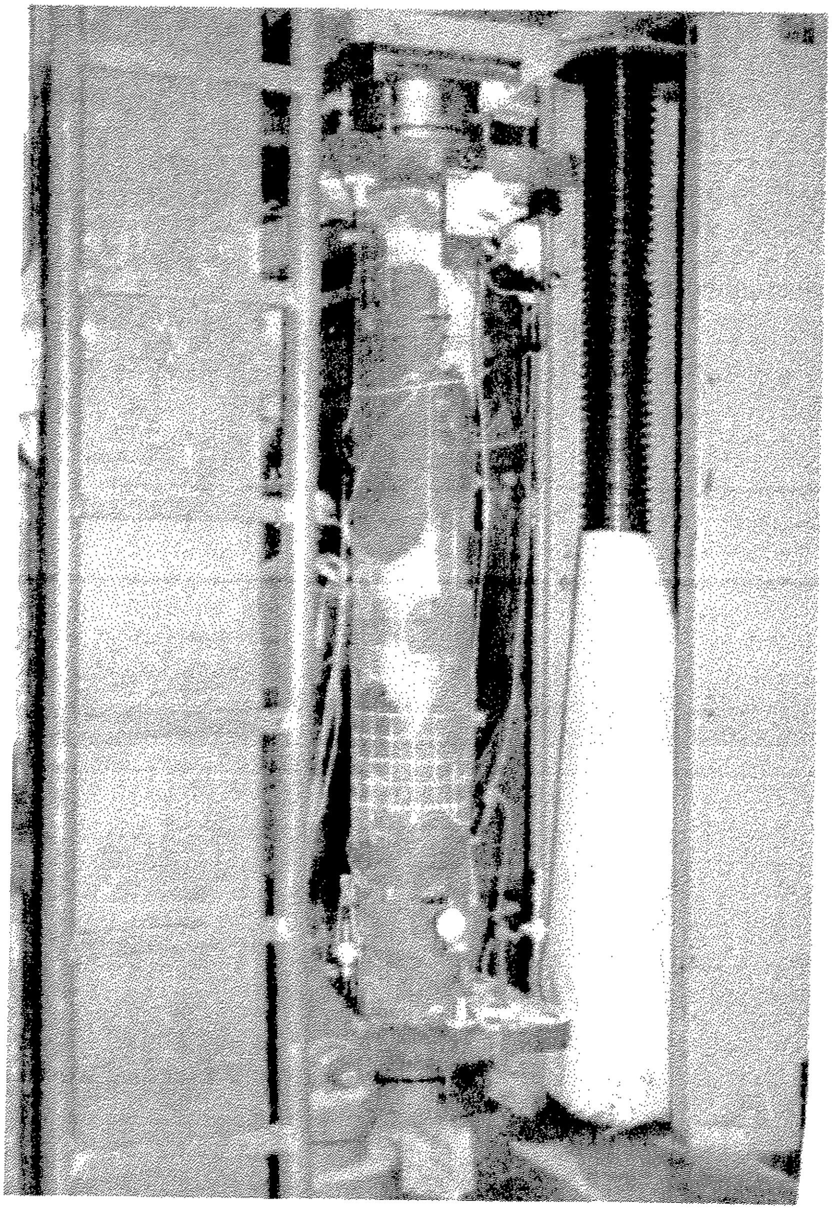

Photo 1-1: Typical Salvaged Corrosion-Damaged Tubular Column

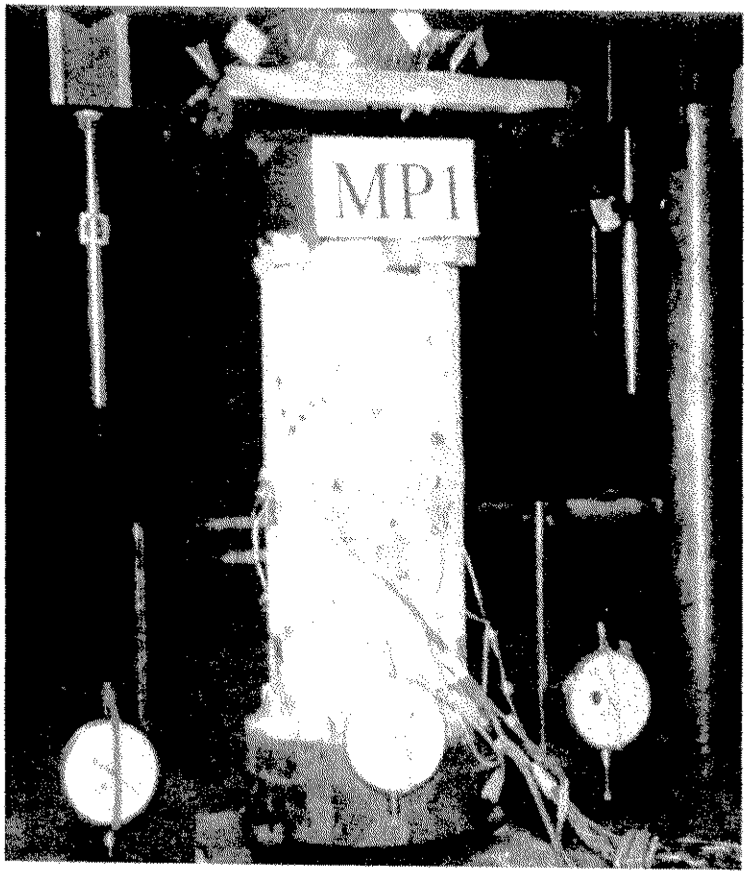

Photo 2-1: Specimen MP1

Photo 2-2: Specimen MP2